Exploring α-subunit heterogeneity in $GABA_A$ receptors

Valentina Dorovykh

A thesis submitted to University College London for the degree of Doctor of Philosophy

March 2023

Department of Neuroscience, Physiology and Pharmacology

University College London

Gower Street

London

WC1E 6BT

Declaration

I, Valentina Dorovykh, confirm that the work presented in this thesis is my own. Where information has been derived from other sources, I confirm that this has been indicated in my thesis.

Abstract

GABA type-A receptors ($GABA_ARs$) are the most abundant proteins responsible for inhibitory signalling in the brain. These proteins assemble into a hetero-pentameric structure, constructed from a selection of α1-6, β1-3 and γ1-3, δ, ε, ρ, π and θ subunits. Although prototypic $GABA_ARs$ are generally considered to be composed of αβγ subunits, the precise composition and arrangement of native $GABA_ARs$ remains poorly defined. It is commonly accepted that distinct GABA receptors comprise only a single type of α subunit, which then dictates their pharmacological profiles influencing neural circuit activity and behaviour.

The aim of this study was to investigate the likelihood of hetero-α subunit assembly in the same receptor pentamer, dissecting the complexity associated with subunit assembly for $GABA_ARs$ and providing novel insight into their structures and functional footprints. To address this, we first electrophysiologically analysed α1 and α2 with β2/3 γ2L wild-type and reporter-mutant subunit mixtures in HEK293 cells to establish the presence of hetero-α-$GABA_AR$ isoforms. We also examined the stoichiometry of hetero-α-receptors and whether there is preferential positioning of α subunit isoforms at α-γ benzodiazepine binding interfaces.

We then demonstrate that hetero-α-$GABA_ARs$ are expressed *in vivo* and measure their abundance and subcellular localisation in hippocampal neurons using proximity ligation assays (PLA). In addition, we assess dynamic regulation of these receptors during long term potentiation (LTP). There is a significant increase in α1α2-containing receptors upon LTP induction, and these receptors are localised preferentially at inhibitory synapses. Finally, homo- and hetero-α1/2 $GABA_AR$ numbers at synapses were estimated using Spatial Intensity Distribution Analysis (SPiDA).

In conclusion, this study demonstrates that hetero-α $GABA_ARs$ do assemble in the brain and proposes their physiological importance for brain inhibition. This study also describes a multidisciplinary approach that is applicable for investigating other $GABA_AR$ hetero-α-subunit assemblies, including the assessment of their pharmacological profiles.

Acknowledgements

Firstly, I would like to thank my supervisor Prof. Trevor Smart, whose enthusiasm, support and positive thinking was instrumental in helping me throughout my PhD. Thank you to my secondary supervisor – Dr. Matthew Gold – for providing his input throughout my project. I would also like to thank Dr. Antoine Godin for his patience and time he has put into SpIDA analysis. Also, I would like to thank UCL for providing the funding for my PhD with the overseas research scholarship.

Also, thanks to all the members of the Smart lab – you make an amazing and friendly community to work and be with! Thanks to Phil for teaching me how to be very meticulous with drug applications and data analysis. Martin – for being an amazing dinner host and courgette 'dealer.' Seth – for constantly being optimistic with my submission timeline. A special thanks goes to Damian – a person who has put in a tremendous amount of time and effort into my project – he is the person who has shown me what good science practice is.

I would like to thank you my family for all the love and support they have given me throughout the years. In particular, to my dad who has given me an opportunity to study abroad and become the best version of myself. To my mom – who would be available all the time to listen to my PhD related worries and achievements and believing in me. She has always been there to encourage me during my academic path. To my sisters and brother – for spamming the family group chat with dog videos and photos – it was a much-appreciated distraction between experiments.

Thank you to all my friends – in London and outside – they have been an excellent company and entertainment within the past few years. I would like to give a special thank you to Reka – a person without whom my day would not start unless we have a coffee and 'chitty-chats' together, and Tibi – for all the fun evenings we spent together during and beyond the pandemic. Also, Harriet, Guido, PB and Fra were always there for me to support me and understand all the PhD related struggles.

Finally, the person who has been by my side through all the highs and lows is my husband – Marco. I am immensely grateful to him for all the support he has given me,

especially when I was writing my thesis. His parmigiana dish (and other not so fancy meals) were the highlight after a busy day at work.

Impact statement

In the brain, fast synaptic inhibition is mediated by $GABA_A$ receptors that are expressed as pentamers comprising of two α, two β and one γ subunits. The $GABA_A$ receptor composition determines receptor agonist sensitivity, pharmacological profiles and subcellular localisation. In particular, the identity of the two α subunits in a $GABA_A$ receptor complex largely dictates receptor GABA potency as well as pharmacological sensitivity and physiological effects of benzodiazepines – $GABA_AR$ positive allosteric modulators. Therefore, establishing $GABA_A$ receptor subunit composition is key to understanding the dynamics of inhibitory transmission within the brain.

Previous studies have mostly focused on functional and pharmacological characterisation of $GABA_A$ receptor subtypes with two identical α subunit isoforms – 'homo-alpha' receptors. Despite some biochemical studies showing the existence of CNS $GABA_A$ receptors with two distinct α subunit isoforms – 'hetero-alpha' receptors, corroborative evidence for such receptor subtypes using other techniques is limited. In this present study, we therefore focused on identifying and investigating the role of hetero-alpha' $GABA_ARs$ containing α1 and α2 subunits – the two most widely expressed α subunit types in the brain. By using a multidisciplinary approach, combining both electrophysiological and imaging techniques, we were able to establish the existence and relative proportion of such receptors in both recombinant and native $GABA_A$ receptor populations.

The expression of receptors with two distinct α subunit isoforms adds a layer of complexity to the assembly, expression and localisation of $GABA_A$ receptors, likely shaping their physiological role in synaptic inhibition. Furthermore, the existence of 'hetero-alpha' $GABA_A$ receptors in the brain is likely to be involved in fine-tuning their pharmacological activity, including physiological effects of benzodiazepines. This may aid the development of therapeutic agents showing greater receptor selectivity and with reduced off-target effects. Overall, this work expands our understanding of $GABA_A$ receptor subtypes, and provides a basis for further research into the fine control of synaptic inhibition.

Contest

Declaration 1

Abstract 2

Acknowledgements 3

Impact statement 5

Contest 6

List of figures 11

List of tables 14

List of abbreviations 15

Chapter 1: Introduction 18

1.1 $GABA_A$ receptors 18

1.1.1 $GABA_A$ subunit and receptor structure 19

1.1.2 $GABA_A$ receptor assembly, stoichiometry and cellular localisation 23

1.1.3 $GABA_A$Rs in vivo expression patterns 27

1.1.4 $GABA_A$R biophysical properties 28

1.1 Post-translational modifications 31

1.2.1 Phosphorylation 31

1.2.2 N-linked glycosylation 36

1.3 $GABA_A$ receptor pharmacology 37

1.3.1 $GABA_A$ receptor agonists 38

1.3.2 $GABA_A$ receptor antagonists 40

1.3.3 Benzodiazepine pharmacology 41

1.3.4 Neurosteroids 43

1.4 'Hetero-alpha' $GABA_A$ receptors 44

1.4.1 'Hetero-alpha' $GABA_A$ receptors: biochemical evidence 45

1.4.2 Concatenated receptor studies 52

1.5 Thesis aims 55

1.5.1 Electrophysiological assessment of $GABA_A$ receptors with two different α subunit isoforms 55

1.5.2 Evidence of existence in vivo 56

1.5.3 Physiological role of α1α2-containg $GABA_A$ receptors 56

1.5.4 Summary of aims 57

Chapter 2: Materials and Methods 58

2.1 Molecular biology 58

2.1.1 $GABA_A$ receptor subunit constructs 58

2.2 HEK293 cell culture and transfection 61

2.2.1 HEK293 cell culture 61
2.2.2 HEK293 cell transfection 62
2.3 Neuronal cell culture and transfection 63
2.3.1 Hippocampal cell culture 63
2.3.2 Neuronal Effectene transfection 64
2.4 Electrophysiology 65
2.4.1 Voltage-clamp electrophysiology (HEK293 cells) 65
2.4.2 Electrophysiology data analysis (HEK293 cells) 67
2.4.3 Voltage-clamp electrophysiology (neurones) 71
2.4.4 Electrophysiology data analysis (neurons) 72
2.5 Neuronal and HEK293 cell immunostaining and confocal imaging 73
2.5.1 Antibody labelling 73
2.5.2 Proximity Ligation Assay (PLA) method 77
2.5.3 PLA fluorescence protocol 77
2.5.4 Image acquisition (confocal microscopy) 80
2.5.5 Image analysis 80
2.5.6 Analogue detector calibration for spatial intensity distribution analysis (SpIDA) 82
2.5.7 Laser beam waist radius measurements 83
2.6 Statistical analysis 83
Chapter 3: Exploring the presence, abundance and subunit arrangement of 'hetero-alpha' $GABA_A$Rs in a transfected HEK293 cells 84
3.1 Introduction 84
3.2 Results: electrophysiological assessment of 'hetero-alpha' wild type receptors 90
3.2.1 Co-expression of α1 and α2 wild-type subunits form distinct population of receptors with higher apparent affinity to GABA 91
3.2.2 Overexpressing either α subunit does not affect the formation of α1α2-containing $GABA_A$ receptors 95
3.2.3 Functional properties of α1α2 – role of the β subunit 99
3.2.4 Functional properties of α1α4 $GABA_A$ receptor mixtures 100
3.2.5 Summary of results from investigating wild-type α1α2 and α1α4 subunit mixtures 102
3.3 Results: Inferring the number of receptor populations with α1α2 co-expression using reporter mutations: $\alpha1^{L263S}$ and $\alpha2^{F65L}$ 103
3.3.1 Substitution of the conserved leucine to serine in α1 subunit increases its GABA sensitivity 103
3.3.2 Co-expression of $\alpha1^{L263S}$ and α2 subunits 107

3.3.3 The F65L substitution in α2 subunit profoundly reduces receptor sensitivity to GABA but does not affect the cell surface expression 111

3.3.4 Co-expression of α1 and $α2^{F65L}$ subunits 114

3.3.5 Co-expression of α2 and $α2^{F65L}$ subunits 117

3.3.6 Summary of results from $α1^{L263S}$ and $α2^{F65L}$ 118

3.4 Results: Insight into subunit arrangement of 'hetero-alpha' $GABA_A$ receptors 120

3.4.1 Validation of benzodiazepine insensitive mutations on α1 and α2 $GABA_AR$ subunits 120

3.4.2 Assessment of subunit arrangement of 'hetero-alpha' β2-containing receptors using reporter mutations $α1^{H101R}$ and $α2^{H101R}$. 126

3.4.3 Assessment of subunit arrangement of 'hetero-alpha' β3-containing receptors using reporter mutations $α1^{H101R}$ and $α2^{H101R}$. 132

3.4.4 Summary of results from $α1^{H101R}$ and $α2^{H101R}$ reporter mutations 139

3.5 Discussion 140

3.5.1 Identities of both α and β subunits determine GABA sensitivity of 'hetero-alpha' $GABA_A$ receptors 140

3.5.2 The β subunit determines the abundance of 'hetero-alpha' $GABA_A$ receptors ... 141

3.5.3 The function of the α/γ interface in 'hetero-alpha' $GABA_A$ receptors 145

3.6 Assumptions and limitations 147

3.6.1 Reporter mutations 147

3.6.2 GABA binding sites 148

3.7 Conclusions 149

Chapter 4: Exploring 'hetero-alpha' $GABA_A$Rs in cultured hippocampal neurons: presence, functional signatures and roles in long-term potentiation 150

4.1 Introduction 150

4.2 Results 153

4.2.1 Assesment of the interaction between $GABA_AR$ α1 and α2 subunits via PLA 153

4.2.2 Nocodazole effects on $GABA_AR$ clustering and α1 and α2 subunit proximity..... 157

4.2.3 $GABA_AR$ γ2 and δ subunits are not in close proximity for PLA probe hybridisation 164

4.2.4 Expression of the α2 subunit leads to an increase in synaptic 'hetero-alpha' $GABA_A$Rs in cultured hippocampal neurons 165

4.2.5 Investigating sIPSCs of α1 and α2 transfected cultured hippocampal neurons.. 169

4.2.6 Exploring effect of chemical inhibitory long-term potentiation on sIPSCs in cultured hippocampal neurons 171

4.2.7 Chemical induction of LTP increases both sIPSC amplitude and frequency 174

4.2.8 Investigating the effect of the glycine LTP protocol on 'hetero-alpha' $GABA_A$Rs using proximity ligation assay..... 177

4.3 Discussion 180
4.3.1 PLA is a reliable method for studying stoichiometry of $GABA_A$ receptors 181
4.3.2 Limitations of proximity ligation assay-based techniques 182
4.3.3 Expression of synaptic 'hetero-alpha' α1α2-containing $GABA_A$ receptors: assembly, subcellular localisation and functional signatures 184
4.3.4 Effects of long-term potentiation on 'hetero-alpha' $GABA_A$ expression 186
4.4 Conclusions 188
Chapter 5: Exploring synaptic $GABA_AR$ composition changes post long-term potentiation induction 189
5.1 Introduction 189
5.1.1 Principle behind spatial intensity distribution analysis 189
5.1.2 SpIDA as a functional tool to study the oligomerisation state of native $GABA_ARs$ 192
5.2 Results 193
5.2.1 Parameter calibration: analogue detector and point spread function (PSF) measurements 193
5.2.2 Mean intensity of α1 and α2 $GABA_AR$ subunit labelling significantly increases post LTP induction 199
5.2.3 Effects of the iLTP induction on α1 $GABA_ARs$ oligomerisation states 203
5.2.4 Effects of the glycine LTP induction on α2 $GABA_AR$ oligomerisation states 205
5.2.5 Effects of the glycine LTP induction on α1 and α2 $GABA_AR$ oligomerisation states 207
5.2.6 Number of α1 and α2 subunits in α1/α2 immunolabelling is consistent with that of α1 + α2 simultaneous immunolabelling 209
5.3 Discussion 211
5.3.1 α1/α2-containing $GABA_AR$ expression in control treated neurons 211
5.3.2 α1/α2-containing $GABA_AR$ expression changes following iLTP induction 214
5.3.3 Limitations of SpIDA 217
5.4 Conclusions 217
Chapter 6: General discussion 219
6.1 Literature overview and project aims 219
6.2 Major findings 220
6.2.1 Existence and abundance of α1α2-containing $GABA_ARs$ in vitro and in vivo 220
6.2.2 Determinants of 'hetero-alpha' $GABA_AR$ expression and assembly 221
6.2.3 Subcellular localisation of 'hetero-alpha' $GABA_ARs$ 223
6.2.4 Functional role of 'hetero-alpha' $GABA_ARs$ 224
6.3 Future directions 227

6.3.1 Concatenated receptor studies 227
6.3.2 Atomic Force and Cryo-electron Microscopy 227
6.4 Concluding Remarks 228
References 229

List of figures

Figure 1.1 *The structure of a $GABA_A$ receptor*……21

Figure 1.2 *$GABA_A$ receptor pharmacology*……..38

Figure 1.3 *'Hetero-alpha' $GABA_A$ receptor subunit arrangement and their benzodiazepine pharmacology*……51

Figure 1.4 *Examples of undesired structural artefacts that could form during the assembly of dimeric subunit concatenated receptors*……54

Figure 2.1 *A schematic representation of U-tube drug application onto a patch-clamped Hek293 cell*……66

Figure 2.2 *Calculating spontaneous activity of recombinant $GABA_A$ receptors*……71

Figure 2.3 *Proximity ligation assay (PLA) principle*……78

Figure 3.1 *Possible number of components comprising the concentration-response relationship from co-expression of $\alpha1^{mut}$ and $\alpha2^{WT}$ subunits together with β and γ*……88

Figure 3.2 *The H101R benzodiazepine insensitive mutation on the α subunit as a functional tool to determine 'hetero-alpha' $GABA_A$ receptor subunit arrangement.*……90

Figure 3.3 *'Hetero-alpha'* β*3-containing recombinant $GABA_A$ receptors are more sensitive to GABA than their homomeric counterparts*……93

Figure 3.4 *α1α2-containing recombinant $GABA_A$ receptors form functional triheteromers (αβγ)*……95

Figure 3.5 *Effects of varying transfection ratios of α1 and α2 cDNAs on GABA concentration-response relationships*……98

Figure 3.6 *Functional properties of recombinant 'hetero-alpha' α1α2-containing $GABA_A$ receptors*……100

Figure 3.7 *Functional properties of recombinant 'hetero-alpha' α1α4-containing $GABA_A$ receptors*……101

Figure 3.8 *Serine substitution of a conserved leucine in TM2 (9′ position) of the α1 subunit increases GABA sensitivity and spontaneous activity*……106

Figure 3.9 *GABA dose-response relationships from co-expression of $\alpha1^{L263S}$ and α2 subunits in HEK293 cells*……109

Figure 3.10 *$GABA_AR$ α2 subunit phenylalanine to leucine substitution at residue position 65 results in a decreased GABA-sensitivity, however does not reduce cell surface expression*……113

Figure 3.11 *GABA dose-response relationships from co-expression of α1 and $α2^{F65L}$ subunits in HEK293 cells*……..116

Figure 3.12 *GABA dose-response relationships from co-expression of α2 and $α2^{F65L}$ subunits in HEK293 cells*……..118

Figure 3.13 *The H101R substitution in the α1/2 $GABA_A$ receptor subunit results in flurazepam insensitivity, however does not affect GABA sensitivity*……..122

Figure 3.14 *The H101R substitution in the α1/2 $GABA_A$ receptor subunit results in flurazepam insensitivity and reduces GABA sensitivity of β3-containing receptors*……..125

Figure 3.15 *Removing benzodiazepine sensitivity of γ2/α1 interface in α1α2β2γ2L transfected HEK293 cells indicates the presence of both γ2/α1 and γ2/α2 interface-containing $GABA_A$ receptor populations*……..128

Figure 3.16 *Mixture of α1 wild type and α2 benzodiazepine insensitive mutant subunits co-expressed with β2 and γ2 subunits results in γ2/α1 and γ2/α2 interface-containing $GABA_A$ receptor populations*……..131

Figure 3.17 *The H101R benzodiazepine insensitive mutation of the α1 subunit in α1α2β3γ2L transfected HEK293 cells indicates the presence of both γ2/α1 and γ2/α2 interface-containing $GABA_A$ receptor populations*……..134

Figure 3.18 *Mixture of α1 wild type and $α2^{H101R}$ mutant subunits co-expressed with β2 and γ2 subunits results in expression of both γ2/α1 and γ2/α2 interface-containing $GABA_A$ receptor populations*……..137

Figure 4.1 *Detection of $GABA_AR$ α1 and α2 subunit interactions in transfected HEK293 cells and cultured hippocampal neurons*……..155

Figure 4.2 *Nocodazole treatment decreases $GABA_AR$ α1 subunit clustering*……..159

Figure 4.3 *Nocodazole treatment promotes $GABA_AR$ α2 subunit declustering*…..161

Figure 4.4 *Nocodazole treatment has no effect on the number of $GABA_AR$ α1 and α2 PLA dots*……163

Figure 4.5 *The $GABA_ARs$ γ2 and δ subunits are not in close proximity to produce a PLA signal*……165

Figure 4.6 *Overexpression of α2, but not α1 $GABA_AR$ subunits leads to an increase in PLA dots that localise at synapses*……..168

Figure 4.7 *sIPSC analysis of eGFP, α1 and α2 transfected hippocampal cultured neurons*……170

Figure 4.8 *Effects on sIPSC frequency and mean amplitude of a chemical iLTP protocol*……..173

Figure 4.9 *Chemical induction of excitatory LTP with glycine significantly increases both sIPSC frequency and amplitude*……..176

Figure 4.10 *Chemical induction of LTP significantly increases $GABA_AR$ α1 and α2 subunit synaptic PLA signal*……..179

Figure 5.1 *Basis of spatial intensity distribution analysis*……..191

Figure 5.2 *Analogue detector calibration procedure*……..195

Figure 5.3 *Measuring the laser beam waist area*……..198

Figure 5.4 *Regions of interest selected for spatial intensity distribution analysis*……200

Figure 5.5 *Mean intensity of $GABA_AR$ labelling increases post iLTP induction in cultured hippocampal neurons*……..202

Figure 5.6 *Effects of the iLTP induction on α1 $GABA_AR$ oligomerisation states*……204

Figure 5.7 *Effects of the glycine LTP induction on α2 $GABA_ARs$ oligomerisation states*……206

Figure 5.8 *Effects of the glycine LTP induction on both α1 and α2 $GABA_ARs$ oligomerisation states*……208

Figure 5.9 *$GABA_AR$ subunit and receptor number for combined α1 and α2 immuno-labelling corresponds to those obtained from α1 + α2 immuno-labelling*……..210

Figure 5.10 *Schematic diagram of $GABA_AR$ changes induced by glycine LTP*……..216

List of tables

Table 1.1 *$GABA_A$ receptor phosphorylation sites*……..33

Table 1.2 *Biochemical evidence for heteromeric $GABA_A$ receptors*……..46

Table 2.1 *PCR reaction concentration and volumes used per reaction*……58

Table 2.2 *PCR primers used to introduce affinity tags or point mutations into $GABA_A$ receptor DNA*……..60

Table 2.3 *Reagents and their volumes used in calcium phosphate HEK293 cell transfection*……..63

Table 2.4 *List of pharmacological compounds used throughout this project*……67

Table 2.5 *List of antibodies used throughout this project*……..75

Table 2.6 *Antibodies used for PLA*……..79

Table 2.7 *DiAna segmentation parameters*……..82

Table 3.1 *The mean GABA EC_{50} values for α1 α2 wild type/mutant mixtures*……138

Table 3.2 *Summary results table of electrophysiological studies in HEK293 cells*……..143

Table 5.1 *Parameters chosen for SpIDA post detector calibration*……..196

List of abbreviations

5HT3R	5-hydroxytryptamine (serotonin) receptor
a.a.	amino acid(s)
AFM	atomic force microscopy
AMPAR	α-amino-3-hydroxy-methyl-4-isoxazoleproionic acid receptor
ANOVA	analysis of variance
APV	(2R)-amino-5-phosphonovaleric acid
ATP	adenosine triphosphate
BAPTA	1,2-bis(o-aminophenoxy) ethane-N,N,N',N'-tetraacetic acid)
BCA assay	bicinchoninic assay
BCIP	5-bromo-4-chloro-3-indolyl phosphate
BDZ	benzodiazepine
BSA	bovine serum albumin
CaMKII	Ca^{2+}/calmodulin-dependent protein kinase II
CLSM	confocal laser-scanning microscopy
CNS	central nervous system
CNQX	cyanquixaline
CRC	concentration response curve
D-AP5	D(-)-2-amino-5-phosphonopentanoic acid
DBI	diazepam binding inhibitor
DIC	differential interference contrast
DIV	day *in vitro*
DMEM	Dulbecco's modified Eagle medium
DNA	deoxyribonucleic acid
dsDNA	double stranded DNA
EGTA	ethylene glycol-bis- N,N,N',N'-tetraacetic acid
eGFP	enhanced green fluorescent protein
EPSC	excitatory post synaptic current
ER	endoplasmic reticulum

FBS	foetal bovine serum
FCS	foetal calf serum
FRET	fluorescence resonance energy transfer
GABA	γ-aminobutyric acid
$GABA_AR$	GABA receptor type A
$GABA_BR$	GABA receptor type B
Gly	glycine
GST	glutathione S-transferase
GTP	guanosine triphosphate
HBS	HEPES-buffered saline
HBSS	Hanks' Balanced Salt Solution
HEK293 cells	Human embryonic kidney 293 cells
HEPES	(4-(2-hydroxyethyl)-1-piperazineethanesulfonic acid)
ICC	immunocytochemistry
ICD	intracellular domain
iLTP	inhibitory long-term potentiation
IPSC	inhibitory postsynaptic current
LB	Lysogeny Broth
LTP	long-term potentiation
KCC2	potassium-chloride co-transporter 2
MAP2	microtubule-associated protein 2
NA	numerical aperture
nAChRs	nicotinic acetylcholine receptors
NBT	p-nitro blue tetrazolium chloride
NGS	normal goat serum
NMDA	N-methyl-D-aspartate
NTD	N-terminal domain
p.i.	protease inhibitors
PBS	phosphate buffered saline

PCR	polymerase chain reaction
PDB	protein data bank
PKA	protein kinase A
PKC	protein kinase C
PLA	proximity ligation assay
PMT	photomultiplier tube
PFA	paraformaldehyde
PIK-3	phosphoinositide 3-kinase
PNK	polynucleotide kinase
PMSF	phenylmethylsulphonyl fluoride
PSF	point spread function
PTX	picrotoxin
QB	quantal brightness
RIPA buffer	radioimmunoprecipitation assay buffer
ROI	region of interest
RT	room temperature
SD	standard deviation
SEM	standard error of the mean
SOC medium	super optimal broth with catabolite repression medium
SpIDA	spatial intensity distribution analysis
TBS	Tris-buffered saline
THIP	4,5,6,7-tetrahydoisoxazolo[5,4-c]pyridine-3(2H)-one
TMD	transmembrane domain
Tris-HCl	**2-Amino-2-(hydroxymethyl)-1,3-propanediol hydrochloride**
Trypsin-EDTA	trypsin-ethylene-diamine-tetra-acetic acid
VIAAT (VGAT) transporter)	vesicular inhibitory amino acid transporter (vesicular GABA
WT	wild type
Zn^{2+}	zinc ion

Chapter 1: Introduction

1.1 $GABA_A$ receptors

In the mammalian brain, γ-aminobutyric acid (GABA) is the main inhibitory neurotransmitter and acts through both fast ionotropic type A receptors $GABA_AR$ and slow metabotropic type B receptors $GABA_BRs$ (Smart and Stephenson, 2019). This introduction gives an insight into the former, as the emphasis of this project lies in the $GABA_A$ receptor family.

$GABA_A$ receptors belong to a superfamily of ligand-gated ion channels (LGICs) previously known as Cys-loop LGICs, and now referred to as pentameric LGICs, which includes glycine receptors (GlyRs) and nicotinic acetylcholine receptors (nAChRs) as two examples (Bowery and Smart, 2006). When two GABA molecules bind to $GABA_A$ receptors, they initiate the gating and opening of the selective ion channel pore through which negatively charged ions, primarily chloride (Cl^-) and bicarbonate (HCO_3^-) flow, mediating phasic and tonic inhibitory synaptic transmission (Olsen and Sieghart, 2009; Thomas et al., 2005). In the mature central nervous system (CNS), the resulting influx of anions into neurones results in a an increased membrane hyperpolarisation and increased membrane conductance, known as 'shunting inhibition' (Farrant and Nusser, 2005; Song et al., 2011). These have an effect on potential changes of other ion channels by reducing their amplitude and duration. Hyperpolarisation and increased membrane conductance act to decrease neuronal excitability, providing the principal mechanism for controlling brain activity.

$GABA_A$ receptors are known for their prominent variety of subunit combinations, that upon assembly produce distinct physiological, kinetic and pharmacological properties (Mortensen et al., 2012b; Olsen and Sieghart, 2009; Semyanov et al., 2004; Sieghart and Sperk, 2002). $GABA_A$ receptors play a major role in CNS signalling, therefore their aberrant function is associated with a multitude of disease states such as epilepsy, memory deficits, schizophrenia, anxiety disorders and depression (Macdonald et al., 2010; Möhler, 2006; Olsen and Sieghart, 2009). Hence, these receptors have an obvious relevance for pharmacotherapy for certain brain disorders (Olsen, 2018). It

is therefore important to understand $GABA_A$ receptors subunit assembly and arrangement to provide better physiological and pharmacological characteristics for such treatments – the underlying rationale for this thesis.

1.1.1 $GABA_A$ subunit and receptor structure

$GABA_AR$ are hetero-pentameric glycoproteins composed from a selection of nineteen subunits: α1-6, β1-3, γ1-3, δ, ε, θ, π, ρ1-3 (receptors containing ρ subunits formerly known as $GABA_C$ receptors) (Barnard et al., 1998; Sigel and Steinmann, 2012). There is ∼70% sequence identity within each subunit family and ∼50% sequence similarity (counting conservative amino acid replacements) between different families of subunits (Davies et al., 1996; Olsen and Tobin, 1990).$GABA_A$ receptor genes consist of nine coding exons and eight noncoding introns, except for γ3 and δ that have ten exons and eight introns (Sigel and Steinmann, 2012; Smart and Stephenson, 2019).

Further diversity of receptor subunits results from the alternative splicing of RNA, generating two forms of a particular subunit (Sieghart, 1995, 1995; Smart and Stephenson, 2019). One of the most prominent examples is the splicing of a γ2 subunit, allowing for existence of short and long variants (γ2S and γ2L respectively). The difference between the two subunit variants lie in an eight amino acid sequence in the intracellular loop region, that contains a consensus sequence for protein kinase C (PKC) binding (Harvey et al., 1994; Whiting et al., 1990). Other $GABA_AR$ subunit sequences undergo RNA alternative splicing (α6, β2, γ3), however the function of these variants is still to be elucidated (Simon et al., 2004; Smart and Stephenson, 2019).

The mature $GABA_A$ receptor subunit is around 450 amino acid residues long (about 50 kDa molecular weight). $GABA_AR$ subunits share a common topology: large N-terminal extracellular domain (NTD), followed by four hydrophobic transmembrane (TM) spanning domains (TM1-4) with a large intracellular loop (ICL) between TM3 and TM4, and an extracellular C-terminus (Carter et al., 2010; Ernst et al., 2005) **(**see ***Figure 1.1*****).** The description as a Cys-loop superfamily results from a conserved 13-residue amino acid loop formed by a disulphide bridge between two cysteine

residues in the extracellular NTD (Connolly and Wafford, 2004; Unwin, 2005). It is located at the base of the NTD and plays a crucial role in forming GABA binding site and ion channel communication (Miller and Smart, 2010). Multiple cryo-electron microscopy (EM) structures of GLIC-$GABA_AR$ chimeras and more physiological $GABA_AR$ heteropentamers (αβγ) are available in various resolutions (Jansen, 2019; Laverty et al., 2017, 2019a; Masiulis et al., 2019a; Miller et al., 2017; Miller and Aricescu, 2014). The dimensions of the overall receptor can be noted from these. The height of the receptor (without the ICL) is ~100 Å, more than a half of which is occupied by the NTD in the extracellular space (Laverty et al. 2019). The width of a $GABA_AR$ ranges between 60 and 80 Å depending on the state of the receptor. The interfaces formed between subunits have a specific nomenclature being labelled as the principal subunit face (+) and a complementary subunit face (-) – these are important for orthosteric and allosteric binding site specification.

The extracellular domain is mostly comprised of a coalescence of orthogonally positioned inner and outer β-sheets (ten in total) that incorporate agonist and allosteric modulator binding sites (Laverty et al. 2019). Two α-helices break the ordered β-sheets: α-helix 1 (α1) positioned at the beginning of the NTD and α2 between β-strands three and four (Laverty et al. 2019). Extensive studies reveal that the NTD forms a binding pocket for GABA (β+ -α- subunit interface) and for allosteric modulators such as the benzodiazepines (α+ -γ- subunit interface) (Michels and Moss, 2007; Sigel, 2002). The NTD is also important for assembly and expression of functional $GABA_A$ receptors.

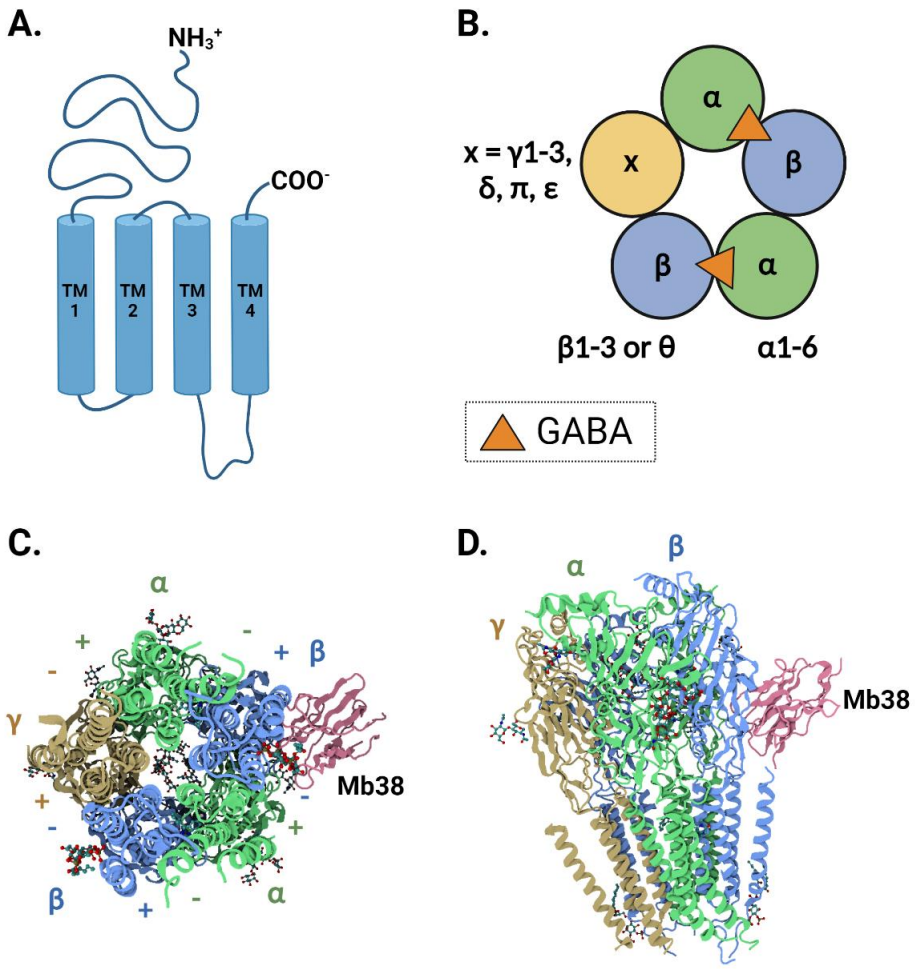

Figure 1.1 The structure of a GABA$_A$ receptor. **A.** Schematic of a subunit structure. The structure of all subunits follows the same topology: large N-terminal domain (NTD), four transmembrane domains (TMs) and a large intracellular loop (ICL) between TM3 and TM4. **B.** Schematic representation of the top (from the extracellular space) view of subunit arrangement in a GABA$_A$ receptor pentamer. Two GABA binding sites are located between β+ (principal) and α- (complementary) interfaces. GABA molecule is represented as an orange triangle. **C and D.** Top and side views of a cryo-EM structure of the α1β3γ2L GABA$_A$ receptor (Masiulis et al. 2019). The α1, β3, and γ2L subunits are shown in green, blue and light brown respectively, with (+) and (-) interfaces indicated. The protein is bound by the megabody, Mb38, shown in pink. **PDB ID is 6HUJ.**

Unlike the NTD, transmembrane domains are α-helical in structure, spanning the lipid bilayer of a cell membrane (Miller and Smart, 2010). The TM2 domains of each subunit in a pentameric complex contribute to the lining of the ion pore and in the absence of GABA are held close together with a pore radius of 3.15 Å (Laverty et al. 2019). The TM2 α-helices are highly conserved throughout the GABA$_A$ receptor subunit family (Miller and Smart, 2010). A selective anion channel pore is formed

from an electropositive ring in the cytosolic portal (Laverty et al. 2019; Keramidas et al. 2004). A prime number notation is used to describe the position of amino acids within the pore-lining TM2 domain: the first highly conserved amino acid residue from the cytoplasmic site of TM2 is denoted as 0' and the extracellular end is denoted as 20' (Miller, 1989). GABA binding leads to the tilting of TM2 domain outward by 9-11° relative to the central vertical axis, allowing the flow of ions (Laverty et al. 2019; Masiulis et al. 2019). The α-helices of TM1, TM3 and TM4 contain the binding sites for various allosteric modulators (Forman and Miller, 2016; Laverty et al., 2017; Miller and Aricescu, 2014). For example, the binding site for anaesthetics is situated in the TM region, β+/α- interface (Forman and Miller, 2016). Another group of drugs – barbiturates, have been shown to bind in the TM domain of the γ2+/β3- interface using photolabelled derivatives (Jayakar et al., 2015).

The large ICL between TM3 and TM4 is where the highest amino acid sequence variability between $GABA_AR$ subunits lies and comprises ~10% of the total subunit molecular mass (Moss and Smart, 2001). It is therefore unsurprising that it plays a critical role in receptor function, trafficking, assembly and distribution via post translational modifications, such as phosphorylation and ubiquitination (Miller and Smart, 2010; Moss and Smart, 2001). For example, ICL of $GABA_A$ receptor β and γ subunits has been shown to comprise multiple consensus sequences recognised by several tyrosine and serine/threonine kinases, such as protein kinase A (PKA) and protein kinase C (PKC) (McDonald et al., 1998; Moss et al., 1992a).

There are two GABA binding sites in each $GABA_A$ receptor located in the extracellular domain of the β+/α- interface (Miller and Smart, 2010). Both of these sites must be occupied by a GABA molecule for full receptor activation in the canonical $GABA_A$ receptor tri-hetero-pentamer (αβγ) (Macdonald et al., 1989; Petrini et al., 2014). Nevertheless, mutagenesis studies (α1 F65L and β2 Y205S at the α1+ and β2- interfaces respectively) in forced concatemeric $GABA_ARs$ have revealed that the two GABA binding sites do not contribute equally to receptor activation (Baumann et al., 2003). This difference is attributed to the subunit variability flanking the binding site. More specifically, one of the β+/α- interfaces is flanked by the γ and β subunits (site 1), whilst the other is surrounded by the α and γ subunits (site 2) (Baumann et al.,

2003; Miller and Aricescu, 2014). Studies in these concatemeric receptors suggested that site 2 had a three-fold higher affinity for GABA, than site 1. In contrast, muscimol (an extrasynaptic $GABA_A$ receptor super-agonist, see ***Section 1.3.1*** for detail) showed a preference to binding site 1 (Baumann et al., 2003).

The GABA binding site is comprised of six domains, known as loops A-F, where the β+ interface provides loops A-C and α- provides loops D-F (Bergmann et al., 2013; Miller and Aricescu, 2014; Miller and Smart, 2010). Initial GABA docking to the tyrosine (β2 Y97) amino acid residue in loop A leads to a series of conformation changes, leading to the opening of the gate (Miller and Smart, 2010; Padgett et al., 2007). This allows Cl^- and HCO_3^- anions to flow through the channel pore following their electrochemical gradients (Masiulis et al. 2019). In the developed adult brain, the Cl^- concentration inside neurons is maintained at a low level by the actions of the K^+-Cl^- co-transporter, KCC2, resulting in a Cl^- reversal potential more hyperpolarised than the resting membrane potential. Therefore, the opening of $GABA_A$ receptors results in the influx of anions into the neurones and subsequent hyperpolarisation of the cell membrane. Contrastingly, in immature neurones, intracellular Cl^- concentration is maintained at higher levels, due to lower expression of KCC2 and higher expression of the Na^+-K^+-Cl^- cotransporter NKCC1. This leads to an efflux of Cl^- upon opening of the $GABA_AR$ pore and an excitatory action of $GABA_A$ receptor activation (Ben-Ari et al., 2007; Olsen and Sieghart, 2009).

1.1.2 $GABA_A$ receptor assembly, stoichiometry and cellular localisation

$GABA_A$ receptors are pentameric in nature, providing an enormous variety for potential subunit assembly partners. Nevertheless, only a limited number of subunit combinations are expressed *in vivo*, which are spatially and developmentally regulated (Michels and Moss, 2007; Olsen and Sieghart, 2009). The receptor subunit stoichiometry and arrangement are important as they define physiological and pharmacological profiles of functional native $GABA_A$ receptors. Most $GABA_A$ receptors have a stoichiometry of 2 α1-6, 2 β1-3 and a γ1-3 or a δ (Olsen and Sieghart, 2009). The major receptor isoform in the mammalian adult brain has a stoichiometry

of 2 α1: 2 β2: 1 γ2 (Farrar et al., 1999; Olsen and Sieghart, 2009; Tretter et al., 1997). Electrophysiological studies using forced concatemeric receptors and studies using atomic force microscopy (AFM) to visualise antibody- and Fab fragment-labelled receptors have confirmed that the subunits are assembled clockwise in a α-β-α-β-γ/δ sequence around the central ion channel pore if viewed from the extracellular matrix (Barrera et al., 2008; Baumann et al., 2002). Receptor folding and assembly occur in the endoplasmic reticulum (ER) and requires chaperones such as calnexin, protein disulphide isomerase and immunoglobulin heavy-chain binding protein (BiP) (Connolly et al., 1996; Sarto-Jackson and Sieghart, 2008).

$GABA_A$ receptors appear to follow specific assembly rules, where only certain combinations of subunits can co-assemble with each other in certain stoichiometries, that determine functional and pharmacological properties of the receptor as well as their cellular localisation (Olsen and Sieghart, 2009). This section will give an outline of the assembly rules, receptor subunit composition and subcellular localisation patterns.

The presence of specific domains, known as 'assembly boxes' is important in homo- and hetero-pentameric $GABA_A$ receptor assembly (Sarto-Jackson and Sieghart, 2008). For instance, the amino acid residues 54-69 in α1 have been shown to be important for correct assembly with the β subunit (Srinivasan et al., 1999; Taylor et al., 1999). Specifically, amino acids (a.a.) Q67 and W69 are of great importance in assembly of the functional α1β3 pentamers (Srinivasan et al., 1999; Taylor et al., 1999). Furthermore, residues 76-89 in β3 sequence, specifically amino acids 85-89 are crucial for correct assembly with the α1 subunit and are located at the β3-/α1+ interface (Ehya et al., 2003). Sequence substitutions of γ2 (a.a. 67-81) and γ3 (a.a. 70-84) with the homologous sequences of ρ1 significantly reduced the assembly between α1 and γ2/3 subunits (Klausberger et al., 2000; Sarto et al., 2002, 2002). Four amino acids on β3 subunits: G171, K173, E179, R180 are essential for the assembly of β3 homomeric $GABA_A$ receptors (Taylor et al., 1999). Other assembly boxes have been identified through the years that are important for $GABA_A$ receptor assembly (Sarto-Jackson and Sieghart, 2008).

The complexity of $GABA_A$ receptor pharmacology and function requires an understanding of how these receptors assemble in the brain. Multiple studies have shown that most single $GABA_A$ receptor subunits are retained in the ER after folding as a means to prevent the unassembled receptors from reaching the cell surface (Connolly et al., 1996; Gorrie et al., 1997; Taylor et al., 1999). Some receptor subunits are able to form homomeric receptors that are expressed on the cell surface. For example, the murine β1 and β3 subunits can form functional Cl^- channels, that are not gated by GABA and are also insensitive to bicuculine or muscimol respectively (Connolly et al., 1996; Krishek et al., 1996a; Wooltorton et al., 1997). β1 homomers can be activated by pentobarbitone and propofol and inhibited with picrotoxin (Krishek et al., 1996a; Sigel et al., 1989). In β3 cDNA injected oocytes, pentobarbitone and bicuculline increased the membrane conductance, whereas picrotoxin and Zn^{2+} had the opposite effect (Wooltorton et al., 1997). Moreover, when the γ2S splice variant but not γ2L is expressed alone in HEK293 cells, single subunits can reach the cell surface and are subsequently internalised (Connolly et al., 1999). However, upon co-expression with α1 and β2 subunits, γ2S monomeric cell surface expression is repressed proving that γ2S subunit is unlikely to be expressed *in vivo* as homomers (Connolly et al., 1999; Moss and Smart, 2001). Three ρ subunit isoforms are known to form both homo- and hetero-pentameric receptors. These receptors are thought to be largely expressed as homomers in the inner plexiform layer of the retina (Koulen et al., 1998). Co-immunoprecipitation studies suggest that ρ isoforms are co-expressed with α1 subunits in Purkinje cells of the mouse cerebral cortex and in certain other brain areas (Harvey et al., 2006; Milligan et al., 2004).

All αγ, βγ, and β3γ2 subunit combinations are retained in the endoplasmic reticulum (Connolly et al., 1999, 1996). Recombinant $GABA_AR$ studies concluded that α and β subunit co-expression is sufficient to form functional GABA-gated ion channels with low single-channel conductance and benzodiazepine insensitivity (Connolly et al., 1996; Verdoorn et al., 1990). There is evidence that these receptors exist *in vivo* and account for up to 10% of the total extrasynaptic pool of receptors in hippocampal pyramidal neurons (Mortensen and Smart, 2006; Sieghart and Sperk, 2002). Inclusion of a γ subunit into the $GABA_AR$ is necessary to produce a receptor with a

benzodiazepine binding site (Angelotti and Macdonald, 1993; Connolly et al., 1996; Sigel et al., 1990; Verdoorn et al., 1990). Because most $GABA_A$ receptors in the brain harbour a benzodiazepine binding site, the majority of $GABA_A$ receptors that exist *in vivo* are thought to be a combination of α, β and γ subunits (Sigel and Steinmann, 2012).

Finally, multiple studies have suggested the possibility of $GABA_A$Rs containing two distinct α or β subunits (Olsen and Sieghart, 2009). The evidence comes mostly from co-localisation, immunodepletion and co-immunoprecipitation studies (Benke et al., 2004a; Chang et al., 1996a; Nakamura et al., 2016; Olsen and Sieghart, 2009). These receptors will be discussed in more detail in ***Section 1.4.***

The subunit composition dictates subcellular distribution: receptors can be localised within the synapse or extrasynaptically (Sieghart and Sperk, 2002). Tri-heteropentameric synaptic $GABA_A$Rs usually encompass a γ subunit isoform, whereas extrasynaptic receptors contain a δ subunit (Farrant and Nusser, 2005; Olsen and Sieghart, 2009). For instance, immunogold labelling localisation studies showed that α1, β2, β3, and γ2 prevail in GABAergic Golgi synapses, whereas the δ subunit was not detected in synaptic junctions, but was present in extrasynaptic locations on somatic and dendritic membranes (Nusser et al., 1995a; Zoltan Nusser et al., 1998). Interestingly, the former pool of subunits has been found extrasynaptically at low levels (Zoltan Nusser et al., 1998). Later, receptors that are clustered synaptically have been confirmed to be localised extrasynaptically (Bogdanov et al., 2006; Thomas et al., 2005). These represent a receptor pool that is involved in a rapid replenishment and dynamic control of receptors at inhibitory synapses (Olsen and Sieghart, 2009; Thomas et al., 2005).

Extrasynaptic receptors usually contain a δ subunit in combination with α4/6 and β1-3 (Olsen and Sieghart, 2009). These receptors are characteristically highly sensitive to GABA and have a slower desensitisation rate than receptors in the synapse which mediate phasic responses. From a pharmacological perspective, these receptors respond to THIP with greater efficacy than GABA, and lack benzodiazepine sensitivity (Brown et al., 2002). There is evidence that α5βγ2 receptors exist extrasynaptically in the forebrain region (Semyanov et al., 2004). α5 and α3 containing receptors can be

both localised synaptically and extrasynaptically, depending on the brain region (Burgard et al., 1996; Pirker et al., 2000).

1.1.3 $GABA_AR$ in vivo expression patterns

Evidence from immunohistochemical, genetic and pharmacological studies has provided an insight into the $GABA_A$ receptor and subunit distribution in the CNS (Chua and Chebib, 2017; Sieghart and Sperk, 2002). The expression patterns of $GABA_A$ receptors in the adult rat brain vary depending on individual subunits and receptor composition (Pirker et al., 2000). The α1β2γ2 subtype is by far the most abundant receptor isoform in the brain, comprising between 50% and 60% of total $GABA_ARs$, and is expressed in most brain areas (Chua and Chebib, 2017; Somogyi et al., 1996). Other α and β isoforms form functional receptors with γ2 subunit, however their expression is more region-specific (Olsen and Sieghart, 2008). For example, α2β3γ2 are expressed in hippocampal pyramidal neurones at high density, whereas the α3β3γ2 isoform is widely expressed in the cholinergic neurones of the basal forebrain (Chua and Chebib 2017). Immunohistochemical staining of the adult rat brain gave indication of the distribution of different α subunits. α1 and α2 expression is widespread throughout the brain, with the latter more localised to olfactory bulb, CA3 area of the hippocampus, dentate molecular layer and amygdala (Fritschy and Mohler, 1995; Pirker et al., 2000). Developmental regulation also occurs with α1-subunit mRNA levels significantly increasing with age in both layer 3 and layer 5 cortical pyramidal cells, whereas α2 mRNA levels decline (Datta et al., 2015). Out of all $GABA_AR$ α subunits, α1 mRNA and protein levels are the most abundant (Hörtnagl et al., 2013).

Other α subunits are more localised in their expression. For example, α3 expression is most prominent in specific areas of the olfactory bulbs and amygdala, whereas α4 is highest in regions of thalamus, striatum and dentate gyrus (Pirker et al., 2000). The expression of α5 and α6 isoforms is significantly different from other α subunits, with wide expression of α5 in the hippocampus and α6 almost exclusively in cerebellar granule cells (Fritschy and Mohler, 1995; Jones et al., 1997; Zoltan Nusser et al., 1998;

Pirker et al., 2000). These findings are consistent with previous *in situ* hybridisation data (Nusser et al., 1996; Thompson et al., 1992).

With regards to β subunits, all three isoforms are widely distributed in the brain. Notably, the expression of the β2 and β3 are complementary in the pallidum and striatum, β2 is highly concentrated in the pallidum, whereas β3 is more concentrated in striatum (Pirker et al., 2000). Furthermore, β subunits follow a cellular localisation preference, with β1 and β2 being highly concentrated in hippocampal interneurons, whereas β1 and β3 appear mainly expressed in the dendrites of principal cells (Pirker et al., 2000). Out of all three γ subunits, γ2 is widely expressed in the brain, whereas γ1 localisation is mainly restricted to pallidum, substantial nigra and septum. γ1 expression is limited to expression in specific somas and dendrites at low levels. Expression of the δ subunit is restricted to thalamus, dentate gyrus and striatum (Olsen and Sieghart, 2008; Pirker et al., 2000).

1.1.4 $GABA_AR$ biophysical properties

The subunit composition of $GABA_A$ receptors not only determines the cellular localisation, but also the biophysical properties of these receptors. Subunit composition influences a number of measurable parameters: the magnitude of the response, agonist sensitivity, and the rates of activation, deactivation and desensitisation (Farrant and Nusser 2005). The affinity of the receptor for the ligand (how avidly the ligand binds to the receptor) and the efficacy of the ligand (how effective the channel gating is) both influence the macroscopic sensitivity of a ligand gated ion channel to its agonists (Colquhoun, 1998). It is worth noting, that the affinity cannot be measured from electrophysiological experiments, therefore the terms 'apparent affinity' or agonist potency are often used to describe the EC_{50} measure (Colquhoun, 1998). Typically, synaptic receptors – those composed of an α1-3, β and γ isoform combinations have a lower GABA apparent affinity than extrasynaptic receptors (α4/6, β and δ containing $GABA_A$ receptors) (Mody, 2001). This is in conjunction with the role of these receptors. Synaptic receptors are exposed to high transient levels of GABA (> 1 mM), released from the presynaptic terminal

into the synaptic cleft, mediating short-lasting phasic inhibition (Farrant and Nusser, 2005; Galarreta and Hestrin, 1997). On the contrary, extrasynaptic receptors are exposed to much lower levels of ambient GABA (0.5-1 μM) in the extrasynaptic space, mediating a persistent level of receptor activation that results in a tonic current (Brickley et al., 1996; Brickley and Mody, 2012; Nusser et al., 1995b).

The GABA potency of tri-heteropentameric $GABA_A$ receptors (α, β, and γ containing) is determined by the α isoform present. Both radioligand binding studies and electrophysiological experiments showed that a four amino acid domain in the GABA binding pocket of an α subunit mediates distinct sensitivities to GABA (Böhme et al., 2004). Electrophysiological studies in transfected HEK293 cells have shown that synaptically localised α2 and α3 containing receptors (α2β3γ2 and α3β3γ2) exhibit the lowest sensitivity to GABA, with EC_{50} values 13.4 μM and 12.5 μM respectively (Mortensen et al., 2012b). The extrasynaptic, α6 δ-containing receptors display the highest potency to GABA (0.17 μM) (Mortensen et al., 2012b). Depending on the cell line used for recombinant receptor studies as well as experimental conditions, GABA potency ranges between 1 μM and 48 μM, with the order of α isoform EC_{50}s being (from low to high): α6 < α1 < α2 < α4 < α5 << α3 (Farrant and Nusser, 2005; Mortensen et al., 2012b; Picton and Fisher, 2007). Therefore, this simple GABA potency relationship is important in underpinning $GABA_A$ receptor activation and subsequent mechanisms of neuronal inhibition (phasic or tonic).

The relative positioning of an α subunit in a pentameric receptor complex with two distinct α subunit isoforms dictates pharmacological properties of GABA. Double and triple concatenated receptors (two linked subunits expressed alongside three linked subunits) containing an α1/α6 isoform mixture expressed in *Xenopus* oocytes exhibited different potency with respect to GABA, with γ2-β2-α1/β2-α6 having a much higher EC_{50} than γ2-β2-α6/β2-α1 (94 μM and 42 μM respectively) (Minier and Sigel, 2004a). Co-expression studies of α1/α3 and α1/α5 subunits determined that – the efficacy of the receptor is dictated by the α1 subunit, whereas the apparent affinity is dictated by both α subunits (Ebert et al., 1994).

The presence of a specific β subunit isoform further dictates GABA sensitivity of the receptors, with the rank order of EC_{50}s being β3 < β2 < β1 in an α1βxγ2 receptor

isoform (Mortensen et al., 2012b). The presence of γ or δ subunits plays an important role in receptor sensitivity to GABA. Pharmacological characterisation of a cell line stably expressing α4β3δ indicated that γ2 subunit replacement with δ, decreased GABA EC_{50} by almost five-fold (from 2.6 μM to 0.5 μM) (Brown et al., 2002). These results are in agreement with the localisation of extrasynaptic δ-containing receptors that are exposed to low concentration of GABA (Olsen and Sieghart, 2008). Interestingly, GABA efficacy at α4β3δ receptors is lower than that of α4β3γ2, indicating that GABA is a partial agonist at these receptors (Brown et al., 2002). Indeed, studies have shown that both 4,5,6,7-tetrahydoisoxazolo[5,4-c]pyridine-3(2H)-one (THIP) and muscimol acted as super-agonists on α4β3δ receptors (Mortensen et al., 2010; Stórustovu and Ebert, 2006). Additionally, δ and γ2 containing receptors present significant differences in kinetic parameters. In α1β2x receptors, γ2 replacement with δ subunits results in a significant decrease of channel opening bursts as well as the mean opening times (Fisher and Macdonald, 1997). This data is consistent with the idea that GABA has a high affinity but low efficacy in δ isoform containing receptors (Adkins et al., 2001; Farrant and Nusser, 2005).

The rates of activation and deactivation are also strongly influenced by $GABA_AR$ subunit composition. The α subunit plays an important role in kinetic profiles of GABA responses (Farrant and Nusser, 2005). Rapid (100 μs) saturating GABA applications to transfected HEK293 or cortical neuron patches, showed that activation of α1β2γ2 is two times faster than of α2β2γ2 (10-90% rise times were 0.5 ms and 1 ms respectively), whereas decay rate was six times slower (208 ms and 31 ms respectively) (Lavoie et al., 1997; McClellan and Twyman, 1999). The presence of an α3 subunit (α3β2γ2) produced a four-fold decrease in the activation rate compared to α1 containing receptors, putting the order of rise times as α2 < α1 < α3 (Gingrich et al., 1995). Activation and deactivation rates are also influenced by the presence of γ or δ subunit isoforms. Activation rate in the presence of γ2 (α1β3γ2) increases by almost four-fold compared with that of α1β3 heterodimers (current rise times of 0.46 ms compared to 1.7 ms) (Haas and Macdonald, 1999). This is only seen with the long splice variant of the subunit (Benkwitz et al., 2004). On the contrary, γ subunit

presence reduces the deactivation rate by two fold (76.1 ms compared to 34.1 ms, α1β3γ2 and α1β3 respectively) (Haas and Macdonald, 1999).

Desensitisation of $GABA_A$ receptors reflects transition to closed receptor states whilst GABA is still bound at the orthosteric site and provides a regulatory mechanism for receptor activation with a likely physiological role. Desensitisation has been shown to play a role in shaping the time course of IPSCs, initiation of inhibitory plasticity of synapses, and modulation of extrasynaptic receptors (Bright et al., 2011; Field et al., 2021; Mortensen et al., 2010). Addition of the δ to α1β3 does not have any significant effect on the receptor activation rate, – however it does decrease both the extent (55.6% compared to 94.6%) as well as the rate (time constants 1260 ms versus 352 ms) of desensitisation (Haas and Macdonald, 1999). These findings correlate with the functional role of δ-containing receptors in mediating tonic inhibition.

1.1 Post-translational modifications

1.2.1 Phosphorylation

A further level of complexity is added to $GABA_A$ receptor function via post-translational modifications. Various receptor modifications can be made but phosphorylation appears to be particularly critical for regulation of $GABA_A$ receptor mediated transmission (Moss and Smart, 1996). Tyrosine and serine/threonine kinases are both known to phosphorylate $GABA_A$Rs. They act via a reversible mechanism consisting of a phosphoryl group (PO_3^-) transfer from adenosine triphosphate (ATP) to a serine/threonine/tyrosine amino acid contained within a consensus sequence (Ardito et al., 2017; Moss and Smart, 1996). This change modifies the phosphorylated protein residue from hydrophobic to hydrophilic polar, potentially altering both protein function and its interaction with other proteins (Ardito et al., 2017). $GABA_A$ receptor phosphorylation is an important modulatory mechanism which affects a multitude of processes including cell surface expression, downstream protein interaction, channel function and pharmacological profiles

(Nakamura et al., 2015). Some of the currently known $GABA_AR$ phosphorylation sites and their physiological consequences are outlined in ***Table 1.1***.

The large intracellular domain between TM3 and TM4 has the highest sequence variability between $GABA_AR$ subunits and contains several consensus sequences recognised by various serine/threonine and tyrosine protein kinases (Moss and Smart, 1996). Pull down assays of glutathione S-transferase (GST) fusion proteins with intracellular loops of various $GABA_AR$ subunits have been used to identify specific kinases and corresponding phosphorylation sites. Studies have largely focused on phosphorylation sites identified in the ICD of β1-3 and γ2 subunits (Brandon et al., 2001; McDonald and Moss, 1997; Moss et al., 1995).

Table 1.1 $GABA_A$ receptor phosphorylation sites. Serine (S)/threonine (T) and tyrosine (Y) residues that are known to be phosphorylated in $GABA_A$ receptor subunits alongside their corresponding kinases are listed in the second and third columns of the table. Physiological effect is indicated, where ↓ stands for a decrease, and ↑ an increase. Original references are noted in the last column.

Subunit	Residue	Kinases	Physiological effect	References
α1	Putative T375	-	↓ synaptic clustering ↓ mIPSC amplitude	(Mukherjee et al., 2011)
α4	S443	PKC	↑ surface expression ↑ tonic inhibition	(Abramian et al., 2014, 2010)
β1	S384	CamKII	-	(McDonald and Moss, 1994)
	S409	CamKII, PKA, PKC, PKG	↓ current amplitude ↓ desensitisation rate	(Brandon et al., 2002; McDonald et al., 1998; McDonald and Moss, 1994; Moss et al., 1992b)
β2	Y372/Y379	PI3-K	↑ surface expression	(Vetiska et al., 2007)
	S410	Akt, CamKII, PKA, PKC, PKG	↓ surface expression ↓ tonic inhibition	(Bright and Smart, 2013; McDonald and Moss, 1997)
β3	S383	CamKII	↑ surface expression ↑ current amplitude ↑ synaptic clustering	(Houston et al., 2007; McDonald and Moss, 1997; Petrini et al., 2014)
	S408/S409	CamKII, PKA, PKC, PKG	Single site: ↓ current amplitude, ↑ neurosteroid-mediated current potentiation. Both sites: ↑ surface expression ↑ current amplitude	(Brandon et al., 2002; Houston et al., 2007; Jovanovic et al., 2004; Kittler et al., 2005; McDonald and Moss, 1997)
γ2S/L	S327	PKC	↑ lateral diffusion, ↓ current amplitude	(Kellenberger et al., 1992; Muir et al., 2010)
	S348/T350	CamKII	-	(Houston et al., 2007; McDonald and Moss, 1994)
	Y365/Y367	Src	↑ surface expression ↑ current amplitude ↑ synaptic cluster size	(Brandon et al., 2001; Tretter et al., 2009)
γ2L	S343	CamKII, PKC	↓ current amplitude	(Krishek et al., 1994; McDonald and Moss, 1994)

A well-studied example of a phosphorylation site is a conserved serine amino acid residue found across all three β subunits (S409 and S410 in β1/3 and β2 respectively). This residue is known to be a target for numerous kinases: protein kinase A (PKA), protein kinase C (PKC), protein kinase G (PKG) and Ca^{2+}/calmodulin-dependent protein kinase II (CamKII) (McDonald and Moss, 1997, 1994). *In vitro* experiments have indicated some discrepancies between the ability of the PKA to phosphorylate β2 S410 residue. Some studies suggest that all three β subunits are phosphorylated by PKA, whereas others suggested that the β2 subunit in α1β2γ2L transfected HEK293 cells is not modulated by PKA (McDonald et al., 1998; McDonald and Moss, 1997; Moss et al., 1992a). Furthermore, the downstream effects of the phosphorylation by PKA at the β1 and β3 subunit residues are opposing: PKA modulation reduces GABAergic currents in β1-containing receptors (α1β1γ2), but increases GABA-evoked currents in β3-containing receptors (α1β3γ2) (McDonald et al., 1998; Moss et al., 1992a). This difference is attributed to the presence of an extra serine residue on the β3 subunit (S408), that can be phosphorylated alongside the S409 defining the direction of modulation with PKA (McDonald et al., 1998). The AP2 complex plays an essential role in clathrin-mediated internalisation of $GABA_A$ receptors (Vithlani and Moss, 2009). Studies suggested that the phosphorylation of S408/S409 residues on β3 subunit results in a significantly reduced affinity for the μ2 subunit of the adaptor protein 2 (AP2), hence preventing $GABA_A$ receptor endocytosis resulting in an increased cell surface expression (Kittler et al., 2005). Therefore, this provides a dynamic phospho-dependent mechanism to regulate receptor internalisation.

Other phosphorylation sites have been identified in β1-3 intracellular domains as targets for various kinases (Nakamura et al., 2015). The S384 residue found on β1 subunits has been shown to be phosphorylated by CaMKII, however the physiological function of such phosphorylation is unknown (McDonald and Moss, 1994). A homologous site on the β3 subunit (S383) is known to be a target for the same kinase (Houston et al., 2009; McDonald and Moss, 1994). Studies have shown that phosphorylation of β3 S383 results in a significant potentiation of GABA-evoked currents in both a recombinant system (NG108-15 cells) and cultured cerebellar granule cells (Houston and Smart, 2006). Two tyrosine residues (Y372 and Y379) on

β2 subunit were established as phosphorylation sites recognised by phosphoinositide 3-kinase (PI3-K) (Nakamura et al., 2015). Following insulin treatment, the association between these residues and PI3-K significantly increased, resulting in the enhanced expression of $GABA_A$ receptors at the membrane and upregulation of mIPSC amplitude (Vetiska et al., 2007).

Numerous phosphorylation sites have been identified in the intracellular domain of the γ2 subunit (Nakamura et al., 2015). Three residues: S327 and S343/T350 have a high affinity to protein kinase C (PKC) and CaMKII serine/threonine kinases respectively (Houston et al., 2007; Krishek et al., 1994; McDonald and Moss, 1994). Phosphorylation of S327 by PKC resulted in a downregulation of GABA-evoked currents when expressed in *Xenopus* oocytes (α1β2γ2S isoform) (Kellenberger et al., 1992). Moreover, S327 phosphorylation caused a decrease in $GABA_A$ receptor lateral mobility within the cell membrane, providing a phospho-dependent control of synaptic inhibition and plasticity (Muir et al., 2010). Another serine residue found only in the eight-amino acid insert of the long splice isoform of γ2, S343, is phosphorylated by CaMKII and results in a significant reduction of GABA-evoked currents (Krishek et al., 1994; Moss et al., 1992a). Src tyrosine kinase has a high affinity for Y365 and Y367 residues of γ2S (Y373 and Y375 on γ2L) and upregulates GABA-evoked currents (Moss et al., 1995). CaMKII phosphorylation of the β3 S383 residue has an indirect residual positive effect on the Y365 and Y367 residues of γ2, further increasing $GABA_A$ receptor currents (Houston et al., 2007).

Unlike numerous identified β and γ phosphorylation sites, evidence for α subunit phosphorylation is limited. The only α subunit that is known to be phosphorylated is α4 at S443 amino acid within the intracellular domain (Abramian et al., 2010; Nakamura et al., 2015). Immunoprecipitation studies from transfected COS7 cells, showed that PKC activation increases phosphorylation of the α4 subunit and subsequently upregulates the cell surface expression of extrasynaptic α4β3 $GABA_A$ receptors (Abramian et al., 2010). Neurosteroids were later shown to potentiate PKC-dependent phosphorylation of α4 subunit, further enhancing cell membrane insertion of extrasynaptic $GABA_A$ receptors (Abramian et al., 2014). On the contrary, immuno-labelling of α4β2δ $GABA_A$ receptors expressed in HEK293 cells revealed a

significant decrease in cell-surface expression following PKC application (Bright and Smart, 2013). Furthermore, a decrease in tonic inhibition in dentate gyrus was observed that was shown to be dependent on β2 subunit phosphorylation at S410 (Bright and Smart, 2013).

1.2.2 N-linked glycosylation

N-linked glycosylation is another important post-translational modification of proteins. This modification occurs in the endoplasmic reticulum (ER), where a multimeric enzyme – oligosaccharyltransferase (OST) – transfers assembled oligosaccharide complexes (comprising glucose, mannose and N-acetylglucosamine monosaccharides) to asparagine (N) residues within the consensus sequence asparagine-X-serine/threonine (N-X-S/T, where X is any amino acid) (Mohorko et al., 2011; Parodi, 2000a). Glycosylation is an essential mechanism for correct protein-folding, trafficking and degradation (Parodi, 2000b). Glycosylation of $GABA_A$ receptors has been shown to be altered in disease states such as schizophrenia and absence epilepsy (Mueller et al., 2014; Tanaka et al., 2008). Samples of patients' grey matter indicated a reduced glycosylation state of α1, β1 and β2 $GABA_A$ receptor subunits (Mueller et al., 2014).

Functional studies in *Xenopus* oocytes were the first to identify the importance of N-linked glycosylation in $GABA_A$ receptor cell surface expression. Applications of tunicamycin, an inhibitor of N-linked glycosylation, caused $GABA_A$ receptor expression in oocytes to be significantly reduced (Sumikawa et al., 1988). Later, site-directed mutagenesis of two N-linked glycosylation sites in the α1 subunit ($\alpha1^{N10Q}$ and $\alpha1^{N110Q}$) revealed that removing these sites reduces expression of α1β2γ2 $GABA_A$ receptors in *Xenopus* oocytes (Buller et al., 1994). Mass spectrometry of purified $GABA_A$ receptors from rat neocortex confirmed the presence of these sites *in vivo* (Chen et al., 2012a). The N110 residue of all α subunits is a well-defined glycosylation site identified based on the sequence analysis and has also been confirmed in later $GABA_A$ receptor structural studies (Blom et al., 2004; Julenius et al., 2005; Laverty et al., 2019b; Phulera et al., 2018). This site is located at the ECD of the receptor and

oligosaccharides tethered at this site occupy a significant portion of the of the vestibule above the channel pore. The carbohydrate side chains of the oligosaccharide are well ordered, making multiple interactions between the sugar groups as well as γ2 subunit residues N101, L112 and W123 (Phulera et al., 2018). This glycosylation site is proposed to be important for $GABA_A$ receptor assembly, potentially blocking the formation of receptor complexes that contain more than two α subunits (Phulera et al., 2018).

Three asparagine residues on the β2 subunit (N8, N80 and N149) were identified as potential glycosylation sites using site-directed mutagenesis experiments (Lo et al., 2010). The same residues were then shown to be glycosylated in a crystal structure of a $GABA_A$ β3 homopentamer (Miller and Aricescu, 2014). Studies in transfected HEK293 cells showed that all three glycosylation sites on the β2 subunit played a role in α1β2 receptor assembly and trafficking. Glycosylation of N80 was identified to play a role in receptor assembly and stability in the ER. Electrophysiological experiments further showed that mutating any of the glycosylated residues reduced GABA-evoked current amplitudes as well as altering the gating properties of α1β2 receptors (Lo et al., 2010).

1.3 $GABA_A$ receptor pharmacology

A defining feature of the $GABA_A$ receptor is the diverse pharmacological profile displayed across receptor subtypes. This profile is altered depending on the structural diversity and arrangement of subunits in a $GABA_A$ receptor complex. Understanding the pharmacological properties of specific receptor isoforms is therefore crucial in predicting the functional profile (Carter et al., 2010; Möhler, 2006). The binding sites of $GABA_A$ receptor modulators are schematically represented in ***Figure 1.2***.

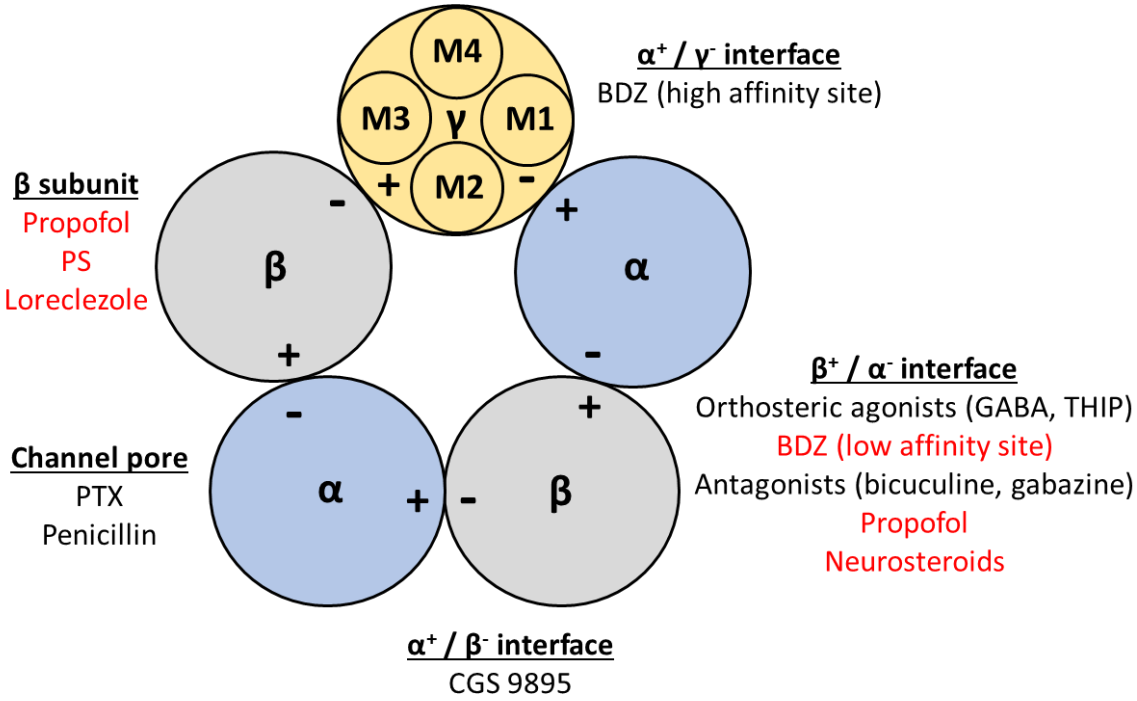

Figure 1.2 αβγ GABA$_A$ receptor pharmacology. GABA$_A$ receptors have a diverse pharmacological profile which is determined by subunit composition and arrangement. Most binding sites are located at the subunit interfaces. Compounds that bind within the N-terminal extracellular domain are highlighted in black. Compounds that have binding sites within the transmembrane region are highlighted in red. Some compounds (PTX and penicillin) bind directly in the channel pore. Abbreviations: BDZ – benzodiazepines, PS – pregnenolone sulfate, PTX – picrotoxin.

1.3.1 GABA$_A$ receptor agonists

Several selective exogeneous GABA$_A$ receptor agonists have been developed as potential therapeutic agents for regulating GABAergic inhibition. The two most commonly known agonists that bind to the orthosteric GABA$_A$ receptor site are muscimol – isolated from *Amanita muscaria* mushroom – and THIP (Johnston, 2014; Krogsgaard-Larsen et al., 2002; Stórustovu and Ebert, 2006).

[3H]Muscimol binding and electrophysiological studies suggested that muscimol acts uniformly on most GABA$_A$ receptors (γ-containing), except for extrasynaptically-located α4β3δ receptors (Ebert et al., 1997). In transfected HEK293 cells, muscimol acted as a super agonist, eliciting between 120-140% of the maximal GABA-evoked currents at α4β3δ receptors (Mortensen et al., 2010; Stórustovu and Ebert, 2006). THIP's pharmacological profile has also been shown to be subunit-selective. It only

acts as a partial agonist on γ-containing $GABA_A$ receptors, whereas it acts as a super-agonist on δ-containing receptors, eliciting peak currents 220% greater than saturating GABA-evoked responses in δ containing receptors (α4β3δ). The potency of both muscimol and THIP has been established (Ebert et al., 1994; Mortensen et al., 2010). Muscimol potency is more than three-fold higher than GABA at α1β3γ2 (0.92±0.34 μM and 3.4±1.0 μM respectively) and two-fold higher in α4β3δ (0.20±0.04 μM and 0.35±0.03 μM respectively). The potency of THIP is much lower than GABA across all these receptor combinations (α1β3γ2, α4β3γ2 and α4β3δ) ranging between 107±31 μM and 13±3.5 μM (Mortensen et al., 2010). The super agonist behaviour of THIP on α4β3δ receptors can be explained by its ability to influence both channel opening dwell times and frequency, resulting in a prolonged burst duration. However, muscimol's moderate super agonist behaviour could be attributed to a decreased desensitisation of extrasynaptic receptors (Mortensen et al., 2010).

Neither muscimol nor THIP show selectivity across $GABA_A$ receptor subtypes, therefore more selective $GABA_A$ receptor agonists have been developed to assess the properties of individual receptor subunit combinations (Johnston, 2014). A group of 5-(4-piperidyl)-3-isoxazolol (4-PIOL) derived analogues have bidirectional effects on $GABA_A$ receptors, acting either as weak partial agonists or antagonists depending on subunit composition (Mortensen et al., 2002; Patel et al., 2016). 4-PIOL exhibits agonist-like effects in synaptic γ-containing receptors, and antagonist-type behaviour in extrasynaptic δ-containing receptors (Patel et al., 2016). Tonic currents were affected by 4-PIOL application to CA1 hippocampal neurones and thalamic relay neurones, that express α5βγ, α4βδ and αβ extrasynaptic receptors. Interestingly, the observed effect on tonic currents was bi-directional, and was dependent on ambient GABA concentration (Caraiscos et al., 2004; Mortensen and Smart, 2006; Patel et al., 2016). Other analogues, piperidine-4-sulforic acid (P4S) and isoguvacine were shown to act as partial and full agonists respectively on α1β2γ2, α6β2γ2 and α1α6β2γ2 receptors (Ebert et al., 1994; Hansen et al., 2001; Mortensen et al., 2002). Another orthosteric $GABA_A$ receptor ligand, thio-4-PIOL acts a partial agonist on α5β3γ2, α4β3δ and α6β3δ receptors, eliciting around 30% of the maximum GABA-evoked response (Hoestgaard-Jensen et al., 2013).

1.3.2 $GABA_A$ receptor antagonists

Apart from agonists, antagonists are also used for probing the functionality of $GABA_A$ receptors. One of the most prominent competitive antagonists of $GABA_A$ receptors is a phthalide isoquinoline alkaloid, bicuculline (Johnston 1996; Johnston 2013; Masiulis et al. 2019). Single channel recordings from cultured mouse spinal cord neurons showed that bicuculline reduced $GABA_A$ receptor currents (Krishek et al., 1996b; Macdonald et al., 1989). Changing the β subunit expressed with α6 and γ2 subunits suggested that bicuculine affinity was significantly weaker in α6β3γ2 compared to α6β1γ2 and α6β2γ2combinations (Ebert et al., 1997). Electrophysiological assessment of mutations in the GABA binding site of the β subunit suggested that bicuculline binds to the orthosteric site, but also interacts with additional sites on the receptor, causing a stabilisation of the receptor in a closed/resting state (Ueno et al., 1997). This was later confirmed with a $GABA_AR$/bicuculline crystal structure (Masiulis et al. 2019). Another $GABA_AR$ competitive antagonist – SR-95531 (gabazine) – does not show any selectivity towards different β subunit-containing $GABA_A$ receptors (Ebert et al., 1997). However, low concentrations (200 nM) of gabazine showed a 71% reduction of phasic but not the tonic current in CA1 hippocampal granule cells (Stell and Mody, 2002).

A non-competitive antagonistic compound – picrotoxin (PTX) – does not bind between subunit interfaces, rather the binding site is located within the channel pore accessible only on the open state conformation of receptor (Korshoej et al., 2010). Early studies involving electrophysiological recordings suggested that PTX inhibition of GABA-evoked currents occurs via stabilisation of the closed/resting state of the receptor (Krishek et al., 1996b; Newland and Cull-Candy, 1992). A latter cryo-EM structure of an α1β3γ2L $GABA_A$ receptor with PTX/+/- GABA has confirmed this idea (Masiulis et al. 2019).

Zn^{2+} is another $GABA_A$ receptor antagonist. Its effectiveness depends on $GABA_A$ receptor subunit composition. Synaptic and extrasynaptic $GABA_A$ receptors not only have different sensitivities to GABA, but also have distinct pharmacological profiles to Zn^{2+} inhibition (Smart et al., 1991). The Zn^{2+} binding site lies within the extracellular

end of the channel pore between the extracellular domains of the two adjacent subunits at the α-β interface. The γ subunit of synaptic αβγ $GABA_A$ receptors disrupts one of the two α-β binding sites, therefore reducing its sensitivity to Zn^{2+} compared with αβ receptors (Hosie et al., 2003; Mortensen and Smart, 2006). Extrasynaptic δ-containing receptors are less sensitive to Zn^{2+} than αβ pentamers (IC_{50} 1.9 μM) but are still highly sensitive to Zn^{2+} inhibition (IC_{50} 16 μM), providing a mechanism for selective negative $GABA_AR$ modulation (Carver et al., 2016; Hosie et al., 2003; Nagaya and Macdonald, 2001).

1.3.3 Benzodiazepine pharmacology

Benzodiazepines (BDZs) are some of the most widely used drugs, prescribed for a variety of conditions such as sleep and anxiety disorders. BDZs are positive allosteric modulators (PAMs) for some $GABA_A$ receptors and have a large spectrum of clinical effects ranging from sedative and hypnotic to anxiolytic and anticonvulsant effects (Möhler, 2006). Single channel recordings suggested that BDZs potentiate GABA-evoked currents without directly activating the receptor. Instead they act via an increased frequency of channel openings and bursts (Rogers et al., 1994).

Subunit composition is crucial in determining $GABA_A$ receptor sensitivity to benzodiazepines. It has been shown that the presence of a γ subunit is essential for BDZ modulation: the disruption of the *GABRG2* gene resulted in the absence of 94% of BDZ binding sites (Günther et al., 1995). The α subunit isoform also plays a crucial role in BDZ sensitivity: extrasynaptic α4 and α6 subunits, expressed as an αβγ pentamer exhibit no diazepam potentiation (Hevers and Lüddens, 1998). Therefore, $GABA_A$ receptors containing an α_x+ / γ_y- interface where x = 1, 2, 3, 5 and y = 1-3 form a high affinity canonical binding site for benzodiazepines (Sigel and Ernst, 2018; Sigel and Lüscher, 2011). In the most abundant $GABA_A$ receptor in mammalian brain, α1β2γ2, the benzodiazepine-binding pocket consists of principal α1 subunit A - C binding loops and complementary γ2 D - F binding loops (Masiulis et al. 2019). Multiple studies have evaluated the functional and pharmacological effects of single point mutations in the α and γ subunits. An α1 histidine to arginine substitution

(H101R), the latter corresponding to the amino acid residue present in this position in α4 and α6, was initially identified using photoaffinity labelling experiments and later characterised in recombinant systems (Knoflach et al., 1996; Korpi and Seeburg, 1993; Whittemore et al., 1996; Wieland et al., 1992a). It was then shown that this conserved amino acid substitution in BDZ-sensitive α subunits ($\alpha1^{H101R}$, $\alpha2^{H101R}$, $\alpha3^{H126R}$ and $\alpha5^{H105R}$) results in diazepam insensitivity (Benson et al., 1998a; Kleingoor et al., 1993a; Rudolph et al., 1999).

Two other residues in the α1 subunit have been instrumental in identifying the orientation of the benzodiazepine, diazepam, in the binding pocket: S205 and T206. When these residues are mutated to cysteines they covalently interact with a cysteine reactive isothiocyanate (-NCS) group attached to nitrazepam acting as an irreversible covalent PAM (Tan et al., 2009). This study indicates that both α1 S205 and T206 play a crucial role in benzodiazepine binding, which was later confirmed via a cryo-EM receptor structure (Masiulis et al. 2019). Further interactions between benzodiazepines and the γ2 subunit in α1β2γ2 have been identified, with key contacts at Y58, N60 and V190 in the benzodiazepine pocket (Middendorp et al., 2014).

Recently, an additional high-affinity binding site for BDZ at the β2+/γ2- interface has been identified, in the absence of α1 subunits (Wongsamitkul et al., 2017). The αβ $GABA_A$ pentamers have also been shown to contain a low affinity benzodiazepine binding site, allowing potentiation of GABA-evoked currents by diazepam and other BDZs at μM concentrations (Baur et al., 2008; Ramerstorfer et al., 2011; Walters et al., 2000). The TM2 mutations in all subunits of α1β2γ2 receptors abolished the μM action of diazepam, while the high affinity component remained unchanged (Walters et al., 2000).

Diazepam is a largely non-selective benzodiazepine known to produce a wide range of effects *in vivo* such as sedation, anxiolysis, muscle relaxation and hypnosis. Genetically modified mice expressing the H101R mutation in individual α subunits have been studied to assess whether specific behavioural effects of benzodiazepines can be attributed to modulation of specific α subunit-containing receptors (Rudolph

et al., 1999; Rudolph and Möhler, 2004; Sigel and Ernst, 2018; Wieland et al., 1992a). Multiple attempts were made to separate the anxiolytic effects from sedation, where the latter was shown to be mediated specifically by α1 receptors (McKernan et al., 2000; Rudolph et al., 1999). The anxiolytic activity of diazepam was shown to be mediated by α2-containing $GABA_A$ receptors, and under conditions of high-receptor occupancy, also by α3-containg receptors (Dias et al., 2005; Löw et al., 2000; Skolnick, 2012).

1.3.4 Neurosteroids

Neurosteroids are a class of modulators that exhibit potent and selective effects on $GABA_A$ receptors (Reddy, 2010; Wang, 2011). Neurosteroids are synthesised endogenously in the brain (principal neurons and glial cells) and in peripheral tissues from cholesterol and neurosteroid precursors (progesterone, deoxycorticosterone and testosterone) (Agís-Balboa et al., 2006; Baulieu et al., 2001). Biosynthesis of several neurosteroids – allopregnanolone, 3α,21-dihydroxy-5α-pregnan-20-one (THDOC), and androstanediol – occur as a sequential reduction of the precursor steroid by 5α-reductase and 3α-hydroxysteroid dehydrogenase (Reddy, 2010). Non-sulphated neurosteroids are lipophilic in nature, therefore can readily cross the blood-brain barrier from the peripheral tissues (Schumacher et al., 1996). Neurosteroids can be classified into three groups: positive allosteric modulatory pregnane-derived steroids that include allopregnanolone and THDOC; androstane-derived neurosteroids that include etiocholanone and androstanediol; and sulphated neurosteroids, which include pregnanolone sulfate (PS) and dehydroepiandrosterone sulfate (DHEAS). Unlike other classes of neurosteroids, sulphated neurosteroids are negative allosteric modulators of $GABA_A$ receptors (Akk et al., 2001; Baker et al., 2010).

The binding site for PAM neurosteroids such as allopregnanolone and THDOC is located within the transmembrane domain (TM1) of an α subunit at the β^+/α^- subunit interface (Hosie et al., 2009; Laverty et al., 2017). A conserved glutamine residue across all α subunit isoforms (Q241 in α1) plays a key role in $GABA_A$R-neurosteroid

interaction, where a single hydrogen bond is formed between the glutamine and C3α hydroxyl ring A of THDOC (Hosie et al., 2009, 2007, 2006; Laverty et al., 2017). Neurosteroids greatly enhance the probability of $GABA_AR$ channel opening, via an increase in both frequency and duration of channel bursts (Hosie et al., 2007; Twyman and Macdonald, 1992). Additionally, high concentrations (>10 μM) of neurosteroids have a direct effect on $GABA_A$ receptor activation and this is mediated by the presence of Y236 and Y284 amino acid residues on α and β subunits respectively (Hosie et al., 2006).

$GABA_A$ receptors containing the δ rather than a γ subunit exhibit a much stronger modulatory response to potentiating neurosteroids, however inhibitory neurosteroids show no subtype selectivity (Belelli et al., 2002; Brown et al., 2002). Potentiating neurosteroid selectivity was suggested to be a consequence of the functional properties of δ-containing $GABA_A$ receptors. Since the efficacy of GABA is low in these receptors, neurosteroids increase GABA efficacy, causing a higher relative enhancement of GABA-mediated currents (Bianchi and Macdonald, 2003; Brown et al., 2002). Slice recordings from CA1 region of hippocampus and dentate gyrus granule cells show that nanomolar concentrations of neurosteroids enhance both tonic inhibitory conductance and IPSC decay time (Harney et al., 2003; Stell et al., 2003).

1.4 'Hetero-alpha' $GABA_A$ receptors

As described earlier, the majority of $GABA_A$ receptor subtypes that occur in the brain are composed of two α, two β, and one γ subunits. The receptor subtypes containing one type of these subunits ('homo-alpha' and 'homo-beta') have been well characterised in recombinant systems (Baumann et al., 2002; Olsen and Sieghart, 2008; Sigel and Steinmann, 2012).

Although only a small number of subunit combinations are thought to be expressed *in vivo*, there is increasing evidence that different α ('hetero-alpha') or β (hetero-beta') subunits may exist in a single receptor complex. This can vastly increase the

possible subunit combinations and receptor isoforms, producing receptor types with unique GABA and allosteric modulator sensitivities (Olsen and Sieghart, 2008; Sieghart and Sperk, 2002). There is extensive biochemical evidence supporting the existence of 'hetero-alpha' and 'hetero-beta' $GABA_A$ receptors from several research groups, which will be described below. ***Table 1.2*** summarises all the biochemical evidence on hetero-subunit type receptors.

1.4.1 'Hetero-alpha' $GABA_A$ receptors: biochemical evidence

Early immunohistochemistry studies based on colocalization analysis proposed that more than one α subunit type could exist in the same $GABA_A$ receptor pentameric complex. Combinations of α1/α2, α1/α3, α1/α5, and α2/α5 subunits were speculated to exist in different brain regions (Bohlhalter et al., 1996; Christie and de Blas, 2002; Fritschy et al., 1992; Fritschy and Mohler, 1995; Zezula and Sieghart, 1991). However, the evidence of the $GABA_A$ receptor subunit composition presented in these studies was not conclusive due to the nature of the colocalization studies.

During the 1990s, a variety of selective $GABA_A$ receptor subunit antibodies were generated, allowing the biochemical assessment of receptor composition. Immunoaffinity studies based on subtractive purification have been performed to estimate the relative abundance of receptor types containing homo- and hetero-subunit combinations (Bencsits et al., 1999; Jechlinger et al., 1998; Nusser et al., 1999). Using this method of purification in rat brain extracts (excluding cerebellum), α4-containing receptors were identified to predominantly exist as α4α4, but also minor populations of α1α4, α2α4, α3α4, (not α5α4) were detected (Bencsits et al., 1999; Benke et al., 1997). Immunoaffinity studies were also performed from calf cerebral cortex extracts, where out of all α1-contaning receptors, minor populations of α1α2 and α1α3 were identified (32±8% and 8±1% respectively) (Duggan et al., 1991). Furthermore, results obtained from rat cerebellum extracts indicated that α6 containing receptors are expressed as α6β*x*γ2 32%, α1α6β*x*γ2 37%, α6β*x*δ 14%, and α1α6β*x*δ 15% (Jechlinger et al., 1998). The same study suggested that 18% of all α6-containing receptors had two different β subunits (Jechlinger et al., 1998). Earlier

immunoprecipitation and immunoaffinity studies also from cerebellum have also identified hetero-α receptors (α1α6) (Pollard et al., 1995, 1993).

Table 1.2 Biochemical evidence for heteromeric $GABA_A$ receptors. The table outlines all the biochemical evidence of 'hetero-alpha' and 'hetero-beta' $GABA_A$ receptors. Publications are categorised by the type of hetero-subunit type assessed (first column). The third column outlines the biochemical techniques used (subtraction immunoaffinity chromatography, immunoprecipitation, or radioligand binding assays). Last column summarises the findings of the reports and the brain area assessed.

Hetero-receptor type	Reference	Assay	Conclusions
α1α2	(Duggan et al., 1991)	Immunoaffinity purification	Calf cerebral cortex extracts, out of all α1-containg receptors: minor populations of α1α2 (32±8%), α1α3 (8±1%), α2α3 *
	(Benke et al., 2004a)	Immunoprecipitation Radioligand binding	Mouse brain extracts, out of α1-, α2-, α3- containing receptors: α1α1 61%, α1α2 13%, α1α3 15%, α2α2 12%, α2α3 2%, α3α3 4%**
	(del Río et al., 2001a)	Immunoprecipitation Immunoaffinity chromatography Radioligand binding	Rat hippocampal and cortical extracts, out of α2-containing receptors, α1α2 36.3 ± 5.2% (hippocampus) and 39.4 ± 5.5% (cortex), α1α2 purified receptors exclusively show α2-BDZ pharmacology
α1α3	(Duggan et al., 1991)	Immunoaffinity purification	See * for details
	(Araujo et al., 1996)	Immunoprecipitation Radioligand binding	Rat cerebral cortex lysates, out of all α1-containing receptors, α1α3 20-25%; out of all α3 -containing receptors α1α3 50-55%, α1 BDZ pharmacology prevails over α3 BDZ pharmacology (70% and 30% respectively)

	(Dietmar Benke et al. 2004)	Immunoprecipitation Radioligand binding	See ** for details
α1α5	(Araujo et al., 1999)	Immunoprecipitation Radioligand binding	Rat hippocampal extracts, out of all α1-containing receptors, α1α5 7-10%, out of all α5-containing receptors, α1α5 18-23%; α1α5 receptors predominantly show an α5 BDZ pharmacology
	(Ju et al., 2009)	Immunoprecipitation Biochemical fractionation Mass spectroscopy	Mouse hippocampal extracts, from α5-containing receptors, α1α5 and α2α5 identified. Different proportions of α1, α2 and α5 in synaptic and extrasynaptic receptors fractions.
α1α6	(Pollard et al., 1993)	Immunoprecipitation	Rat cerebral cortex lysates, α1α6 minor population
	(Pollard et al., 1995)	Immunoaffinity Radioligand binding	Rat cerebellum extracts, out of all α6-containing receptors: α1α6 41 ± 12%, α1α6 receptors predominantly show an α6 BDZ pharmacology (BDZ insensitive)
	(Khan et al., 1996)	Immunoprecipitation Radioligand binding	Cerebellum, α1 59-65%, α6 22-28%, α1α6 11-17%
	(Jechlinger et al., 1998)	Immunoaffinity chromatography	Rat cerebellum extracts, out of all α6-containing receptors: α6β*x*γ2 32%, α1α6β*x*γ2 37%, α6β*x*δ 14%, α1α6β*x*δ 15%
	(Nusser et al., 1999)	Immunoprecipitation Radioligand binding	Mouse cerebellar extracts (α6 gene disruption, α6 -/-), in control group (α6 +/+) α1α6 present. In α6 -/- mice 26% reduction of α1 expression
	(Pöltl et al., 2003)	Immunoprecipitation Radioligand binding	Mouse or rat cerebellum extracts. Mouse: out of α1-

			and α6-containing receptors, α1βxγ2 40.5 ± 2.4%, α6βxγ2 6.8 ± 0.8%, **α1α6βxγ2 22.4 ± 1.4%**, α1βxδ 0.8 ± 0.7%, α6βxδ 17.7 ± 1.0%, **α1α6βxδ 10.4 ± 1.2%.** 56% of all receptors contain α6 subunits and 59% contain both α1 and α6 subunits.
	(Ogris et al., 2006)	Immunoaffinity purification Radioligand binding RT-PCR	Mouse cerebellar extracts (α1 gene disruption, α1 -/-), in control group (α1 +/+). In α1 -/- mice, α6 subunit expression is increased by 54 % (replacing α1 subunits)
	(Scholze et al., 2020)	Immunoprecipitation Radioligand binding	Rat cerebellum extracts, out of all γ2 containing receptors: α1γ2βxα1βx 57%, α6γ2βxα6βx 19%, α1γ2βxα6βx 9%, 6γ2βxα1βx 15%
α2α3	(Duggan et al., 1991)	Immunoaffinity purification	See * for details
	(Benke et al., 2004a)	Immunoprecipitation Radioligand binding	See ** for details
α2α5	(del Río et al., 2001a)	Immunoprecipitation Immunoaffinity chromatography Radioligand binding	Rat hippocampal extracts, out of α2-containing receptors, α2α5 20.2 ± 2.1%, α2α5 purified receptors exclusively show α5-BDZ pharmacology
α2α*x*, where *x* is 1, 3, 4 or 5	(Pöltl et al., 2003)	Immunoprecipitation Immunoaffinity chromatography	Mouse or rat cerebellum extracts. Mouse: out of all $GABA_A$ receptors: α1α2 α2α3, α2α4, α2α5 were identified (between 1.3 and 7.3 % each)
	(Nakamura et al., 2016)	Immunoprecipitation Proteomic analysis	Mouse brain extracts (pHluorin-tagged α2 mouse model). α1α2 α2α3, α2α4, α2α5 were identified

α4α*x*, where *x* is 1, 2 or 3	(Benke et al., 1997)	Immunoprecipitation Immunoaffinity chromatography Radioligand binding	Rat brain lysates (different regions): out of α4-containing receptors, α1α4 α2α4 α3α4, but not α5α4 was detected
	(Bencsits et al., 1999)	Immunoaffinity	Rat brain extracts (no cerebellum), α1α4, α2α4, α3α4 identified (not α5α4)
α5α*x*, where *x* is 1, 2 or 3	(Mertens et al., 1993)	Immunoprecipitation Radioligand binding	Rat brain extracts (various regions), α1α5 α2α5 and α3α5 were identified
	(Sieghart et al., 1993)	Immunoprecipitation	Rat brain extracts, out of α5-containing receptors, α1α5 α2α5 and α3α5 were identified
β1β2	(Li and De Blas, 1997)	Immunoprecipitation	Rat brain extracts, out of all β-containing receptors, β1β2 8%
β1β3	(Li and De Blas, 1997)	Immunoprecipitation	Rat brain extracts, out of all β-containing receptors, β1β3 19%
β2β3	(Li and De Blas, 1997)	Immunoprecipitation	Rat brain extracts, out of all β-containing receptors, β2β3 33%
2 different β	(Jechlinger et al., 1998)	Immunoaffinity chromatography	Rat cerebellum extracts, 18 % of α6 receptors contain 2 different β subunits

The subunit composition of α6-containing $GABA_A$ receptors has been widely studied. Cerebellar granule cells almost exclusively express α1, α6, β1-3, γ2, and δ subunits, making it an obvious target for studying hetero-α receptors (Fritschy and Mohler, 1995; Laurie et al., 1992; Pirker et al., 2000). Immunogold labelling of α1 and α6 $GABA_A$ receptors showed colocalization of these subunits in cerebellar granule cells, suggesting the possibility that α1 and α6 can co-exist in the same pentamer (Zoltan Nusser et al., 1998). Later, the same group utilised an α6 knock-out mice to study the effect α6-containing receptor populations. The results showed a 26% reduction of α1-subunit expression in α6 (-/-) mice compared to α6 (+/+) mice (Nusser et al., 1999). A similar study of α1 (-/-) mice cerebellar extracts suggested a 54% increase in

α6 subunits in α1-defficient mice compared to the wild-type ones, suggesting that α1 is replaced by α6 subunit in α1α6 $GABA_A$ receptors (Ogris et al., 2006). These finding are in agreement with the previous reports (59% of all cerebellar receptors contain both α1 and α6 subunits) (Pöltl et al., 2003). Quantitative immunoprecipitation assays further identified hetero-α $GABA_A$ receptors containing both α1α6 subunits, as well as proposed their subunit arrangement. One study estimated that out of all α6-containg receptors, 41 ± 12% are α1α6 and these predominantly show an α6 BDZ pharmacology (BDZ insensitive, i.e. α6-β-α1-β-γ arrangement around the central pore, top view) (Pollard et al., 1995). In accordance with these findings, ^{3}H-Ro 15-4513 binding experiments of γ2-prurified $GABA_A$ receptors concluded that the majority of α1α6βxγ2 cerebellar receptor are benzodiazepine insensitive (α6γ2βxα1βx 15% and α1γ2βxα6βx 9%) (Scholze et al., 2020).

Numerous reports provide evidence for hetero-α $GABA_A$ receptors containing an α1 subunit. Immunoprecipitation from whole mouse brain extracts suggested that out of all α1-, α2-, α3- subunit containing $GABA_A$ receptors the majority are α1α1 (61%), whereas α1α2 and α1α3 containing receptors account for a 13% and 15% respectively (Dietmar Benke et al. 2004). Immunodepletion experiments showed that α1α3 $GABA_A$ receptors constitute a large proportion of α3- but not of α1- containing receptors (54% and 24% respectively) in rat cerebral cortex (Araujo et al., 1996). Furthermore, α1α5 containing receptors represent 7-10% of all α1-containg $GABA_A$ receptor population in rat hippocampal neurones (Araujo et al., 1999). These α1-'hetero-alpha' receptors constitute significant populations for the non-α1-subunit (i.e. α3, α5) but represent a smaller proportion of α1-receptors, probably due to their high expression levels (Datta et al., 2015; Hutcheon et al., 2004; Pirker et al., 2000).

There is some evidence suggesting the existence of 'hetero-beta' $GABA_A$ receptors, however it is limited. Mixtures of two different β subunits were identified in 18% of all α6-containing receptors (α6βxγ2, α1α6βxγ2, α6βxδ, and α1α6βxδ) from rat cerebellum (Jechlinger et al., 1998). In addition, various combinations of 'hetero-beta' $GABA_A$ receptors were found from total rat brain extracts, comprising around 60% of all β-subunit containing receptors (Li and De Blas, 1997).

Insight into subunit arrangement in hetero-α receptor complex was assessed *via* benzodiazepine binding properties of immunoprecipitated $GABA_A$ receptors (Araujo et al., 1996, 1999; del Río et al., 2001a; Pollard et al., 1995; Scholze et al., 2020). Interestingly, results from these show that from purified $\alpha1\alpha_x$-containing $GABA_A$ receptors (where x is 2, 5 or 6), α_x benzodiazepine pharmacology prevails over α1 (Araujo et al., 1999; del Río et al., 2001a; Pollard et al., 1995; Scholze et al., 2020). Hence, the majority of 'hetero-alpha' $GABA_A$ receptor subunit could present an **α_xγ2βα1β** subunit arrangement. One exception appears to be α1α3-containing receptors, where α1 benzodiazepine pharmacology prevails over that of α3 (70% and 30% respectively) (Araujo et al., 1996). The proposed subunit arrangements from these data are outlined in ***Figure 1.3***.

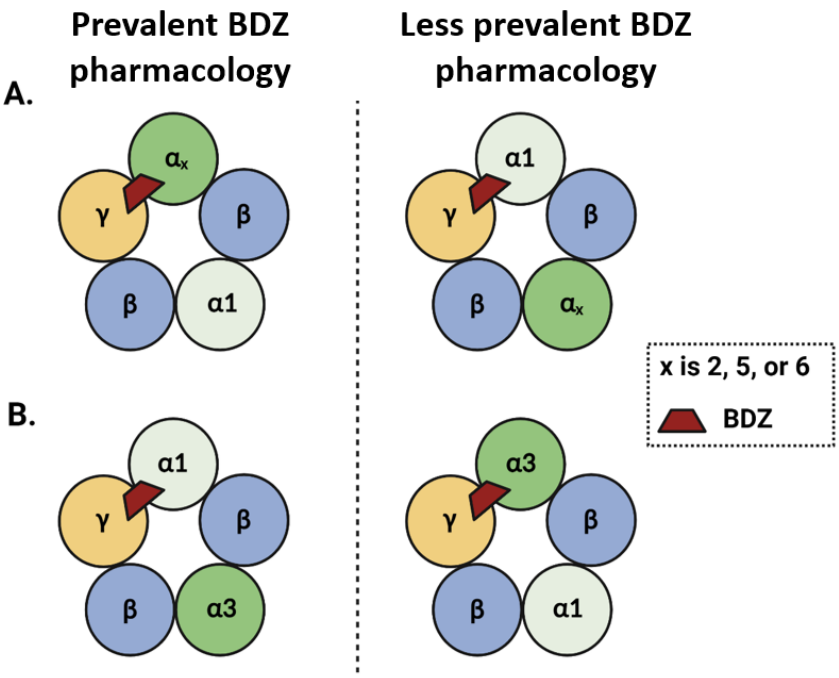

Figure 1.3 'Hetero-alpha' $GABA_A$ receptor subunit arrangement and their benzodiazepine pharmacology. **A.** and **B.** Schematic representation of $GABA_AR$ subunit arrangement around the central pore (top view). The high-affinity benzodiazepine site, BDZ, at the αγ interface is shown as a dark red trapezoid. **A.** The α_x (where x is 2, 5 or 6) BDZ pharmacology prevails over the α1 BDZ pharmacology in $\alpha1\alpha_x$ – containing $GABA_A$ receptors (>50% of receptors contain an α_x+ / γ- interface) (Araujo et al., 1999; del Río et al., 2001a; Pollard et al., 1995; Scholze et al., 2020). **B.** In α1α3-containg receptors, α1 BDZ pharmacology prevails over α3 (>50% of receptors contain an α1+ / γ- interface) (Araujo et al., 1996) .

The evidence described above suggests that a significant part of the $GABA_A$ receptors in the brain comprise of two distinct α and /or β subunit isoforms (Sieghart and Sperk, 2002). Nevertheless, to establish the existence of these receptors in the brain, functional electrophysiological and pharmacological *in vivo* studies are required. It is, however, difficult to study the receptor composition, arrangement and pharmacology of a receptor type that is composed of a mixture of three or more distinct subunit isoforms. This is because various receptor subtypes with different subunit combinations and arrangements can be formed. Therefore, to study the pharmacological fingerprints of $GABA_A$ receptors with two different isoforms of α or β subunits it is essential to know the positioning of subunits in a pentameric complex. This can be achieved by forced assembly of receptors, known as concatenation. The next section will outline the benefits and caveats of concatenated receptor studies and how these contribute to the understanding of 'heteroalpha' $GABA_AR$ pharmacological profiles.

1.4.2 Concatenated receptor studies

The principle behind the concatenation of subunits was firstly applied to successfully study nicotinic acetylcholine receptors, nAChRs, and subsequently has been widely used to link Cys-loop receptor architecture with function (Im et al., 1995; Liao et al., 2020). Receptor concatenation is a technique in which multiple subunits are expressed as a covalently linked fusion protein. The N-terminus of a subunit is linked to a C-terminus of a preceding subunit via a glutamine linker sequence of an optimal length (E. Sigel et al. 2006; Minier and Sigel 2004, 200; S. W. Baumann, Baur, and Sigel 2001). Various combinations of concatenated oligomers (monomer/tetramer, dimer/trimer and pentamer) have been used to study the impact of subunit position and number on the function of receptors as well as positional effects of mutations in specific subunits that occur multiple times in a receptor (Baumann, Baur, and Sigel 2003; Gallagher et al. 2004; Absalom et al. 2019; Baumann, Baur, and Sigel 2002; Boileau, Pearce, and Czajkowski 2005; Minier and Sigel 2004). There is a clear

advantage for the use of concatenated receptors to study multi subunit $GABA_A$ receptors due to the ability to define subunit arrangement and stoichiometry.

Dimer/trimer concatenated subunit constructs with two α subunit isoforms (α1 and α6) were designed to functionally assess γ2β2**α1**β2**α1**, γ2β2**α6**β2**α6**, γ2β2**α1**β2**α6**, and γ2β2**α6**β2**α1** $GABA_A$ receptors (Minier and Sigel, 2004a). The GABA apparent affinity of γ2β2**α6**β2**α1** was found to be two times higher than of γ2β2**α1**β2**α6** (42 ± 14 μM and 94 ± 38 μM respectively). Furthermore, inhibition with furosemide – a $GABA_AR$ α6 subunit selective non-competitive inhibitor (Thompson et al., 1999) and diazepam potentiation were also assessed. An α6 subunit positioning next to the γ2 resulted in high sensitivity to furosemide, whereas an α1 neighbouring γ2 subunit in concatenated constructs (γ2β2**α1**β2**α1** and γ2β2**α6**β2**α1**) resulted in diazepam sensitivity (Minier and Sigel, 2004a). This study pioneered the use of concatenated receptors as a diagnostic tool to study pharmacological signatures of 'hetero-alpha' $GABA_A$ receptors. Indeed, a recent study used a forced receptor assembly approach to study pyrazoloquinolinone (PQ) allosteric modulation of α1α6-containg $GABA_A$ receptors (Simeone et al., 2019). Concatenated receptors with two different β subunit isoforms were also used to assess the functional signatures of these receptors to β2-selective compounds: etomidate and loreclezole (Boulineau et al., 2005). The results from this study showed that the response to these compounds is independent of β2 positioning in the receptor complex.

Whilst receptor concatenation is a powerful technique, there are precautions that need to be taken in the experimental design. Firstly, structural artefacts could result during concatenated receptor assembly (Sigel et al., 2006). Examples include: one subunit of a dimeric concatenated construct lining the channel pore and the other sticking out, concatenated subunit constructs connecting two pentameric receptors, incorrect arrangement or subunits within the pentamer or linker proteolysis (see ***Figure 1.4*** for details) (Minier and Sigel 2004). Some concatenated constructs of Cys-loop receptors were also found to assemble in both clockwise and anticlockwise directions (Ahring et al., 2018; Liao et al., 2020). However, these artefacts can be avoided by optimising the cDNA concatenated constructs (omitting signal peptides and adjusting the length of the linker between concatenated subunits) and adjusting

the ratios of cDNAs used (Ericksen and Boileau, 2007; Sigel et al., 2009). Another major pitfall of forced arrangement receptor studies is small agonist-evoked current amplitude (Boileau et al., 2005). Increasing the cDNA amount and using *Xenopus* oocytes as an expression system can, to some extent, overcome this problem (Baumann et al., 2001; Sigel et al., 2006).

Despite the caveats of this techniques, receptor concatenation can vastly contribute to the understanding of $GABA_A$ receptors with two different α and β isoforms. Nevertheless, the results obtained from such studies need to be assessed with caution.

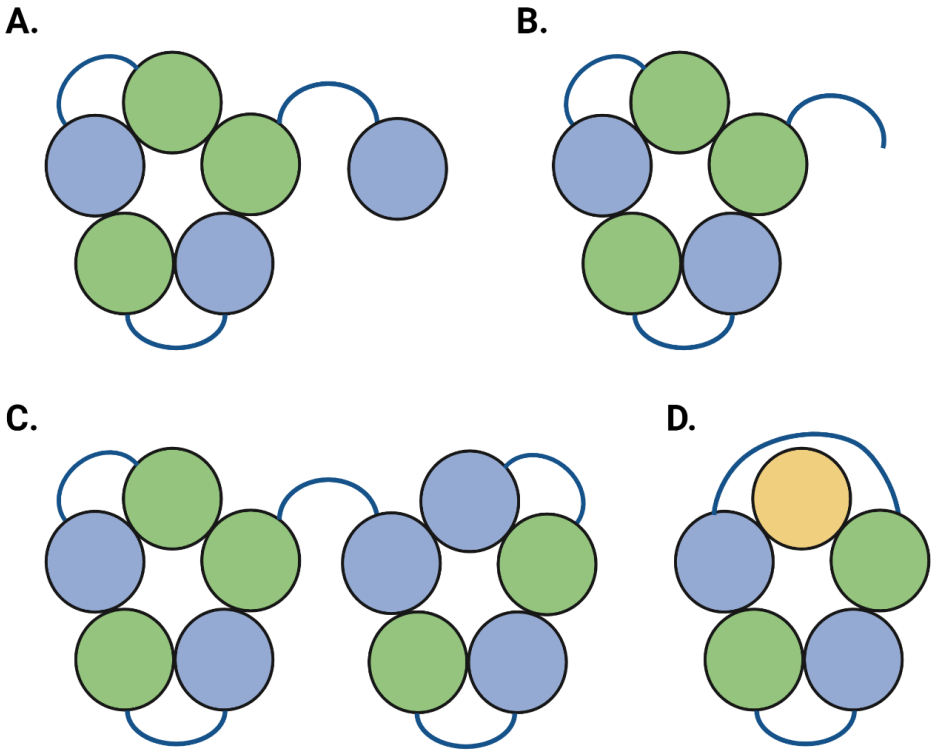

Figure 1.4 Examples of undesired structural artefacts that could form during the assembly of dimeric subunit concatenated receptors. Dimeric subunit constructs are shown as green and blue circles (corresponding to each subunit) joined by a linker chain (dark blue). **A.** One subunit of a dimeric construct lines the channel pore of the receptor, whereas the other subunit is sticking out. **B.** Proteolysis in the linker region between two concatenated subunits can result in its false inclusion into the receptor pentamer. **C.** Dimeric subunit constructs can incorporate into two different receptor pentamers. **D.** If the linker chain between two concatenated subunits is too long, another subunit can get incorporated in between (Minier and Sigel 2004).

1.5 Thesis aims

1.5.1 Electrophysiological assessment of $GABA_A$ receptors with two different α subunit isoforms

Despite a multitude of biochemical evidence pointing to the existence of 'hetero-alpha' $GABA_A$ receptors, functional assessment of these in a recombinant system is lacking. Our first aim, therefore, was to electrophysiologically identify and study $GABA_A$ receptors with two distinct α subunit isoforms. The α1 and α2 subunits were chosen, due to their abundance in the brain (both expression levels and localisation) (Pirker et al., 2000). Single α1 and α2 subunits or their mixtures were expressed with β2/3 γ2 to form functional $GABA_A$ receptors in HEK293 cells. This allowed for a comparison of functional signatures of 'hetero-alpha' receptors with those of 'homo-alpha' populations. A selection of reporter mutations was then used to help distinguish between 'homo'- and 'hetero'-alpha receptor populations as well as estimate their relative abundances.

Subunit arrangement is key in determining $GABA_A$ receptor sensitivity to benzodiazepines. The canonical benzodiazepine binding site lies between the α+ / γ- interface, where α1 H101, α1 N103, α1 S206, and γ2 N60 play crucial roles in BDZ binding (Masiulis et al. 2019). The α1 and α2 subunit BDZ pharmacology mediate distinct effects in the brain: sedative and anxiolytic affects respectively (Dias et al., 2005; McKernan et al., 2000; Skolnick, 2012). $GABA_A$ receptor populations with two distinct α subunit isoforms could therefore present either α1 or α2 BDZ pharmacology or a mix of both. Here, a well characterised reporter mutation – α1 H101R – was used to study the subunit arrangement in 'hetero-alpha' $GABA_A$ receptors (Benson et al. 1998; Dietmar Benke et al. 2004). We aimed, through mutagenesis and pharmacological studies, to determine whether the presence of a specific α subunit is more abundant at the α+ / γ- interface or indeed, is exclusively expressed at this interface.

From these data, we hypothesised that $GABA_A$ receptors containing both α1 and α2 isoforms assemble in a recombinant system and present distinct pharmacological fingerprints.

1.5.2 Evidence of existence in vivo

After the *in vitro* assessment of 'hetero-alpha' $GABA_A$ receptors, our next aim was to establish the existence of these receptors *in vivo*. Even though, immunoaffinity purification and coimmunoprecipitation studies have been widely used to study receptor composition, most of these assess α1α6-containg receptors. Furthermore, biochemical conditions vastly determine coimmunoprecipitation outcomes (Nakamura et al., 2016). Here, we use proximity ligation assay (PLA) to visualise native α1α2-containg $GABA_A$ receptors in cultured hippocampal neurons and to assess their subcellular localisations. The PLA technique fluorescently labels proteins in close proximity (30 nm) and therefore allows us to detect α1 and α2 subunits within the same receptor. We also validated the reliability of the technique by using the microtubule inhibitor, nocodazole, and γ/δ $GABA_A$ receptor interactions.

Our next aim was to elucidate the determinants of assembly of α1α2-containing $GABA_A$ receptors. This was attempted by transfecting either α1 or α2 subunits into hippocampal neurons and investigating the changes in PLA signals. Additionally, electrophysiological recording and IPSC kinetic analysis was used to explore functional fingerprints of 'hetero-alpha' $GABA_A$ receptor populations underpinning inhibitory synaptic transmission.

1.5.3 Physiological role of α1α2-containg $GABA_A$ receptors

To date, there is no evidence regarding the physiological role of $GABA_A$ receptors containing both α1 and α2 subunit isoforms. Therefore, the last aim was to investigate 'hetero-alpha' receptor importance and changes after the induction of

long-term potentiation (LTP). This was achieved through PLA and imaging techniques in hippocampal cultured neurons.

1.5.4 Summary of aims

1. To determine the existence, abundance and subunit composition of $GABA_A$ receptors with two distinct α subunit isoforms in a recombinant system (***Chapter 3***).

2. To investigate two potential subunit arrangements of α1α2-containg receptors: γ2βx**α1**βx**α2** and γ2βx**α2**βx**α1** (***Chapter 3***).

3. To establish the existence and determine the subcellular localisation of α1α2-containg $GABA_A$ receptors in cultured hippocampal neurons (***Chapter 4***).

4. To investigate functional fingerprints of these receptors using iPSC kinetic analysis (***Chapter 4***).

5. To examine the physiological function of 'hetero-alpha' $GABA_A$ receptors using a long-term potentiation protocol (***Chapter 5***).

Chapter 2: Materials and Methods

2.1 Molecular biology

2.1.1 $GABA_A$ receptor subunit constructs

All point mutant and affinity-tagged subunits were made using our stocks of wild type subunit constructs. The wild type constructs were cloned into pRK5 vector with the Kozak sequence upstream of the signalling peptide for optimal mammalian expression. The murine $GABA_A$ receptor DNA of α1 (UniProtKB: P62812), α2 (UniProtKB: P26048), β2 (UniProtKB: P63137) β3 (UniProtKB: P63080), and γ2L (UniProtKB: P22723) were used as templates for mutagenesis. Point mutations and affinity-tag insertions were introduced by inverse PCR method using Phusion Hot Start DNA polymerase kit (Thermo Fisher Scientific, F549), see ***Table 2.1*** for details. Primers used in DNA mutagenesis are listed below (***see Table 2.2***).

Table 2.1 PCR reaction concentration and volumes used per reaction. Reagents are listed in the left column, for more detail about the primers and DNA template used for each PCR see ***Table 2.2***.

Reagent	Stock [conc.]	Final [conc.]	Volume
Template cDNA	2.5 µg/ml (125 ng)	50 ng/ml (2.5 ng)	1 µl
Forward primer	15 µM	0.3 µM	1 µl
Reverse primer	15 µM	0.3 µM	1 µl
dNTP mixture (concentration per each nucleotide (nt))	10 mM each nt	0.2 µM each nt	1 µl
Phusion Buffer HF/GC	5X	1X	10 µl
Phusion DNA Polymerase	2 U/µl	0.02 U/µl	0.5 µl
$MgCl_2$ (where required)	50 mM	Between 1 and 2.5 mM	1 to 2.5 µl
ddH_2O	—	—	To 50 µl
Total volume:			50 µl

PCR products were separated on the 0.8% agarose gel (100 V for 45 minutes). Ethidium bromide was used as a fluorescent probe to label the DNA. All PCR products were mixed with 6X loading dye (New England BioLabs, B7024) to visualise the gel front and run alongside 1 kb DNA ladder (New England BioLabs, B7025). The DNA band of the correct molecular weight was cut out of the agarose gel and subsequently purified using a DNA Gel Extraction kit (New England BioLabs, Monarch, T1020).

The linear cDNA was then ligated using T4 Polynucleotide kinase (PNK) and T4 DNA ligase (New England Biolabs, M0201, M0202). Briefly, 16 µl of linear DNA gel-extraction product was incubated at 72 ˚C for 5 minutes to separate the ends of dsDNA and cooled down on ice for 1 minute. T4 ligase buffer and PNK (2 and 1 µl respectively) were added to the gel extraction product and incubated for 40 minutes at 37 ˚C. Following this step, 1 µl of T4 DNA ligase was added to the mixture to ligate the linear DNA at 4 ˚C overnight.

Table 2.2 PCR primers used to introduce affinity tags or point mutations into $GABA_A$ receptor DNA. Primers are shown in the 5' to 3' direction. Nucleotides that correspond to the template sequence are shown as upper-case letters, nucleotides that have been added or changed are shown as lower-case letters. The template used to produce each construct (left column) is stated in the right column and corresponds to the wild type $GABA_A$ receptor subunit.

Mutation/ affinity tag	Forward primer (sequence 5'-3')	Reverse primer (sequence 5'-3')	Template
GABAA α1 F65L	ATGTGTTTTTaCGTCAAAGTT GGAAGG	CTATTGTATACTCCATATCGTG GTCTG	GABAA α1
GABAA α1 H101C	CAATGGAAAGAAGTCTGTG GCCCACAA	caGAAAAATGTATCTGGAGTC CAGATT	GABAA α1
GABAA α1 H101R	CgCAATGGAAAGAAGTCTGT GGCCCAC	GAAAAATGTATCTGGAGTCCA GATTTT	GABAA α1
GABAA α1-HA	ttccagattacgctGATGAACTT AAAGACAACACCACT	catcgtatgggtaTTGGGAGGGCT GTCCATAGCTTCT	GABAA α1
GABAA α1-myc	tcagaagaggatctgGATGAACT TAAAGACAACACCACT	gatgagtttttgttcTTGGGAGGGC TGTCCATAGCTTCT	GABAA α1
GABAA α2 F65L	ATGTTTTaTTTCGGCAAAAA TGGAAAGG	CTATTGTATACTCCATATCTGT ATCTGG	GABAA α2
GABAA α2 H101C	CAATGGGAAAAAGTCAGTG GCCCATAA	caAAAGAAGGTATCAGGAGTC CAGATT	GABAA α2
GABAA α2 H101R	CgCAATGGGAAAAAGTCAG TGGCCCATAAC	AAAGAAGGTATCAGGAGTCC AGATTTTGCT	GABAA α2
GABAA α2-myc	tcagaagaggatctgGATGAGG CTAAAAATAACATCACC	gatgagtttttgttcTTCTTGGATGT TAGCCAGCACCAA	GABAA α2

Ligated cDNA was then transformed into 5α competent *Escherichia coli (E. coli)* (New England Biolabs, C2987). Ligated DNA product (1-2 µl) was gently pipetted and mixed with 25 µl of competent *E. coli* and left on ice for 30 minutes. The bacteria were then heat shocked (42 ˚C) for 40 seconds to take up the ligated DNA product. Following 1-minute incubation on ice, SOC medium (100 µl) was added to the *E. coli* and incubated with robust shaking for 25 minutes. This mixture was then plated onto Luria Broth (LB) agar plates with a suitable antibiotic: ampicillin or kanamycin (100 µg/ml and 50 µg/ml respectively). The plates with the transformed 5α competent *E. coli* bacteria were placed in the incubator (37^o C) overnight for colony growth. The

colonies were picked the next day and incubated in 2.5 ml of LB broth supplemented with an antibiotic with shaking overnight at 37^{o} C. The DNA was then purified using Plasmid Miniprep Kit (New England BioLabs, Monarch, NEB T1010). DNA concentration was measured using a Nanodrop (Thermo Fisher) at 260 nm wavelength. DNA plasmids were subjected to sequencing to identify successful constructs (SP6 was used as a forward primer and P5 was used as a reverse primer). The bacterial culture of a successful colony was grown in 150-250 ml of LB broth under the same conditions. The DNA was then subjected to purification using either a Midi or a Maxi HiSpeed Plasmid DNA Kit (Qiagen, 12643/12662). DNA concentration was measured and adjusted to 1 mg/ml for ease of use for HEK293 or neuronal transfections. Prior to use all constructs were sequenced one more time to confirm the correct sequence of the plasmid.

2.2 HEK293 cell culture and transfection

2.2.1 HEK293 cell culture

Human embryonic kidney (HEK293) cells were cultured on 10 cm dishes in Dulbecco's modified Eagle medium (DMEM) (Gibco, Thermo Fisher Scientific) supplemented with 10% foetal calf serum (FCS) (Gibco, Thermo Fisher Scientific), 0.1 mg/ml penicillin and 0.1 mg/ml streptomycin (Gibco, Thermo Fisher Scientific) kept in 37°C/5 % CO_2 humidified incubator. Cells were passaged when they reached around 80% confluency, which was monitored regularly to prevent overgrowth. To passage, the DMEM media was aspirated and cells were carefully washed with Ca^{2+}/Mg^{2+} free Hanks' Balanced Salt Solution (HBSS) (Gibco, Thermo Fisher Scientific) and lifted using 0.05% trypsin-ethylene-diamine-tetra-acetic acid (trypsin-EDTA) (Gibco, Thermo Fisher Scientific). EDTA is a divalent cation chelator that inhibits adhering proteins and trypsin is a proteolytic enzyme that breaks them down, therefore lifting the cells off the dish. To inactivate trypsin-EDTA, 10 ml of DMEM media was added and cells were collected and centrifuged at 168 x g for 2 minutes. Supernatant was then aspirated, and cells were resuspended in 1-5 ml of DMEM culture media. Cells were

subsequently plated at a lower confluence (20 or 50%) on 10 cm dishes for cell line maintenance or pull downs; or on 22 mm coverslips coated in poly-L-lysine (Sigma, P7280) for subsequent transfection.

2.2.2 HEK293 cell transfection

HEK293 cells plated on 22 mm coverslips were used for electrophysiological and imaging experiments, whereas 10 cm dishes were used for pull-down assays of specific $GABA_A$ receptor subunits. HEK293 cells were transfected using a calcium phosphate transfection method. Specifically, 1 µg or 6 µg (for 22 mm coverslips or 10 cm dishes, respectively) of cDNA for each $GABA_A$ receptor subunit was used per transfection. A transfection ratio of 1:1:1 (α:β:γ) was used for the $GABA_A$ receptor subunits unless otherwise stated. In addition, 1 µg of eGFP cDNA was added to the DNA mixture used for 22 mm coverslips for identification of transfected cells. In brief, cDNA was added to 20 µl or 120 µl (coverslips or dishes respectively) 340 mM $CaCl_2$ and vigorously shaken with 24 µl or 144 µl (coverslips or dishes respectively) HEPES-buffered saline (HBS: 50 mM HEPES, 280 mM NaCl, 1.1 mM Na_2HPO_4, pH 7.12). After transfection, cells were incubated for 24 to 48 h at 37°C, to allow the expression of receptors. The details of concentrations and volumes of reagents used can be found in ***Table 2.3***.

Table 2.3 Reagents and their volumes used in calcium phosphate HEK293 cell transfection. Transfection ratio of $GABA_A$ receptor subunits was 1:1:1 (α:β:γ) unless otherwise stated. The total volume of the transfection reaction was pipetted onto 22 mm coverslips or 10 cm dishes as appropriate.

Reagent	Concentration	22 mm coverslip	10 cm dish
$GABA_A$ receptor cDNA	1 mg/ml	1 µl/subunit	6 µl/subunit
eGFP cDNA	1 mg/ml	1 µl	—
$CaCl_2$	340 mM	20 µl	120 µl
HBS		24 µl	144 µl
Total volume:		**48 µl**	**282 µl**

2.3 Neuronal cell culture and transfection

2.3.1 Hippocampal cell culture

Hippocampal neurons were prepared from E18 Sprague-Dawley rat embryos. Briefly, the brains were removed and placed in a 35 mm dish containing pre-chilled Ca^{2+}/Mg^{2+} HBSS (Gibco, Thermo Fisher Scientific). The brains were separated into two hemispheres using a sharp blade. Working under the dissecting microscope, each hemisphere was treated in the following way to isolate the hippocampi: first, the cerebellum was cleaved off and then meninges were cautiously removed with a pair of fine forceps. This step is crucial, since meninges contain fibroblasts and can overgrow hippocampal neuronal cultures if not removed correctly. Lastly, hippocampi were extracted by carefully cutting around their outline. Dissected hippocampi were collected and transferred into a 35 mm dish containing pre-warmed (37°C) 0.1% w/v trypsin (Gibco, Thermo Fisher Scientific) in Ca^{2+}/Mg^{2+} HBSS for 10 minutes. Working in a sterile tissue culture hood, hippocampi were washed two times in 5 ml of fresh Ca^{2+}/Mg^{2+} HBSS to remove any residual trypsin. The tissue was then triturated using fire-polished Pasteur pipettes with progressively smaller apertures in 2 ml plating media [Minimum essential medium (Gibco, Thermo Fisher Scientific,

11095080) containing 2 mM L-glutamine, 20 mM glucose, 10 µg/mL penicillin, 10 µg/mL streptomycin, 5% (v/v) horse serum and 5% foetal bovine serum (FCS)]. Once the mixture was homogeneous, plating media was added to the desired final volume (1 ml plating media per two hippocampi). Cells were then plated onto 18 mm coverslips coated with poly-L-ornithine (Sigma, P4957) (250 µl/coverslip). Cells were placed into the 37°C/5 % CO_2 humidified incubator for three hours to allow for cell attachment to the coverslips. Plating media was then aspirated and replaced with 2 ml maintenance media [Neurobasal-A Medium (Gibco, Thermo Fisher Scientific, 10888022) supplemented with 0.5% (v/v) GlutaMAX supplement (Gibco, 35050061), 1 % (v/v) B-27 supplement (Gibco, 17504044), 35 mM glucose, 50 µg/mL penicillin and 10 µg/mL streptomycin]. The maintenance media was changed weekly to replenish the nutrients necessary for neuronal growth.

2.3.2 Neuronal Effectene transfection

Neurons were transfected with a $GABA_AR$ subunit of interest on day 7 after plating using Effectene as per manufacturers protocol (Qiagen, 301425). EGFP cDNA was used alongside $GABA_A$ receptor subunit cDNA as an identification method for successfully transfected neurons. In brief, a total of 0.8 µl of 1 mg/ml cDNA was mixed with 6.4 µl Enhancer and 100 µl Effectene buffer. The mixture was left for 5 minutes before the addition of 10 µl Effectene. The solution was left for further 10 minutes. During this incubation, neuron-plated coverslips were briefly washed with room temperature HBSS (Ca^{2+}/Mg^{2+}, +/+) and replenished with 1.5 ml maintenance media. The effectene transfection mix was then added directly onto the coverslips and incubated for 2 hours before replacing the mixture with fresh media. Neurons were then left to express the proteins of interest and used for electrophysiological and imaging experiments 5-10 days later.

2.4 Electrophysiology

2.4.1 Voltage-clamp electrophysiology (HEK293 cells)

Electrophysiological recordings were undertaken 24-48 h after HEK293 cell transfection. Coverslips carrying HEK cells were transferred to a recording chamber and transfected cells were identified by their EGFP fluorescence (excitation at 465-495 nm wavelength) using a Nikon Eclipse E600FN microscope (Nikon Instruments).

Cells were constantly perfused with Kreb's solution (5 mM HEPES, 140 mM NaCl, 4.7 mM KCl, 1.2 mM $MgCl_2$, 2.5 mM $CaCl_2$, 11 mM glucose, pH 7.4 with NaCl,). Whole-cell patch-clamp electrophysiology was performed using thin wall borosilicate glass electrodes (World Precision Instruments, TW150-4) with a tip resistance between 2 and 4 MΩ filled with internal solution (10 mM HEPES, 140 mM KCl, 1 mM $MgCl_2$, 4 mM MgATP, 10 mM ethylene glycol-bis(2-aminoethylether)-*N,N,N',N'*-tetraacetic acid (EGTA), pH7.2). Osmolarity of the internal solution (300 ± 10 mOsm/l) was measured with a vapour pressure osmometer (Wecsor Inc, Model 5520). Prior to any measurements the osmometer was calibrated with a standard osmolarity solution of 290 mOsm/l (Reagecon Osmolarity standard, Fisher Scientific).

Membrane currents were recorded using an Axopatch 200B amplifier (Axon Instruments, Molecular Devices); voltage-clamp configuration was used for recording from HEK293 cells with a holding potential of -30 mV ± 10 mV (unless otherwise stated). Membrane currents were filtered at 4 kHz and digitised at 50 kHz (Digidata 1320A, Molecular Devices). Data was acquired using Clampex software (version 10.2, Molecular Devices).

Responses to brief applications (3-5 s) of GABA +/- drugs of interest (see ***Table 2.4*** for full list of drugs used) were recorded. Local drug application onto the recorded cell was achieved using a U-tube (made by Prof. Trevor Smart), with 2 minutes in between the doses to achieve optimum recovery from desensitisation. U-tube has an approximate solution exchange time between 100 and 200 ms (Mortensen and Smart, 2006). ***Figure 2.1*** shows a representation of a 'patched' HEK293 cell and the U-tube setup.

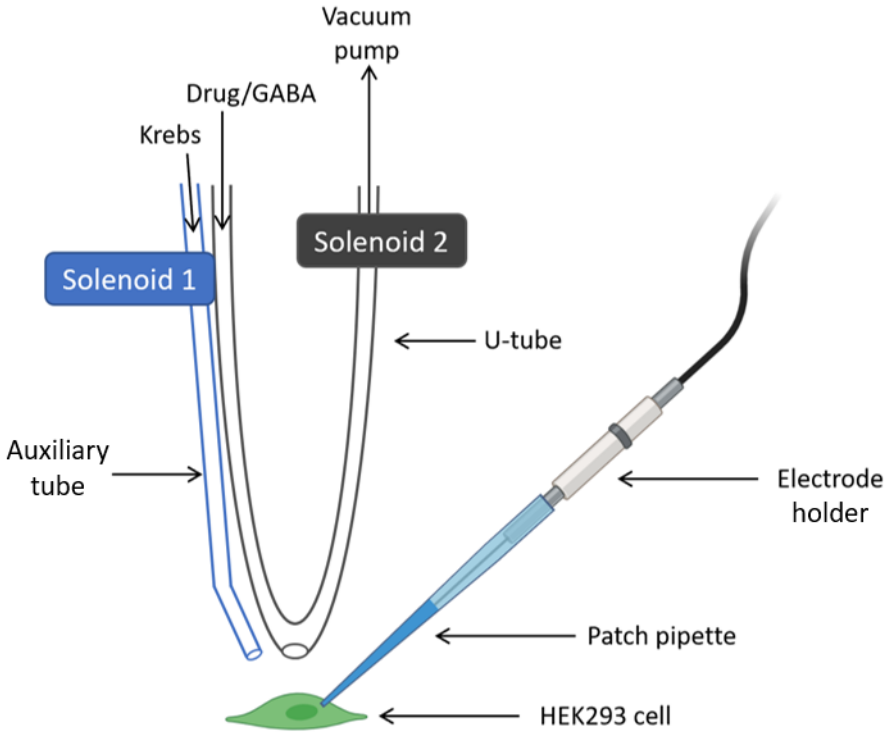

Figure 2.1 A schematic representation of U-tube drug application onto a patch-clamped HEK293 cell. eGFP transfected HEK293 cell (shown in green) patched with electrode fabricated as described in text. The electrode is connected to the head stage, amplifier and digitiser (not shown) to record changes of membrane currents upon GABA +/- drug application. The U-tube (represented in grey) delivers GABA +/- drugs to the cell, whereas the auxiliary tube (shown in blue) carries Krebs solution to the cell. Flow in each tube is controlled by a separate solenoid, which allows for rapid precise drug application. When both solenoids are open, drug passes around the U-tube small hole directly to the waste (not shown) under suction from the vacuum pump whilst the auxiliary tube successfully carries Krebs into the bath chamber (not shown). When the solenoids are closed, Krebs delivery onto the cell stops, and GABA +/- drug no longer circulates around the U-tube but instead flows onto to the HEK293 cell via a small hole in the tip.

Table 2.4 List of pharmacological compounds used throughout this project. Drug stock concentrations were prepared in an appropriate solvent. Where DMSO was used, its final concentration was below 0.1% (v/v).

Compound	Source	Solvent	Stock [conc.]	Final [conc.]
(+)-Bicuculline-methiodide	Sigma	DMSO	50 mM	50 µM
D-AP5	Sigma	ddH_2O	50 mM	50 µM
Diazepam	Roche	DMSO	1 mM	≤ 1 µM
Flurazepam		DMSO	1 mM	≤ 1 µM
GABA	Sigma	ddH_2O	1-3 M	≤ 30 mM
Glycine	Sigma	ddH_2O	200 mM	200 µM
Kynurenic acid	Sigma	Kreb's solution	Powder	1 mM
Nocodazole	Sigma	DMSO	10 mM	10 µM
Picrotoxin	Sigma	DMSO	100 mM	100 µM
PF-06372865	Pfizer	DMSO	1 mM	≤ 1 µM
$ZnCl_2$	Sigma	ddH_2O	10 mM	10 µM

2.4.2 Electrophysiology data analysis (HEK293 cells)

All HEK293 cell recordings were processed and analysed using Clampfit software (version 11.2, Molecular devices).

At the start of all recordings, a high dose of GABA (EC_{80}-EC_{100}) was applied at least three times at regular intervals (2 minutes) to ensure a stable current response. Throughout the experiment, the series resistance (R_s) was monitored closely for any changes. If R_s changed of more than 20%, the experiment was terminated. To produce a robust concentration-response curve, the order of GABA (+/- drug) concentrations applied was randomised to avoid any systematic error (e.g. desensitisation between consecutive dose applications). Every third dose, a reference concentration of GABA was applied (usually the maximum concentration), to which the responses were normalised to. Current responses for each concentration were normalised to the current evoked by this maximum dose of GABA, and expressed as a percentage, using a formula:

Equation 1:

$$X_{norm} = \frac{X}{X_{max}} \times 100\%$$

Where X_{norm} is the normalised current evoked by the concentration of interest, X is the observed current at a concentration of interest and X_{max} is the current evoked by the maximum dose to which the current is normalised to. Concentration-response profiles were then plotted by fitting the normalised current response data using the Hill equation:

Equation 2:

$$\frac{I_{[A]}}{I_{max}} = \frac{1}{1 + (\frac{EC_{50}}{[A]})^n}$$

Where $I_{[A]}$ is the peak current amplitude evoked by a defined concentration *[A]* of agonist (here i.e. GABA), I_{max} is the maximal current, EC_{50} is the concentration required to elicit a half maximal response and *n* is the Hill coefficient. Single component concentration response curves were plotted and fitted using GraphPad Prism software (version 8.4.2).

For multicomponent concentration-response curves fitting, a modified Hill equation was used:

Equation 3:

$$I_{[A]} = \sum_{y=1}^{x} \frac{I_{max}}{1 + (\frac{EC_{50}}{[A]})^n}$$

Where *x* is the number of fitted components. All $\alpha\alpha^{mut}\beta\gamma 2$ concentration response profiles were fitted with two and three Hill components. Fits were ranked according to χ^2 value where a better fit corresponded to the smallest χ^2 value of the two. EC50 and Imax were allowed to differ for each component, while the Hill coefficient was assumed to be the same for all components to reduce the degrees of freedom during

the fitting procedure. This Hill coefficient is referred to as cumulative Hill coefficient in Chapter 3.

Experiments where the optimum concentration of benzodiazepine (BDZ) potentiation was determined, were set up in the following way: first, GABA concentration-response profiles for a construct of interest (α1β2γ2L or α2β2γ2L) were obtained and EC_{15} ($EC_{10\text{-}20}$) was estimated. This dose was then selected to determine BDZ potentiation profiles. The following equation was used to estimate the percentage potentiation of EC_{15} GABA concentration with BDZ:

Equation 4:

$$\%\ potentiantion\ EC_{15}\ GABA = \frac{I_{EC_{15}[GABA+BDZ]} - I_{EC_{15}[GABA]}}{I_{EC_{15}[GABA]}} \times 100\%$$

Where *I* is the peak current amplitude, *EC_{15}[GABA+BDZ]* is the concentration of GABA producing 15% maximal response with a concentration of BDZ, and *EC_{15}[GABA]* is the GABA concentration EC_{15} alone. BDZ potentiation curve was fit using the Hill equation described above (***Equation 2***).

Once the BDZ concentration-response curve was plotted, a sub maximum dose of BDZ (usually 300 nM) was noted and used for further experiments. To determine the degree of BDZ potentiation on the whole GABA response profiles, a fixed dose (300 nM) of BDZ was used. Firstly, range of GABA concentrations were applied as described above to obtain the dose-response relationship. Then, a maximum dose of GABA (1 mM) with 300 nM BDZ was applied to make sure that the maximum GABA response with or without BDZ is the same. Subsequently, the concentration-response relationship was obtained for the same GABA doses with 300 nM BDZ. Experiments were performed with BDZ pre-incubation prior to GABA+BDZ application, unless otherwise stated. BDZ in Krebs was delivered through the auxiliary tube (see ***Figure 2.1***) for 20 seconds – 2 minutes (depending on the BDZ used) prior to a rapid GABA (+BDZ) application through the U-tube. Peak currents were normalised, plotted and fitted using ***Equation 1 and 2***. The GABA EC_{50} values in the presence of drug (GABA + BDZ) were obtained in the same way as EC_{50} GABA values alone.

Zn^{2+} inhibition experiments were also performed to check for the incorporation of the γ subunit in $GABA_A$ receptors (αβ or αβγ pentamers). To do this, a low concentration of Zn^{2+} was used (10 µM) (Hosie et al., 2003). This concentration blocks αβ-containing $GABA_A$ receptors, but not αβγ-containing receptors. From the GABA concentration-response profiles, an EC_{80} was estimated for each transfection (~30 µM for α1β3γ2L, α2β3γ2L, α1α2β3γ2L and α1α2β3) and used to determine Zn^{2+} inhibition. This was achieved by preincubating transfected HEK293 cells with 10 µM Zn^{2+} through the auxiliary tube (see ***Figure 2.1***) and subsequently applying an EC_{80} GABA + 10 µM Zn^{2+}. To calculate the Zn^{2+} inhibition percentage, the following formula was used:

Equation 5:

$$\%\ EC_{80}\ GABA\ inhibition = \frac{I_{EC_{80}[GABA]} - I_{EC_{80}[GABA+Zn^{2+}]}}{I_{EC_{80}[GABA]}} \times 100\%$$

Where $EC_{80}[GABA]$ is the current of GABA concentration producing 80% maximal response, and $[GABA+Zn^{2+}]$ is GABA applied with pre-incubated Zn^{2+}. The data was plotted as a bar chart with the mean percentage inhibition EC_{80} GABA ± s.e.

In some experiments, transfected receptors showed a high level of spontaneous activity in the absence of GABA. To quantify this spontaneous current, a saturating dose of GABA was applied to determine maximal whole cell current. Subsequently, when the current baseline was reached a high concentration of picrotoxin (PTX), 100 µM, was applied to block the spontaneous $GABA_A$ receptor activation (see ***Figure 2.2***). Spontaneous currents were then calculated as a percentage of the total $GABA_A$ receptor current using the following equation:

Equation 6:

$$\%\ I_{Spontaneous} = \frac{I_{PTX}}{I_{PTX} + I_{EC_{max}[GABA]}} \times 100\%$$

Where I_{PTX} is the current inhibited by PTX.

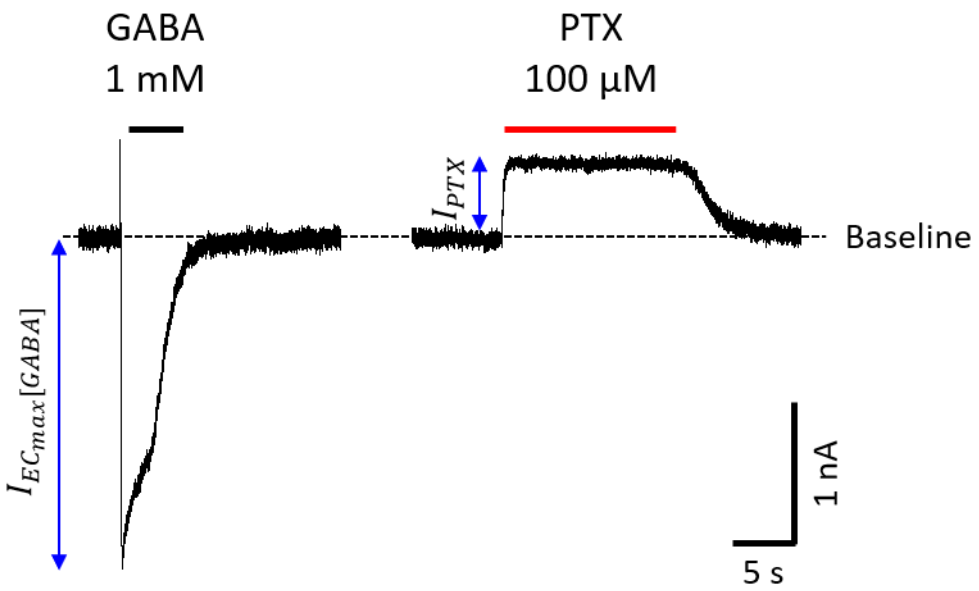

Figure 2.2 Calculating spontaneous activity of recombinant GABA$_A$ receptors. A saturating GABA concentration (1 mM GABA) was applied to HEK293 cells transfected with GABA$_A$ receptor subunit combinations. GABA-activated current amplitude was noted as $I_{EC_{max}[GABA]}$. Once the current returned to baseline, a high dose of PTX (100 µM) was applied, revealing the spontaneous activity of the construct (I_{PTX}). These two values were used to calculate the percentage spontaneous activity, as described in ***Equation 6***.

2.4.3 Voltage-clamp electrophysiology (neurones)

Neuronal electrophysiological recordings were undertaken using the same experimental set-up as described in ***Section 2.4.1***. Generally, a slightly higher resistance of the electrode tip was used (between 3 and 5 MΩ) compared to that for HEK293 cells. Electrode tips were filled with internal solution (10 mM HEPES, 2 mM NaCl, 2 mM $MgCl_2$, 0.5 mM $CaCl_2$, 140 mM CsCl, 5 mM ethylene glycol-bis- N,N,N',N'-tetraacetic acid (EGTA), 2 mM Na_2ATP, 0.5 mM Na_2GTP, 2 mM QX-314, pH7.3) with osmolarity of 300 ± 10 mOsm/l.

Cells were constantly perfused with a modified Kreb's solution, pH7.3 (see recipe in ***Section 2.4.1***), to which 2 mM kynurenic acid was added to block excitatory post synaptic currents (EPSCs). Neuronal recordings were performed at a holding potential of -60 mV. Drugs (if used) were bath-applied by addition to the perfusing Kreb's solution.

Recording were briefly interrupted at 1-minute intervals, where the series resistance (R_s) was calculated, to monitor any changes. If R_s changed by more than 20%, the voltage-clamp experiment was terminated, and all data gathered for this neurone was discarded.

2.4.4 Electrophysiology data analysis (neurons)

The analysis of GABA-mediated spontaneous inhibitory postsynaptic currents (sIPSCs) was performed using programmes: WinEDR (version3.9.4, John Dempster) for event detection and WinWCP (version 5.5.5, John Dempster) for further analysis.

Recordings were firstl imported to WinEDR, where parameters were set for optimal synaptic event detection. Depending on the recording baseline stability and noise, the following threshold parameters were used: amplitude of 6-9 pA deviation from the baseline (negative), with a duration of 1-2 ms. The events were then detected by the programme and all events were manually checked before exporting to WinWCP. Here, all validated events were used to calculate the average sIPSC amplitude and frequency. For further analysis of sIPSC kinetics, at least 50 'clean' events (uncontaminated rise and decay phases) were selected. These selected events were aligned at the start of their rise phases before averaging to create mean sIPSC waveforms. The averaged waveforms were then used for fitting mono- or bi-exponential curves to the sIPSC decay phase. A better fit (usually bi-exponential) was used for comparison afterwards. From a bi-exponential fitting, a weighted tau (τ_w) value was calculated using the following formula:

Equation 8:

$$\tau_W = \frac{A_1 \times \tau_1 + A_2 \times \tau_2}{A_1 + A_2}$$

Where τ_1 and τ_2 are the time constants of each exponential component, and A_1 and A_2 are the relative amplitude contributions to the overall bi-exponential fit.

2.5 Neuronal and HEK293 cell immunostaining and confocal imaging

2.5.1 Antibody labelling

HEK293 cells were stained 48 hours after transfection. Hippocampal E18 neuronal cultures were fixed and stained on day 14 (D14) after the culture. Neurons were immuno-labelled for either endogenously expressed $GABA_ARs$, or for exogenously transfected receptor subunits. For the latter, hippocampal cultured neurons were transfected on day 7 (D7) after plating.

The same protocol of immunostaining was used for neurons and HEK293 cells. Cells were cultured on 22 mm coverslips (HEK293 cells) and 18 mm coverslips (hippocampal neurons). Cells were thoroughly washed with phosphate buffered saline (PBS) (Sigma, P4417) before they were fixed in 4% paraformaldehyde (PFA) / 4% sucrose (w/v) in PBS for 5 minutes at room temperature (RT). After extensive washing, cells were incubated with 10% normal goat serum (NGS) in PBS for 20 min to block any non-specific binding of primary antibodies and subsequently washed with 1% bovine serum albumin (BSA) in PBS. Extracellular primary antibodies were added to coverslips to label surface protein of interest for 1 hour. All antibodies (primary and secondary) were diluted in 3% NGS in PBS to a desired concentration. A complete list of antibodies used in this project can be found in ***Table 2.5***. To minimise the amount of antibodies used, 50 µl of diluted antibody mixture was pipetted onto parafilm to give a droplet. Coverslips were taken out of 35 mm dishes, excess liquid removed carefully with a tissue, before being inverted onto the antibody mixture droplet. To prevent evaporation of the antibody solution, the coverslips were covered with the cap from the dishes. At the end of the incubation, coverslips were gently lifted and placed back into the dishes, where they were washed with 1% BSA in PBS before permeabilization (where necessary to label intracellular proteins). To permeabilise the cells, coverslips were incubated in PBS with 0.1% Triton X-100 for 5 minutes and then extensively washed. Before adding antibodies to label intracellular proteins, cells were incubated with the same blocking mixture as before (10% NGS in PBS, 20 minutes). After extensive washing with 1% BSA in PBS to remove unbound antibodies, cells were subjected to secondary antibody labelling. Secondary

antibodies were Alexa Fluor® labelled (see ***Table 2.5*** for details), therefore coverslips were protected from light during subsequent incubations to prevent fluorophore bleaching. Coverslips were then washed 4 times with 1% BSA in PBS for 5 minutes to wash off all the unbound secondary antibodies, before being mounted onto the glass slides using the Prolong Gold mounting reagent (Thermo Fisher Scientific, P36930) and left at RT to cure overnight. For storage, slides were kept in the dark at 4^{o}C.

Table 2.5 List of antibodies used throughout this project. Primary antibodies were used for immunocytochemistry (ICC) and/or proximity ligation assay (PLA) at a concentration stated in column 5 of the table. Secondary antibodies were conjugated to Alexa Fluor®.

	Antibody	Species	Epitope	Dilution	Catalogue number	Source
Primary Antibodies	Polyclonal anti-$GABA_A$ α1	Rabbit	Amino acids 1-15 from rat $GABA_A$ α1	1:500	Ab33299	Abcam
	Polyclonal anti-$GABA_A$ α1	Rabbit	Cytoplasmic loop from rat $GABA_A$ α1	1:500	06-868	Upstate
	Polyclonal anti-$GABA_A$ α2	Rabbit	Amino acids 29-37 from rat $GABA_A$ α2	1:500	224-103	Synaptic Systems
	Monoclonal anti-$GABA_A$ α5	Mouse	Amino acids 368-419 from human $GABA_A$ α5	1:500	N415/24	NeuroMab
	Monoclonal anti- $GABA_A$ β2,3 (Clone BD17)	Mouse	Extracellular domain (β chain) from bovine $GABA_A$ β2,3	1:500	MAB341	Sigma-Aldrich
	Polyclonal anti-$GABA_A$ γ2	Rabbit	Amino acids 39-53 from rat $GABA_A$ γ2	1:100	AGA-005	Alomone labs
	Polyclonal anti-$GABA_A$ γ2	Rabbit	Cytoplasmic loop from rat $GABA_A$ γ2	1:300	832A-GG2C	PhosphoSolutions
	Monoclonal anti-$GABA_A$ δ	Mouse	Internal region from rat $GABA_A$ δ	1:500	200-301-F33	Rockland
	Monoclonal anti-gephyrin	Mouse	Amino acids 326-550 from rat gephyrin	1:500	147-111	Synaptic Systems
	Polyclonal anti-MAP2	Chicken	Full length protein of cow MAP2	1:100	Ab92434	Abcam
	Polyclonal anti-Vesicular inhibitory amino acid transporter (VIAAT)	Guinea Pig	Amino acids 106-120 from rat VIAAT	1:200	AGP-129	Alomone labs
Secondary Antibodies	Alexa Fluor® 488 anti-chicken IgY (H+L)	Goat	n/a	1:750	A32931	Invitrogen
	Alexa Fluor® 488 anti-rabbit IgG (H+L)	Goat	n/a	1:750	A32731	Invitrogen
	Alexa Fluor® 555 anti-guinea pig IgG (H+L)	Goat	n/a	1:750	A21435	Invitrogen
	Alexa Fluor® 555 anti-mouse IgG (H+L)	Goat	n/a	1:750	A31570	Invitrogen

	Alexa Fluor® 555 rabbit IgG (H+L)	Goat	n/a	1:750	A21428	Invitrogen
	Alexa Fluor® 647 anti-chicken IgY (H+L)	Goat	n/a	1:750	A21449	Invitrogen
	Alexa Fluor® 647 anti-guinea pig IgG (H+L)	Goat	n/a	1:750	A21450	Invitrogen

2.5.2 Proximity Ligation Assay (PLA) method

Proximity ligation assay (PLA) is a powerful method that allows sensitive and highly specific detection of protein interactions at a single molecule resolution. It employs the basis of immunofluorescent labelling and, therefore, can be visualised using conventional confocal microscopy. The principle of the PLA methodology is briefly outlined in ***Figure 2.3***. Normally, two primary antibodies (raised against different species) are used to detect the epitopes of interest. Then, two secondary antibodies coupled to a specific oligonucleotide sequences (known as PLA PLUS and MINUS probes) bind to the primary antibodies. If the PLA probes are in close proximity (≤30 nm), the oligonucleotides from the complimentary PLA probes hybridise and are subsequently ligated to form a closed circular DNA template. At this point, DNA polymerase and fluorescently labelled oligonucleotides are added, and the circular DNA loop acts as a template for rolling circle amplification. This allows ~1000-fold amplification of the PLA signal that can then be directly visualised with confocal microscopy. The signals are discrete PLA dots, each representing a single interaction (Gomes et al., 2016b).

2.5.3 PLA fluorescence protocol

This protocol was performed on HEK293 cells and cultured hippocampal neurons. Neurones were either transfected (see ***Sections 2.2.2 and 2.3.2*** for details) or used to identify native protein interactions. PLA was performed on its own in HEK293 cells or alongside immunostaining in neurones. Cells were washed, fixed and blocked as described in **Section 2.5.1**. PLA was performed between α1 and α2, α1 and α5, or γ and δ $GABA_AR$ subunits. If the antibodies used for PLA recognised intracellular epitopes, the cells were permeabilised prior to PLA. Details can be found in ***Table 2.6***.

All incubations were performed on parafilm with coverslips inverted and in a heated humidity chamber at 37 ˚C. Between incubations, cells were washed twice with 1X wash buffer A (Duolink®, DUO82049) for 5 minutes, unless otherwise stated. The final volumes of reagents added to each coverslip were 40 µl per incubation.

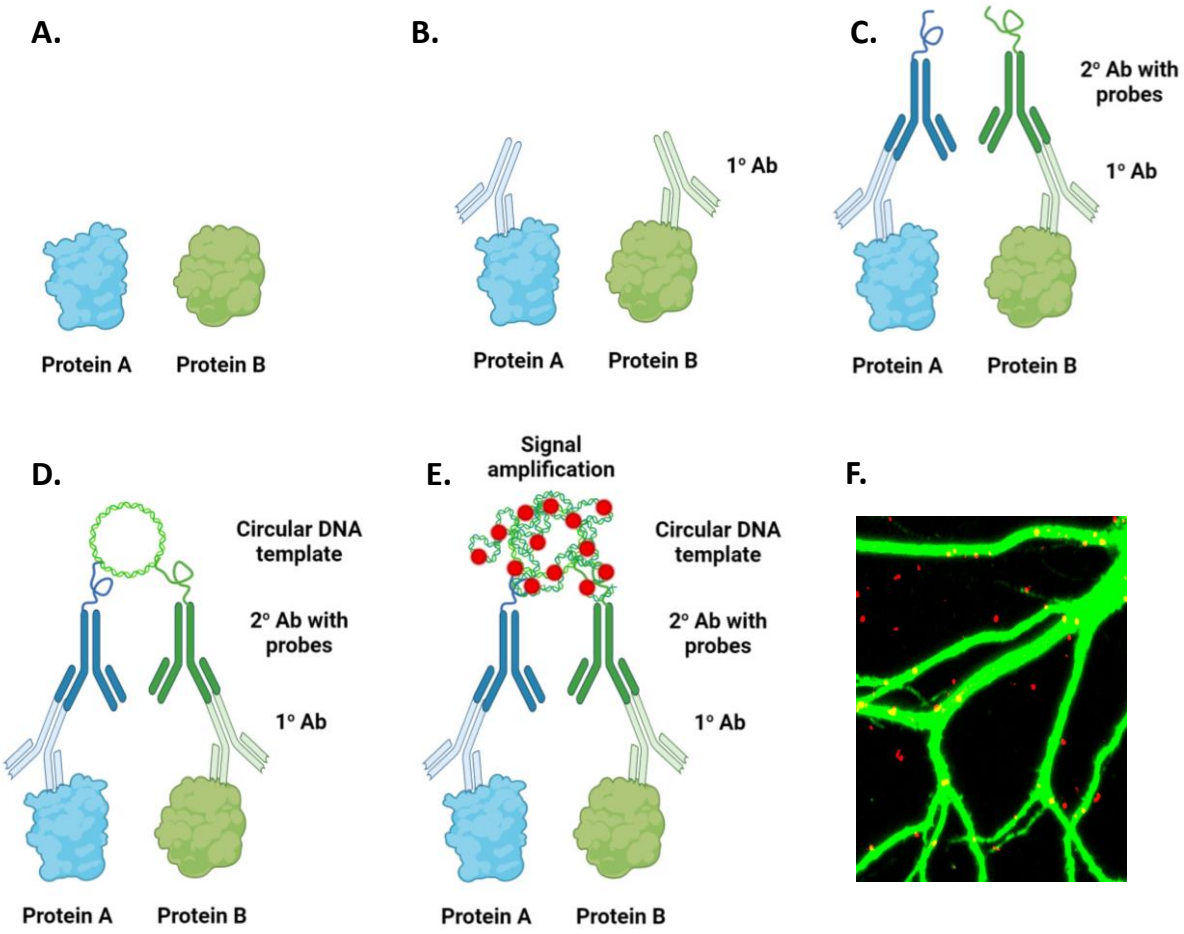

Figure 2.3 Proximity ligation assay (PLA) principle. **A.** Two proteins that are in close spatial proximity. **B.** Primary antibodies raised in different species bind to target protein epitopes. **C.** Secondary antibodies coupled to oligonucleotides (PLA probes) recognise primary antibodies. **D.** The oligonucleotides are in close proximity, hybridise and form a close circular DNA template following ligation. **E.** DNA template is amplified with addition of DNA polymerase and fluorescently labelled oligonucleotides. **F.** PLA signal can be detected with confocal microscopy, where each PLA dot represents a discrete protein interaction.

After blocking, primary antibodies were diluted in Duolink® antibody diluent at a concentration used for ICC and coverslips incubated for 1 hour. After washes, PLA probes (PLUS and MINUS) were diluted in antibody diluent, applied to the coverslips and subsequently incubated for 1 hour. Following PLA probe incubation, 5X Duolink ligation buffer was diluted in ddH_2O and ligase (Duolink®, DUO92008) was added to

1X ligation buffer (1:40). This mixture was applied to the coverslips and incubated for 40 minutes. During the washes, 5X Amplification buffer was diluted in ddH_2O and DNA polymerase (Duolink®, DUO92008) was added to it at 1:80 dilution. The mixture was then added to the coverslips and incubated for 110-120 minutes. The final washes were subsequently performed: two washes for 10 minutes with 1X wash buffer B ((Duolink®, DUO82049) followed by two 1-minute washes with 0.01X wash buffer B. The coverslips were mounted with a small volume of Duolink® *in situ* mounting medium with DAPI (DUO82040) and left in the fridge overnight before the edges were sealed with nail varnish. The coverslips were then imaged within 3 days with a confocal microscope.

Table 2.6 Antibodies used for PLA. Primary and secondary antibodies used for a detection of protein interaction are listed in columns 2 and 3 of the table. For more details of target epitopes and dilutions see ***Table 2.5***. (*****) - rabbit polyclonal anti-$GABA_A$ α2 antibodies (224-103) were conjugated to the PLUS probe using *In Situ* Probemaker PLUS kit (Duolink®, DUO92009) as per manufacturer's instructions. This antibody was used during the primary incubation step of the protocol.

PLA targets	Primary antibodies	Secondary probes	Permeabilised?
α1 and α2	Rabbit polyclonal anti-$GABA_A$ α1 (ab33299)	Anti-rabbit MINUS probe (DUO 92005)	No
	Rabbit polyclonal anti-$GABA_A$ α2 (224-103) conjugated to PLUS probe*****	n/a	
α1 and α5	Rabbit polyclonal anti-$GABA_A$ α1 antibody (06-868)	Anti-rabbit MINUS probe (DUO 92005)	Yes
	Mouse monoclonal anti-$GABA_A$ α5 (N415/24)	Anti-mouse PLUS probe (DUO 92001)	
γ2 and δ	Rabbit polyclonal anti-$GABA_A$ γ2 (832A-GG2C)	Anti-rabbit MINUS probe (DUO 92005)	Yes
	Mouse monoclonal anti-$GABA_A$ δ (200-301-F33)	Anti-mouse PLUS probe (DUO 92001)	

2.5.4 Image acquisition (confocal microscopy)

Fluorescence images were acquired using a Zeiss Axiscop LSM510 confocal microscope (Carl Zeiss Ltd.) and Zeiss acquisition software. The wavelength of lasers used for image collection were 488 nm (Alexa Fluor 488), 543 nm (Alexa Fluor 555) and 643 nm (Alexa Fluor 647). Plan-NEOFLUAR 40X/1.4NA (numerical aperture) oil DIC, and Plan-Achroplan 40X/0.8NA water, Plan-APOCHROMAT 63X/1.4NA oil DIC objective lenses (Zeiss) were used. Images were acquired using Zeiss LSM software. 8-bit images were taken at 1024x1024 pixel resolution. Normally, scan speeds 6 or 7 were used (translating to pixel dwell times of 7.68 µs and 3.84 µs respectively). Laser intensity, detector gain, and detector offset were optimised on the control (wt and control treated) coverslip and kept constant throughout the day for the same experiment.

An area to be imaged was selected using 488nm wavelength laser. For HEK293 cells, eGFP was used as a transfection marker. For hippocampal cultured neurones, either eGFP was used for transfected cells or MAP2 labelling as a means to identify pyramidal neurones morphology. Ten to fifteen images were taken for each condition and this process was repeated on three different cultures for neurones/batch of transfected HEK293 cells. For PLA, images were taken as Z-stacks, where the top and bottom of the neurone was marked, and consecutive optical slices of optimal thickness were taken (0.36 µm for Plan-APOCHROMAT 63X/1.4NA oil DIC lens).

2.5.5 Image analysis

All confocal images were analysed using Image J software (version 1.52p). For HEK293 cells, the mean fluorescence of cell surface proteins was determined for each cell by selecting a region of interest (ROI) around the cell membrane using the eGFP signal. For neurones, an ROI was selected as a dendritic area with proximity to the soma using either MAP2 reactivity or the eGFP fluorescence signal. Average fluorescence of the channel of interest was then calculated. Background fluorescence, quantified

using an area with no cells, was subtracted from the average value to get a background-adjusted fluorescence intensity. The mean fluorescence intensities were then calculated in Prism GraphPad software (version 9.2.0) and compared using an appropriate statistical test.

For $GABA_AR$ cluster analysis using ICC, dendritic ROIs were selected as described above. The background fluorescence of the appropriate channel was then noted. This was used to set a threshold for image segmentation (10X background intensity) and subsequent cluster analysis. Parameters quantified from the cluster analysis were average particle size and percentage of ROI area occupied by all clusters.

For the analysis of PLA images, the z-stacks were first superimposed to aid drawing a ROI (same process as above). The ROI was saved and used on the non-superimposed images thereafter. The PLA signal channel (red) was selected, and the mean background intensity was noted. The area outside of the ROI was subsequently deleted, and the remaining image was used for analysis (PLA dot count and co-localisation with synaptic markers). The same process was applied to VIAAT or gephyrin immunolabelling (blue channel). Here, the Distance Analysis (DiAna) Image J plug-in (version 1.48) was used (Gilles et al., 2017). Both red and blue channels were filtered and segmented to generate binarized images suitable to apply object-based colocalization method within DiAna (see parameters in **Table 2.7**). The objects delineated by this process are PLA dots or VIIAT/gephyrin clusters. Segmented images were then analysed, to quantify percentage colocalization between PLA dots and synaptic markers (VIAAT or gephyrin) using spatial overlap between clusters to define colocalization. Average cluster volume and intensity were also quantified.

Table 2.7 DiAna segmentation parameters. The parameters used were optimised by visual inspection.

Channel	PLA signal (red)	VIIAT/gephyrin (blue)
Segmentation type	Classic	Classic
Filter type	Median	None
Threshold	4X background	10X background
Minimum object size (pxl)	27	27

2.5.6 Analogue detector calibration for spatial intensity distribution analysis (SpIDA)

To allow us to take into account the inherent detector noise, we determined the analogue detector signal for the 488 nm Argon laser line of the Zeiss LSM510 confocal microscope using Plan-APOCHROMAT 63X/1.4NA oil DIC objective lenses (***Section 2.5.4***). Here, we followed the methods described by Barbeau et al., 2013. Briefly, green chroma-slides (Chroma, 82001) were used to determine the broadening of the signal from photomultiplier tubes, PMTs. A spot scanning mode on the Zeiss LSM510 confocal microscope was applied to measure the PMT shot noise by systematically increasing the intensity of the laser from 0 to 90 % (while the tube current, detector and amplifier gain were kept constant). The detected signal resulted in a uniform illumination profile. The mean variance of the resulting signals was obtained using Image J software (version 1.52p) and plotted against the mean intensity. For more detail, see ***Section 5.2.1***. All images were obtained at 12-bit data depth, with a 1024x1024 pixels in size. Three scan speeds were used to calibrate the detector: scan speed 8 (dwell time 3.04 µs/pixel), scan speed 7 (dwell time 3.84 µs/pixel), scan speed 6 (dwell time 7.68 µs/pixel). Two PMT detector gains were tested 450 V and 500 V, with an amplifier offset of 0. Pinhole size was kept constant at 1 Airy unit.

2.5.7 Laser beam waist radius measurements

To measure the laser beam waist radius, fluorescent 100 nm sized TetraSpec microspheres (Invitrogen, T14792) were imaged as Z-stacks with the 488 nm line of the Argon laser. Obtained images were analysed with MetroloJ plugin (Matthews and Cordelieres, n.d.) of the Image J software (version 1.52p). This plugin generates the point spread function report (PSF) from which the beam waist area can be calculated. The fluorescent spheres used in our system were below its resolution (Cole et al., 2011). This will be described in more detail in ***Section 5.2.1***.

2.6 Statistical analysis

To assess potential differences in GABApotency on $GABA_AR$ constructs (Chapter 3), statistical analyses were performed on pEC_{50} values, where pEC_{50}= -log(EC_{50}).

All the data was plotted (mean ± s.e.m.), and statistical analysis performed in Prism GraphPad software (version 9.2.0). All datasets were tested for normality using D'Agostino-Pearson normality test. If the n number was too small to pass the D'Agostino-Pearson normality test or if the data was not normally distributed, Shapiro-Wilk test was used instead. If the data was normally distributed, an un-/paired t-test or one-way ANOVA with Tukey's post hoc multiple comparisons tests were used (two variables and multiple variables respectively). However, if the data was not normally distributed, Mann-Whitney or Kruskal-Wallis with Dunn's post hoc tests were performed. The threshold for statistical significance for all tests was set to p-value ≤ 0.05 (denoted by one asterisk (*)). P values lower than 0.05 were denoted as ** (p-value ≤ 0.01) or *** (p-value ≤ 0.001), **** (p-value ≤ 0.0001).

Chapter 3: Exploring the presence, abundance and subunit arrangement of 'hetero-alpha' $GABA_A$Rs in a transfected HEK293 cells

3.1 Introduction

The majority of $GABA_A$ receptor subtypes that occur in the brain are composed of two α, two β, and one γ subunits. The receptor subtypes containing one type of α subunit isoform ('homo-alpha') are well characterised in recombinant systems (Baumann et al., 2002; Olsen and Sieghart, 2008; Sigel and Steinmann, 2012). A multitude of biochemical including brain lysate co-immunoprecipitation and radioligand binding studies suggest that $GABA_A$ receptors with two distinct α subunit isoforms are expressed in various brain regions (Bohlhalter et al., 1996; Christie and de Blas, 2002; Fritschy et al., 1992; Fritschy and Mohler, 1995; Zezula and Sieghart, 1991). However, it is currently poorly understood what the physiological and pharmacological relevance of receptors with two heterologous α subunits is.

So far, electrophysiological studies of recombinant α1α3β2γ2, α1α5β2γ2, and α1α6β2γ2 $GABA_A$ receptors have shown that they display distinct GABA-activated kinetics and sensitivities (Ebert et al. 1994; Tia et al. 1996; Verdoorn 1994). Characterisation of GABA concentration response profiles in both HEK293 cells and *Xenopus* oocytes co-expressing α1, α3, β2, and γ2 subunits indicated that α1α3β2γ2 GABA sensitivity lies between that of α1β2γ2 and α3β2γ2 (Verdoorn 1994; Ebert et al. 1994). However, the GABA concentration response profile of α1α5β2γ2-injected Xenopus oocytes presented a leftward shift compared to its 'homo-alpha' counterparts: α1β2γ2 and α5β2γ2. Interestingly, some studies reported that the identities of both α subunits determine both the efficacy and apparent affinity of P4S – partial $GABA_A$ agonist (Hansen et al. 2001; Mortensen et al. 2002; Ebert et al. 1994). For example, when α1/α3 or α1/α5 subunits are co-expressed, the maximum efficacy of the 'hetero-alpha' injected oocytes is dictated by α1 subunit, whereas the P4S apparent affinity is dictated by both α subunit subtypes (Ebert et al. 1994). A different study reported conflicting evidence, demonstrating that both the efficacy and

apparent P4S affinity of α1α6β2γ2-expressing *Xenopus* oocytes is higher than α1β2γ2- and α6β2γ2- injected oocytes (S. L. Hansen et al., 2001). Later work on concatenated receptors have not observed the same P4S effect of any of the α1α6-containing receptors, suggesting that Hansen et al., was predominantly looking at αβ rather than αβγ $GABA_A$ receptors (Minier and Sigel, 2004c).

Additionally, 'hetero-alpha' $GABA_A$ receptors were suggested to have distinct kinetics upon fast GABA applications (Tia et al., 1996; Verdoorn, 1994). Both groups claim that τ of the fast component as well as its relative percentage in a double-exponential decay analysis of α1α3β2γ2 and α1α6β2γ2 expressing HEK 293 cells / oocytes is distinct from α1β2γ2/α3β2γ2 and α1β2γ2/α6β2γ2 receptors. However, from the data presented in those studies deactivation kinetics of 'hetero-alpha' α1-containing $GABA_A$ receptors resemble the decay phases of α1β2γ2 receptors (Tia et al., 1996; Verdoorn, 1994). Given this similarity with deactivation of α1-containing receptors, the current evidence of 'hetero-alpha' α1α3 and α1α6 populations is inconclusive and requires a more in-depth analysis.

A study of recombinant $GABA_A$ receptors indicated that 1 μM benzodiazepine potentiation of GABA-evoked currents α1α3β2γ2 expressing cells, resulted in a 5-fold shift in GABA EC_{50}, compared to only a two- and a three-fold shifts in α1β2γ2- and α3β2γ2-expressing cells (Verdoorn, 1994). This could potentially implicate that the 'hetero-alpha' $GABA_A$ receptor populations show distinct benzodiazepine pharmacological properties. However, radioligand binding studies of purified rat cortical α1α3-containing receptors suggest that these receptors predominantly show α1-BDZ pharmacology, rather than that of α3 (Araujo et al., 1996). This could imply that the benzodiazepine pharmacology of 'hetero-alpha' receptors depends on the subunit arrangement in the pentamer, specifically on identity of the α subunit at the α/γ interface. However, up to this moment, our understanding of pharmacological signature of 'hetero-alpha' $GABA_A$ receptors is limited.

In this study, we investigated the existence of 'hetero-alpha' $GABA_A$ receptors using electrophysiology. Since α1 and α2 subunits are widely expressed across all brain regions, this work focused on electrophysiological analysis of α1α2-containing $GABA_A$ receptors (Pirker et al., 2000). So far, the abundance of α1α2-$GABA_A$ receptors has

been estimated to constitute the minority of all α1-containing receptors in cortical and total brain extracts (Benke et al., 2004a; del Río et al., 2001a; Duggan et al., 1991). However, α1α2 combination in the α2-containing receptors population of rat hippocampal and cortical extracts represented 36 % and 39 % respectively (Benke et al., 1997; del Río et al., 2001b). This mismatch of hetero-alpha receptors' relative abundance could be due to α1 $GABA_AR$ prevalence in expression over other α subunit isoforms (Hörtnagl et al., 2013).

Since $GABA_ARs$ containing both α1 and α2 subunits in the same receptor complex appear to be expressed at significant levels, it seems plausible that the inclusion of more than one α subunit isoform may affect $GABA_A$ receptor function. One of the obvious physiological properties that these receptors could have is their distinct GABA sensitivity signature, as observed with α1α3β2γ2 and α1α5β2γ2 receptor mixtures (Ebert et al., 1994; Verdoorn, 1994). It is well established that GABA sensitivity is determined by the identity of the α subunit present in the pentamer (Böhme et al., 2004). Furthermore, the two GABA binding sites at the β+/α- interface do not carry the same contribution to receptor activation, with site 2 having a threefold higher GABA affinity than site 1 (Baumann et al., 2003). Therefore, having two distinct α subunits could potentially bring greater pharmacological diversity to $GABA_A$ receptor function. Additionally, it is unknown how the expression of $GABA_A$ receptors with two distinct α-subunits would affect the benzodiazepine pharmacology of the receptor.

The first aim of this chapter was to co-express α1 and α2 subunits with either β2 and β3 subunits (plus γ2L) in HEK293 cells to examine their functional properties. Here, we wanted to assess whether 'hetero-alpha' subunit expression results in receptor combinations with unique properties (***Section 3.2***).

The second aim was to infer the number of distinct receptor populations (i.e. a mixture of α1β2/3γ2, α2β2/3γ2, α1α2β2/3γ2) when α1 and α2 subunits are co-expressed (***Section 3.3***). A modified version of the method (outlined below), first described by Chang et al., (1996) was applied. This approach has been widely used to study the stoichiometry of other $GABA_A$ receptor combinations as well as nAChRs and 5-HT3Rs.

The method is based on co-expression of wild-type and mutant subunits of each class (e.g. α^{WT} and α^{mut}) to infer the number of mutant subunit per receptor from the number of fitted components of a GABA concentration-response relationships (Chang et al., 1996a). In this study, a conserved leucine substitution at the 9' position in the TM2 domain was used as a reporter mutation, as it produces a profound leftward shift of the agonist concentration response profile (Chang et al., 1996a). The extent of the shift is directly correlated with the number of leucine substitutions per ion channel (one or two) and can therefore be used to infer the number of mutant subunits within each pentamer (one or two) (Chang et al., 1996a; Chang and Weiss, 1999).

Figure 3.1 outlines the principle behind inferring the number of receptor populations from multicomponent Hill equation fits. Assume that co-expression of $\alpha1^{mut}$ and $\alpha2^{WT}$ along with β2 and γ2L subunits will result only in expression of one type of α subunit per receptor pentamer: either $\alpha1^{mut}\beta2\gamma2L$ or $\alpha2\beta2\gamma2L$. Therefore, the GABA concentration-response profile would have two components representing GABA-evoked currents of 'homoalpha' receptor populations (one component from $\alpha1^{mut}$-containing and another from $\alpha2^{WT}$-containing receptors). The EC_{50} values for each component should be the same as those obtained from expression of pure $\alpha1^{mut}\beta2\gamma2L$ or $\alpha2\beta2\gamma2L$ receptors. Alternatively, if a $GABA_AR$ mixture resulting from $\alpha1^{mut}$ and $\alpha2^{WT}$ co-expression contained three distinct receptor populations: two 'homo-alpha' and one 'hetero-alpha' receptor populations, the concentration response relationship would be described as a sum of three Hill equations and therefore would produce three components ($\alpha1^{mut}\beta2\gamma2L$, $\alpha2^{WT}\beta2\gamma2L$, $\alpha1^{mut}\alpha2^{WT}\beta2\gamma2L$). The EC_{50} values for the first and third components would be equivalent to their 'homo-alpha' counterparts ($\alpha1^{mut}$ and $\alpha2^{WT}$). The intermediate component would represent receptors containing both $\alpha1^{mut}$ and $\alpha2^{WT}$ subunits in the same receptor complex. The EC_{50} value for this component can be calculated based on EC_{50} predictions from Chang et al., (1996). Briefly, the shift in GABA sensitivity with one copy of $\alpha1^{mut}$ in a receptor complex would be the square root of the EC_{50} shift observed with two copies of the mutation present ($\alpha1^{mut}\alpha1^{mut}$) (Chang

et al., 1996a) (see ***Section 3.3.2***). The same principle can be applied for $\alpha1^{WT}$ and $\alpha2^{mut}$ co-expression.

Here, $\alpha1^{L263S}$ and $\alpha2^{F65L}$ were used as reporter mutations to separate the concentration response profiles of α1β2/3γ2L and α2β2/3γ2L receptors. From the number of inflections in GABA dose response relationship of wild-type and mutant mixtures, we could infer the number of distinct receptor populations and their relative abundances.

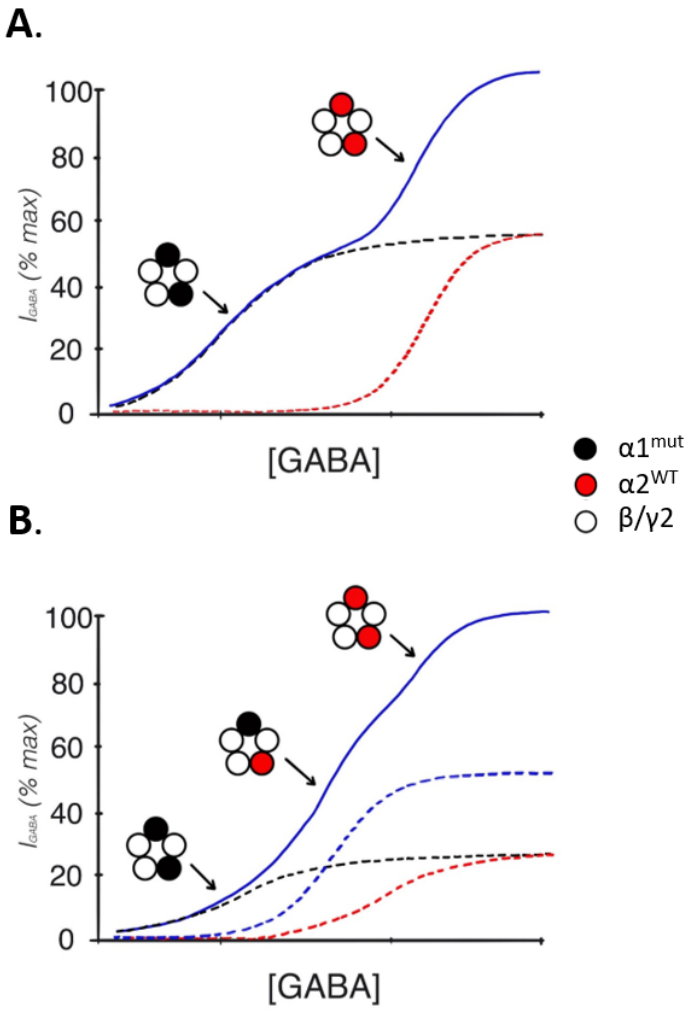

Figure 3.1 Possible number of components comprising the concentration-response relationship from co-expression of $\alpha1^{mut}$ and $\alpha2^{WT}$ subunits together with β and γ. Here, a reporter mutation in the α1 subunit was used (***see text***) to separate GABA apparent affinities of α1 and α2- containing receptors. Co-expression of $\alpha1^{mut}$ and $\alpha2^{WT}$ subunits allows the generation of multiple receptor populations within the same cell potentially containing zero,

one or two copies of the mutant subunits with distinct apparent GABA affinities which can be discerned from the number of components in the GABA curve fit. **A.** With the expression of two receptor populations containing only one type of α subunit per $GABA_A$ receptor complex, the concentration response curve, CRC, will be fit with a two-component Hill equation. The first component theoretically represents the activation of $\alpha1^{mut}$ $\alpha1^{mut}\beta\gamma2$ receptors, whereas the second component is due to $\alpha2^{WT}\alpha2^{WT}\beta\gamma2$ receptors. The GABA EC_{50} values for these two components should be approximately equal to the EC_{50} values obtained from expression of pure $\alpha1^{mut}\beta\gamma2$ and $\alpha2^{WT}\beta\gamma2$ receptors respectively. **B.** If $\alpha1^{mut}$ and $\alpha2^{WT}$ co-expression results in three populations (two 'homo-alpha' and one 'hetero-alpha'), the CRC should show three components. The first and third components in the GABA CRC represent $\alpha1^{mut}$ $\alpha1^{mut}\beta\gamma2$ and $\alpha2^{WT}\alpha2^{WT}\beta\gamma2$ populations, whereas the middle component is observed from activation of 'hetero-alpha' receptors, $\alpha1^{mut}\alpha2^{WT}\beta\gamma2$ and $\alpha2^{WT}\alpha1^{mut}\beta\gamma2$ (assuming subunit arrangement in a 'hetero-alpha' pentameric complex has no effect in GABA apparent affinity). The same logic can be applied with $\alpha1^{WT}$ and $\alpha2^{mut}$ co-expression. Figure modified from Chang et al., (1996).

The last aim of this chapter was to distinguish between the relative α subunit positioning in a 'hetero-alpha' $GABA_A$ receptor complex (i.e. α1γ2Lβα2β or α2γ2Lβα1β) (***Section 3.4***). Given that the benzodiazepine BDZ high affinity binding site is located at the α/γ interface, ablation of this site using a well characterised H101R mutation allows us to use this as a functional reporter to identify which α subunit sits adjacent to the γ subunit (Benson et al., 1998a; Kleingoor et al., 1993a; Rudolph et al., 1999). For example, by co-expressing $\alpha1^{H101R}$ and α2 subunits (+ β2/3 γ2L), all the α1/γ interfaces are BDZ insensitive (α1γ2Lβα1β and α1γ2Lβα2β), therefore potentiation of receptors only with α2/γ interfaces will be observed (α2γ2Lβα2β and α2γ2Lβα1β) and vice versa (see ***Figure 3.2***). In addition, a comparison between subunit arrangement of β2- and β3-containing 'hetero-alpha' $GABA_A$ receptors was made.

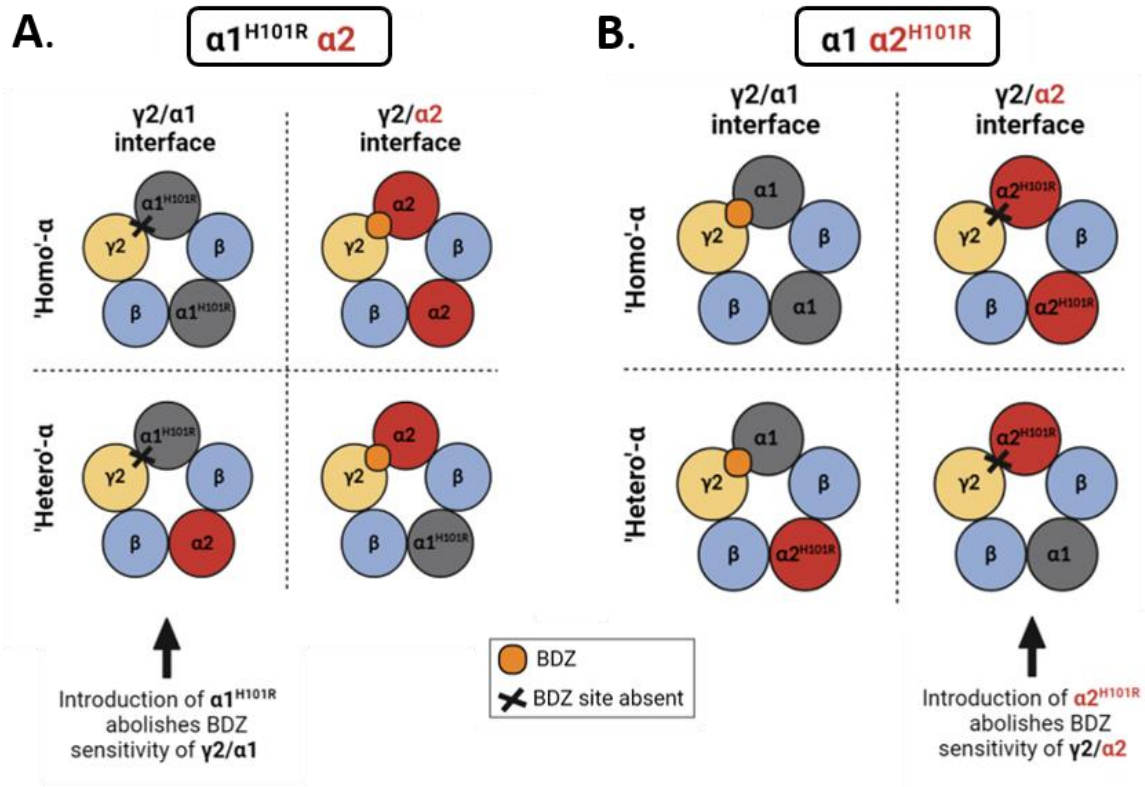

Figure 3.2 The H101R benzodiazepine insensitive mutation on the α subunit as a functional tool to determine 'hetero-alpha' $GABA_A$ receptor subunit arrangement. Co-transfection of α1 and α2 with β and γ2 subunits into HEK293 cells can result in four distinct receptor populations: α1γ2βα1β, α2γ2βα2β, α1γ2βα2β, α2γ2βα1β – all sensitive to BDZ at γ2/α interface. Introduction of an H101R substitution on an α subunit abolishes the sensitivity of BDZ at the γ2/α interface. **A.** Co-transfection of $α1^{H101R}$ and α2 (β, γ2) will result in $GABA_A$ receptor populations, which are either BDZ insensitive (γ2/$α1^{H101R}$) or γ2/α2 BDZ sensitive (γ2/α2). **B.** Co-transfection of α1 and $α2^{H101R}$ (β, γ2) results in $GABA_A$ receptor populations with two γ2/α interfaces: γ2/α1 (BDZ sensitive) and γ2/$α2^{H101R}$ (BDZ insensitive).

3.2 Results: electrophysiological assessment of 'hetero-alpha' wild type receptors

The first part of this electrophysiological examination of receptor heterogeneity was to establish the likelihood of two different isoforms of α subunits being co-assembled into single $GABA_A$ receptor pentamers. Initially, this was undertaken using wild-type α1 and α2 subunits.

3.2.1 Co-expression of α1 and α2 wild-type subunits form distinct population of receptors with higher apparent affinity to GABA

To assess the electrophysiological properties of 'hetero-alpha' subunit mixtures, α1 and α2 $GABA_A$ receptor subunits were expressed separately or as a combination. This was achieved by co-expressing equimolar ratios of α1 and/or α2 subunit cDNA constructs with β3, γ2L and eGFP – the latter construct was required to successfully identify transfected HEK293 cells. Green fluorescent (transfected) cells were identified and whole-cell voltage clamp was performed. The peak current responses to a range of briefly applied (4s) GABA concentrations (0.3 μM, 1 μM, 3 μM, 10 μM, 30 μM, 100 μM, 300 μM and 1 mM) were measured. GABA concentrations were applied to the cells in a random order and all responses were normalised to a saturating (maximal) GABA concentration that was applied at regular intervals to monitor response stability over time. The data were then fitted with the Hill equation (***Equation 2, Section 2.4.2***). Representative examples for GABA-evoked currents of α1β3γ2L, α2β3γ2L, α1α2β3 and α1α2β3γ2L are shown in ***Figure 3.3***.

The GABA EC_{50} values for α1β3γ2L and α2β3γ2L expressing HEK293 cells were 6.2 ± 1.0 μM and 15.3 ± 2.6 μM respectively (***Figure 3.3 B and C***) indicating that GABA is 2-fold more potent at the α1-receptor. These values are in agreement with the previously reported values (Mortensen et al., 2012b). Interestingly, when α1 and α2 were co-expressed with β3 and γ2L subunits, the GABA concentration response curve (CRC) was shifted to the left of both 'homo-alpha' control curves. The EC_{50} value of α1α2β3γ2L was measured at 3.6 ± 0.4 μM, statistically different from α2β3γ2L (P value ≤ 0.001). This could imply that α1 and α2 subunit co-expression in a heterologous expression system results in the formation of a new receptor complex since only three expression outcomes are likely with regard to α subunits: α1α1, α2α2 and α1α2. It is unlikely that the observed leftward shift of α1α2β3γ2L CRC is due to the expression of single subunit isoforms (α1/2, β3, γ2L homo-pentamers), αγ, or βγ combinations, since these receptors are retained in the endoplasmic reticulum (Connolly et al., 1999, 1996). However, $GABA_A$ receptors formed of αβ pentamers

(lacking γ2L) were previously shown to form functional receptors with higher apparent affinity for GABA (Connolly et al., 1996; Sigel et al., 1990; Verdoorn et al., 1990). Therefore, the newly formed receptor population is likely to consist of either α1α2β3 or α1α2β3γ2L receptors.

To clarify this point, we first obtained GABA-evoked concentration response profiles of α1α2β3 transfected HEK293 cells and compared the resulting CRC to those transfected with α1α2β3γ2L (***Figure 3.3 B and C***). There is a clear distinction in GABA potency for these presumed receptor assemblies. The mean EC_{50} value of α1α2β3 was significantly higher than that of α1α2β3γ2L (12.7 ± 2.3 μM and 3.6 ± 0.4 μM respectively), and similar to that for α2α2β3γ2L, suggesting that the CRC curve shift observed with the latter most likely is due to the formation of 'hetero-alpha' αβγ-heterotrimers. It is important to note that we assumed that 'hetero' and 'homo-alpha' $GABA_A$Rs have a similar single channel conductance and that the open probability (P_0) is not different between α1 and α2 subunit isoforms.

To further ensure that the receptors co-expressing α1 and α2 formed αβγ-heterotrimers with the expected high affinity benzodiazepine binding site (i.e. that they contained the γ2/α interface indicating the presence of the γ subunit), sensitivity to Zn^{2+} inhibition was tested (Draguhn et al., 1990; Smart et al., 1991; Walters et al., 2000).

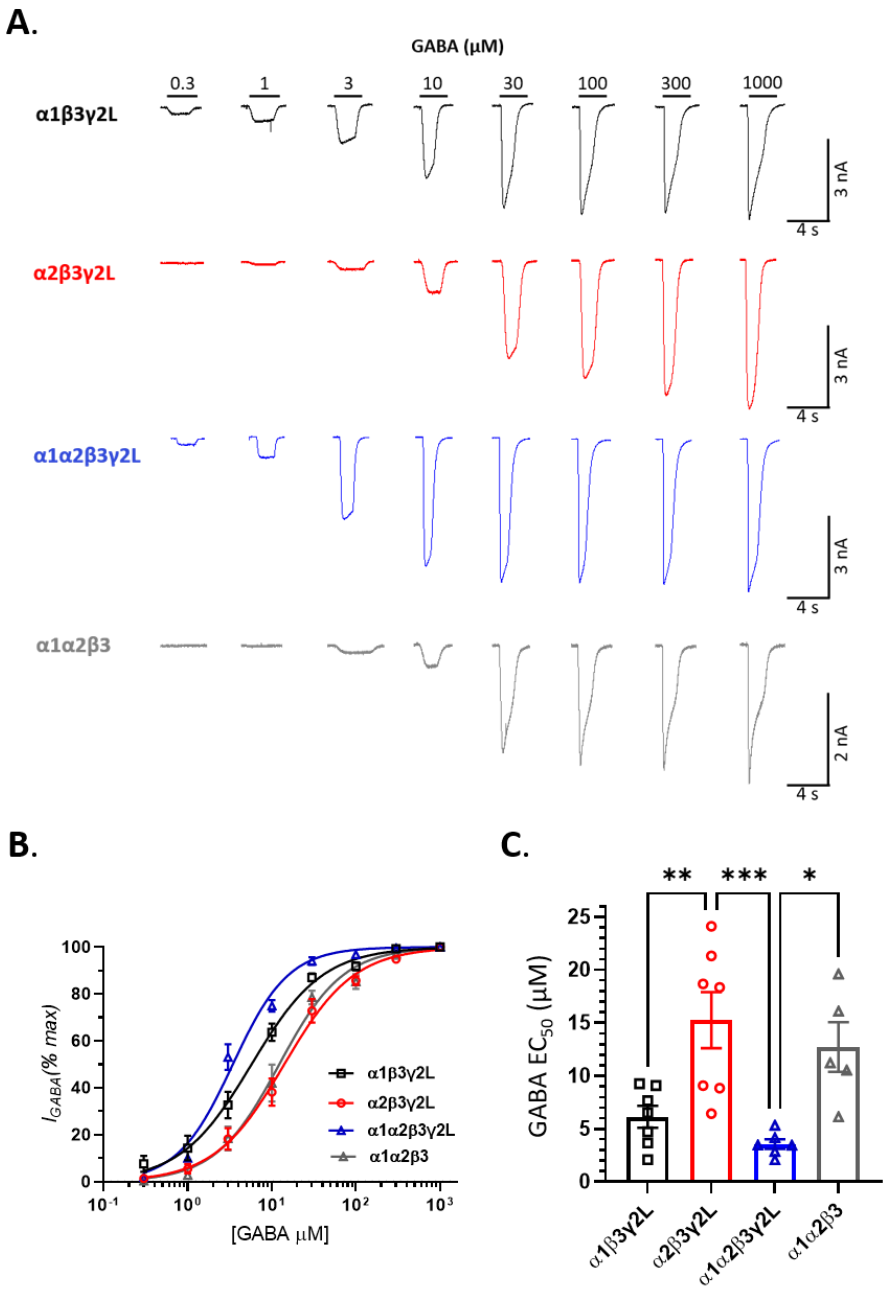

Figure 3.3 'Hetero-alpha' β3-containing recombinant GABA$_A$ receptors are more sensitive to GABA than their homomeric-α counterparts. **A.** Representative membrane current responses to GABA concentrations (μM) of α1β3γ2L (black), α3β3γ2L (red), α1α2β3γ2L (blue), and α1α2β3 (grey) receptors expressed in HEK293 cells. **B.** GABA concentration-response relationships of α1β3γ2L (□) (n = 7, n_H = 1.1 ± 0.1), α2β3γ2L (○) (n = 7, n_H = 1.2 ± 0.1), α1α2β3γ2L (△) (n = 6, n_H = 1.4 ± 0.1), α1α2β3 (△) (n = 5, n_H = 1.4 ± 0.2). **C.** The mean GABA EC_{50} values for α1β3γ2L (□) (n = 7, EC_{50} = 6.2 ± 1.0 μM), α2β3γ2L (○) (n = 7, EC_{50} = 15.3 ± 2.6 μM), α1α2β3γ2L (△) (n = 6, EC_{50} = 3.6 ± 0.4 μM), α1α2β3 (△) (n = 5, EC_{50} = 12.7 ± 2.3 μM). In the graph, all columns and error bars represent means and SEMs respectively (one-way ANOVA with Tukey's post hoc test for multiple comparisons between all groups, P values: ≤ 0.05 *, ≤ 0.01 **, ≤ 0.001 ***). Individual data points are shown in this and all proceeding figures.

$GABA_A$ receptors have been previously shown to form αβ pentamers with higher apparent GABA affinity as well as a much higher (nanomolar) sensitivity to Zn^{2+} inhibition of GABA evoked currents (Hosie et al., 2003; Mortensen and Smart, 2006). Here, a low discriminatory concentration of Zn^{2+} (10 μM) was used: this concentration completely inhibits the GABA-evoked currents of αβ pentamers, but has minimal effect on αβγ-heterotrimers (Mortensen and Smart, 2006). A high concentration of GABA (30 μM, EC_{70-90}) was first applied to HEK293 cells expressing either αβ-heterodimers (α1α2β3) or αβγ-heterodimers (α1β3γ2L, α2β3γ2L, and α1α2β3γ2L) (***Figure 3.4***). The same cell was then preincubated with 10 μM Zn^{2+} for 10 s before the GABA EC_{70-90} concentration was re-applied. Current amplitudes were recorded for GABA -/+ Zn^{2+} and the percentage inhibition was calculated using ***Equation 5*** (see ***Methods, Section 2.4.2***). As expected for αβ heterodimers, the average GABA response was abolished after Zn^{2+} application (n = 5, 4.0±1.3 % response). By contrast, the average response of EC_{70-90} after Zn^{2+} preincubation for γ-containing $GABA_A$ receptors was unchanged (α1β3γ2L: 97.9 ± 2.1 %, n = 7; α2β3γ2L: 96.7 ± 2.3 %, n = 7; α1α2β3γ2L: 97.8 ± 1.2 % n = 6, P value: ≤0.0001****). These data further support that α1α2-containing $GABA_A$ receptors, when co-expressed with β3 and γ2L subunit, form fully functional αβγ-heterotrimers.

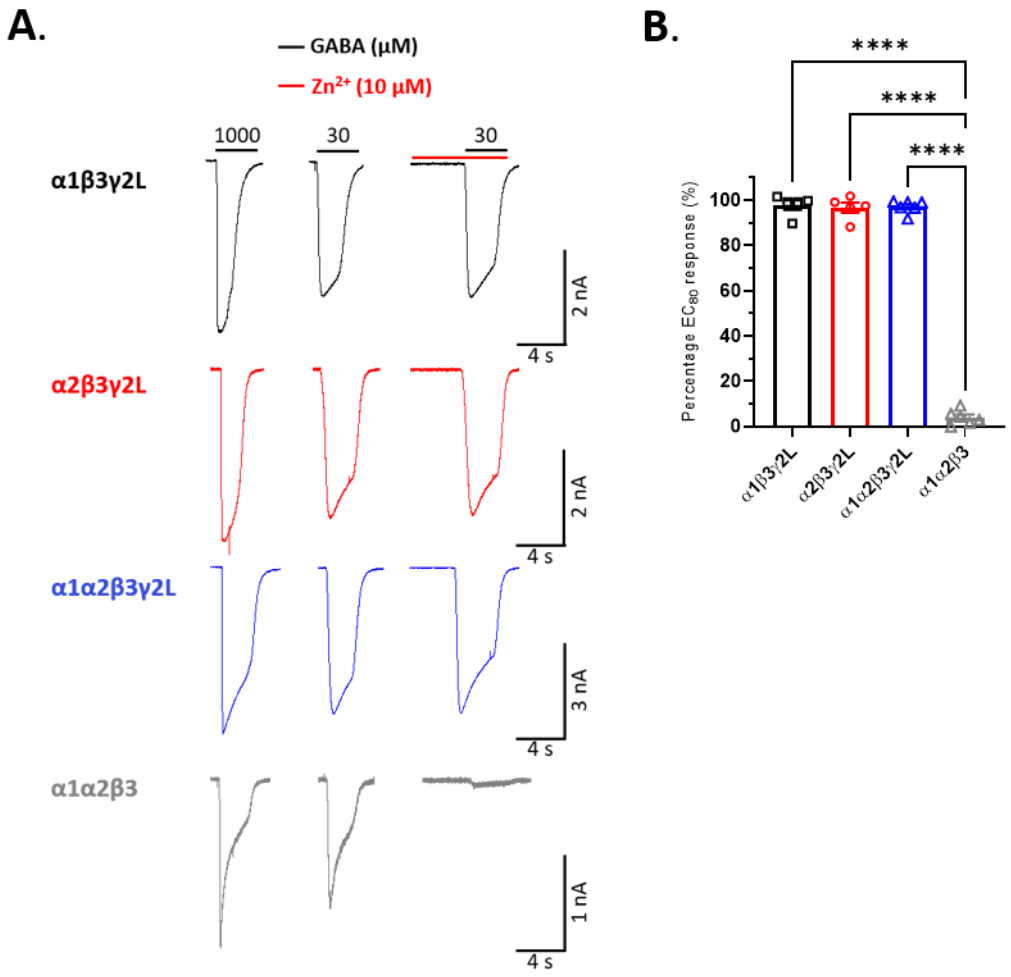

Figure 3.4 α1α2-containing recombinant GABA$_A$ receptors form functional triheteromers (αβγ). **A.** Representative GABA-activated current responses (μM) of α1β3γ2L (black), α3β3γ2L (red), α1α2β3γ2L (blue), α1α2β3 (grey) and their sensitivities to 10 μM Zn^{2+} pre-application. **B.** Bar chart representing percentage response of $EC_{70\text{-}90}$ GABA with 10 μM Zn^{2+}: of α1β3γ2L (□) (n = 7, 97.9 ± 2.1 %), α2β3γ2L (○) (n = 7, 96.7 ± 2.3 %), α1α2β3γ2L (△) (n = 6, 97.8 ± 1.2 %), α1α2β3 (△) (n = 5, 4.0 ± 1.3 %). Columns and error bars represent means and SEMs respectively (one-way ANOVA with Tukey's post-hoc test for multiple comparisons between all groups, P value: ≤ 0.0001 ****).

3.2.2 Overexpressing either α subunit does not affect the formation of α1α2-containing GABA$_A$ receptors

Once we established that the co-expression of α1 and α2 subunits results in a formation of a receptor population with a higher apparent affinity for GABA (likely to be α1α2β3γ2L), the next aim was to examine whether overexpression of either α subunits could alter the relative proportion of these receptors. It can be assumed that

co-transfection of α1, α2, β3 and γ2L produces three populations of receptors: two 'homo-alpha' populations (i.e. α1β3γ2L and α2β3γ2L) and one 'hetero-alpha' population (α1α2β3γ2L), all present at a certain proportion (and not distinguishing between hetero-alpha receptors that have the α subunits occupying different locations in the pentamer). Increasing the amount of α1 subunit cDNA in the co-transfection mixture should theoretically result in higher proportions of α1-containing receptors, either α1α1β3γ2L or α1α2β3γ2L. If the assembly of α1α1-containing receptors is predominant over α1α2-containg receptors, a shift towards the α1β3γ2L CRC would also be expected. If, however, the assembly of α1α2 containing receptors is preferred, this effect on the CRC shift should be minimal, as α1 subunit incorporation into the receptor is limited by the α2 subunit. The same logic can be applied to α2 subunit overexpression.

To elucidate the effects of overexpression for either α subunit, α1, α2, β3, γ2L (+eGFP) cDNAs were transfected in the following ratios: 10:1:1:1 (ignoring eGFP) and 1:10:1:1 (α1:α2:β3:γ2L). The final cDNA amount per transfection reaction remained constant at 4 μg. GABA concentration response profiles of these transfections is shown in ***Figure 3.5***. The data shows that there is no difference between the GABA EC_{50} values determined for equal and 10-fold excess cDNA amounts of α2 in α1α2β3γ2L transfected HEK 293 cells (α1:α2 1:1 (blue triangles) 3.6 ± 0.5 μM n = 6; α1:α2 1:10 (light blue inverted triangles) 5.5 ± 1.0 μM n = 6). Furthermore, the apparent GABA affinity of α1α2-containing receptors (1:1 and 1:10) is 4.2- and 3.1-fold higher than that of α2β3γ2L receptors ($P \leq 0.001$ and ≤ 0.01 respectively). These data suggest that providing more α2 subunits to the α1α2 mixture does not result in an increased assembly of $GABA_A$ receptors with two copies of α2 subunits in the pentameric complex. Since the amounts of α1, β3 and γ2L subunits are the limiting factors for assembly, the result suggests that 'hetero-alpha' receptor assembly is preferential over 'homo'-α2 receptors.

A similar outcome was apparent with α1 overexpression in the α1α2-containing transfection mixture, again suggesting there is little effect on the preferential subunit assembly. The EC_{50} value for the 10:1 cDNA ratio (α1:α2 (dark blue diamonds) 7.1±2.1 μM n=8) is doubled in comparison to that of the 1:1 ratio (α1:α2 (blue triangles) 3.6

± 0.5 μM n = 6), but this is not statistically different. Similarly, no clear difference is observed between the curves for the α1α2-mixture (10:1) and α1α1 pure population. The absence of any clear curve separation makes the preference for either 'hetero-alpha' or 'homo'-α1 $GABA_A$ receptor expression difficult to observe. It could be attributed to the fact that there is not enough separation in the apparent affinity for GABA between α1α2β3γ2L (equimolar transfection ratios) and α1β3γ2L, so any changes in EC_{50} values will be subtle.

Interestingly, increasing the amounts of either α1 or α2 subunit cDNAs (10:1 and 1:10) consistently results in the same overlapping concentration response profiles for the α1α2 hetero-trimers (see ***Figure 3.5 A and B***). This could suggest, unexpectedly, that the proportion of 'hetero-alpha' $GABA_A$ receptors (here α1 and α2) is seemingly independent of the α subunit type availability, and therefore assembly could be tightly regulated. Taking all these results into consideration, the conclusions are based on the assumption that there are three distinct receptor populations present for an α1α2 subunit mixture: α1β3γ2L, α2β3γ2L, and α1α2β3γ2L.

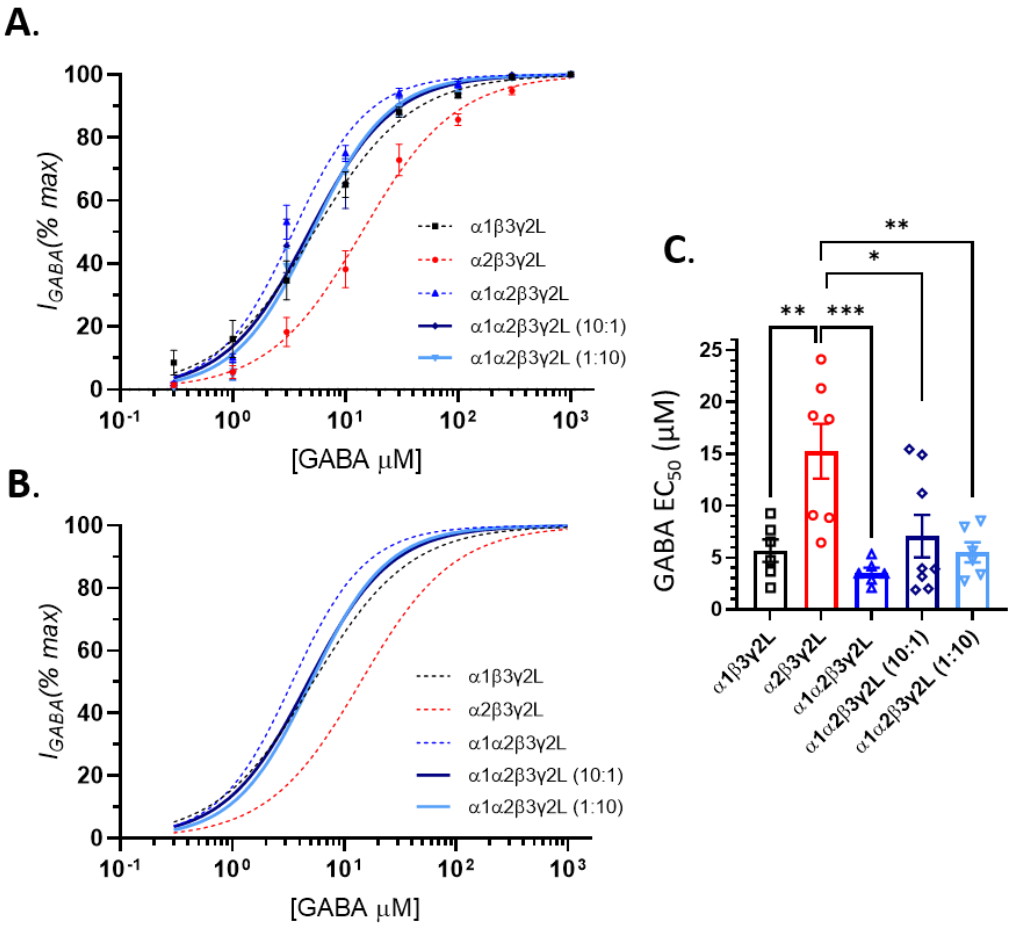

Figure 3.5 Effects of varying transfection ratios of α1 and α2 cDNAs on GABA concentration-response relationships. HEK293 cells were transfected with cDNAs of α1 and/or α2, β3 and γ2L subunits at a 1:1:1:1 ratio (4 μg cDNA total). The α1α2β3γ2L (10:1) and α1α2β3γ2L (10:1) were transfected as 10:1:1:1 and 1:10:1:1 (α1:α2:β3:γ2L) ratios, respectively. **A.** GABA concentration-response curves of α1β3γ2L (■) (n = 6, n_H = 1.1 ± 0.1), α2β3γ2L (●) (n = 7, n_H = 1.2 ± 0.1), α1α2β3γ2L (▲) (n = 6, n_H = 1.5 ± 0.1), α1α2β3γ2L **(10:1)** (◆) (n=8, n_H = 1.6 ± 0.1), and α1α2β3γ2L **(1:10)** (▼) (n=6, n_H = 1.4 ± 0.1). Points are mean ± SEM. **B.** For clarity, this graph shows the fits of GABA concentration-response curves from panel **A** without the data points. **C.** Bar chart showing the mean (± SEM) GABA EC_{50} values for α1β3γ2L (□) (EC_{50} = 5.7 ± 1.1 μM), α2β3γ2L (○) (EC_{50}=15.3 ± 2.6 μM), α1α2β3γ2L (△) (EC_{50} = 3.6 ± 0.5 μM), α1α2β3γ2L **(10:1)** (◇) (EC_{50} = 7.1 ± 2.1 μM), α1α2β3γ2L **(1:10)** (▽) (EC_{50} = 5.5 ± 1.0 μM). One-way ANOVA with Tukey's post hoc test was used for multiple comparisons between all groups, P ≤ 0.05 *, ≤ 0.01 **, ≤ 0.001 ***).

3.2.3 Functional properties of α1α2 – role of the β subunit

The identity of the β subunit determines the biophysical properties of $GABA_A$ receptors, including GABA potency and receptor's spontaneous activity, and strongly affects the receptor's response to modulation by allosteric ligands, e.g. loreclezole, mefenamic acid, and etomidate. Both, β2 and β3 subunits are widely expressed in the brain, however there are some differential regional and cellular localisation patterns, and deletion of each gene (*GABRB2/3*) has significantly different effects on the host organism ranging from phenotypically near normal (β2-/-) to a catastrophic life-limiting effect, mimicking Angelman's syndrome (β3-/-) (DeLorey et al., 1998; Korpi et al., 2002; Pirker et al., 2000; Sur et al., 2001). The next step for exploring the hetero-alpha receptors was, therefore, to investigate whether there are any differences in GABA response profiles of α1α2-containing receptors expressed either with β2 or β3 subunits. The previous results with β3 subunits, described in ***Section 3.2.1***, indicated a leftward shift of α1α2β3γ2L CRC, suggesting expression of 'hetero-alpha' receptor population increased the potency of GABA.

To establish, whether a similar effect is observed with β2-containing receptors, GABA response profiles of α1α2β2γ2L mixture was compared to respective 'homo-alpha' receptor populations (***Figure 3.6***). The first notable feature was that the GABA EC_{50}s for homo-alpha receptors, α1β2γ2L and α2β2γ2L were similar, contrasting with the data obtained for β3 subunit-containing receptors. In addition, the apparent affinity for GABA of α1α2β2γ2L was also similar to that of α1β2γ2L and α2β2γ2L recombinant receptors (EC_{50} values: 10.4 ± 2.0 μM n = 5; 11.0 ± 2.6 μM n = 6; and 14.7 ± 1.8 μM n =10 respectively), i.e. there was no leftwards displacement of the curve. From these data with β2 subunits, it is difficult to deduce whether there are two (pure α1β2γ2L and α2β2γ2L) or three (two 'homo-alpha' and one 'hetero-alpha') distinct populations of receptors. Furthermore, if we assume that a 'hetero-alpha' population is indeed present in the mixture, its GABA sensitivity is indistinguishable to that of 'homo-alpha' receptors. Thus, in terms of conclusions, the data suggest that there are differences in the GABA concentration response profiles of α1α2-containing receptors depending upon whether they are expressed with β2 or β3 subunits.

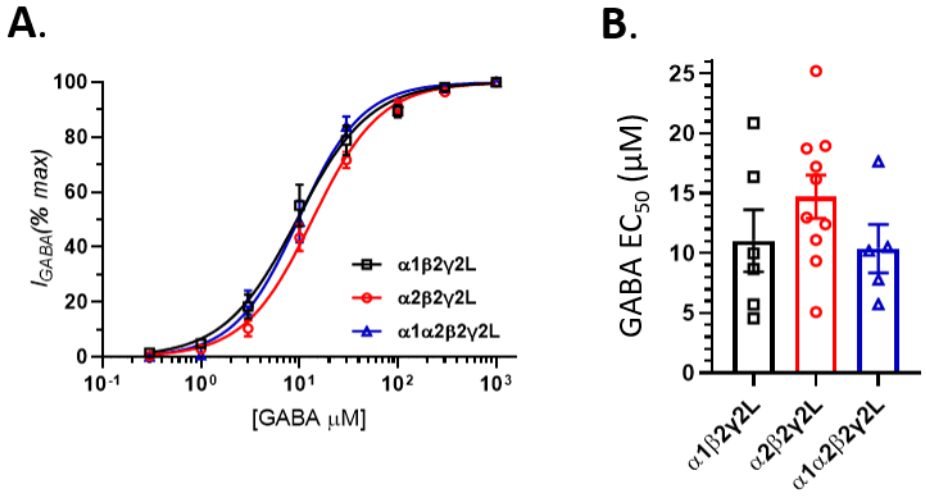

Figure 3.6 Functional properties of recombinant 'hetero-alpha' α1α2-containing GABA$_A$ receptors. **A.** GABA concentration-response relationships of α1β2γ2L (□) (n = 6, n_H = 1.4±0.1), α2β2γ2L (○) (n = 10, n_H = 1.1 ± 0.1), α1α2β2γ2L (△) (n = 5, n_H = 1.5 ± 0.1). **B.** The mean GABA EC_{50} values for α1β2γ2L (□) (n = 6, EC_{50} = 11.0 ± 2.6 μM), α2β2γ2L (○) (n = 10, EC_{50} = 14.7 ± 1.8 μM), α1α2β2γ2L (△) (n = 5, EC_{50} = 10.4 ± 2.0 μM. Means and SEMs of EC_{50} values are shown in the bar chart (one-way ANOVA with Tukey's post hoc test for multiple comparisons between all groups, P value: n.s. not significant).

3.2.4 Functional properties of α1α4 GABA$_A$ receptor mixtures

So far, electrophysiological properties of α1 and α2 subunit mixtures – most widely expressed subunits in the brain – were assessed (Pirker et al., 2000). The next aim was to establish whether there are any differences that can be established in GABA response profiles of unlikely subunit mixtures. Expression of the α4 GABA$_A$ receptor subunit is at low abundance and is predominantly localised to olfactory bulbs, thalamus, striatum and dentate gyrus (Pirker et al., 2000). Immunoaffinity purification from those four regions (rat brain lysates) suggests that α4 subunit co-immunoprecipitated with α1, α2, and α3 subunits (Benke et al., 1997). However, the majority α4 subunits were associated with α3 (Benke et al., 1997). Furthermore, only a third of α4-containing receptors were associated with both β2/3 and γ2 subunits (Bencsits et al., 1999). These data together, suggest that α1 and α4 subunits are

unlikely to be expressed in the same $GABA_AR$ pentameric complex, making it a suitable candidate for our study.

To test the effects of α1 and α4 co-expression on GABA concentration response profiles, HEK293 cells were transfected with either α1, α4, or α1α4 mixtures of subunits along with equimolar ratios of β3 and γ2L (+ eGFP). GABA concentration response profiles were obtained for each construct (***Figure 3.7***). GABA EC_{50} value of α1α4β3γ2L was statistically different from that of α4β3γ2L, but not of α1β3γ2L (7.7 ± 1.6 µM n = 6; 15.4 ± 3.0 µM n = 6; and 5.7 ± 1.1 µM n = 6 respectively). This data could imply that the CRC of the α1α4 lies in the middle of two pure population α1- and α4-receptor curves. In comparison to α1α2β3γ2L (***Figure 3.3***), no leftward shift of the CRC α1α4-mixture curve is observed. This could suggest that a 'hetero-alpha' $GABA_A$ receptor population is absent for the α1α4β3γ2L receptor mixture. However, this result is similar to that of α1α2β2γ2L receptor mixture, which could imply that if the 'hetero-alpha' receptors are present.

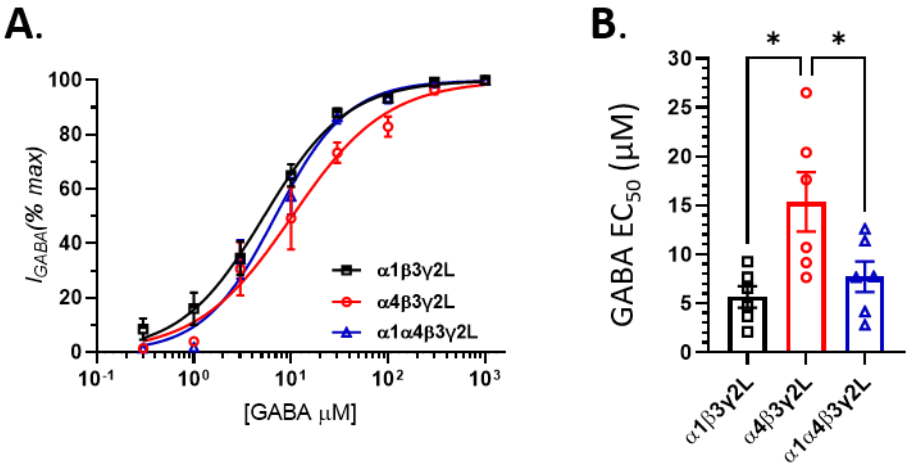

Figure 3.7 Functional properties of recombinant 'hetero-alpha' α1α4-containing $GABA_A$ receptors. **A.** Concentration response curves of α1β3γ2L (□) (n = 6, n_H = 1.1 ± 0.1), α4β3γ2L (○) (n = 6, n_H = 1.2 ± 0.1), α1α4β3γ2L (△) (n = 6, n_H = 1.4 ± 0.1). **B.** The mean GABA EC_{50} values for α1β3γ2L (□) (n = 6, EC_{50} = 5.7 ± 1.1 µM), α4β3γ2L (○) (n = 6, EC_{50} = 15.4 ± 3.0 µM), α1α4β3γ2L (△) (n = 6, EC_{50} = 7.7 ± 1.6 µM). Means and SEMs of EC_{50} values are shown in the bar chart (one-way ANOVA with Tukey's post hoc test for multiple comparisons between all groups, P value: ≤ 0.05 *).

3.2.5 Summary of results from investigating wild-type α1α2 and α1α4 subunit mixtures

In this section two wild-type α-subunit combinations were recombinantly expressed to establish the existence of 'hetero-alpha' $GABA_A$ receptor populations and further identify their pharmacological footprints. From the data accrued so far, a number of conclusions could be noted.

Firstly, co-expression of α1 and α2 subunits with β3 and γ2, results in a leftward CRC shift, compared to either of the pure α1 or α2 constructs (***Figure 3.3***). This data suggests the presence of a new receptor population with a higher apparent affinity for GABA. Furthermore, we showed that this receptor population is expressed as an αβγ-heterotrimer according to its sensitivity to Zn^{2+} block (***Figure 3.4***). It can therefore be concluded, that this receptor population is most likely composed of α1α2β3γ2. We cannot make any conclusions regarding specific subunit arrangement around the channel pore (i.e. reading counter clockwise around the pentamer: α1-γ2L-β3-α2-β3 versus α2-γ2L-β3-α1-β3).

Increasing the relative proportion of either α subunit cDNA had little effect on aligning the apparent GABA affinity shift with the GABA curves for 'homo-alpha' mixtures (e.g. α1α1, α2α2). This could indicate that there is an assembly mechanism that strictly reserves a minimal threshold of 'hetero-alpha' receptor production, irrespective of the α subunit cDNA proportion. Furthermore, overexpressing α2 subunits in α1α2β3γ2L recombinant receptors suggests that there is a preference towards assembly of α1α2-containing receptors over that of α2α2-containing receptors.

There was also a difference in the GABA response profiles between β2- and β3-containing α1α2 receptors. A clear shift in GABA potency was noted for α1α2β3γ2L receptors but not for α1α2β2γ2L, possibly indicating that hetero-alpha subunit co-assembly may be facilitated by the β3, but not the β2, subunit. Collectively, we cannot conclude here exactly how many receptor populations are present when co-expressing α1 and α2 subunits (the same dilemma applies to α1 and α4 co-expression). One of the main reasons for this is that the EC_{50} values of the pure α subunit populations are too close to observe any clear separation of the α-subunit

mixtures, apart from α1α2β3γ2L. In order to establish the number of populations present in each mixture, we require a reporter mutation in one of the α subunits to increase the separation of the GABA EC_{50}s. This would allow for a larger separation between CRCs, and hence an improved ability to resolve mixed receptor populations with distinct GABA sensitivities. The next section will focus on two such reporter mutations: $\alpha1^{L263S}$ and $\alpha2^{F65L}$.

3.3 Results: Inferring the number of receptor populations with α1α2 co-expression using reporter mutations: $\alpha1^{L263S}$ and $\alpha2^{F65L}$

3.3.1 Substitution of the conserved leucine 263 to serine in α1 subunit increases its GABA sensitivity

A conserved leucine amino acid residue in the putative transmembrane domain 2 (TM2) was substituted to serine in the α1 subunit (L263S) as described in ***Methods 2.1.1***. This residue is located at an approximate midpoint of the TM2, at the 9' position, and is conserved across most LGIC subunits (Lester, 1992). The amino acid substitution of a conserved leucine residue in a single subunit profoundly increased agonist receptor sensitivity, resulting in a 10- to 49-fold rightward shift of the agonist dose-response curve, depending on the nature of the subunit and type of a receptor tested (Chang et al., 1996a; Labarca et al., 1995; Patel et al., 2014). The L9'S mutation has been widely used to study the stoichiometry and receptor activation mechanisms of both nAChRs, 5-HT3Rs, and $GABA_A$Rs (Chang et al., 1996a; Chang and Weiss, 1999; Filatov and White, 1995; Labarca et al., 1995; Patel et al., 2014; Yakel et al., 1993).

The aim was to first validate the previously observed GABA sensitivity increase due to the L9'S mutation. To do so, HEK293 cells were transfected with either $\alpha1^{L263S}$ or α1 (WT) along with the β2 and γ2L subunits (+ eGFP) cDNAs. The dose-response relationships of these constructs were then compared (***Figure 3.8 A***). ***Figure 3.8 B*** shows a 36-fold decrease in GABA EC_{50} of $\alpha1^{L263S}$β2γ2L compared to α1β2γ2L (0.2 ± 0.04 μM, n = 7; 7.1 ± 0.8 μM, n = 7 respectively). Previously reported CRC shift caused by this mutation in the α1β2γ2L was 153-fold, from 45.8 ± 3.6 μM to 0.3 ± 0.1 μM

(mean± standard deviation, SD) (Chang et al., 1996a). The effect on the GABA sensitivity observed in our experimental system is less extreme, which could be attributed to the difference of the expression system used (HEK293 cells versus *Xenopus laevis* oocytes).

Interestingly, the channel gating of $\alpha1^{L263S}\beta2\gamma2L$ showed spontaneous activity of this receptor combination in the absence of exogeneous GABA, revealed via picrotoxin (PTX), 100 µM, application (***Figure 3.8 C***). PTX is a non-competitive antagonist of $GABA_AR$ which binds within the channel pore thereby antagonising the activity of constitutively active receptors and blocking spontaneous currents (Smart and Constanti 1986; Newland and Cull-Candy 1992). Cryo-electron microscopy has revealed that PTX binding pocket is sequestered within the channel pore between 2' and 9' rings of M2 domains (Masiulis et al., 2019b). Therefore, we expected that the α1 9' substitution would influence channel gating and receptor activation. HEK293 cells transfected with the $\alpha1^{L263S}\beta2\gamma2L$ showed a significantly higher spontaneous activity than its α1 wild-type counted part (I_{spont}: $\alpha1^{L263S}\beta2\gamma2L$ 25.7 ± 4.0%; α1β2γ2L 0.2 ± 0.05 %; Kruskal-Wallis with Dunn's post hoc test, P value: ≤ 0.05). These results are in agreement with previous studies, in both *Xenopus laevis* oocytes and HEK293 recombinant systems (Chang and Weiss, 1999; Patel et al., 2014). The spontaneous activity of the holding current was estimated to be 22.0 ± 3.0 % in $\alpha1^{L263S}\beta2\gamma2L$ (*Xenopus* oocytes) and 21.9 ± 5.3 in $\alpha4^{L263S}\beta3\delta$ (HEK293 cells), suggesting that the mutation of the conserved leucine residue in the α $GABA_AR$ subunit contributes to ~ 20 % of spontaneous channel opening (Chang and Weiss, 1999; Patel et al., 2014). Furthermore, mutations of this conserved leucine residue in M2 domain in other $GABA_A$ receptor subunits and nACh receptor subunits revealed constitutively open channels, suggesting that this residue may play an important role in receptor activation (Akabas et al., 1992; Chang and Weiss, 1999; Pan et al., 1997; Patel et al., 2014).

Notably, the Hill coefficient of the DRC obtained for $\alpha1^{L263S}\beta2\gamma2L$ (n_H = 0.8 ± 0.04) was significantly lower than that of α1β2γ2L (n_H = 1.3 ± 0.1) receptors (unpaired *t*-test, P = 0.003). Even though the change in the Hill coefficient cannot be directly ascribed to the number of agonist binding sites or cooperativity, it could be that the mutation at

the 9' M2 domain could alter receptor gating. Furthermore, a low Hill coefficient (n_H = 0.8 ± 0.04) could potentially indicate the presence of two distinct $GABA_AR$ populations, probably $\alpha1^{L263S}\beta2\gamma2L$ and for $\alpha1^{L263S}\beta2$.

Additionally, the spontaneous activity of $\alpha1^{L263S}\alpha2\beta2\gamma2L$ transfected HEK293 cells was calculated to be only 4.6 ± 1.3 %, not exhibiting the spontaneous activity equal to the mean of its 'homo' α-subunit counterparts ($\alpha1^{L263S}\beta2\gamma2L$ and $\alpha2\beta2\gamma2L$; 25.7 ± 4.0 % and 0.1 ± 0.03 % respectively) (***Figure 3.8 D***).

Overall, due to the prominent leftward shift of the $\alpha1^{L263S}\beta2\gamma2L$ DRC, this leucine to serine substitution in α1 subunit can be used as a reporter mutation to study receptor populations present during an α1/α2 co-expression (***Section 3.3.2***).

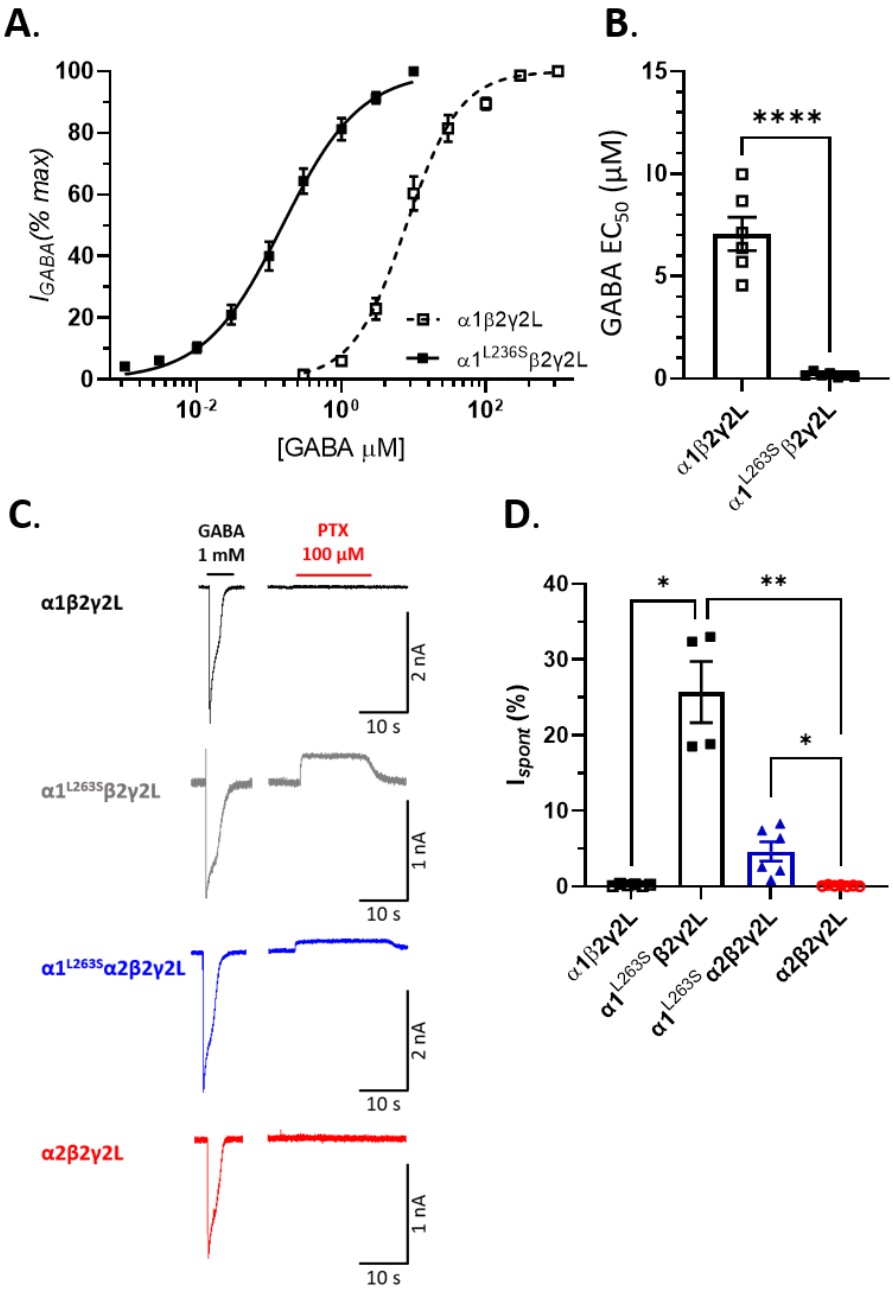

Figure 3.8 Serine substitution of a conserved leucine in TM2 (9′ position) of the α1 subunit increases GABA sensitivity and spontaneous activity. **A.** GABA concentration-response profiles of α1β2γ2L (□) (n = 7, n_H = 1.3 ± 0.1) and α1^{L263S}β2γ2L (■) (n = 7, n_H = 0.8 ± 0.04). **B.** Bar chart representing the mean ± SEM GABA EC_{50} values for α1β2γ2L (□) (n = 7, EC_{50} = 7.1 ± 0.8 µM) and α1^{L263S}β3γ2L (■) (n = 7, EC_{50} = 0.2 ± 0.04 µM) (unpaired *t*-test, P ≤ 0.0001 ****). **C.** Representative traces of maximal GABA-activated current responses (1 mM) followed by an application of a saturating dose of PTX (100 µM) to reveal the level of spontaneous activity of α1β2γ2L (black), α1^{L263S}β2γ2L (grey), α1^{L263S}α2β2γ2L (blue), and α2β2γ2L (red). **D.** Comparison of spontaneous activity (I_{spont}) values for α1β2γ2L (□) (0.2 ± 0.05 %), α1^{L263S}β2γ2L (■) (25.7 ± 4.0 %), α1^{L263S}α2β2γ2L (▲) (4.6 ± 1.3 %), and α2β2γ2L (○) (0.1 ± 0.03 %) (Kruskal-Wallis with Dunn's post hoc test, P value: ≤ 0.05 *, ≤ 0.01 **).

3.3.2 Co-expression of α1^{L263S} and α2 subunits

The 9' mutation in M2 domain has been widely used to study the receptor stoichiometry $GABA_A$Rs (α1β2γ2 and α4β3δ), nAChRs and 5-HT3Rs (Chang et al., 1996a; Filatov and White, 1995; Labarca et al., 1995; Patel et al., 2014; Yakel et al., 1993). Since the substitution of this conserved residue results in a profound increase in agonist sensitivity (i.e. leftward DCR shift), it was used as a reporter mutation to correlate the multiple receptor populations with distinct agonist potencies expressed in the same cell (see ***Introduction 3.1***). Chang et al., (1996) proposed a method to deduce the subunit stoichiometry in a $GABA_A$ receptor complex, where co-expression of the same subunit wild type and 9' mutant mixture would generate populations of receptors with distinct GABA apparent affinities. Here, this approach was modified to establish the number of receptor populations in HEK293 cells co-expressing α1 and α2 subunits (see ***Figure 3.1*** for details). For every α1/α2 mixture, two and three component Hill equations were fitted. The number of true components were established from the goodness of fit (lower χ^2 statistic).

We first expressed α1^{L263S} or α2 with β2, γ2L subunits (+eGFP) cDNAs in HEK293 cells and obtained the GABA concentration response profiles. The average GABA EC_{50} values of α1^{L263S}β2γ2L and α2β2γ2L were 0.2 ± 0.04 μM and 13.4 ± 0.9 μM respectively, accounting for a 67-fold shift in GABA sensitivity between two recombinant receptor constructs. From these, a predicted EC_{50} value of a middle component (assuming three distinct populations with α1^{L263S}α2 co-expression) can be calculated. The middle component will contain only one copy of the α1^{L263S} in a receptor pentamer and therefore will contribute to 8.2 ($\sqrt{67}$) fold increase in GABA sensitivity. Assuming the GABA sensitivity is unchanged regardless of the positioning of a single α1^{L263S} subunit in the pentamer complex, the predicted EC_{50} value for 'hetero-alpha' receptor population would be 1.6 μM (8.2 x 0.2 μM). Similar logic can be applied to predicting GABA sensitivities of other 'hetero-alpha' receptors.

The concentration response relationship of α1^{L263S}α2β2γ2L-expressing cells was better described as a sum of three rather than two Hill equations (χ^2 5.77 and 4.94

respectively) (see ***Figure 3.9 C***). The first and third components accounted for 6.1 ± 2.8 % and 49.1 ± 4.3 % of the total pool of receptors with respective GABA EC_{50} values of 0.04 ± 0.02 µM and 18.4 ±3.3 µM, which are in agreement with previous studies of multi-component $GABA_A$ receptor curve fits (Chang et al. 1996; Patel, Mortensen, and Smart 2014). These EC_{50} values are consistent with the EC_{50} values obtained for $\alpha1^{L263S}\beta2\gamma2L$- and $\alpha2\beta2\gamma2L$-expressing cells (0.2 ± 0.04 µM and 13.4 ± 0.9 µM respectively), indicating that first and third component GABA sensitivities correspond to activation of 'homo-alpha' receptor populations: $\alpha1^{L263S}\beta2\gamma2L$ and $\alpha2\beta2\gamma2L$. Furthermore, the multi-component CRC fit revealed a presence of an intermediate component with an EC_{50} value of 0.8 ± 0.2 µM, which contributed to 44.7 ± 3.9 % of the total receptor number. This component is likely to be attributed to the expression of receptors containing one copy of $\alpha1^{L263S}\beta$ and one copy of α2 in the same pentamer. Moreover, GABA apparent affinity obtained from the Hill equation fits is in good agreement with the theoretical EC_{50} value (1.6 µM).

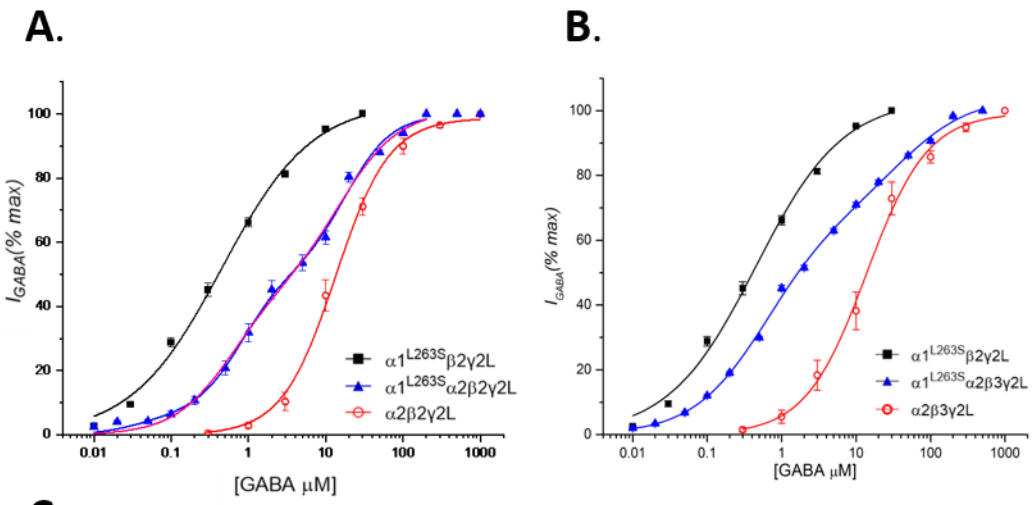

C.

Hill equation components	Two-component fit (blue)		Three-component fit (magenta)	
	EC_{50} (μM)	Percentage (%)	EC_{50} (μM)	Percentage (%)
1st component	0.6 ± 0.1	46.9 ± 5.5	0.04 ± 0.02	6.1 ± 2.8
2nd component	16.3 ± 3.8	54.3 ± 5.2	0.8 ± 0.2	44.7 ± 3.9
3rd component	-	-	18.4 ± 3.3	49.1 ± 4.3
χ^2	5.77		4.94	

D.

Hill equation components	Two-component fit (blue)		Three-component fit (magenta)	
	EC_{50} (μM)	Percentage (%)	EC_{50} (μM)	Percentage (%)
1st component	0.6 ± 0.1	67.7 ± 4.1	0.6 ± 0.4	10.0 ± 1.3
2nd component	41.6 ± 15.4	36.7 ± 3.0	0.6 ± 0.1	57.7 ± 2.9
3rd component	-	-	41.6 ± 12.6	36.7 ± 2.4
χ^2	1.76		1.59	

Figure 3.9 GABA dose-response relationships from co-expression of α1^{L263S} and α2 subunits in HEK293 cells. **A.** Dose response relationships of α1^{L263S}β2γ2L (■) (n = 7, n_H = 0.8±0.04), α2β2γ2L (○) (n = 7, n_H = 1.3 ± 0.1) and α1^{L263S}α2β2γ2L (▲) (n = 6). The latter was fit with the sum of two (blue) or three (magenta) Hill equations (two and three components respectively). Cumulative Hill coefficient (n_H) values are 1.1 ± 0.1 (two-component fit) and 1.5 ± 0.2 (three-component fit). The EC_{50} values for α1^{L263S}β2γ2L (■) and α2β2γ2L (○) are 0.2 ± 0.04 μM and 13.4 ± 0.9 μM respectively. **B.** Dose response relationships of α1^{L263S}β2γ2L (■) (n = 7, n_H = 0.8 ± 0.04), α2β3γ2L (○) (n = 8, n_H = 1.1±0.1) and α1^{L263S}α2β3γ2L (▲) (n = 7). The latter was fit with the sum of two (blue) or three (magenta) Hill equations (two and three components respectively). Cumulative Hill coefficient (n_H) values are 0.9 ± 0.1 (two-component fit) and 0.9 ± 0.1 (three-component fit). The GABA EC_{50} values for α1^{L263S}β2γ2L

(■) and α2β3γ2L (○) are 0.2 ± 0.04 μM and 13.8 ± 1.4 μM respectively. Note that the control $\alpha1^{L263S}$ DRC is β2 subunit containing. **C** and **D.** Table summarising the EC_{50} values (μM) and relative percentages (%) of $\alpha1^{L263S}\alpha2\beta2\gamma2L$ (**B**) and $\alpha1^{L263S}\alpha2\beta3\gamma2L$ (**D**) Hill equations-fitted components. The value of the χ^2 distribution statistic indicates the goodness of fit.

Similarly, multi-component concentration response relationship Hill equations were fitted to the GABA-activated currents of $\alpha1^{L263S}\alpha2\beta3\gamma2L$-expressing cells (***Figure 3.9 B***). Table from ***Figure 3.9 D*** shows that two and three component curve fits had similar χ^2 statistic (1.76 and 1.59 respectively), suggesting that a sum of two components of Hill equations is sufficient to describe the $\alpha1^{L263S}\alpha2\beta3\gamma2L$ data. The second component accounted for the activation of 36.7 ± 3.0 % of total receptors with an EC_{50} value of 41.6 ± 15.4 μM, corresponding to the α2β3γ2L receptor population. Interestingly, the first component's EC_{50} value was determined to be 0.6 ± 0.1 μM and attributed to 67.7 ±4.1 % of the total receptor population. The GABA sensitivity of this component is close to the EC_{50} value of a middle component in $\alpha1^{L263S}\alpha2\beta2\gamma2L$-transfected cells (0.8 ± 0.2 μM). This could imply that the first component in β3-expressing cells corresponds to the receptor population with $\alpha1^{L263S}\alpha2$ mixture (one of each in a pentamer), rather than $\alpha1^{L263S}$-only receptor population. This data together suggests that only two receptor populations are expressed ($\alpha1^{L263S}\alpha2$- and α2α2-containing) in $\alpha1^{L263S}\alpha2\beta3\gamma2L$-transfected cells. It is also worth mentioning, that the EC_{50} values of first and intermediate components of the curve fit described by three Hill equations are equal (0.6 ±0.4 μM and 0.6 ± 0.1 μM respectively). Furthermore, the relative receptor population sum of these components (10.0 ± 1.3 % and 57.7 ± 2.9 %) is equal to the percentage of the first component in a two-receptor population fit (67.7 ±4.1 %). This further strengthens the idea of two, rather than three receptor populations in $\alpha1^{L263S}\alpha2\beta2\gamma2L$-transfected cells.

Using the $\alpha1^{L263S}$ reporter mutation as a functional tool to dissect the number of distinct receptor populations in $\alpha1^{L263S}\alpha2\beta\gamma2L$-transfected HEK293 cells revealed some differences between β2 and β3-containing receptors. Firstly, $\alpha1^{L263S}\alpha2\beta\gamma2L$ receptor mixtures with the β2 subunit seem to form three distinct receptor populations (two 'homo-alpha' and one 'hetero-alpha'), whereas the same

combinations with the β3 subunit only form two distinct receptor populations: $\alpha1^{L263S}\alpha2\beta3\gamma2L$ and $\alpha2\alpha2\beta3\gamma2L$. From the data presented, the $\alpha1^{L263S}\alpha1^{L263S}\beta3\gamma2L$ population seems to be absent when co-expressing $\alpha1^{L263S}$ and α2. Additionally, the proportion of 'homo-alpha' receptor populations in β2-containing receptors is 1.5 times higher than that in β3-containing receptors. Also, the proportion of $\alpha1^{L263S}\alpha1^{L263S}$-containing receptor population co-expressed with β2 subunit accounts for only 6.1 ± 0.1 % of the total receptor pool. Since these differences were observed, the next aim was to confirm these differences using the same principle with a reporter mutation on an α2 subunit: phenylalanine to leucine substitution at position 65.

3.3.3 The F65L substitution in α2 subunit profoundly reduces receptor sensitivity to GABA but does not affect the cell surface expression

The mutation on the α1 $GABA_AR$ subunit, F65L has previously been used to study $GABA_A$ receptor agonist-dependent gating as well as GABA binding sites in concatenated receptors (Baumann et al., 2003; Sigel et al., 1992). The $\alpha1^{F65L}$ substitution has been previously shown to decrease the GABA sensitivity of α1β2γ2 receptors by ~210 fold (from EC_{50} value of 6 ± 2 μM to 1260 ± 380 μM) as well as reducing bicuculline sensitivity by ~200 fold (Baumann et al., 2003). Since this mutation causes such a profound rightward shift of the GABA dose response relationships, it was a next obvious candidate to use for dissecting the multicomponent Hill equation fits, similar to $\alpha1^{L263S}$ (***Section 3.3.2***).

The substitution of phenylalanine to leucine at position 65 of the α2 subunit was performed using site directed mutagenesis (see ***Methods, Section 2.1***). The reason why an α2 subunit was chosen for the mutation over the α1 subunit was the relative positioning of the wild type dose response relations of α1β2/3γ2L and α2β2/3γ2L constructs (***Figures 3.3 C and 3.6 A***). The α2-containing receptors have a higher EC_{50} that those containing α1 subunit, therefore introducing the mutation in the former would result in greater separation of the α1 and $\alpha2^{F65L}$ CRCs. To validate the $\alpha2^{F65L}$ substitution has an effect on the GABA apparent affinity, concentration response

relationships obtained from $\alpha2^{F65L}\beta2\gamma2L$-expressing HEK293 cells were compared to α2β2γ2L transfected combination. The EC_{50} value increased from 13.4 ± 0.1 μM to 947.1 ± 101.1 μM (wild type and mutant respectively), resulting in a ~70-fold shift in GABA potency (***Figure 3.10 B***).

Given a significant reduction in GABA sensitivity on $\alpha2^{F65L}\beta2\gamma2L$-expressing HEK293-expressing cells, the effect of the F65L mutation on the α2-containing receptors cell surface expression was assessed. Impaired $\alpha2^{F65L}$ subunit trafficking to the cell surface membrane could affect the 'hetero-alpha' receptor formation in favour of α1α1-containing receptors. To assess the levels of cell surface expression, either α2 or $\alpha2^{F65L}$ N-terminus *myc*-tagged subunits, co-expressed with β2 and γ2L subunit (+ eGFP) were expressed in HEK293 cells and immunolabelled with anti-*myc* antibodies (see ***Methods, Section 2.5.1***). ***Figure 3.10, D*** shows that there is no significant difference between α2 or $\alpha2^{F65L}$ cell surface fluorescence, suggesting that F65L mutation does not affect α2 subunit trafficking to the membrane.

These data together indicate that $\alpha2^{F65L}$ mutation is a good candidate to study 'hetero-alpha' receptor mixtures' populations and their relative abundances in HEK293 cells.

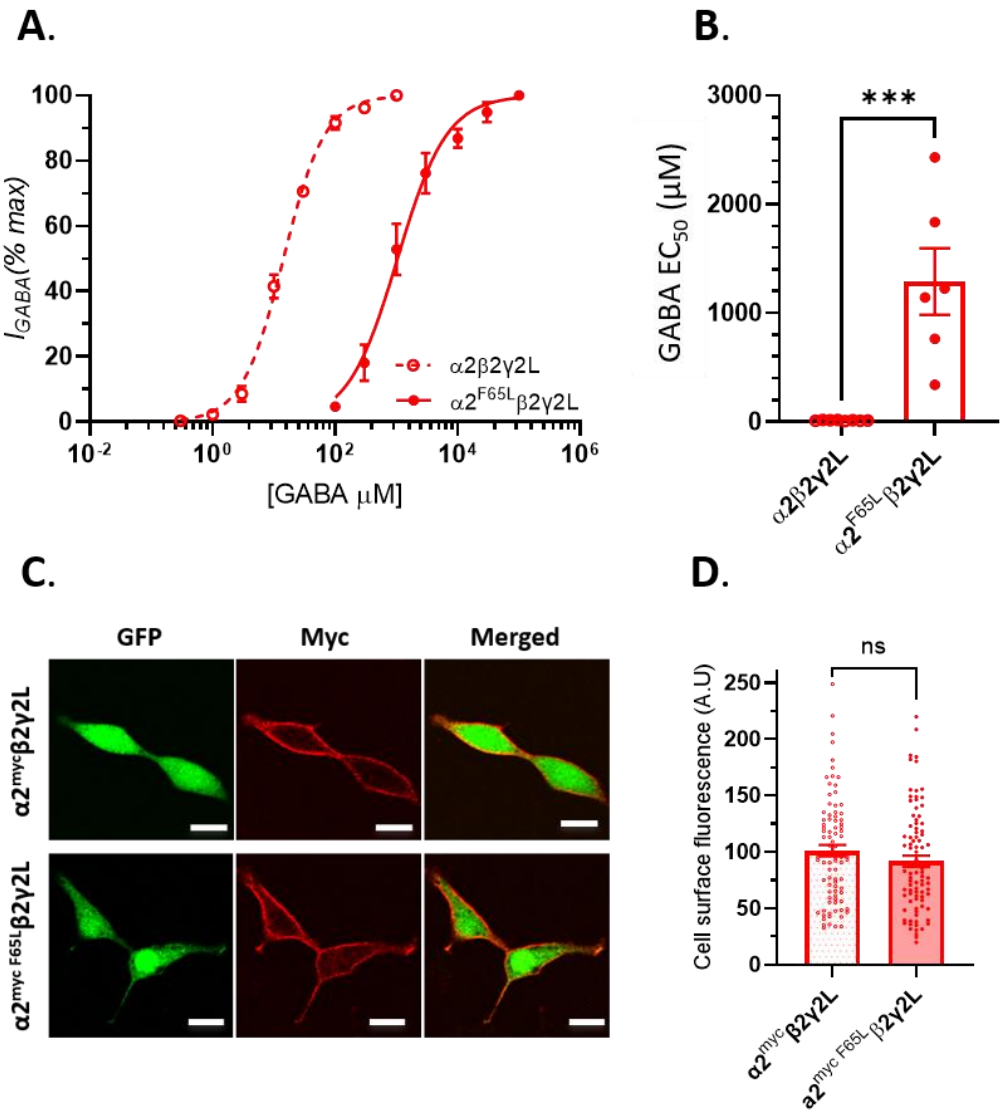

Figure 3.10 GABA$_A$R α2 subunit phenylalanine to leucine substitution at residue position 65 results in a decreased GABA-sensitivity, however does not reduce cell surface expression. **A.** Concentration response relationships of α2β2γ2L (○) (n = 7, n_H = 1.2 ± 0.1) and α2^{F65L}β2γ2L (●) (n = 5, n_H = 1.2±0.1). **B.** Bar chart representing the mean ± SEM GABA EC_{50} values α2β2γ2L (○) and α2^{F65L}β2γ2L (●) are 13.4 ± 0.1 μM and 947.1 ± 101.1 μM (unpaired *t*-test, P ≤ 0.001 ***). **C.** Representative confocal images of cell surface labelling in HEK293 cells expressing α2^{myc}β2γ2L (top row) α2$^{myc\ F65L}$β2γ2L (bottom row) GABA$_A$ receptors. Cells were co-transfected with eGFP for identification. Scale bars = 10 μm. **D.** Quantification of mean fluorescence intensities for myc-tagged α2 and α2^{F65L} containing GABA$_A$ receptors (101.1 ± 5.0 a. u. and 91.7 ± 5.0 a. u. respectively, unpaired t-test, P value n. s., not significant), n=3 cultures.

3.3.4 Co-expression of α1 and $\alpha2^{F65L}$ subunits

Here an F65L mutation on the α2 $GABA_A$ receptor subunit was used to establish the number of receptor populations in α1 and $\alpha2^{F65L}$ co-expressing HEK293 cells. The same approach was applied as that described in ***Section 3.3.2***. Firstly, the GABA EC_{50} values were obtained for 'homo-alpha' expressing receptors: α1β2γ2L and $\alpha2^{F65L}$β2γ2L (9.0 ± 0.7 μM and 947.1 ± 101.1 μM respectively) (***Figure 3.11 A***). Since there was a ~ 105-fold difference between α1 and $\alpha2^{F65L}$ containing receptors GABA apparent affinities, the EC_{50} value of the middle component (α1$\alpha2^{F65L}$β2γ2L) was estimated to be ~ 92 μM.

Next, equimolar ratios of α1, $\alpha2^{F65L}$, β2, γ2L subunits (+eGFP) cDNAs were expressed in HEK293 cells. The mean concentration response profile obtained for this subunit combination was fitted with both two and three component Hill equations to establish which gave a better fit of the data. Since there was no difference between χ^2 values of two- and three-component fits (3.03 and 3.06 respectively) of α1$\alpha2^{F65L}$β2γ2L-expressing cells (***Figure 3.11 C***), a sum of two Hill equations was considered to be a better fit. The EC_{50} value of the first component was 16.0 ± 0.8 μM likely to represent the α1α1β2γ2L $GABA_A$ receptor population. This receptor population accounted for the majority of the receptor pool (85.2 ± 1.3 %). The GABA sensitivity of a second component was 3005.1 ± 971.7 μM and accounted for the remaining 13.9 ± 1.6 % of receptors. This receptor population could represent the $\alpha2^{F65L}\alpha2^{F65L}$β2γ2L receptors.

Concentration response profiles of α1$\alpha2^{F65L}$β3γ2L-expressing HEK293 cells were fitted with the sum of two and three Hill equations (***Figure 3.11 B and C***). Similar to β2-containing receptors, no difference was observed in two- and three-component fits (χ^2 3.04 and 3.11 respectively). The sum of two Hill equations revealed the first component is dominating over the second one (85.2 ± 1.3 % and 13.9 ± 1.6 %). The EC_{50} value of the first component was estimated at 16.0 ± 0.8 μM and is likely to represent the α1α1β3γ2L $GABA_A$ receptor population. The second component had a GABA apparent affinity of 3005.1 ± 971.7 μM and is likely to represent the $\alpha2^{F65L}\alpha2^{F65L}$β3γ2L receptor population.

Using the $\alpha2^{F65L}$ reporter mutation as a tool to dissect the number of receptor populations and their relative abundance in both β2- and β3- containing 'hetero-alpha'-expressing HEK293 cells suggested that there are only two receptor populations in the mixture pool: α1α1βγ2L and $\alpha2^{F65L}\alpha2^{F65L}$βγ2L. This was surprising, as all the data presented so far indicates the presence of 'hetero-alpha' receptors when co-expressing α1 and α2 subunits. A possible explanation for a two-, rather than a three-component fit could be that, when a mutant α subunit is co-transfected with a wild type α subunit, the expression of the wild-type α receptors predominates. This is observed in both β2- and β3- containing receptors, where the α1α1βγ2L is largely prevalent over other receptor populations (85.2 ± 1.3 %). The remaining 13.9 ± 1.6 % could comprise of both α1$\alpha2^{F65L}$βγ2L and $\alpha2^{F65L}\alpha2^{F65L}$βγ2L receptor populations, however it would be hard to observe at the 'top-end' of the curve.

A. **B.**

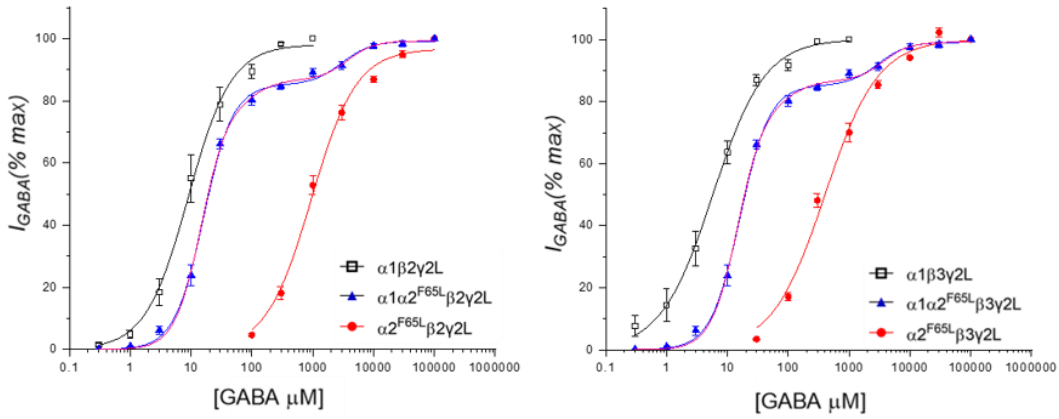

C.

Hill equation components	Two-component fit (blue)		Three-component fit (magenta)	
	EC_{50} (µM)	Percentage (%)	EC_{50} (µM)	Percentage (%)
1st component	16.0±0.8	85.2±1.3	14.8±1.4	80.3±4.8
2nd component	3005.1±971.7	13.9±1.6	120.0±0.0	6.4±5.9
3rd component	-	-	3699.7±1353.4	12.5±2.0
χ^2	3.03		3.06	

D.

Hill equation components	Two-component fit (blue)		Three-component fit (magenta)	
	EC_{50} (µM)	Percentage (%)	EC_{50} (µM)	Percentage (%)
1st component	16.0±0.8	85.2±1.3	14.8±1.5	80.3±5.1
2nd component	3005.1±971.7	13.9±1.6	115.0±0.0	6.4±6.2
3rd component	-	-	3651.9±1333.6	12.6±2.0
χ^2	3.04		3.11	

Figure 3.11 GABA dose-response relationships from co-expression of α1 and α2^{F65L} subunits in HEK293 cells. **A.** Concentration response relationships of α1β2γ2L (□) (n = 7, n_H = 1.2 ± 0.1), α2^{F65L}β2γ2L (●) (n = 5, n_H = 1.2 ± 0.1) and α1α2^{F65L}β2γ2L (▲) (n = 6). The fit for α1α2^{F65L}β2γ2L was done with two (blue) or three (magenta) Hill equations. Cumulative Hill coefficient (n_H) values are 1.8 ± 0.1 (two-component fit) and 2.0 ± 0.2 (three-component fit). The GABA EC_{50} values for α1β2γ2L (□) and α2^{F65L}β2γ2L (●) are 9.0 ± 0.7 µM and 947.1 ± 101.1 µM respectively. **B.** Concentration response relationships of α1β3γ2L (□) (n = 6, n_H = 1.1 ± 0.1), α2^{F65L}β3γ2L (●) (n = 6, n_H = 1.0 ± 0.1) and α1α2^{F65L}β3γ2L (▲) (n = 6). The latter was fit with two (blue) or three (magenta) Hill equations. Cumulative Hill coefficient (n_H) values are 1.8 ± 0.1 (two-component fit) and 2.0 ± 0.2 (three-component fit). The GABA EC_{50} values for α1β3γ2L (□) and α2^{F65L}β3γ2L (●) are 5.8 ± 0.5 µM and 401.2 ± 52.4 µM respectively. Tables **C** and **D** summarise the EC_{50} values (µM) and relative percentages (%) of α1α2^{F65L}β2γ2L (C) and α1α2^{F65L}β3γ2L (**D**) Hill equation-fitted components.

3.3.5 Co-expression of α2 and $\alpha2^{F65L}$ subunits

To establish whether co-expression of wild type and F65L mutant α subunits affects the assembly of 'hetero-alpha' and 'homo-alpha' mutant populations, the same receptors subtype was co-expressed in HEK293 cells: α2 and $\alpha2^{F65L}$. In theory, co-expression of α2 and $\alpha2^{F65L}$ (plus β2 γ2L) subunits would result in three receptor populations (α2α2β2γ2L, α2$\alpha2^{F65L}$β2γ2L, and $\alpha2^{F65L}\alpha2^{F65L}$β2γ2L) and their relative abundance would follow a binomial distribution (25 : 50 : 25) (Chang et al., 1996a).

To do that, equimolar ratios of α2, $\alpha2^{F65L}$, β2, γ2L subunits (+eGFP) cDNAs were expressed in HEK293 cells and GABA concentration response profiles were obtained (***Figure 3.12***). The curve was described using a sum of two and three component Hill equations (χ^2 5.19 and 4.18 respectively). The EC_{50} of the three components of a three-component fit were 12.9 ± 1.5 μM, 44.1 ± 34.0 μM, and 2642.9 ± 1184.0 μM and accounted for 78.9 ± 2.3 %, 7.6 ± 0.9 %, and 14.0 ± 1.5 % respectively. These are likely to represent α2α2β2γ2L, α2$\alpha2^{F65L}$β2γ2L, and $\alpha2^{F65L}\alpha2^{F65L}$β2γ2L respectively. As expected the 'homo-alpha' wild type α2 receptor population accounts for more than two thirds of the total receptor pool. The 'hetero-alpha' receptor population represents only a small fraction (7.6 ± 0.9 %) of the total receptor pool. From this data is clear that co-expression of α2 and $\alpha2^{F65L}$ subunits results in the minimal expression of receptors containing both subunit isoforms. Furthermore, most of the receptors, when subunits are expressed in equimolar ratios, form 'homo-alpha' wild-type containing $GABA_A$ receptors.

Overall, the $\alpha2^{F65L}$ substitution has proven to not be a good tool to establish the stoichiometry of receptor populations and their relative abundance, when co-expressing α1 and $\alpha2^{F65L}$ subunits. Even though immunolabelling of wild type and mutant $\alpha2^{myc}$ subunits revealed no change in subunit expression on the cell surface (***Figure 3.10 D***), electrophysiological assessment of α2$\alpha2^{F65L}$β2γ2L-transfected HEK293 cells demonstrate a strong prevalence of α2α2-containing population over other receptor stoichiometries (***Figure 3.12***).

A.

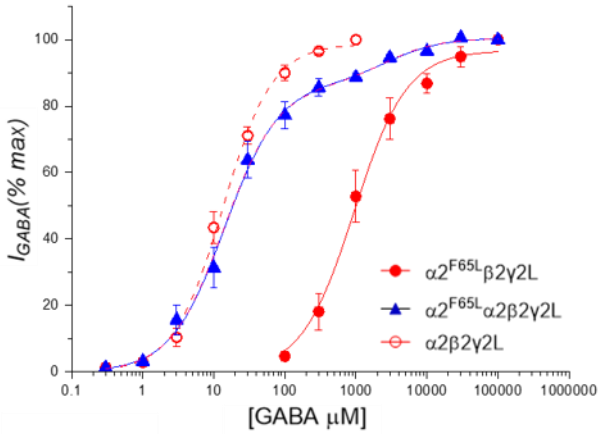

B.

Hill equation components	Two-component fit (blue)		Three-component fit (magenta)	
	EC_{50} (µM)	Percentage (%)	EC_{50} (µM)	Percentage (%)
1st component	14.2 ± 1.5	86.7 ± 2.9	12.9 ± 1.5	78.9 ± 2.3
2nd component	2827.8 ± 2194.5	13.8 ± 2.9	44.1 ± 34.0	7.6 ± 0.9
3rd component	-	-	2642.9 ± 1184.0	14.0 ± 1.5
χ^2	5.19		4.18	

Figure 3.12 GABA dose-response relationships from co-expression of α2 and α2^{F65L} subunits in HEK293 cells. **A.** Concentration response relationships of α2β2γ2L (○) (n = 7, n_H = 1.2±0.1), α2^{F65L}β2γ2L (●) (n = 5, n_H = 1.2 ± 0.1) and α2α2^{F65L}β2γ2L (▲) (n = 6). The latter was fit with the sum of two (blue) or three (magenta) Hill equations (two and three components respectively). Cumulative Hill coefficient (n_H) values are 1.1 ± 0.1 (two-component fit) and 1.2 ± 0.1 (three-component fit). The EC_{50} values for α2β2γ2L (○) and α2^{F65L}β2γ2L (●) are 13.4 ± 0.1 µM and 947.1 ± 101.1 µM respectively. **B.** Table summarising the EC_{50} values (µM) and relative percentages (%) of α2α2^{F65L}β2γ2L Hill equation-fitted components. The value of the χ^2 distribution is lower for a fit of three components, suggesting that there are three receptor populations with distinct GABA sensitivities (α2β2γ2L, α2α2^{F65L}β2γ2L, and α2^{F65L}β2γ2L).

3.3.6 Summary of results from α1^{L263S} and α2^{F65L}

Here, two reporter mutations, α1^{L263S} and α2^{F65L}, were used to dissect the number and types of receptor populations as well as their relative abundances when co-

expressing α1 and α2 subunits. Furthermore, differences between β2- and β3-containing receptors were investigated. A method initially described by Chang. et al., 1996 was used to determine curve fits comprising a sum of either two or three Hill equations. From this subsection, a few conclusions can be drawn. The limitations of this technique will be described in the discussion section of this chapter.

Firstly, characterisation of $\alpha1^{L263S}$ and $\alpha2^{F65L}$ reporter mutations was done, prior to using them to characterise multicomponent concentration response profiles. The data obtained for these mutations are in good agreement with the previous data (Baumann et al., 2003; Chang et al., 1996b; Chang and Weiss, 1999; Patel et al., 2014; Sigel et al., 1992).

Co-expression of $\alpha1^{L263S}$ and α2 with β2, and γ2L subunits revealed the presence of three distinct receptor populations: two 'homo-alpha' and one 'hetero-alpha' populations. The 'hetero-alpha' population accounted for ~45% of the total receptor pool, whereas the $\alpha1^{L263S}\alpha1^{L263S}$-containing receptor population comprised a small percentage of the total receptor number (~ 6 %). Interestingly, the same α subunit combination co-expressed with a β3 (+ γ2L) seemed to form only two receptor populations which are likely to be $\alpha1^{L263S}$α2β3γ2L and α2α2β3γ2L. This implies that in β3-containing 'hetero-alpha' mixtures might not express the $\alpha1^{L263S}\alpha1^{L263}$ receptors. Additionally, the $\alpha1^{L263S}$α2β3γ2L population accounted for more than 67% of the total receptor pool. It is worth mentioning. However, that the two and three component fits for the β3-containing receptors had very similar goodness of fit values (χ^2 1.76 and 1.59 respectively), so it could be possible that the $\alpha1^{L263S}\alpha1^{L263}$ receptors are present at a very small percentage (~ 10 %) (***Figure 3.9 D***).

The data obtained from α1 and $\alpha2^{F65L}$ co-expression suggested that both β2- and β3-containing receptors form two 'homo-alpha' populations, where α1α1-containing receptor stoichiometry accounts for the majority of the receptor number (~ 85 %). The χ^2 statistics between the two and three component fits were very similar (see ***Figure 3.11 C and D***). This could imply that the third component is thus present, however its relative abundance is low (~ 6 %).

Taken together, this data indicates that 'hetero-alpha' receptors are expressed in HEK293 cells. Furthermore, β3-containing receptors seem to have a preference towards a 'hetero-alpha' receptor assembly, over β2-containing receptors.

3.4 Results: Insight into subunit arrangement of 'hetero-alpha' $GABA_A$ receptors

So far, the evidence towards the presence of 'hetero-alpha' receptor populations in HEK293 cells was presented. The next aim of this project was to establish the subunit arrangement of the receptors incorporating two distinct α subunit isoforms: α1 and α2. Here, we investigate the subunit arrangement of tri-heteromeric $GABA_A$ receptors in α1α2β2/3γ2L-expressing HEK293 cells. As mentioned in ***Section 3.1*** of this chapter, a well characterised H101R substitution in the α subunit will be used.

3.4.1 Validation of benzodiazepine insensitive mutations on α1 and α2 $GABA_AR$ subunits

Here, a mutation of a conserved amino acid residue in the α subunit (H101R) was used. This mutation has been previously well characterised in HEK293 cells and used in knock-in animal models to study α subunit selective BDZ effects (Benson et al., 1998b; Kleingoor et al., 1993b; Löw et al., 2000; Rudolph et al., 1999; Wieland et al., 1992b). Our first objective was to validate the $\alpha1^{H101R}$ and $\alpha2^{H101R}$ constructs in HEK293 system. Firstly, an optimal potentiating dose of benzodiazepine – flurazepam (FLU) was obtained by potentiating GABA $EC_{15\text{-}25}$ (3 μM) with varying FLU concentrations in α1β2γ2L-expressing HEK293 cells (***Figure 3.13 A***). All FLU potentiating experiments were done with 30-second pre-application of FLU through the wash tube, followed by co-application of FLU + GABA. From ***Figure 3.13 A***, a concentration of 300 nM FLU was taken as an optimal dose for all following experiments.

Next, the extent of FLU potentiation on the GABA concentration response profiles of α1β2γ2L- and α2β2γ2L-transfected HEK293 cells was measured. The GABA EC_{50} decreased 1.4- and 1.9-fold with 300 nM FLU application for α1β2γ2L and α2β2γ2L constructs respectively (***Figure 3.13 B and C***). Similar increases in GABA apparent potencies were observed previously with 300 nM flurazepam in *Xenopus* oocytes and 1 μM diazepam in HEK293 cells (Benson et al., 1998a; Reynolds and Maitra, 1996).

The effects of the H101R mutation in α1 and α2 subunits on the BDZ potentiation of GABA activated-currents was assessed. Relying on the previous literature, we expected to see a complete ablation of potentiation at 300 nM BDZ (Benson et al., 1998a; Kleingoor et al., 1993a; Wieland et al., 1992a). Indeed, the GABA EC_{50} of $\alpha1^{H101R}$β2γ2L- and $\alpha1^{H101R}$β2γ2 -expressing HEK293 cells did not change in the presence of 300 nM flurazepam (P values: 0.82 and 0.98 respectively), consistent with previously published values (Benson et al., 1998a).

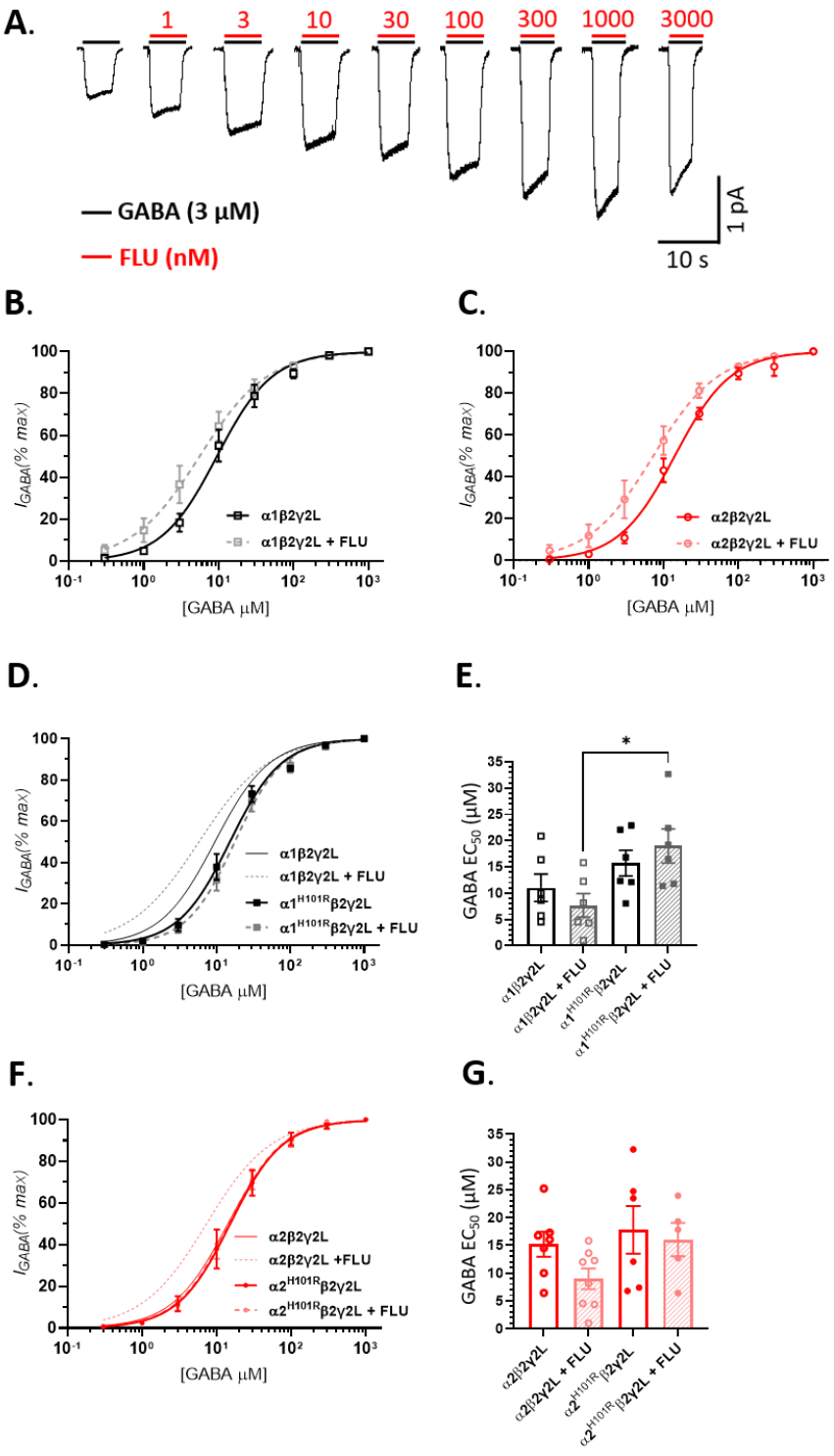

Figure 3.13 The H101R substitution in the α1/2 GABA$_A$ receptor subunit results in flurazepam insensitivity, however does not affect GABA sensitivity. **A.** Representative GABA-activated current traces (3 µM, EC_{15-25}) with the 30-second pre-application of increasing doses of flurazepam (FLU) to reveal the optimum FLU dose for $GABA_A$ receptor current potentiation. The FLU dose that was chosen for later experiments was 300 nM. **B.** and **C.** GABA concentration response profiles of α1β2γ2L (**B.**) and α2β2γ2L (**C.**) with/without flurazepam. **D.** GABA concentration response profiles of α1β2γ2L and $α1^{H101R}$β2γ2L +/- 300

nM flurazepam. The data points for α1β2γ2L are shown in panel **B.** The Hill coefficients are: α1β2γ2L (n = 6, n_H = 1.4 ± 0.1), α1β2γ2L + FLU (n = 6, n_H = 1.1 ± 0.04), α1^{H101R}β2γ2L (n = 6, n_H = 1.3 ± 0.1), α1^{H101R}β2γ2L + FLU (n = 6, n_H = 1.4 ± 0.1). **E.** Bar chart representing the mean GABA EC_{50} values for α1β2γ2L (□, black) (n = 6, EC_{50} = 11.0 ± 2.6 μM), α1β2γ2L + FLU (□, grey) (n = 6, EC_{50} = 7.6 ± 2.3 μM), α1^{H101R}β2γ2L (■) (n = 6, EC_{50} = 15.7 ± 2.4 μM), α1^{H101R}β2γ2L + FLU (■) (n = 6, EC_{50} = 17.3 ± 2.0 μM), (one-way ANOVA with Tukey's post hoc test for multiple comparisons between all groups, P value: ≤ 0.05 *). **F.** GABA concentration response relationships of α2β2γ2L and α2^{H101R}β2γ2L +/- 300 nM flurazepam. The data points for α1β2γ2L are shown in panel **C.** The Hill coefficients from the curve fits are: α2β2γ2L (n = 7, n_H = 1.2±0.1), α2β2γ2L + FLU (n = 8, n_H = 1.2 ± 0.1), α2^{H101R}β2γ2L (n = 6, n_H = 1.4 ± 0.03), α2^{H101R}β2γ2L + FLU (n = 6, n_H = 1.4 ± 0.1). **G**. The mean GABA EC_{50} values for α2β2γ2L (○, red) (n = 7, EC_{50} = 15.2 ± 2.5 μM), α2β2γ2L + FLU (○, light red) (n = 8, EC_{50} = 9.0 ± 1.9 μM), α2^{H101R}β2γ2L (●) (n = 6, EC_{50} = 17.8 ± 4.3 μM), α2^{H101R}β2γ2L + FLU (●) (n = 6, EC_{50} = 16.0 ± 3.0 μM). The mean EC_{50} values with SEMs are represented in the bar chart (one-way ANOVA with Tukey's post hoc test for multiple comparisons between all groups, P value: ≥ 0.05, n.s.).

Similarly, the ablation of benzodiazepine sensitivity of α1^{H101R} and α2^{H101R} mutant subunits in β3-containing receptors was validated. We first examined the extent of FLU potentiation in wild type receptors. The α1β3γ2L mean EC_{50} GABA shifted leftwards from 5.7 ± 1.1 μM to 4.0 ± 0.8 μM with FLU, whereas α2β3γ2L GABA potency increased from 15.2 ± 2.6 μM to 9.6 ± 2.1 μM, contributing to 42 % and 58 % increase in apparent GABA affinity respectively (***Figure 3.14 A and B***). Interestingly, the GABA dose response relationship of α1^{H101R}β3γ2L (5.7 ± 1.1 μM) experienced a significant rightward shift compared to its wild type counterpart, α1β3γ2L (110.0 ± 21.8 μM) (P value ≤ 0.001) (***Figure 13 C and D***). A statistically significant decrease in GABA apparent affinity was also observed between α2β3γ2L- and α2^{H101R}β3γ2L-expressing HEK293 cells (15.2 ± 2.6 μM and 95.7 ± 15.6 μM respectively, P value ≤ 0.01) (***Figure 3.14 E and F***). This rightward shift of the GABA CRC with H101R mutation introduction into the α subunit in recombinant β3-containing $GABA_A$ receptors was previously observed (Benson et al., 1998a).

The potentiating effect of flurazepam on α1^{H101R}β3γ2L GABA EC_{50} was abolished (110.0 ± 21.8 μM and 97.7 ± 22.5 μM, without and with FLU respectively), similar to α2^{H101R}β3γ2L (73.5 ± 17.0 μM and 95.7 ± 15.6 μM, without and with FLU respectively) (***Figure 3.14 C-F***).

Overall, the H101R mutation of the α1 and α2 subunits was shown to ablate the effects of FLU potentiation of the GABA concentration response profiles, making this amino acid substitution a useful tool to assess subunit arrangement of 'hetero-alpha' transfected HEK293 cells.

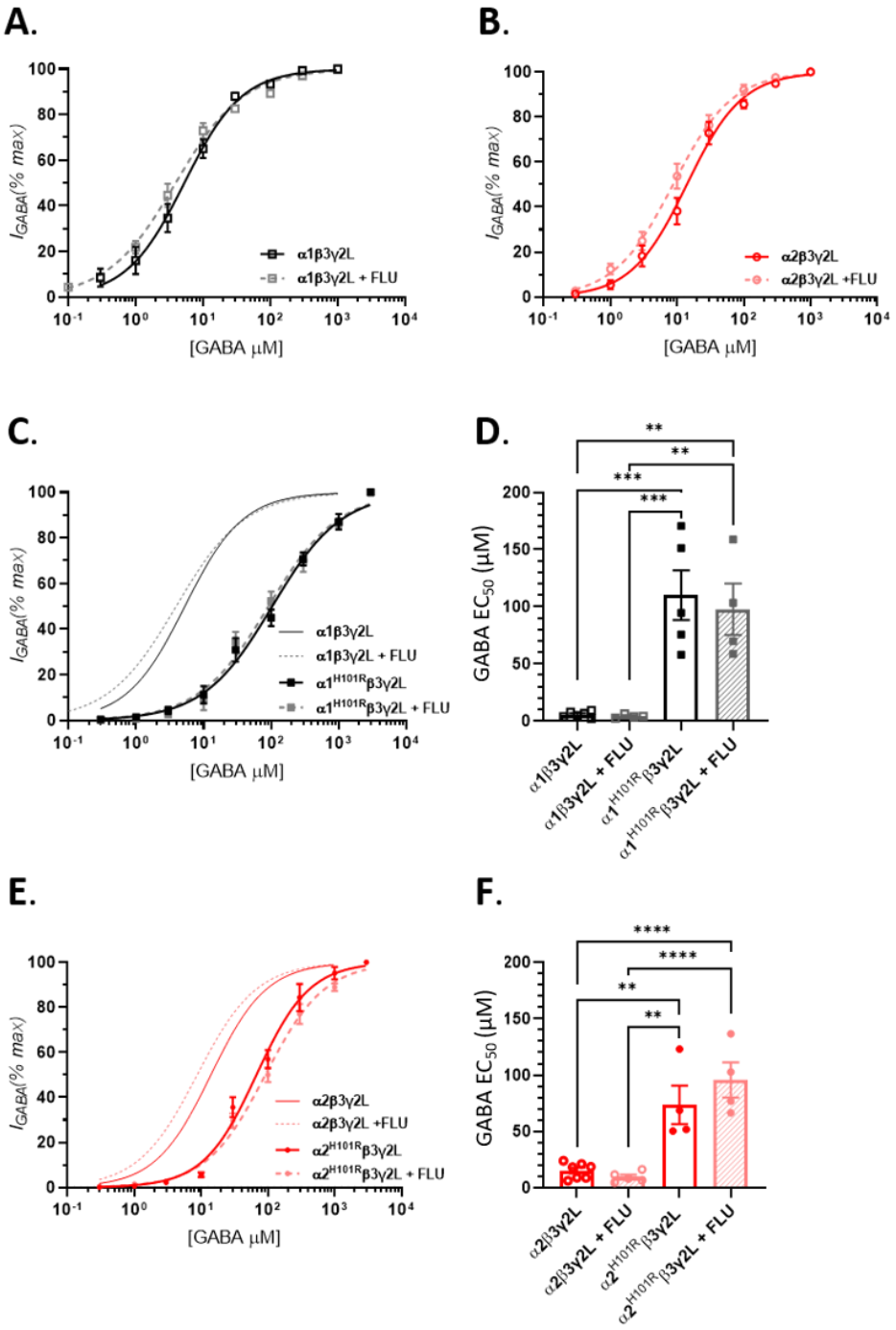

Figure 3.14 The H101R substitution in the α1/2 GABA$_A$ receptor subunit results in flurazepam insensitivity and reduces GABA sensitivity of β3-containing receptors. **A.** and **B.** GABA concentration response profiles of α1β3γ2L (**A.**) and α2β3γ2L (**B.**) with/without flurazepam. The n_H and EC_{50} values are given below. **C.** GABA concentration response profiles of α1β3γ2L and $\alpha1^{H101R}$β3γ2L +/- flurazepam (300 nM). The data points for α1β3γ2L are shown in panel **A.** The Hill coefficients are: α1β3γ2L (n = 6, n_H = 1.1 ± 0.1), α1β3γ2L + FLU (n = 4, n_H = 0.9 ± 0.01), $\alpha1^{H101R}$β3γ2L (n = 5, n_H =0.9 ± 0.1), $\alpha1^{H101R}$β3γ2L + FLU (n = 4, n_H = 0.9 ± 0.1). **D.** Bar chart representing the mean GABA EC_{50} values for α1β3γ2L (□, black) (n = 6, EC_{50} = 5.7 ± 1.1 µM), α1β3γ2L + FLU (□, grey) (n = 4, EC_{50} = 4.0 ± 0.8 µM), $\alpha1^{H101R}$β3γ2L (■) (n = 5,

EC_{50} = 110.0 ± 21.8 µM), $\alpha1^{H101R}\beta3\gamma2L$ + FLU (■) (n = 4, EC_{50} = 97.7 ± 22.5 µM), (one-way ANOVA with Tukey's post hoc test for multiple comparisons between all groups, P value: ≤ 0.01 **, ≤ 0.001 ***). **E.** GABA concentration response relationships of α2β3γ2L and $\alpha2^{H101R}\beta3\gamma2L$ +/- flurazepam (300 nM). The data points for α1β3γ2L are shown in panel **B.** The Hill coefficients from the curve fits are: α2β3γ2L (n = 7, n_H = 1.2 ± 0.1), α2β3γ2L + FLU (n = 5, n_H = 1.0 ± 0.04), $\alpha2^{H101R}\beta3\gamma2L$ (n = 4, n_H = 1.1 ± 0.1), $\alpha2^{H101R}\beta3\gamma2L$ + FLU (n = 4, n_H = 1.0 ± 0.02). **F**. The mean GABA EC_{50} values for α2β3γ2L (○, red) (n = 7, EC_{50} = 15.2 ± 2.6 µM), α2β3γ2L + FLU (○, light red) (n = 5, EC_{50} = 9.6 ± 2.1 µM), $\alpha2^{H101R}\beta3\gamma2L$ (●) (n = 4, EC_{50} = 73.5 ± 17.0 µM), $\alpha2^{H101R}\beta3\gamma2L$ + FLU (●) (n = 4, EC_{50} = 95.7 ± 15.6 µM), (one-way ANOVA with Tukey's post hoc test for multiple comparisons between all groups, P value: ≤ 0.01 **, ≤ 0.001 ***).

3.4.2 Assessment of subunit arrangement of 'hetero-alpha' β2-containing receptors using reporter mutations $\alpha1^{H101R}$ and $\alpha2^{H101R}$.

As described in ***Section 3.1*** of this chapter, the aim was to infer the relative subunit positioning of α1α2-containing $GABA_A$ receptor mixtures at the α/γ interface. By co-transfecting α1 and α2 subunits (+β2 and γ2L), where one of the α subunits presents an H101R substitution, the α/γ interface could be established. For example, co-expression of $\alpha1^{H101R}$ and α2, would theoretically yield four distinct receptor population, two of which contain an $\alpha1^{H101R}$/γ2L interface, and therefore are BDZ insensitive: $\alpha1^{H101R}\gamma2L\beta2\alpha1^{H101R}\beta2$ and $\alpha1^{H101R}\gamma2L\beta2\alpha2\beta2$; and two with an α2/γ2L high-affinity BDZ site: α2γ2Lβ2α2β2 and $\alpha2\gamma2L\beta2\alpha1^{H101R}\beta2$ (***Figure 3.2 A***). Examination of whether the receptors are potentiated, and if so the extent of this potentiation allows us to determine identity of the α subunit adjacent to γ2L as well as the most likely subunit combination arrangements.

Firstly, the α1/γ2L interface sensitivity to BDZ was ablated by co-transfecting equimolar ratios of $\alpha1^{H101R}$, α2, β2 and γ2L subunits cDNAs in HEK293 cells. The GABA concentration response relationships in the absence/presence of 300 nM flurazepam were obtained (***Figure 3.15 A***). There was an overall 1.6-fold decrease in GABA apparent affinity from 13.2 ± 3.3 µM to 8.5 ± 1.4 µM. For the ease of data interpretation and reference, ***Table 3.1*** shows all the GABA EC_{50}s for various constructs tested in the absence / presence of flurazepam. Furthermore, the GABA concentration response relationship of $\alpha1^{H101R}\alpha2\beta2\gamma2L$ + FLU was better described

by a sum of two, rather than one component Hill equations (χ^2 2.53 and 2.92 respectively), indicating the presence of two distinct populations (***Figure 3.15 F***). The first component of the $\alpha1^{H101R}\alpha2\beta2\gamma2L$ + FLU is leftward shifted (EC_{50} 2.8 ±0.8 μM), corresponding to the $GABA_A$ receptors with α2/γ2L BDZ-sensitive interface, whereas the second component corresponds to $\alpha1^{H101R}$/γ2L BDZ-insensitive interface-containing $GABA_A$Rs (21.3 ± 6.3 μM) (***Figure 3.15 E***). The relative proportion of the two components was similar, accounting for 51.1 ± 10.8 % (α2/γ2L interface-containing) and 48.1 ± 10.4 % ($\alpha1^{H101R}$/γ2L interface-containing).

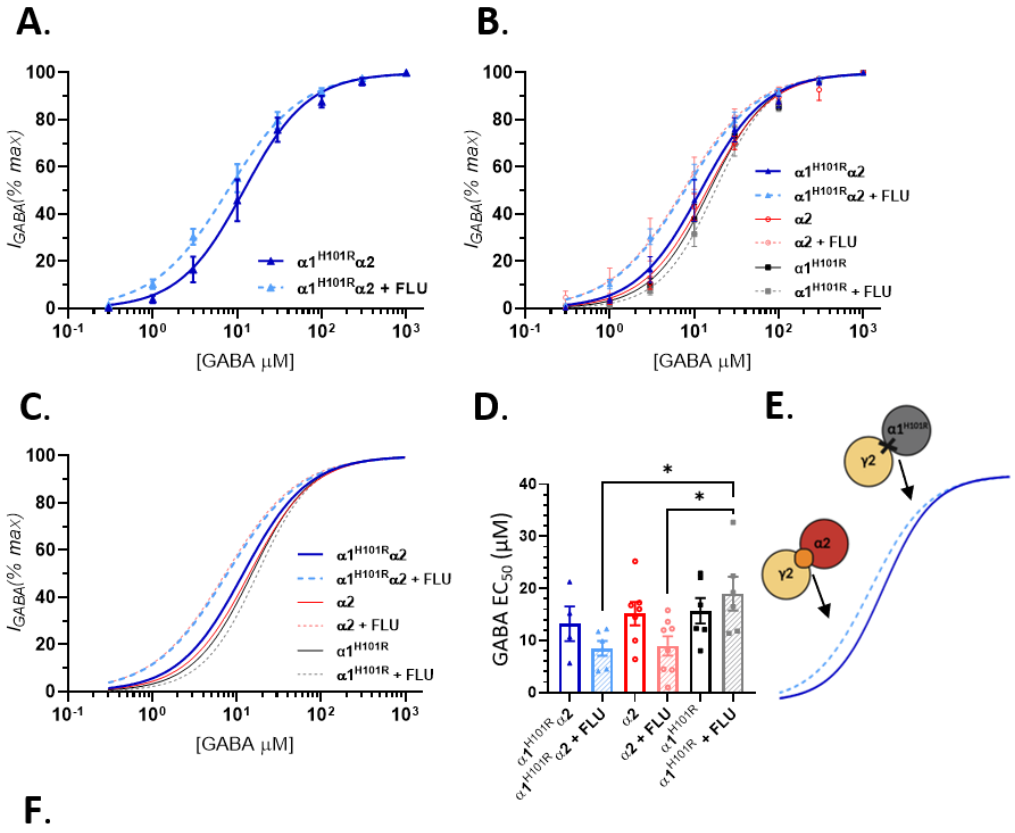

$\alpha1^{H101R}\alpha2\beta2\gamma2L$	GABA			GABA + FLU		
Hill equation components	**One-component fit**	**Two-component fit**		**One-component fit**	**Two-component fit**	
	EC_{50} (μM)	**EC_{50} (μM)**	**Percentage (%)**	**EC_{50} (μM)**	**EC_{50} (μM)**	**Percentage (%)**
1st component	13.2 ± 3.3	9.4 ± 0.8	89.6 ± 4.0	8.5 ± 1.4	2.8 ± 0.8	51.1 ± 10.8
2nd component	-	260.9 ± 205.7	12.5 ± 3.3	-	21.3 ± 6.3	48.1 ± 10.4
χ^2	4.31	1.39		2.92	2.53	

Figure 3.15 Removing benzodiazepine sensitivity of γ2/α1 interface in α1α2β2γ2L transfected HEK293 cells indicates the presence of both γ2/α1 and γ2/α2 interface-containing $GABA_A$ receptor populations. **A.** GABA concentration response profiles of $\alpha1^{H101R}\alpha2\beta2\gamma2L$ (▲) and $\alpha1^{H101R}$ $\alpha2\beta2\gamma2L$ plus flurazepam (FLU) (▲). **B** and **C.** GABA concentration response relationships of $\alpha1^{H101R}\alpha2\beta2\gamma2L$ (▲), $\alpha1^{H101R}\alpha2\beta2\gamma2L$ + FLU (▲), $\alpha2\beta2\gamma2L$ (○, red), $\alpha2\beta2\gamma2L$ + FLU (○, light red), $\alpha1^{H101R}\beta2\gamma2L$ (■), and $\alpha1^{H101R}\beta2\gamma2L$ + FLU (■). The hill coefficients from the curve fits are: (n = 4, n_H = 1.2±0.04), (n = 6, n_H = 1.1 ± 0.05), (n = 7, n_H = 1.2 ± 0.1), (n = 8, n_H = 1.2 ± 0.1), (n = 6, n_H = 1.3 ± 0.1), and (n = 6, n_H = 1.4 ± 0.1) respectively. Panel **C** represents the hill equation fits of panel **B**. **D**. Bar chart representing the mean ± SEM GABA EC_{50} values for $\alpha1^{H101R}\alpha2\beta2\gamma2L$ (▲) (n = 4, EC_{50} = 13.2 ± 3.3 μM), $\alpha1^{H101R}\alpha2\beta2\gamma2L$ + FLU (▲) (n = 6, EC_{50} = 8.5 ± 1.4 μM), $\alpha2\beta2\gamma2L$ (○, red) (n = 7, EC_{50} = 15.2 ±

2.2 µM), α2β2γ2L + FLU (○, light red) (n = 8, EC_{50} = 9.0 ± 1.9 µM), $\alpha1^{H101R}$β2γ2L (■) (n = 6, EC_{50} = 15.7 ± 2.4 µM), and $\alpha1^{H101R}$β2γ2L + FLU (■) (n = 6, EC_{50} = 19.0 ± 3.2 µM), (one-way ANOVA with Tukey's post hoc test for multiple comparisons between all groups, P value: ≤ 0.05 *). The EC_{50} values are summarised in ***Table 3.1*** of this chapter (see below). **E**. Cartoon representation of the γ2/α interfaces that could potentially result from the GABA CRC shifts shown in panel **A** (assuming double component fit of $\alpha1^{H101R}$α2β2γ2L + FLU). Bottom-end component is rightward shifted in the presence of FLU, indicating the γ2/α2 interface, whereas the top-end component indicated the presence of the γ2/$\alpha1^{H101R}$ interface (FLU insensitive). **F.** Table summarising single and double component EC_{50} and χ^2 values for $\alpha1^{H101R}$α2β2γ2L -/+ FLU.

Taking a similar approach for looking at α2/γ interface, we looked at the effect of the $\alpha2^{H101R}$ on the GABA concentration response profiles and BDZ potentiation of α1$\alpha2^{H101R}$β2γ2L-expressing HEK293 cells. By using this reporter mutation, BDZ sensitivity of α2/γ2L interfaces in possible receptor mixtures (α1γ2Lβ2α1β2, $\alpha2^{H101R}$γ2Lβ2$\alpha2^{H101R}$β2, α1γ2Lβ2$\alpha2^{H101R}$β2, and $\alpha2^{H101R}$γ2Lβ2α1β2) is predicted to be ablated. We generated GABA concentration response profiles (+/- 300 nM FLU) for HEK293 cells co-transfected with equimolar ratios of α1, $\alpha2^{H101R}$, β2, and γ2L subunits. The α1$\alpha2^{H101R}$β2γ2L GABA CRC exhibited a 2-fold leftward shift in the presence of 300 nM flurazepam (EC_{50} from 19.6 ± 4.2 µM to 9.7 ± 1.4 µM) (***Figure 3.16 A***). Similar to $\alpha1^{H101R}$α2β2γ2L, the potentiation of α1$\alpha2^{H101R}$β2γ2L GABA CRC by flurazepam was described as a sum of a two component Hill equations (***Figure 3.16 F***). The first and second components accounted for 60.6 ± 3.8 % and 40.0 ± 3.4 % of the total receptor pool, with GABA EC_{50} values of 3.5 ± 0.4 µM and 50.0 ± 8.7 µM respectively. This suggests that there are receptor populations with two distinct α/γ2L interfaces: a first component that experiences the decrease in GABA apparent affinity corresponds to receptor population(s) with α1/γ2L interface, whereas a second receptor population is BDZ-insensitive and therefore contains an $\alpha2^{H101R}$/γ2L interface (***Figure 3.16 E***).

Overall, experiments with H101R reporter mutations on the α1 and α2 $GABA_A$ receptor subunits suggest that, co-expression of both subunits together with β2 and γ2L are likely to yield receptor populations with both α1/γ2L and α2/γ2L interfaces. Furthermore, our data suggests that the relative proportion of these interfaces is similar, between 48.1 % and 60.6 % are α1/γ2L interface-containing and from 40.0 % to 51.1 % are α2/γ2L interface-containing. Since the GABA CRC leftward curve shifts

upon BDZ potentiation are minor (between 1.4- and 2-fold shift), it is hard to establish what curve shifts corresponds to potentiation of which receptor populations, i.e. ‘homo-alpha’ or ‘hetero-alpha’ $GABA_AR$s.

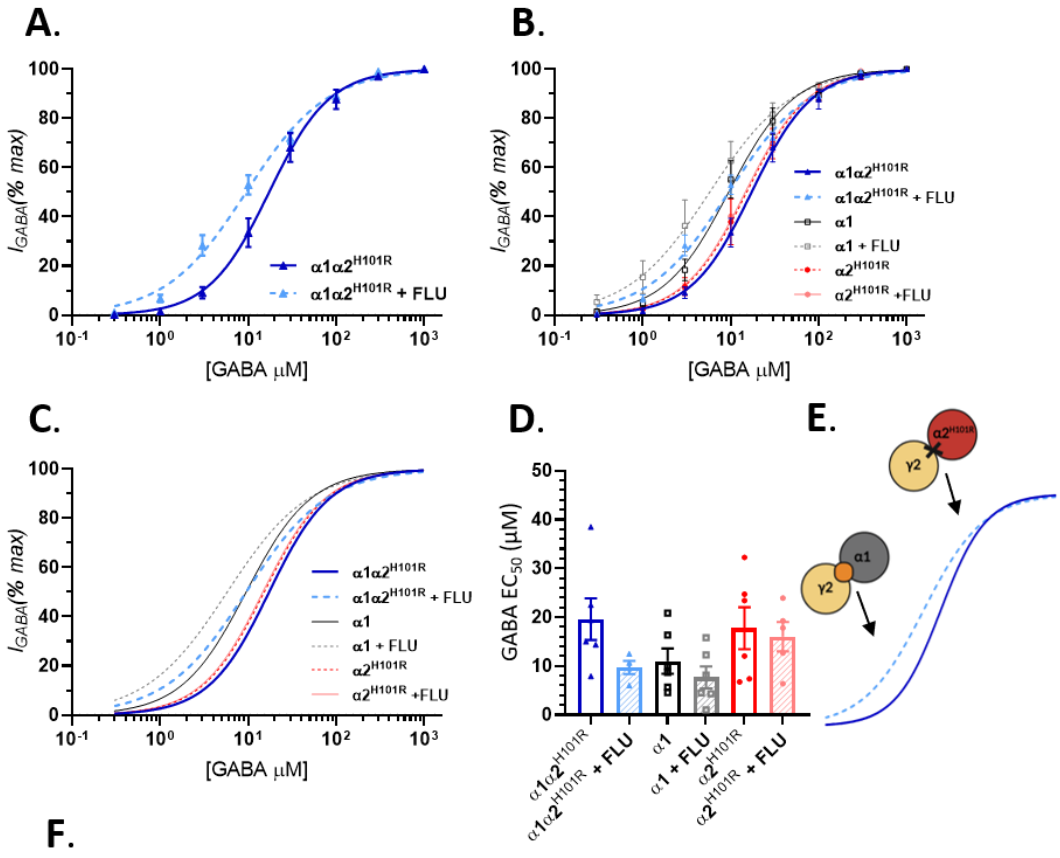

α1α2^{H101R}β2γ2L	GABA			GABA + FLU		
Hill equation components	**One-component fit**	**Two-component fit**		**One-component fit**	**Two-component fit**	
	EC_{50} (μM)	**EC_{50} (μM)**	**Percentage (%)**	**EC_{50} (μM)**	**EC_{50} (μM)**	**Percentage (%)**
1st component	19.6 ± 4.2	17.0 ± 1.4	48.2 ± 1.1	9.7 ± 1.4	3.5 ± 0.4	60.6 ± 3.8
2nd component	-	17.0 ± 1.4	51.1 ± 1.1	-	50.0 ± 8.7	40.0 ± 3.4
χ^2	1.94	1.94		10.19	1.85	

Figure 3.16 Mixture of α1 wild type and α2 benzodiazepine insensitive mutant subunits co-expressed with β2 and γ2 subunits results in γ2/α1 and γ2/α2 interface-containing $GABA_A$ receptor populations. **A.** GABA concentration response curves of α1α2^{H101R}β2γ2L (▲) and α1α2^{H101R}β2γ2L plus FLU (▲). **B** and **C.** GABA concentration response relationships of α1α2^{H101R}β2γ2L (▲) (n = 6, n_H = 1.4 ± 0.05), α1α2^{H101R} β2γ2L + FLU (▲) (n = 4, n_H = 1.0 ± 0.02), α1β2γ2L (□, black) (n = 6, n_H = 1.4 ± 0.1), α1β2γ2L + FLU (□, grey) (n = 6, n_H = 1.1 ± 0.04), α2^{H101R}β2γ2L (●) (n = 6, n_H = 1.4 ± 0.03), and α2^{H101R}β2γ2L + FLU (●) (n = 5, n_H = 1.4 ± 0.1). Panel **C** shows only the hill equation fits of **B** (no data points). **D**. Bar chart representing the mean GABA EC_{50} values of α1α2^{H101R}β2γ2L (▲) (n = 6, EC_{50} = 19.6 ± 4.3 μM), α1α2^{H101R} β2γ2L + FLU (▲) (n = 4, EC_{50} = 9.7 ± 1.4 μM), α1β2γ2L (□, black) (n = 6, EC_{50} = 11.0 ± 2.6 μM), α1β2γ2L + FLU (□, grey) (n = 6, EC_{50} = 7.7 ± 2.3 μM), α2^{H101R}β2γ2L (●) (n = 6, EC_{50} = 17.8 ± 4.3 μM), and

$\alpha2^{H101R}\beta2\gamma2L$ + FLU (●) (n = 5, EC_{50} = 16.0 ± 3.0 µM) transfected HEK293 cells. Statistical test: one-way ANOVA with Tukey's post hoc test for multiple comparisons between all groups was performed, P value: ≥ 0.05 n.s. The EC_{50} values are summarised in ***Table 3.1*** of this chapter (see below). **E**. Cartoon representation of the γ2/α interfaces that could be potentially result from the GABA CRC shifts shown in panel **A** (assuming double component fit of $\alpha1\alpha2^{H101R}\beta2\gamma2L$ + FLU). Higher apparent affinity component indicates the presence of an γ2/α1 interface that can be potentiated with FLU, whereas the lower apparent affinity component is FLU insensitive (γ2/$\alpha2^{H101R}$ interface containing $GABA_A$ receptors). **F.** Table summarising single and double component fit EC_{50} and χ^2 values for $\alpha1^{H101}\alpha2\beta2\gamma2L$ -/+ FLU.

3.4.3 Assessment of subunit arrangement of 'hetero-alpha' β3-containing receptors using reporter mutations $\alpha1^{H101R}$ and $\alpha2^{H101R}$.

So far, differences between β2- and β3-containing receptors in HEK293 cells co-expressing α1 and α2 subunits were established (***Sections 3.2 and 3.3*** of this chapter). It was, therefore, interesting to establish, whether subunit arrangement of β3-containing receptors could differ from that of β2-containing receptors. To achieve this aim, H101R reporter mutation was used to establish the identity of the α subunit at the α/γ2L interface, similarly to β2-containing receptors (***Section 3.4.2***). As shown in ***Figure 3.14 C and E***, the GABA concentration response profiles of $\alpha1^{H101R}\beta3\gamma2L$ and $\alpha2^{H101R}\beta3\gamma2L$ co-transfected HEK293 cells exhibit a prominent rightward shift compared to α1β3γ2L and α2β3γ2L (P values ≤ 0.001 and ≤ 0.01 respectively). This decrease in GABA apparent affinity allows for higher curve separation when establishing the respective receptor populations in multi-component Hill equation fits of $\alpha1^{H101R}\alpha2\beta3\gamma2L$ / $\alpha1\alpha2^{H101R}\beta3\gamma2L$ GABA CRC flurazepam potentiation.

We first ablated the BDZ sensitivity of all α1/γ2L interfaces high affinity BDZ sites by using an $\alpha1^{H101R}$ DNA construct. The GABA concentration response relationships were obtained in the absence or presence of 300 nM flurazepam in $\alpha1^{H101R}\beta3\gamma2L$-expressing HEK293 cells (***Figure 3.17 A***). The GABA EC_{50} value for $\alpha1^{H101R}\alpha2\beta3\gamma2L$ exhibited a 1.4-fold decrease in the presence of FLU (from 15.1 ± 2.9 µM to 10.5 ± 2.6 µM). Furthermore, the data obtained for flurazepam potentiation of the GABA CRC was better described by the sum of two Hill equations, rather than a single Hill equation component (χ^2 0.46 and 3.62 respectively) (***Figure 3.17 F***). The first component accounted for 77.5 ± 3.6 % of the total $GABA_A$ receptor population with

an EC_{50} value of 5.1 ± 0.5 µM, whereas the second component accounted for 23.9 ± 3.3 % (GABA EC_{50} 111.3 ± 27.3 µM). This suggests that there are two distinct receptor populations: the former correspond to $GABA_A$Rs with α2/γ2L BDZ-sensitive interface, and the latter represent the $\alpha1^{H101R}$/γ2L interface-containing receptors (***Figure 3.17 E***).

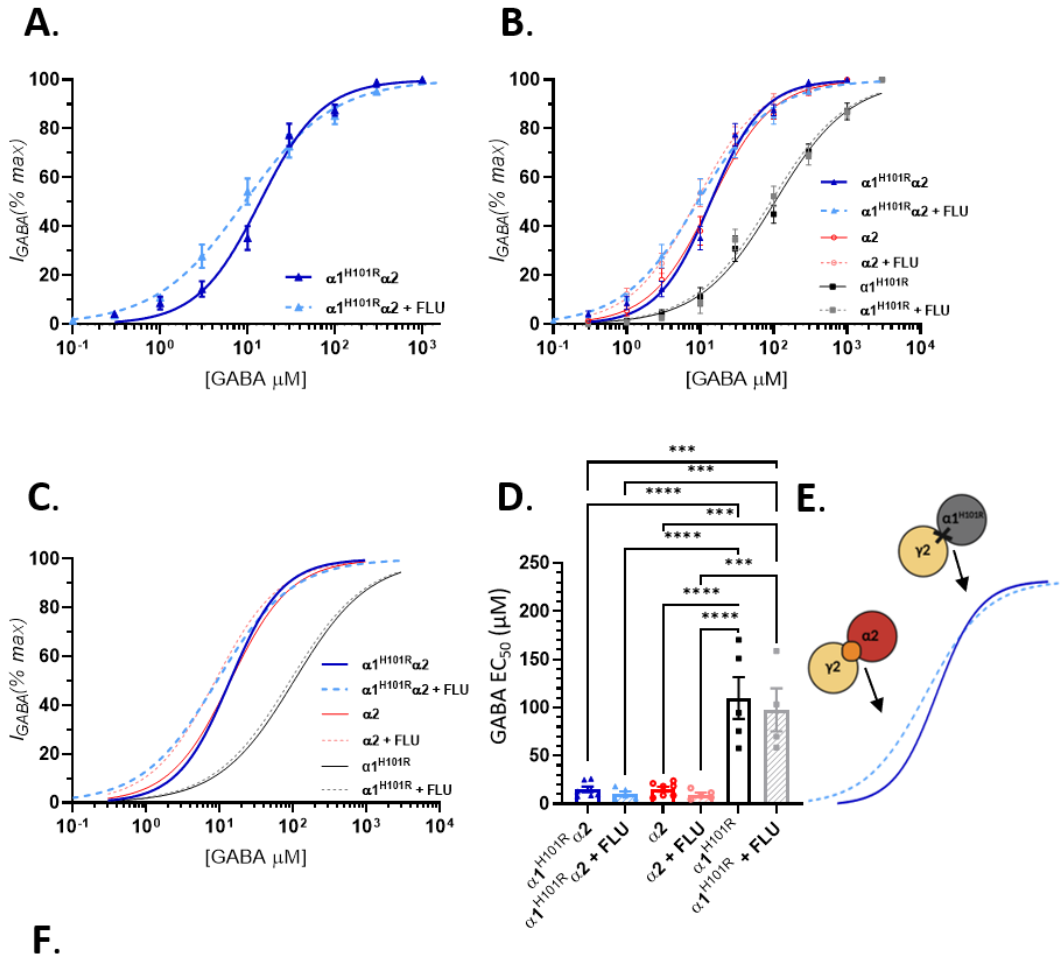

$\alpha1^{H101R}\alpha2\beta3\gamma2L$	GABA			GABA + FLU		
Hill equation components	**One-component fit**	**Two-component fit**		**One-component fit**	**Two-component fit**	
	EC_{50} (μM)	**EC_{50} (μM)**	**Percentage (%)**	**EC_{50} (μM)**	**EC_{50} (μM)**	**Percentage (%)**
1^{st} component	15.1 ± 2.9	14.0 ± 4.0	49.9 ± 3.7	10.5 ± 2.6	5.1 ± 0.5	77.5 ± 3.6
2^{nd} component	-	14.0 ± 4.0	50.5 ± 3.7	-	111.3 ± 27.3	23.9 ± 3.3
χ^2	21.93	21.93		3.62	0.46	

Figure 3.17 The H101R benzodiazepine insensitive mutation of the α1 subunit in α1α2β3γ2L transfected HEK293 cells indicates the presence of both γ2/α1 and γ2/α2 interface-containing $GABA_A$ receptor populations. **A.** GABA concentration response profiles of $\alpha1^{H101R}\alpha2\beta3\gamma2L$ (▲) and $\alpha1^{H101R}\alpha3\beta2\gamma2L$ plus FLU (▲). **B** and **C.** GABA concentration response relationships of $\alpha1^{H101R}\alpha2\beta3\gamma2L$ (▲) (n = 7, n_H = 1.3 ± 0.1), $\alpha1^{H101R}\alpha2\beta3\gamma2L$ + FLU (▲) (n = 5, n_H = 0.9 ± 0.03), α2β3γ2L (○, red) (n = 7, n_H = 1.2 ± 0.1), α2β3γ2L + FLU (○, light red) (n = 5, n_H = 1.0 ± 0.05), $\alpha1^{H101R}\beta3\gamma2L$ (■) (n = 5, n_H = 0.9 ± 0.1), and $\alpha1^{H101R}\beta3\gamma2L$ + FLU (■) (n = 4, n_H = 0.9 ± 0.05). Panel **C** shows the hill equation fits of panel **B** (no data points). **D**. Bar chart

representing the mean GABA EC_{50} values for $\alpha1^{H101R}\alpha2\beta3\gamma2L$ (▲) (n = 7, EC_{50} = 15.1 ± 2.9 µM), $\alpha1^{H101R}\alpha2\beta3\gamma2L$ + FLU (▲) (n = 5, EC_{50} = 10.5 ± 2.6 µM), α2β3γ2L (○, red) (n = 7, EC_{50} = 15.3 ± 2.6 µM), α2β3γ2L + FLU (○, light red) (n = 5, EC_{50} = 9.6 ± 2.1 µM), $\alpha1^{H101R}\beta3\gamma2L$ (■) (n = 5, EC_{50}=110.0±21.8 µM), and $\alpha1^{H101R}\beta3\gamma2L$ + FLU (■) (n=4, EC_{50}=97.7±22.5 µM), (one-way ANOVA with Tukey's post hoc test for multiple comparisons between all groups, P value: ≤ 0.001 ***, ≤ 0.0001 ****). The EC_{50} values are summarised in ***Table 3.1*** of this chapter (see below). **E**. Cartoon representation of the γ2/α interfaces that could be potentially result from the GABA CRC shifts shown in panel **A** (assuming double component fit of $\alpha1^{H101R}\alpha2\beta3\gamma2L$ + FLU). Higher apparent affinity component suggests the presence of γ2/α2 interface-containing receptor population, whereas the lower apparent affinity component suggests the presence of the $\gamma2/\alpha1^{H101R}$ interface (FLU insensitive $GABA_A$ receptors). **F.** Table summarising single and double component fit EC_{50} and χ^2 values for $\alpha1^{H101}\alpha2\beta3\gamma2L$ -/+ FLU.

Next, the effect of α2/γ2L BDZ-sensitivity ablation was investigated. Equimolar ratios of α1, $\alpha2^{H101R}$, β3, and γ2L subunit cDNA were co-expressed in HEK293 cells, and GABA concentration response profiles without and with flurazepam were obtained. The $\alpha1\alpha2^{H101R}\beta3\gamma2L$ GABA EC_{50} exhibited a 2.9-fold decrease in the presence of 300 nM flurazepam (from 11.6 ± 2.0 µM to 4.0 ± 1.0 µM) (***Figure 3.18 A***). Similar to $\alpha1^{H101R}\alpha2\beta3\gamma2L$, the potentiation of $\alpha1\alpha2^{H101R}\beta3\gamma2L$ GABA CRC by flurazepam was described as a sum of two components (***Figure 3.18 F***). The EC_{50} values of those two components were 1.9 ± 0.3 µM and 28.4 ± 10.8 µM and accounted for 73.9 ± 7.1 % and 26.0 ±6.7 % of the total receptor pool respectively. These results suggest that there are receptor populations with two distinct α/γ2L interfaces in $\alpha1\alpha2^{H101R}\beta3\gamma2L$ co-expressing HEK293 cells: first component, exhibiting a decrease in GABA EC_{50} corresponds to receptor population(s) with α1/γ2L interface, whereas the second receptor population is BDZ-insensitive and therefore contains an $\alpha2^{H101R}$/γ2L interface (***Figure 3.18 E***). It is worth noting that the relative proportion of α1/γ2L to α2/γ2L is reversed, compared to the results obtained from $\alpha1^{H101R}\alpha2\beta3\gamma2L$-expressing cells. Interestingly, the $\alpha5^{H105R}$ mutation has been shown to disrupt the assembly of α5 in $GABA_A$ receptors containing two distinct α subunits, specifically by affecting the relative positioning of the α subunits (Balic et al., 2009). This could explain the complete switch in α1/γ2L and α2/γ2L interface proportions that was observed in our results (***Figure 3.17 E and 3.18 E***).

Together, these results suggest that co-expression of two distinct $GABA_AR$ α subunits, α1 and α2 (+ β3 and γ2L), probably assemble as receptor populations with both α1/γ2L and α2/γ2L interfaces. Discrepancies between α1/γ2L and α2/γ2L interfaces proportions obtained from $\alpha1^{H101R}\alpha2\beta3\gamma2L$ and $\alpha1\alpha2^{H101R}\beta3\gamma2L$ GABA CRC flurazepam potentiation data (***Figure 3.17 F and 3.18 F***) are likely to be attributed to subunit positioning changes upon H101R mutation introduction (Balic et al., 2009). Furthermore, from the data presented above, it is not possible to correlate receptor interfaces and $GABA_AR$ population identities ('homo-alpha' or 'hetero-alpha').

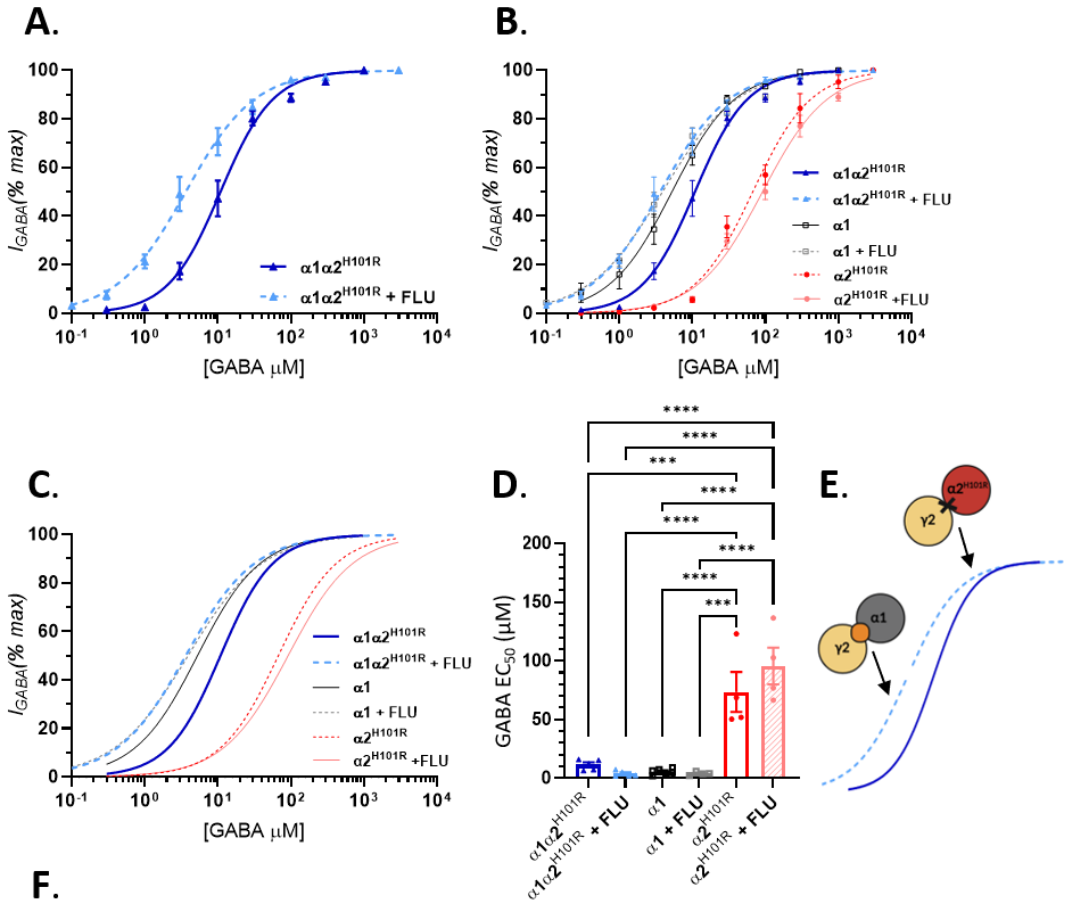

α1α2^{H101R}β3γ2L	GABA			GABA + FLU		
Hill equation components	**One-component fit**	**Two-component fit**		**One-component fit**	**Two-component fit**	
	EC_{50} (μM)	**EC_{50} (μM)**	**Percentage (%)**	**EC_{50} (μM)**	**EC_{50} (μM)**	**Percentage (%)**
1st component	11.6 ± 2.0	10.1 ± 1.6	45.9 ± 1.8	4.0 ± 1.0	1.9 ± 0.3	73.9 ± 7.1
2nd component	-	10.2 ± 0.02	51.4 ± 0.01	-	28.4 ± 10.8	26.0 ± 6.7
χ^2	6.83	6.83		4.17	1.90	

Figure 3.18 Mixture of α1 wild type and α2^{H101R} mutant subunits co-expressed with β2 and γ2 subunits results in expression of both γ2/α1 and γ2/α2 interface-containing GABA$_A$ receptor populations. **A.** GABA concentration response curves of α1α2^{H101R}β3γ2L (▲) and α1α2^{H101R}β3γ2L plus FLU (▲). **B** and **C.** GABA concentration response relationships of α1α2^{H101R}β3γ2L (▲) (n = 5, n_H = 1.3 ± 0.1), α1α2^{H101R} β3γ2L + FLU (▲) (n = 5, n_H = 1.0 ± 0.03), α1β3γ2L (□, black) (n = 6, n_H = 1.1 ± 0.1), α1β3γ2L + FLU (□, grey) (n = 4, n_H = 0.9 ± 0.01), α2^{H101R}β3γ2L (●) (n = 4, n_H = 1.1 ± 0.1), and α2^{H101R}β3γ2L + FLU (●) (n = 4, n_H = 1.0 ± 0.02). Panel **C** shows the hill equation fits of **B** (no data points). **D**. Bar chart representing the mean GABA EC_{50} values of α1α2^{H101R}β3γ2L (▲) (n = 5, EC_{50} = 11.6 ± 2.0 μM), α1α2^{H101R} β3γ2L + FLU (▲) (n = 5, EC_{50} = 4.0 ± 1.0 μM), α1β3γ2L (□, black) (n = 6, EC_{50} = 5.7 ± 1.1 μM), α1β3γ2L + FLU

(□, grey) (n = 4, EC_{50} = 4.1 ± 0.8 µM), $\alpha2^{H101R}\beta3\gamma2L$ (●) (n = 4, EC_{50} = 73.5 ± 17.0 µM), and $\alpha2^{H101R}\beta3\gamma2L$ + FLU (●) (n = 4, EC_{50} = 95.7 ± 15.6 µM) transfected HEK293 cells(one-way ANOVA with Tukey's post hoc test for multiple comparisons between all groups was performed, P value: ≤ 0.001 ***, ≤ 0.0001 ****). The EC_{50} values are summarised in ***Table 3.1*** of this chapter (see below). **E**. Cartoon representation of the γ2/α interfaces that could be potentially result from the GABA CRC shifts shown in panel **A** (assuming double component fit of $\alpha1\alpha2^{H101R}\beta3\gamma2L$ + FLU). Bottom-end component is shifted rightwards suggesting the presence of an γ2/α1 interface that can is potentiated by FLU pre-application, whereas the top-end component is FLU insensitive (γ2/$\alpha2^{H101R}$ interface containing $GABA_A$ receptors). **F.** Table summarising single and double component fit EC_{50} and χ^2 values for $\alpha1^{H101}\alpha2\beta3\gamma2L$ -/+ FLU.

Table 3.1 The mean GABA EC_{50} values for α1 α2 wild type/mutant mixtures. The table summarises the GABA EC_{50} values (µM) of $\alpha_x\beta2\gamma2$ and $\alpha_x\beta3\gamma2$ $GABA_A$ receptor mixtures in the absence or presence of flurazepam (see ***Figures 3.12-3.15***). The α_x stands for the mixtures of α wild type and H101R mutant (see second column for detail). The fold increase in apparent affinity between GABA and GABA + FLU is given in the last column.

$GABA_AR$ mixture	The α subunit	GABA EC_{50} (µM)	GABA + FLU EC_{50} (µM)	Fold increase in apparent potency
$\alpha_x\beta2\gamma2$ (β2-containing)	$\alpha1^{H101R}$	15.7 ± 2.4	19.0 ± 3.2	0.8
	$\alpha1^{H101R}\alpha2$	13.2 ± 3.3	8.5 ± 1.4	1.6
	α2	15.2 ± 2.2	9.0 ± 1.8	1.7
	α1	11.0 ± 2.6	7.7 ± 2.3	1.4
	$\alpha1\alpha2^{H101R}$	19.6 ± 4.2	9.7 ± 1.4	2.0
	$\alpha2^{H101R}$	17.8 ± 4.3	16.0 ± 3.0	1.1
$\alpha_x\beta3\gamma2$ (β3-containing)	$\alpha1^{H101R}$	110.0 ± 21.8	97.7 ± 22.5	1.1
	$\alpha1^{H101R}\alpha2$	15.1 ± 2.9	10.5 ± 2.6	1.4
	α2	15.3 ± 2.6	9.6 ± 2.1	1.6
	α1	5.7 ± 1.1	4.1 ± 0.8	1.4
	$\alpha1\alpha2^{H101R}$	11.6 ± 2.0	4.0 ± 1.0	2.9
	$\alpha2^{H101R}$	73.5 ± 17.0	95.7 ± 15.6	0.8

3.4.4 Summary of results from α1^{H101R} and α2^{H101R} reporter mutations

In this section a histidine to arginine substitution, H101R, on two distinct α subunits: α1 and α2 was used as a reporter tool to establish the identity of α subunit at the α/γ2L interface in α1α2βγ2L-expressing HEK293 cells. Furthermore, the goal was to assess, whether there are any differences in the identity and abundance of this interface between β2- and β3-containing receptors.

Our first aim was to assess the effects of H101R mutation on the α1β2/3γ2L and α2β2/3γ2L GABA concentration response profiles. Our results show an ablation of flurazepam potentiation of the GABA responses (***Figures 3.12 and 3.13***). This is in agreement with previous reports studying the effects of diazepam on receptors containing an α subunit with H101R substitution (Benson et al., 1998b; Kleingoor et al., 1993b; Löw et al., 2000; Rudolph et al., 1999; Wieland et al., 1992b).

By introducing an H101R mutation in either α subunit of interest (α1 and α2) and assessing the GABA responses potentiation profiles of α1α2βγ2L-expressing HEK293 cells, we were able to identify the identities of α/γ2L interfaces. Both β2- and β3-containing receptor data (***Figures 3.15 - 3.18***) exhibited two Hill equation components, suggesting that either α subunits can be present at the α/γ2L interface. Unfortunately, this data alone does not provide the full insight into the receptor populations and their subunit arrangements i.e. 'homo-alpha' and 'hetero-alpha' $GABA_A$ receptors.

Notably, the GABA EC_{50} values of α1^{H101R}α2β3γ2L (15.1 ± 2.9 μM) and α1α2^{H101R}β3γ2L (11.6 ± 2.0 μM) are in close proximity to their wild-type counterparts: α2β3γ2L (15.3 ± 2.6 μM) and α1β3γ2L (5.7 ± 1.1 μM), rather than mutation-containing receptors: α1^{H101R}β3γ2L (110.0 ± 21.8 μM) and α2^{H101R}β3γ2L (73.5 ± 17.0 μM) (***Figures 3.17 and 3.18***). The possible explanation could be that the expression or post-translational events (assembly, receptor trafficking) of α1^{H101R} mutant subunit could be affected. Immunohistochemical and biochemical evidence from α1^{H101R} mice suggested that the mutation does not affect α1 subunit protein levels (Rudolph et al., 1999). Nevertheless, a homologous mutation in the α5 subunit – α5^{H101R}, leads to a ~ 20 %

reduction of α5 protein levels in hippocampal cultured neurones, however it does not reduce α5 mRNA levels (Crestani et al., 2002).

Taken together, we tried to dissect the subunit arrangement and hence the identity of the α subunit at the α/γ2L interface in 'hetero-alpha' $GABA_A$ receptors.

3.5 Discussion

Although the structural heterogeneity of $GABA_A$ receptors has been widely studied, the majority of these studies include only biochemical analyses (Bohlhalter et al., 1996; Christie and de Blas, 2002; Fritschy et al., 1992; Fritschy and Mohler, 1995; Zezula and Sieghart, 1991) as described in ***Section 1.4.1***. The consensus support for existence of $GABA_A$ receptors with two distinct α subunits remains unclear. In this study, we have examined the electrophysiological properties of α1 and α2 subunit-containing $GABA_A$ receptors. Here, we have assessed the behaviour of GABA concentration response relationships of α1α2-transfected HEK293 cells. We also used $\alpha1^{L263S}$, $\alpha2^{F65L}$, $\alpha1^{H101R}$, and $\alpha2^{H101R}$ reporter mutations as functional tools to dissect the abundance and subunit arrangement in populations formed by α1 and α2 co-expression (Baumann et al., 2003; Benson et al., 1998a; Chang et al., 1996a; Kleingoor et al., 1993a; Sigel et al., 1992; Wieland et al., 1992a).

3.5.1 Identities of both α and β subunits determine GABA sensitivity of 'hetero-alpha' $GABA_A$ receptors

Conclusions from each set of experiments can be found in summary ***Sections 3.2.4, 3.3.4, and 3.4.4***. ***Table 3.2*** outlines the main outcomes of electrophysiological analyses of 'hetero-alpha' $GABA_A$ receptors. Our data from α1α2β2γ2L wild-type and $\alpha1^{L263S}$β2γ2L expressing HEK293 cells collectively indicates the presence of 'hetero-alpha' $GABA_A$ receptor population that comprises ~ 45 % of the total receptor pool. However, the GABA sensitivity of this receptor population is not distinct compared to 'homo-alpha' counterparts: α1β2γ2L and α2β2γ2L. Interestingly, our data indicates

that α1α2β3γ2L wild-type mixtures experience a leftward shift of GABA sensitivity compared to 'homo-alpha' populations (***Figure 3.3***). This suggests that a population of 'hetero-alpha' $GABA_A$ receptors is formed within the mixture and has a higher GABA apparent affinity than α1α1- and α2α2-containing receptors. Previous studies on recombinant $GABA_A$ receptors: α1α3β2γ2 and α1α5β2γ2, have shown that the GABA sensitivity of the former lies between α1- and α3-contaning receptors, whereas the latter shows an increased GABA apparent affinity compared to α1 and α5 'homo-alpha' $GABA_A$ receptors (Ebert et al. 1994; Tia et al. 1996; Verdoorn 1994). It has been well documented that the identity of both α and β subunits determines GABA potency of 'homo-alpha' $GABA_A$ receptors ($\alpha_x\beta_y\gamma$-tri-heteropentamers), suggesting that the same principle could be applied to 'hetero-alpha' receptors (Böhme et al., 2004; Mortensen et al., 2012a). Expression of 'hetero-alpha' combinations could therefore provide greater pharmacological diversity of $GABA_A$ receptors. Given that α1 and α2 subunits' expression prevails over other α subunit types (Pirker et al., 2000), collective α1α1, α1α2 and α2α2 $GABA_A$ receptor mixtures could be implicated in fine tuning of GABA-evoked responses in the brain.

A study of recombinant α1/α3- and α1/α5-co-injected oocytes suggested that the maximum efficacy and potency towards P4S – a partial $GABA_AR$ agonist, is determined by the relative identities of α subunits (α1 and α3/α5 respectively) (Ebert et al. 1994). This further strengthens the hypothesis of α subunits playing a crucial role in determining 'hetero-alpha' $GABA_A$ receptor pharmacology.

3.5.2 The β subunit determines the abundance of 'hetero-alpha' $GABA_A$ receptors

Results from wild type electrophysiological analysis, with varying the ratios of α1 : α2 cDNAs in β3-containing receptors indicates that not only the relative proportion of α1α2-containing $GABA_A$ receptors is 'fixed', but also the expression of α1α2 receptors predominates over α2α2-containing receptors (***Figure 3.8***). The multi-component Hill-equation fits of $\alpha1^{L263S}$α2β3γ2L are in agreement with the wild-type data, estimating the relative proportion of α1α2 'hetero-alpha' and α2α2 'homo-alpha' $GABA_A$ receptor populations to be 67.7 ± 4.1 % and 36.7 ± 3.0 % respectively (***Figure***

3.9). Interestingly, the relative proportion of $\alpha1^{L263S}\alpha2$: $\alpha2\alpha2$ β2-containing $GABA_A$ receptors is 44.7 % to 49.1 %, suggesting that both of these populations are expressed at similar levels (***Figure 3.9***). It is important to note that co-expression of $\alpha1^{L263S}$ and α2 subunits revealed that there is no pure $\alpha1^{L263S}\alpha1^{L263S}$ receptor populations detected in β3-containing receptors. Furthermore, the same receptor population ($\alpha1^{L263S}\alpha1^{L263S}$) in the β2-expressing receptors comprises the minority of the total receptor pool: ~ 6 %. Taken together, our data could indicate that the identity of the β subunit dictates the relative expression of α1α2 'hetero-alpha' receptors.

The β subunit identity influences $GABA_A$ receptor assembly, clustering and trafficking (Jacob et al., 2008). Evidence on subcellular localisation of β2/3-containing $GABA_A$ receptors is conflicting, with some studies suggesting that β2-containing receptors predominantly localise synaptically, whereas β3-containing receptors are localised peri-synaptically and vice versa depending on the brain area (Herd et al., 2008; Kasugai et al., 2010; Thomas et al., 2005). Furthermore, a study that assessed differential solubilisation of $GABA_A$ receptors suggested that the number of α5-containing 'hetero-alpha' receptors (α1- or α2-containing) depends on the subcellular localisation (Ju et al., 2009). It is, therefore, possible that the identity of both α subunits ('homo-alpha' or 'hetero-alpha') could be dictated by their β assembly partners (β2 or β3) and, hence, subcellular localisation.

Table 3.2 Summary results table of electrophysiological studies in HEK293 cells. The table summarises the results from each set of electrophysiological experiments: wild-type α1α2 subunit co-expression, and reporter mutations: $\alpha1^{L263S}$ and $\alpha2^{F65L}$ - receptor population number studies based upon multi-component Hill equation fits; $\alpha1^{H101R}$ and $\alpha2^{H101R}$ – benzodiazepine insensitive mutations to establish α/γ2L interfaces.

		The β2-containing	The β3-containing	Notes
Wild-type		The α1α2 CRC curve lies between the α1α1 and α2α2. There could be a middle component receptor population (α1α2), but reporter mutations are needed to separate α1α1 and α2α2 CRCs.	Co-expression of α1α2 subunits results in a DRC leftward shift, compared to α1α1 and α2α2 CRC. This could indicate that α1α2 receptor population has a higher GABA apparent affinity. The α1α2 receptors are tri-heteromers, i.e. αβγ. Altering α1:α2 ratios does not have an effect on CRC dynamics, suggesting that there is a minimum number of α1α2 receptors that need to assemble. The assembly of α1α2 receptors predominates over α2α2.	The GABA EC_{50} of α1α1 and α2α2 lie too close to one another, therefore it is hard to distinguish the receptor populations.
Reporter mutation	$\alpha1^{L263S}$	The CRC of $\alpha1^{L263S}\alpha2$ fits three-component Hill equation with respective percentages of the total receptor population: 6.1 ± 2.8 % (α1α1*), 44.7 ± 3.9 % (α1α2*), 49.1 ± 4.3 % (α2α2*).	The CRC of $\alpha1^{L263S}\alpha2$ has two distinct populations with the relative percentages of 67.7 ± 4.1 % (α1α2*), 36.7 ± 3.0 % (α2α2). The 'homo-alpha' α1α1 is not observed in the Hill-equation fit and could therefore be absent.	* - probable receptor populations.
	$\alpha2^{F65L}$	Two-population Hill equation fit is best for $\alpha1\alpha2^{F65L}$, with respective receptor percentages of 85.3 ± 1.3 % and 13.9 ± 1.6 %**.	The CRC of $\alpha1\alpha2^{F65L}$ revealed two distinct receptor populations and account for 85.2 ± 1.3 % and 13.9 ± 1.6 % of the total receptor pool**.	** The χ2 statistics of the two- and three-component fit are similar.

				The $\alpha2\alpha2^{F65L}$ mixture contains three components, where the first component predominates over other two (78.9 ± 2.3 %).
Reporter mutation	$\alpha1^{H101R}$	Both α1/γ2L and α2/γ2L interfaces are present upon $\alpha1^{H101R}$ and α2 subunit co-expression (48.1 ± 10.4 % of α1/γ2L- and 51.1 ± 10.8 % of α2/γ2L-interface containing).	Both interfaces are present (α1/γ2L and α2/γ2L) when co-expressing $\alpha1^{H101R}$ and α2 subunits. Relative percentages of α1/γ2L and α2/γ2L interfaces are 23.9 ± 3.3 % and 77.5 ± 3.6 % respectively.	The results only show the α/γ2L interfaces present in a subunit mixture, not the stoichiometry or the full arrangement of receptor populations. The H101R substitution has been shown to affect subunit positioning of the α5 subunits (Balic et al., 2009).
	$\alpha2^{H101R}$	Both α1/γ2L (60.6 ± 3.8 %) and α2/γ2L (40.0 ± 3.4 %) interfaces are present upon α1 and $\alpha2^{H101R}$ subunit co-expression.	Both α1/γ2L (73.9 ± 7.1 %) and α2/γ2L (26.0 ± 6.7 %) interfaces are present upon α1 and $\alpha2^{H101R}$ subunit co-expression.	The results only show the α/γ2L interfaces present in a subunit mixture, not the stoichiometry or the full arrangement of receptor populations.
				The H101R substitution has been shown to affect subunit positioning of the α5 subunits (Balic et al., 2009).

Previous studies identified 'hetero-alpha' $GABA_A$ receptor mixtures from brain lysates using biochemical methods (see ***Introduction Table 1.2*** for more detail). A spectrum of α1α2-containing receptor percentages was reported, varying between 13 % and 36 % of the total α1-, α2- and α3-containing $GABA_A$ receptors (Benke et al., 2004a; del Río et al., 2001a; Duggan et al., 1991). These values are lower than the ones we obtained from multi-component Hill equation fits: 44.7 ± 3.9 % and 67.7 ± 4.1 % for $\alpha1^{L263S}\alpha2\beta2\gamma2L$ and $\alpha1^{L263S}\alpha2\beta3\gamma2L$ receptor populations respectively (***Figure 3.9***). The discrepancies could be attributed to multiple reasons. Firstly, biochemical analyses were performed from brain lysates, whereas our study was performed in a recombinant system. Neurones and HEK293 cells could have different assembly machinery, which would then dictate the assembly preferences of 'hetero-alpha' $GABA_A$ receptors. Furthermore, western blotting heavily relies on the quantity and quality of purified protein as well as antibody specificity and affinity, and therefore carries significant systematic and random errors in quantification analysis. Also, the detergent and its percentage used for solubilisation of $GABA_A$ receptors determines both the efficiency of extraction and receptor type (synaptic or extrasynaptic) (Ju et al., 2009). Finally, the biochemical data does not distinguish between 'hetero-alpha' β2 or β3-containing $GABA_A$ receptors.

3.5.3 The function of the α/γ interface in 'hetero-alpha' $GABA_A$ receptors

It has been previously elucidated that high affinity benzodiazepine site in $GABA_A$ receptors lies between the α^+/γ^- interface (Masiulis et al., 2019b; Minier and Sigel, 2004c; Walters et al., 2000). This implies that the pharmacological activity of 'hetero-alpha' $GABA_AR$ benzodiazepine modulation is governed by the identity of the α subunit adjacent to the γ subunit. Our data from $\alpha1^{L263S}$ and α2 subunits mixtures together with β3 and γ2 subunits suggested that the pure 'homo-alpha' $\alpha1^{L263S}$ receptor population is not present in the mixture (***Figure 3.9***). Furthermore, experiments with BDZ-insensitive mutation, H101R, in the α2 subunit, revealed that $\alpha1\alpha2^{H101R}\beta3\gamma2L$-expressing HEK293 cells experience a 2.9-fold decrease in GABA apparent affinity (***Table 3.1***). Taken together, these data imply that the α1

benzodiazepine sensitivity in the α1α2β3γ2L-expressing HEK293 cells is purely mediated by 'hetero-alpha' $GABA_A$ receptors with the **α1**γ2β3**α2**β3 subunit arrangement.

Previous biochemical studies have tried to assess the subunit arrangement of the 'hetero-alpha' $GABA_A$ receptors by establishing their benzodiazepine binding properties (Araujo et al., 1999, 1996; del Río et al., 2001a; Pollard et al., 1995; Scholze et al., 2020). The results suggested that the 'hetero-alpha' α1-containing $GABA_A$ receptor arrangement is dictated by the identity of the other α subunit. Both arrangements **α*x***γ2β**α1**β and **α1**γ2β**α*x***β (where *x* – 2, 3, 4, 5) could be identified, but the prevalence of each complex was determined by the α*x* subunit. Our data also suggests that both **α2**γ2Lβ2/3**α1**β2/3 and **α1**γ2Lβ2/3**α2**β2/3 'hetero-alpha' receptors are present within the α1α2-receptor mixture; however, we could not establish the prevalence of each population (***Figures 3.15-3.18***). As discussed in ***Section 3.4.4***, one of the possible explanations for inability to accurately estimate the receptor population prevalence with the H101R reporter mutation is the effect it has on the relative positioning of the α BDZ insensitive subunit positioning in the 'hetero-alpha' $GABA_A$ receptor complex (Balic et al., 2009).

Behavioural studies of the H101R BDZ-insensitive mutant mouse models have correlated benzodiazepine actions with the α subunit isoform. As such, α1 subunit containing $GABA_A$ receptors have been associated with sedation, α2/3 – anxiolysis, and α5 – cognitive enhancement (Collinson et al., 2002; Löw et al., 2000; Rudolph et al., 1999). Our findings suggest that in α1α2-co-expressing HEK293 cells with either β2 or β3 subunits, both α1/γ2L and α2/γ2 interfaces are present (***Figures 3.15-3.18***). Thus, it is possible that the mode of benzodiazepines action in 'hetero-alpha' $GABA_A$ receptors could be more complex than initially anticipated in H101R mouse models. Possible permutations and arrangements of α subunits in the receptor pentamer could translate into multicomponent patterns of behaviour. Therefore, understanding composition and pharmacology of 'hetero-alpha' $GABA_A$ receptor mixtures, specifically their benzodiazepine modulation is crucial.

3.6 Assumptions and limitations

3.6.1 Reporter mutations

In this chapter we took the advantage of three reporter mutations: $\alpha1^{L263S}$, $\alpha2^{F65L}$, and $\alpha1^{H101R}/\alpha2^{H101R}$ to dissect the abundance and pharmacology of the 'hetero-alpha' $GABA_A$ receptors (Baumann et al., 2003; Benson et al., 1998a; Chang et al., 1996a; Kleingoor et al., 1993a; Sigel et al., 1992; Wieland et al., 1992a). We have characterised each amino acid substitution in our recombinant system – HEK293 cells.

Our conclusions with the $\alpha1^{L263S}$ and $\alpha2^{F65L}$ are strongly based on the assumption that these mutations do not after the stoichiometry and arrangement of the α1β2/3γ2L and α2β2/3γ2L $GABA_A$ receptors. The mutations in the $GABA_AR$ TM2 domain, one of which is L9'S, are thought to have little effect on the subunit interface interactions, and therefore should not affect the subunit stoichiometry (Xu and Akabas, 1996). Indeed, the L9'S mutation of the conserved amino acid has been previously used to study the stoichiometry of the γ2- and δ-containing $GABA_A$ receptors, as well as nAChRs, and 5-HT3Rs (Chang et al., 1996a; Chang and Weiss, 1999; Filatov and White, 1995; Labarca et al., 1995; Patel et al., 2014; Yakel et al., 1993).

The $\alpha2^{F65L}$ mutation, a homologous amino acid substitution to the $\alpha1^{F65L}$, was previously used to study $GABA_A$ receptor agonist-dependent gating as well as GABA binding sites in concatenated receptors (Baumann et al., 2003; Sigel et al., 1992). Since the subunit arrangement in the concatenated receptors is fixed, we cannot infer the effect of the F65L mutant on the stoichiometry of freely expressed 'hetero-alpha' $GABA_A$ receptors from the previous studies. However, from our data using $\alpha2\alpha2^{F65L}$-co-expression (***Figure 3.12***), we established that the α2α2 wild-type receptor population GABA-evoked currents predominate over those containing an $\alpha2^{F65L}$. Ideally, the receptor population percentages upon co-expression of the same wild-type and mutant subunit isoform, assuming the stoichiometry and expression are not affected, should follow a binomial distribution: 1:2:1 ratio (Chang et al., 1996a). Nevertheless, the data presented in ***Figure 3.9*** largely deviates from this

prediction. This could imply that the mutant $\alpha2^{F65L}$ subunit does not assemble as efficiently as the α2 wild type, or the assembly is reduced, indicating that the F65L mutation could affect subunit assembly.

With regards to $\alpha1^{H101R}/\alpha2^{H101R}$, it is worth reiterating that the H101R benzodiazepine mutation in the α5 subunit has been previously implicated in alternation of relative subunit positioning in the $GABA_AR$ pentamers (Balic et al., 2009). Even though the $\alpha1^{H101R}$ mutation does not seem to affect the subunit protein levels and hence the expression, other studies suggested that the homologous substitution on the α5 subunit reduces its protein levels by ~ 20 % (Crestani et al., 2002; Rudolph et al., 1999).

Furthermore, it is worth noting that even though $\alpha1^{L263S}$ and $\alpha2^{F65L}$ mutants do not impair $GABA_AR$ cell surface expression (***Figure 3.10***), both mutations could skew the results of multi-component Hill equation fits (***Section 3.3***). One of the most prominent limitations is that both mutations have been suggested to alter the gating kinetics of the $GABA_A$ receptor (Baumann et al., 2003; Chang et al., 1996a). This is not surprising given that both amino acids (L263 and F65) are located within the TM2 domain lining the channel pore and the α^- side of the GABA binding pocket respectively (Laverty et al., 2019b; Masiulis et al., 2019b; Miller and Aricescu, 2014; Miller and Smart, 2010). Changes in gating kinetics would subsequently lead to altered relative proportions in the multi-component Hill equation fits.

3.6.2 GABA binding sites

In this study, we also assumed that the two possible subunit arrangements: **α1**γ2β**α2**β **α2**γ2β**α1**β, of α1α2-containing 'hetero-alpha' $GABA_A$ receptors are functionally equivalent in terms of GABA-evoked responses. The two GABA binding sites are located at the extracellular domain of the β+/α- interface and both sites must be occupied for full receptor activation (Miller and Smart, 2010). Nevertheless, two binding sites were shown to not carry the same contribution to the receptor activation, with site 1 (flaked by the γ and β subunits) carrying a three-fold lower

GABA affinity than site 2 (flanked by the α and γ subunits) (Baumann et al., 2003). This suggests that in a receptor pentamer with two distinct α subunits, the relative positioning of the two will largely dictate the receptor's apparent affinity to GABA. Indeed, concatenated receptor studies with α1/α6 subunit mixtures show that the γ2β2α1/β2α6 construct has a much higher GABA EC_{50} than γ2β2α6/β2α1 (Minier and Sigel, 2004a). Nonetheless, from our data (***Figures 3.2 and 3.6***) and previous reports the subunits that were chosen for this study: α1 and α2, were shown to have very similar potencies to GABA (Mortensen et al., 2012a). Minimising the potency differences of 'homo-alpha' receptor populations (α1α1- and α2α2-containing) should in theory have very little effect on the GABA potency differences between **α1**γ2β**α2**β **α2**γ2β**α1**β 'hetero-alpha' $GABA_A$ receptors. Further work should aim at assessing the GABA potencies of those receptor populations using forced assembly studies.

3.7 Conclusions

1. Wild-type α1α2β3γ2L $GABA_A$ receptors have a higher potency to GABA than 'homo-alpha' counterparts, which is indicative of a distinct receptor population formation. Furthermore, this receptor population has a high-benzodiazepine site i.e. αβγ stoichiometry.

2. Both β2 and β3 containing $GABA_A$ receptors, when co-expressed with α1 and α2 subunits (+ γ2L) form 'hetero-alpha' receptor populations. The abundance of these populations is possibly influenced by the identity of the β subunit.

3. Co-expression of α1, α2, β3, and γ2 does not produce a α1β3γ2L $GABA_AR$ population pool. Additionally, 'hetero-alpha' receptor population is predominant over the α2α2-containing population.

4. The α1 benzodiazepine sensitivity in the α1α2β3γ2L-expressing HEK293 cells is purely mediated by 'hetero-alpha' $GABA_A$ receptors within the **α1**γ2β3**α2**β3 subunit arrangement.

Chapter 4: Exploring 'hetero-alpha' $GABA_A$Rs in cultured hippocampal neurons: presence, functional signatures and roles in long-term potentiation

4.1 Introduction

In the previous chapter, the existence and abundance of 'hetero-alpha' $GABA_A$ receptors, specifically α1α2-containing receptors, was investigated in a recombinant HEK293 system. Our results indicate that α1α2-containing $GABA_A$Rs do indeed form upon co-transfection of α1, α2, β2/3, and γ2L subunits, and receptor assembly permutations as well as subunit arrangements within the pentamer are potentially dictated by the identities of both α and β subunit isoforms. Our next aim was to assess the presence of these 'hetero-alpha' receptors and their sub-cellular localisation – synaptic or extrasynaptic – in neurons.

As outlined in the ***Introduction Section 1.4.1***, previous studies identified various 'hetero-alpha' $GABA_A$ receptors by using immunohistochemistry and co-immunoprecipitation methods (Araujo et al., 1999; Benke et al., 2004a; Bohlhalter et al., 1996; Christie and de Blas, 2002; del Río et al., 2001a; Fritschy et al., 1992; Fritschy and Mohler, 1995; Zezula and Sieghart, 1991). However, the evidence for native 'hetero-alpha' $GABA_A$Rs is not conclusive due to the nature of the techniques used. Firstly, while co-localisation studies can give insight on whether two receptor subunits are present in the same subcellular compartment, the resolution of such techniques is not high enough to reveal whether subunits of interest are in the same pentameric complex. For example, the resolution of confocal microscopes could reach 180 nm in the *xy* plane, whereas the diameter of a single $GABA_A$R pentamer ranges between only 6 to 8 nm (Heintzmann and Huser, 2017; Laverty et al., 2019a; Miller and Aricescu, 2014).

Similarly, biochemical techniques, including co-immunoprecipitation (co-IP) of 'hetero-alpha' $GABA_A$ receptors could inform on whether two distinct subunit isoforms are present in a 'pulled-down' protein complex. However, these subunits could be connected by a string of other proteins that are associated with them,

therefore two distinct α subunits could be co-immunoprecipitated due to inter-, rather than an intra-receptor interaction (Gomes et al., 2016a). Furthermore, artefacts can arise in co-IP protocols, which are influenced by detergent type and its concentration in the lysis buffer, specificity of antibodies and other experimental conditions (Burckhardt et al., 2021; Nakamura et al., 2016). Lastly, identification of proteins with low-level expression could also be challenging.

Due to these issues, we wanted to find an alternative method that could assess the existence of native 'hetero-alpha' $GABA_A$ receptors. Our aim was not only to demonstrate the presence of two distinct α subunit isoforms within the same native receptor complex in neurons, but also to assess their subcellular compartmentalisation.

To achieve this goal, we used the proximity ligation assay (PLA) to study the existence of 'hetero-alpha' $GABA_A$ receptors in cultured hippocampal neurons. The principle behind PLA is outlined in detail in the ***Methods Section 2.5.2***. Briefly, PLA is used to detect interactions between endogenous proteins of interest by giving a fluoresent readout after incubations with relevant antigen-specific primary antibodies and oligo-tagged secondary probes. Following hybridisation and amplification cycles, the fluorescent signal can be detected by confocal microscopy. For the amplification to work, the two protein targets need to be ≤ 30 nm apart, ie, in sufficiently close proximity; however some studies claim that the distance should be ≤ 17 nm for signal amplification to occur (Gomes et al., 2016a; Söderberg et al., 2006; Weibrecht et al., 2010). This distance is comparable to fluorescent resonance energy transfer (FRET) methods, which relies on expression of fluorophore tagged proteins and have a resolution of 5 - 10 nm (Jaeger et al., 2014; Lecat-Guillet et al., 2017). Overall, this makes PLA a valuable technique to study protein-protein interactions *in situ* without the caveats of target protein overexpression.

Indeed, the PLA technique has been widely used to study heteromerization states of G-protein coupled receptors (GPCRs) *in vitro* using heterologous cells expressing receptors of interest, as well as native receptors in cultured neurons and brain slices (Berg et al., 2012; Gomes et al., 2016a, 2016b; Sierra et al., 2015). Hence, PLA has been used to investigate heteromerization states of cannabinoid (CB1 and CB2)

receptors, δ and κ opioid receptors, D2-type dopamine receptors (D2Rs) and A2-type adenosine receptors (A2ARs) in various brain regions (Berg et al., 2012; Callén et al., 2012; Sierra et al., 2015). Furthermore, PLA has been used to study mitochondrial dynamics, the effect of upregulating CYFIP1 protein on synaptic excitation/inhibition balance, as well as phophorylation-induced despersal of synaptic Neuroligin-2 (NL2) (Davenport et al., 2019; Halff et al., 2020; Norkett et al., 2016).

Here, we performed the PLA for native α1 and α2 $GABA_A$ receptor subunits to assess their proximity in cultured hippocampal neurons. To validate that the PLA interaction is indeed occuring at the intra-receptor level, two controls were performed. We treated neurons with a microtubule polymerisation inhibitor – nocodazole, that was previously shown to decluster synaptic $GABA_A$ receptors (Petrini et al., 2003) and thus would split any inter-receptor associations and therefore generate false PLA signal. Additionally, PLA was used to analyse γ2 and δ $GABA_AR$ subunit proximity – these subunits are not assembled in the same receptor complex –thus they should not be close enough to generate a PLA signal.

Our next aim was to understand whether the overexpression of either one of the α $GABA_AR$ subunits (α1 or α2) could influence the number of 'hetero-alpha' receptors. To do so we performed PLA in cultured hippocampal neurons transfected with either α1 or α2 cDNAs. Recordings of spontaneous inhibitory post synaptic currents (sIPSCs) from the same neuronal transfections were analysed to establish any kinetic signatures of α1α2-containing $GABA_A$ receptors.

Lastly, we used PLA to quantify the expression of α1α2-containing $GABA_A$ receptors after induction of chemical inhibitory long-term potentiation (iLTP) using a protocol validated by electrophysiology (Molnár, 2011). iLTP has been shown to induce changes in receptor lateral mobility and $GABA_AR$ number at inhibitory synapses (Goldin et al., 2001; Molnár, 2011).

Throughout the PLA experiments, immunostaining of the vesicular inhibitory amino acid transporter (VIAAT) was performed. VIAAT has been widely used as an inhibitory presynaptic marker for both GABAergic and glycinergic synapses. At the developmental stage of cultured hippocampal neurons used here, (days *in vitro*

DIV12-15), VIAAT colocalisation with glutamic acid decarboxylase (GAD65) – is reported to be between 96.6 ± 0.8 % and 99.3 ± 0.4 %, proving it a reliable marker for GABAergic synapses (Danglot et al., 2003; Sagné et al., 1997). Co-localisation of PLA fluorescence with VIAAT was quantified in all experiments to identify the subcellular localisation of the 'hetero-alpha' $GABA_A$ receptors.

4.2 Results

4.2.1 Assesment of the interaction between $GABA_AR$ α1 and α2 subunits via PLA

As mentioned above, PLA is a widely used method to establish whether two proteins of interest are in direct contact in native tissues (Gomes et al., 2016a). With regards to using PLA to study ion channels, puromycin-proximity ligation assays (puro-PLA), which exploits the incorporation of puromycin into the newly synthesised proteins and its subsequent labelling, were used to investigate *de novo* synthesis of NMDA and $GABA_A$ receptors (Dieck et al., 2015; Rajgor et al., 2020, 2018). Hence, to our knowledge, PLA has not been previously used to directly assess subunit composition of ligand-gated ion channels. Therefore, preliminary experiments in both transfected HEK293 cells and cultured hippocampal neurons were required to validate the PLA assay protocol for 'hetero-alpha' $GABA_A$ receptor assesment.

The size of a single $GABA_A$ receptor is estimated to be 8 nm in diameter at the N-terminal domain and 11 nm in height (excluding the large intracellular loop) (Laverty et al., 2019b; Miller and Aricescu, 2014). Furhermore, each IgG antibody is estimated to be 8.5 nm in height (Tan et al., 2008). Therefore, the theoretical maximal distance between two α subunits in a single $GABA_A$ receptor with two antibodies would be 25 nm (8.5+8+8.5), which is within the sensitivity range of PLA – less than 30 nm between the secondary probes (refer to ***Figure 2.3***) (Weibrecht et al., 2010).

Our first aim was to assess whether PLA detects an interaction between two distinct $GABA_AR$ subunits: α1 and α2. To do so, HEK293 cells were co-transfected with α1, α2, β2/3 and γ2 $GABA_AR$ subunits and eGFP cDNAs in equimolar ratios – the latter

construct was required for identification of transfected cells. We used two subunit-specific rabbit antibodies: anti-α1 (Abcam, 33299) and anti-α2 (Synaptic Systems, 224-103) – both well characterised and widely used (Arama et al., 2015; Ding et al., 2017; Kasugai et al., 2010; Maric et al., 2017; Nakamura et al., 2020, 2016) – to assess the proximity between α1 and α2 subunits (see ***Methods 2.5.3*** for detail). Since the antibodies were derived from the same species, the anti-α2 antibody was directly conjugated to a short PLUS oligonucleotide probe to avoid secondary PLA probe cross-reactivity. Throughout this chapter, the PLA was performed after fixation of the cultured neurons, but prior to permeabilisation. All PLA probes were amplified with the red detection reagents in the amplification cycle of the protocol (***Methods 2.5.3***), which generates a signal visible as a distinct red fluorescent spot detectable by confocal fluorecence microscopy, indicating close (<30 nm) proximity two proteins.

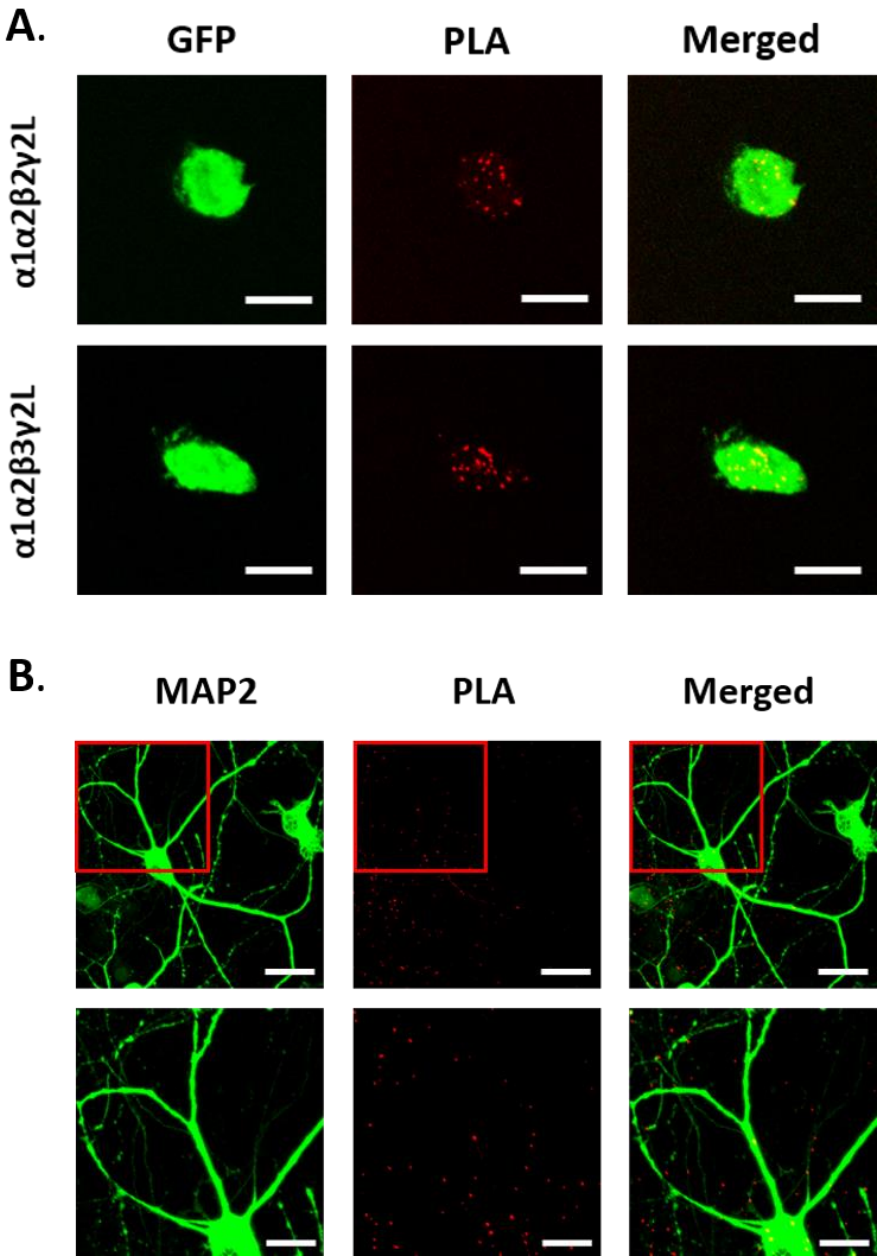

Figure 4.1 Detection of GABA$_A$R α1 and α2 subunit interactions in transfected HEK293 cells and cultured hippocampal neurons. **A.** Representative confocal microscopy images of PLA in HEK293 cells expressing either α1α2β2γ2L (top row) or α1α2β3γ2L (bottom row). Cells were co-transfected with eGFP for identification (green). PLA signal (red) indicates the proximity between GABA$_A$R α1 and α2 subunit antibodies. Scale bar 20 µm. **B.** Confocal microscopy images of PLA in cultured hippocampal neurons, immunostained for MAP2 (green); PLA signal – red dots indicate the proximity between native GABA$_A$R α1 and α2 subunit antibodies. Scale bars 50 µm (top panels) and 30 µm (zoomed images). Representative images for PLA signals are maximal projections of multiple z-sections in these and all subsequent figures in this chapter.

Figure 4.1 A shows example images of maximum projections of PLA signal between α1 and α2 subunits obtained from α1α2β2γ2L- (top row) and α1α2β3γ2L- transfected HEK293 cells (bottom row). Throughout this chapter, each individual PLA puncta will be referred to as a 'PLA dot'. These images show that both α1α2β2γ2L- and α1α2β3γ2L-expressing HEK293 cells have PLA dots, suggesting that α1 and α2 $GABA_A$Rs are in close (< 30nm) proximity, most likely to be in the same receptor complex. This further strengthens the data from ***Section 3.2***, suggesting that wild-type $GABA_A$ receptors form α1α2-containing pentamers in HEK293 cells.

After validating the PLA protocol in a recombinant system, our next aim was to assess whether this technique works with native receptors. PLA directed against extracellular α1 and α2 native $GABA_A$R subunit epitopes was performed in DIV 12-14 cultured hippocampal neurons followed by immunolabelling for microtubule associated protein 2 (MAP2) (see ***Sections 2.5.1 and 2.5.3***). MAP2 staining was performed to visualise the soma and dentritic projections of neurons. Briefly, neurons were fixed with PFA and cell surface α1 and α2 subunits were probed with selective antibodies: rabbit anti-α1 (1:500 dilution) and rabbit anti-α2 congugated to the PLUS probe (1:200 dilution) antibodies respectively. Neurons were then incubated with anti-rabbit MINUS PLA probe (1:5 dilution), following which ligation and amplification incubations were performed. The neurons were permeabilised and intracellular MAP2 was labelled with chicken anti-MAP2 antibody (1:100 dilution) and subsequently labelled with Alexa Fluor® 488 secondary antibodies. Neurons were imaged with confocal microscopy as Z-stacks***. Figure 4.1 B*** shows representative images of pyramidal neurons with MAP2 labelling (green) and PLA performed between α1 and α2 $GABA_A$R subunits (red). The presence of the PLA dots on dendrites suggest that these two subunits are in close proximity and are probably in the same receptor complex.

Taken together, this suggest that α1 and α2 $GABA_A$R subunits are in close enough proximity to be detected by PLA. Nevertheless, the PLA signal could arise between α1 and α2 $GABA_A$R subunits in adjacent receptors, rather than originating from the same

pentamer. The next section will outline the controls performed to validate that the signal arises at the intra-, not inter-receptor level.

4.2.2 Nocodazole effects on $GABA_AR$ clustering and α1 and α2 subunit proximity.

$GABA_A$ receptors are known to form clusters at postsynaptic membranes directly opposite GABAergic presynaptic terminals to ensure effective fast synaptic inhibition (Moss and Smart, 2001). Various proteins have been implicated in synaptic $GABA_AR$ clustering, with the most prominent example being the post-synaptic scaffolding protein - gephyrin (Tyagarajan and Fritschy, 2014). This tubulin-binding protein co-localises with various $GABA_A$ receptor subunits and its ablation leads to loss of synaptic $GABA_AR$ clusters (Essrich et al., 1998; Feng et al., 1998; Kneussel et al., 1999; Tretter et al., 2008). Additionally, the stability of the cytoskeleton is crucial for $GABA_AR$ clustering, with manipulation of microtubule polymerisation leading to modulation of $GABA_AR$ activity and cluster assembly (Chen et al., 2000; Petrini et al., 2003). Treatment with a microtubule polymerisation inhibitor – nocodazole – has been shown to lead to declustering of both synaptic and extrasynaptic $GABA_A$ receptors and induces changes in kinetic profiles of GABAergic currents in cultured hippocampal neurons (Petrini et al., 2004, 2003).

So far, we have shown that α1 and α2 $GABA_ARs$ are in sufficiently close proximity to allow for PLA signal formation in both transfected HEK293 cells and cultured hippocampal neurons (***Figure 4.1***). However, the signal could arise due to PLA probe hybridisation between adjacent $GABA_A$ receptors each containing only one type of α subunit: α1 or α2 (inter-receptor interaction), rather than two distinct α subunit isoforms in the same pentameric complex (intra-receptor interaction). Since $GABA_A$ receptors are densely packed at postsynaptic junctions, with tens to few hundreds of $GABA_A$ receptors clustered in a small membrane area (0.04 to 0.15 μm^2; Kasugai et al. 2010; Nusser, Cull-Candy, and Farrant 1997; Specht et al. 2013), it is indeed possible that PLA signal could be inter-receptor driven. To test the identity of the PLA α1/α2 interaction, we used nocodazole treatment that has been previously used to disperse $GABA_A$ receptors from synapses (Petrini et al., 2003).

To do so, cultured hippocampal neurons were subjected to treatment with nocodazole. In brief, 10 µM nocodazole in DMSO was added to maintenance media (1:1000 dilution) and applied to cultured hippocampal neurons as described previously (Petrini et al., 2003). A control treatment with DMSO was applied in parallel. Neurons were incubated with the treatments for 1 hour before proceeding with either PLA or ICC protocols. For ICC, either cell surface $GABA_AR$ α1 or α2 subunits were labelled, to test nocodazole's effectiveness in dispersing $GABA_A$ receptors *via* microtubule depolymerisation.

Cell surface labelling of $GABA_AR$ α1 subunit (red) in cultured hippocampal neurons with control and nocodazole treatments is shown in ***Figure 4.2 A and B***. It is clear that after 10 µM nocodazole treatment, the $GABA_AR$ α1 subunit is diffusely expressed throughout the cell surface membrane, rather than localised as discrete puncta. Quantification of α1 subunit clusters using the built-in ImageJ particle analysis plug-in revealed a significant reduction of total cluster area within the MAP2 mask (green) in nocodazole treated neurons compared to control treatment (P value ≤ 0.0001) (***Figure 4.2 C***). Furthermore, the mean intensity of the $GABA_AR$ α1 subunit surface labelling significantly decreases with nocodazole treatment (P value ≤ 0.0001) (***Figure 4.2 D***).

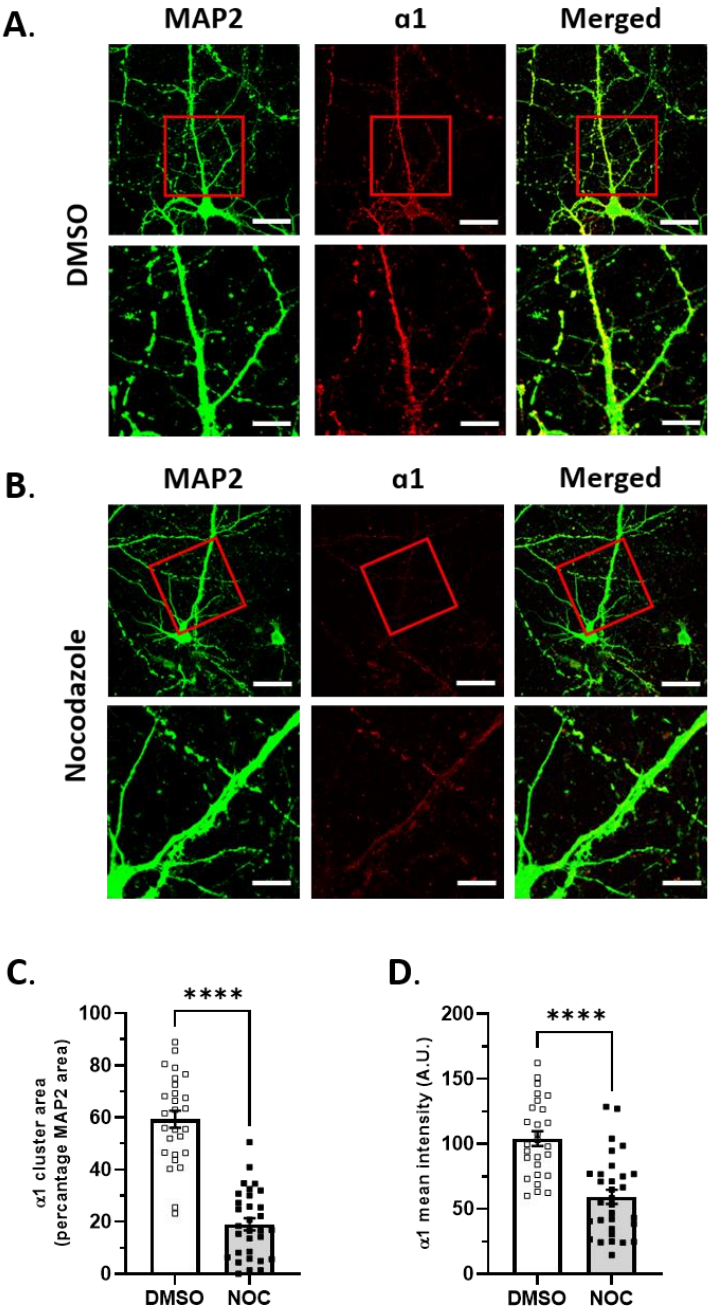

Figure 4.2 Nocodazole treatment decreases GABA$_A$R α1 subunit clustering. **A and B.** Example confocal microscopy images of cultured hippocampal neurons with cell surface labelling of GABA$_A$ receptor α1 subunit (red) and post-permeabilization labelling with MAP2 (green). Neurons were treated either with 10 µM nocodazole in DMSO (1:1000) (**B**) or with control treatment, DMSO (1:1000) (**A**). Scale bars 60 µm (overview) and 30 µm (zoomed inserts). **C**. Bar chart representing the total area of GABA$_A$R α1 subunit clusters within the MAP2 mask (normalised to MAP2 area) in DMSO (□) (n = 27, 59.3 ± 3.3 %) or nocodazole (■) (n = 31, 19.1 ± 2.3 %) treated neurons. **D**. The mean intensity of GABA$_A$R α1 subunit surface labelling in control, DMSO, (□) (n = 27, 104.1 ± 5.6 a.u.) or nocodazole (■) (n = 31, 59.4 ± 5.4 a.u) treated neurons. Unpaired t-test for both **C and D**, P value ≤ 0.0001 ****. Bars represent mean ± SEM with individual data points representing single cells in this and proceeding figures.

Next, cell surface immunolabelling of $GABA_AR$ α2 subunits was also performed after the same treatment of cultured hippocampal neurons (***Figure 4.3***). Similar to α1-, α2-containing $GABA_A$ receptors were dispersed after nocodazole treatment compared to control (***Figure 4.3 A and B***). As expected the mean total area of $GABA_AR$ α2 subunit clusters within the MAP2 mask was significantly decreased post nocodazole application compared to control ($P \leq 0.0001$) (***Figure 4.3 C***). The mean cell surface $GABA_AR$ α2 subunit intensity decreased by 2.2-fold, from 112.2 ± 7.6 a.u. with control treatment to 50.2 ±4.8 a.u. after nocodazole treatment ($P \leq 0.0001$) (***Figure 4.3 D***).

These findings together, provide evidence that nocodazole promotes $GABA_A$ receptor declustering in cultured hippocampal neurons by inhibiting microtubule polymerisation, which is in agreement with previous studies (Petrini et al., 2004, 2003).

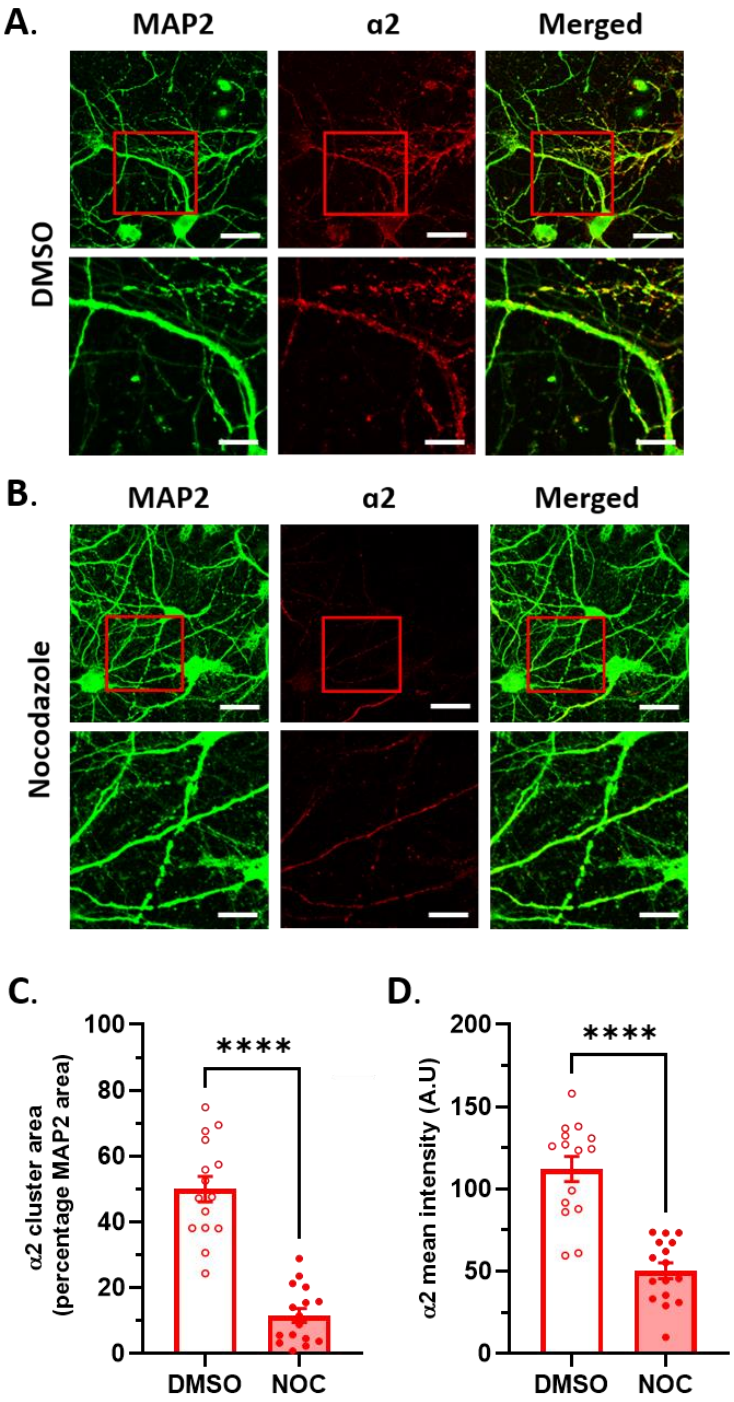

Figure 4.3 Nocodazole treatment promotes GABA$_A$R α2 subunit declustering. **A and B**. Cell surface staining of GABA$_A$ receptor α2 subunit followed by permeabilization and MAP2 staining (green) in control, DMSO (**A**) or 10 µM nocodazole treated (**B**). **C**. Bar chart showing the mean total area of GABA$_A$R α2 subunit clusters within the MAP2 mask (normalised to the MAP2 area) in control, DMSO, (○) (n = 15, 50.0 ± 3.9 %) or nocodazole (●) (n = 16, 11.6 ± 2.1 %) treated cultured hippocampal neurons. Scale bars 60 µm (top panels) and 30 µm (zoomed images). **D**. Bar chart representing the mean GABA$_A$R α2 subunit cluster intensity in DMSO (○) (n = 15, 112.2 ± 7.6 a.u.) or nocodazole (●) (n = 16, 50.2 ±4.8 a.u.) treated neurons. Unpaired t-test for both **C and D**, P ≤ 0.0001 ****.

Next, we performed the proximity ligation assay between α1 and α2 $GABA_AR$ subunits on nocodazole treated hippocampal cultured neurons. If the PLA α1/α2 signals in ***Figure 4.1 B*** arise due to inter-receptor PLA probe interactions, the number of PLA dots is expected to decrease upon treatment with nocodazole as it induces $GABA_A$ receptor declustering and hence increases the distance between single receptor pentamers.

In PLA experiments (here and in all proceeding sections), the quantitative analysis of PLA signal is presented in three distinct ways. The first quantifies the number of PLA dots within the MAP2 mask area (***Figure 4.4 C***). This is the most reliable and direct method of assessment. Second, the total number of PLA dots in the zoomed confocal image was calculated and normalised to the MAP2 mask area (***Figure 4.4 D***). The rationale for this was that MAP2 labelling could potentially be missed in the finer dendrites. Lastly, we measured the total number of PLA signals and normalised to the whole image area (***Figure 4.4 E***). This appears the most indirect method for quantification, but has been used by others (Gomes et al., 2016a). We chose the first method as a standard throughout this chapter for establishing any changes, however all three measures gave similar results.

Figure 4.4 illustrates the PLA results between α1 and α2 subunits in cultured hippocampal neurons. ***Figures 4.4 A and B*** show representative confocal images of pyramidal neurons labelled with cell surface PLA (red) and intracellular MAP2 immunolabelling (green). No significant differences were observed between PLA dots within the MAP2 area in control and nocodazole treated neurons (P value ≥ 0.05) (***Figure 4.4 C***). This suggests that the proximity of α1 and α2 subunits does not change, regardless of nocodazole-induced $GABA_A$ receptor declusterising (***Figures 4.2 and 4.3***), indicating that these subunits are likely to be present in the same receptor pentamers. Hence, the proximity ligation-based method is likely to be a reliable technique for assessment of native 'hetero-alpha' $GABA_A$ receptors.

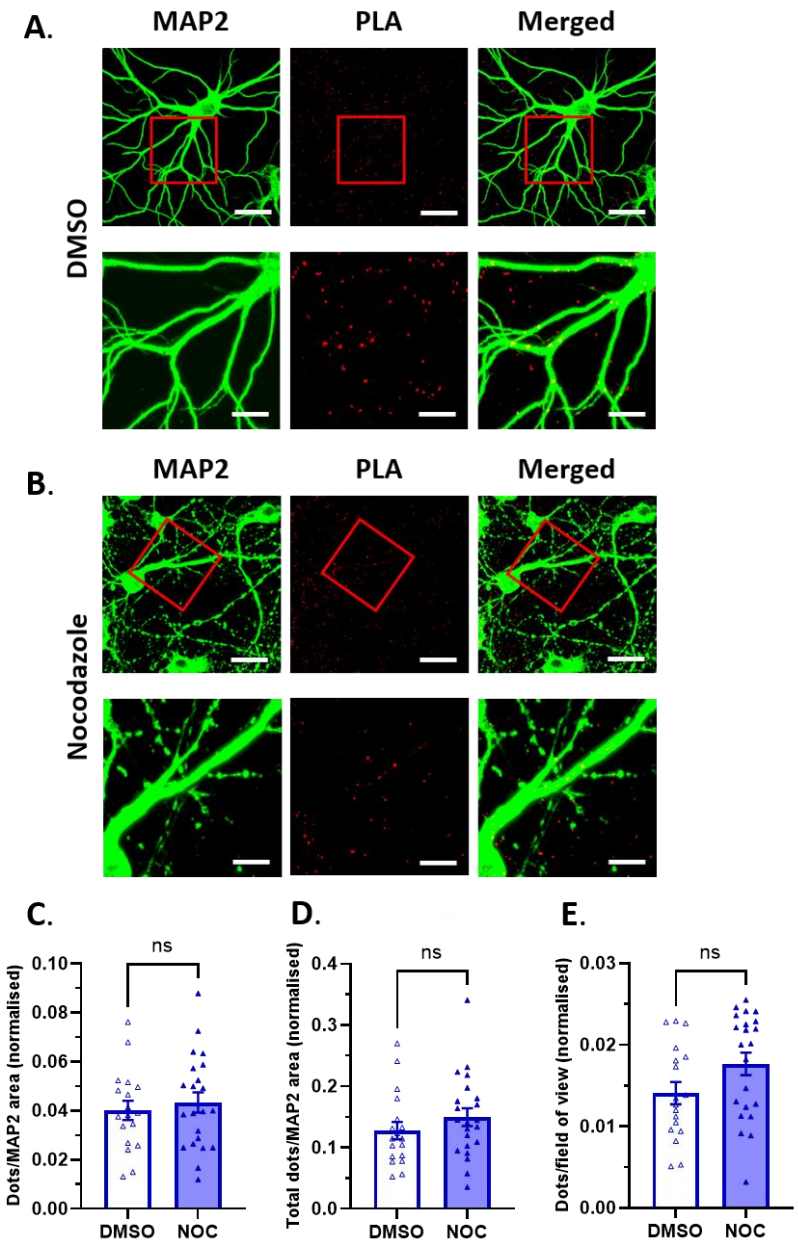

Figure 4.4 Nocodazole treatment has no effect on the number of GABA$_A$R α1 and α2 PLA dots. **A and B**. Representative confocal images showing PLA dots (red) between GABA$_A$R α1 and α2 subunit antibodies and MAP2 intracellular labelling (green). The PLA was performed prior to permeabilization to assess the proximity of cell surface GABA$_A$R subunits. Cultured hippocampal neurons were treated with 10 µM nocodazole in DMSO (1:1000) (panel **B**) or sham treated with DMSO (1:1000) (panel **A**). Scale bars 60 µm (top panels) and 30 µm (zoomed images). **C**. Bar chart showing the mean number of PLA dots within the MAP2 mask (normalised to MAP2 mask area) for DMSO (△) (n = 18, 0.04 ± 0.003) and nocodazole (▲) (n = 22, 0.04 ± 0.004) treated neurons. Unpaired t-test, P ≥ 0.05 n.s. **D**. Bar chart representing the total number of PLA dots per field of view (zoomed images; normalised to MAP2 mask area) for DMSO (△) (n = 18, 0.13 ± 0.014) or nocodazole (▲) (n = 18, 0.15 ± 0.014) treated neurons. Unpaired t-test, P ≥ 0.05 n.s. **E**. Bar chart showing total number of PLA dots per field of view (normalised to area) for DMSO (△) (n = 18, 0.01 ± 0.001) and nocodazole (▲) (n = 22, 0.02 ± 0.001) treated neurons. Mann-Whitney test, P ≥ 0.05 n.s.

4.2.3 $GABA_AR$ γ2 and δ subunits are not in close proximity for PLA probe hybridisation

To further validate PLA as a method for quantifying native hetero-alpha $GABA_A$ receptors in cultured hippocampal neurons we performed another control to assess whether this technique is likely to detect inter-receptor subunit interactions: assessment of proximity between γ2 and δ subunits. The δ $GABA_A$ receptor is localised mainly extrasynaptically although there is some evidence that these receptors can be localised perisynaptically and may contribute to sIPCSCs (Kasugai et al., 2010; Sun et al., 2018; Wei et al., 2003). The γ2 subunit has been shown to exist in synaptic junctions as well as at extrasynaptic locations (Bogdanov et al., 2006; Kasugai et al., 2010; Zoltan Nusser et al., 1998; Thomas et al., 2005). Therefore, it is possible that these two subunits could co-exist in close proximity within the same subcellular compartments, both in synapses and extrasynaptic membranes. Nevertheless, their presence in the single $GABA_AR$ receptor pentamer is mutually exclusive (Martenson et al., 2017; Olsen and Sieghart, 2009). Since γ2 and δ subunits cannot exist in the same $GABA_AR$ complex, any PLA dots would imply that these subunits are present in distinct $GABA_A$ receptors that are in sufficiently close proximity to generate an inter-receptor PLA signal.

To test this hypothesis, a PLA assay between γ2 and δ subunits was performed in cultured hippocampal neurons. First, the antibodies used for PLA were tested by immunocytochemistry. The first two rows in ***Figure 4.5 A*** shows representative images of neuronal dendrites labelled with either rabbit anti-γ2 antibodies (top row, red) or mouse anti-δ antibodies (middle row, red) alongside MAP2 labelling (green). Immunocytochemistry with both $GABA_A$ receptor subunit antibodies gives rise to clear $GABA_A$ receptor immunolabelling along MAP2-positive dendrites, indicating the presence of both γ2- and δ-containing receptors in these neurons.

The bottom row in ***Figure 4.5*** shows confocal images of PLA (red) performed between γ2 and δ subunits with the same antibodies as above. Quantification analysis indicated that no PLA γ2/δ dots were observed in the images taken, suggesting these two $GABA_AR$ subunits are not in close enough proximity for the PLA probes to

hybridise. This observation further strengthens the validity of PLA use to assess $GABA_A$ receptor stoichiometry at a single receptor level.

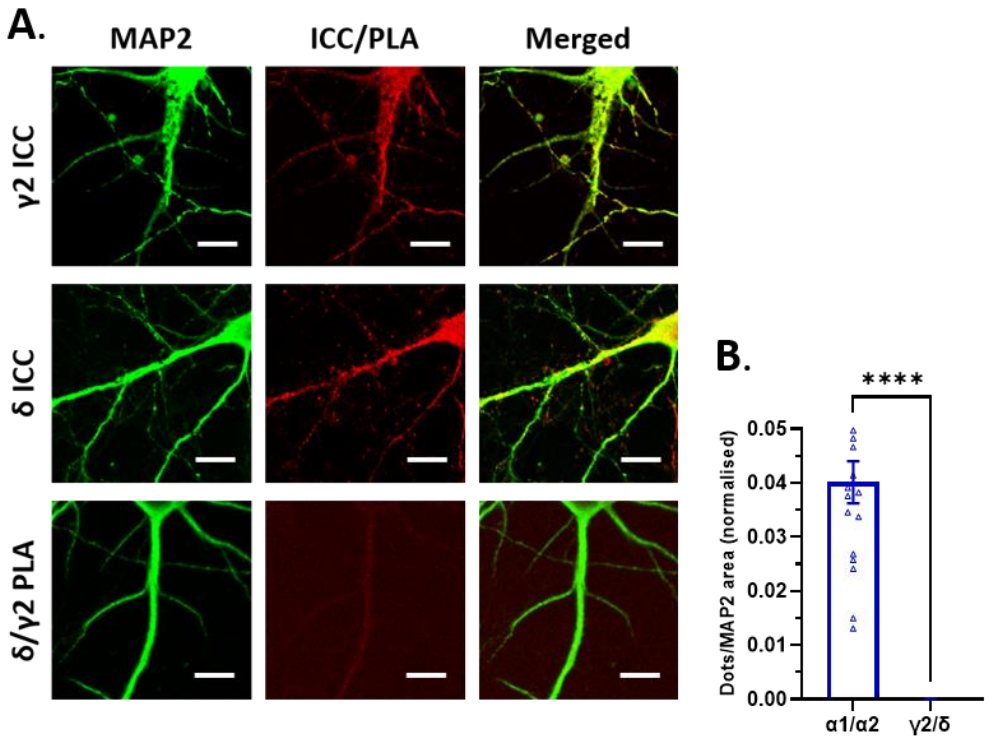

Figure 4.5 The $GABA_A$Rs γ2 and δ subunits are not in close proximity to produce a PLA signal. **A.** Representative confocal images of $GABA_A$R γ2 (top row) and δ (middle row) subunit cell surface staining in cultured hippocampal neurons. The bottom row shows a representative neuronal dendrite after application of PLA between γ2 and δ subunits (red channel). MAP2 immunostaining was performed after permeabilization (green). Scale bar 50 µm (all images). **B**. Bar chart quantifying the mean ± SEM values of PLA dots between $GABA_A$R α1 and α2 (△) (n = 18, 0.04 ± 0.004), or γ2 and δ (▲) (n = 12, 0) subunits. Mann-Whitney test, P ≤ 0.0001 ****.

4.2.4 Expression of the α2 subunit leads to an increase in synaptic 'hetero-alpha' $GABA_A$Rs in cultured hippocampal neurons

From the previous chapter we concluded that the expression of 'hetero-alpha' $GABA_A$Rs is likely to be tightly regulated and depends on the identity of both α and β subunits. To assess the effects of expressing either α subunit (α1 and α2) on numbers of α1α2-containing receptors and their subcellular localisation, we transfected DIV7

cultured hippocampal neurons with either subunit cDNA construct. These subunit constructs were co-transfected with eGFP in equimolar ratios and included a control eGFP only transfection performed in parallel. Unlike HEK293 cells transfection, the β2/3 and γ2 were not co-transfected with the α subunits. This is due to the fact that neurons endogenously express $GABA_A$Rs, thereby by transfecting cultured neurons with only α subunits, the assembly and expression of receptors is limited by endogenous β2/3 and γ2 subunit availability.

On DIV12-14 neurons were fixed and cell surface PLA between α1 and α2 was performed as described previously. Neurons were then permeabilised and labelled with guinea-pig anti-VIAAT antibodies. Subsequent confocal imaging was used to produce Z-stacks with optimum slices of eGFP positive neurons.

For analysis, an ImageJ plug-in DiAna (see ***Methods Section 2.5.3***) was used, which allows for three-dimensional object segmentation and automatically performs object-based co-localisation and distance analyses (Gilles et al., 2017). We measured co-localisation between PLA dots and VIAAT puncta. Since VIAAT is a synaptically-localised vesicular co-transporter of GABA, the role of which is to package vesicles containing GABA molecules for synaptic release, it serves as a reliable presynaptic marker for GABAergic terminals (Danglot et al., 2003; Juge et al., 2009; Sagné et al., 1997). Therefore, all PLA α1/α2 dots co-localising with VIAAT were considered as synaptic, whereas PLA dots that did not overlap with VIAAT were regarded as extrasynaptic.

PLA signal between anti-α1 and anti-α2 $GABA_A$ receptor antibodies revealed the presence of 'hetero-alpha' α1α2-containing receptors in eGFP, α1 or α2 transfected neurons (***Figure 4.6 A***). The number of PLA dots did not change upon α1 subunit overexpression compared to control, eGFP (0.04 ± 0.005 per μm^2 and 0.04 ± 0.005 per μm^2 respectively, $P \geq 0.05$) (***Figure 4.6 B***). Interestingly, the number of PLA dots in α2-transfected neurons (n = 16, 0.07 ± 0.007) significantly increased compared to both eGFP- (n = 14, 0.04 ± 0.005) and α1-transfected (n = 14, 0.04 ± 0.005) neurons ($P \leq 0.05$ and ≤ 0.001 respectively). This suggests that overexpression of α2, but not α1 $GABA_A$R subunits leads to an increased number of 'hetero-alpha' α1α2-containing $GABA_A$ receptors. It is possible that increasing the number of available α2 subunits

upregulates the assembly and cell surface expression of α1α2-containing $GABA_A$Rs, indicating that α2 subunit synthesis could be a limiting factor in formation of these receptors.

Co-localisation analysis of α1/α2 PLA dots with VIAAT clusters revealed that there was no significant difference in the proportion of synaptic PLA dots in α1 transfected neurons compared with eGFP controls (P value ≥ 0.05). However, there was a significant increase in both PLA with VIAAT puncta and VIAAT puncta with PLA dots in α2-transfected neurons, 42.3 ± 4.6 % and 63.9 ± 5.5 % respectively, compared to control eGFP transfected neurons, 21.3 ± 3.6 % and 17.3 ± 2.9 % respectively, (P ≤ 0.01 and ≤ 0.0001) and α1-transfected neurons 24.3 ± 5.1 % and 17.5 ± 3.6 % respectively (***Figure 4.6 E and F***). Additionally, a 1.7-fold increase in PLA colocalization with VIAAT puncta (P ≤ 0.05), and a 3.6-fold increase in PLA-positive VIAAT puncta (P ≤ 0.0001) were observed in α2- compared to α1-transfected neurons. Since the overall number of α1α2-containing $GABA_A$Rs increases with α2 subunit overexpression (***Figure 4.6 B***), it is likely that the newly assembled 'hetero-alpha' $GABA_A$Rs have a preference to cluster at synapses, rather than localise extrasynaptically.

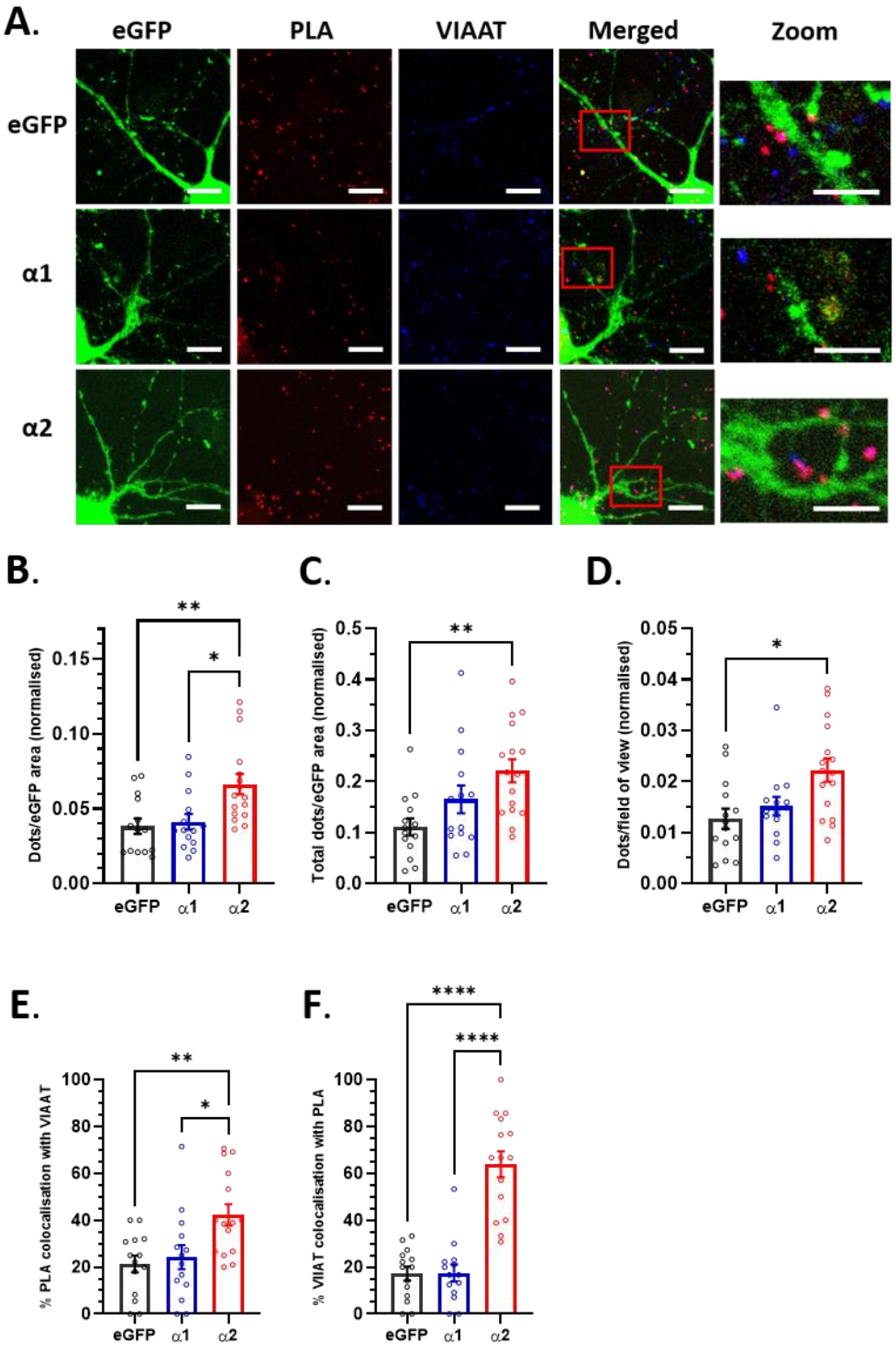

Figure 4.6 Overexpression of α2, but not α1 GABA$_A$R subunits leads to an increase in PLA dots that localise at synapses. **A.** Example confocal images of PLA signal (red) between GABA$_A$R α1 and α2 subunit antibodies, eGFP (green) and VIAAT (blue). PLA was performed prior to permeabilization to assess the proximity of surface α1 and α2 subunits. Cultured hippocampal neurons were transfected with eGFP (top row), eGFP + α1 subunit (middle row), or eGFP + α2 subunit (bottom row) cDNAs (equimolar ratios) on DIV7 and stained on DIV14-16. Scale bar 30 µm (overview) and 15 µm (zoomed inserts). **B.** Bar chart representing number of PLA dots within the eGFP mask (normalised to MAP2 mask area). The mean ± SEM

of PLA signals of eGFP (○) (n = 14, 0.04 ± 0.005), α1 (○) (n = 14, 0.04 ± 0.005), and α2 (○) (n = 16, 0.07 ± 0.007) transfected neurons. Kruskal-Wallis test with Tukey's post hoc test for multiple comparisons between all groups, P ≤ 0.05 *, ≤ 0.001 **. **C.** Bar chart representing the total number of PLA dots in the field of view (zoomed images; normalised to eGFP mask area). Neurons were transfected with eGFP (○) (n = 14, 0.11 ± 0.017), α1 +eGFP (○) (n = 14, 0.17 ± 0.027), or α2 + eGFP (○) (n = 16, 0.22 ± 0.023) cDNAs. Ordinary one-way ANOVA test with Tukey's post hoc test for multiple comparisons between all groups, P ≤ 0.05 *. **D**. Total number of PLA dots per field of view (normalised to area). The mean ± SEM of PLA signals of eGFP (○) (n = 14, 0.01 ± 0.002), α1 (○) (n = 14, 0.02 ± 0.002), and α2 (○) (n = 16, 0.02 ± 0.002) transfected neurons. Kruskal-Wallis test with Tukey's post hoc test for multiple comparisons between all groups, P ≤ 0.05 *, ≤ 0.001 **. **E.** Percentage of PLA dots colocalising with VIAAT clusters for EGFP (○) (n = 14, 21.3 ± 3.6 %), α1 (○) (n = 14, 24.3 ± 5.1 %), and α2 (○) (n = 15, 42.3 ± 4.6 %) transfected neurons. **F.** Bar chart representing percentage means ± SEMs of VIAAT clusters colocalising with PLA dots for eGFP (○) (n = 14, 17.3 ± 2.9 %), α1 (○) (n = 14, 17.5 ± 3.6 %), and α2 (○) (n = 15, 63.9 ± 5.5 %) transfected neurons. For **E and F**, Ordinary one-way ANOVA test with Tukey's post hoc test, P ≤ 0.05 *, ≤ 0.01 **, ≤ 0.0001 ****.

4.2.5 Investigating sIPSCs of α1 and α2 transfected cultured hippocampal neurons

Following the results obtained from investigating the effects of either α1 or α2 subunit overexpression on 'hetero-alpha' $GABA_A$ receptor cell surface numbers and their localisation patterns, the effects of these transfections on inhibitory synaptic transmission in cultured hippocampal neurons were investigated. Specifically, our aim was to elucidate any functional signatures of 'hetero-alpha' α1α2-containing $GABA_A$Rs. Since overexpression of the α2 subunit results in an increased synaptic expression of 'hetero-alpha' $GABA_A$R, we hypothesised that these could potentially have a role in regulating inhibitory synaptic transmission.

To test this hypothesis, cultured hippocampal neurons were transfected with either α1 or α2 $GABA_A$R subunit cDNAs (+ eGFP), and a control transfection with eGFP cDNA only was performed in parallel. The transfection protocol was performed in the same way as described in ***Section 4.2.3***. Transfected neurons were subjected to whole-cell voltage-clamp electrophysiology, where membrane currents were recorded and spontaneous inhibitory post-synaptic currents (sIPSCs) were analysed (see ***Methods 2.4.4***). Example mean sIPSC waveforms of eGFP (black), α1 (blue) and α2 (red) transfected neurons are shown in ***Figure 4.7 A***. No significant differences in sIPSC frequency and mean amplitude (***Figure 4.7 B and C*** respectively) were observed

between eGFP, α1, and α2 subunit cDNA transfections (P value ≥ 0.05 between all groups). Despite lack of statistical significance, a trend towards increased sIPSC frequency of α2-transfected neurons (2.7 ± 0.5 Hz) could be noted, compared to the control, eGFP (1.4 ± 0.2 Hz) and α1 (1.7 ± 1.04 Hz) transfections.

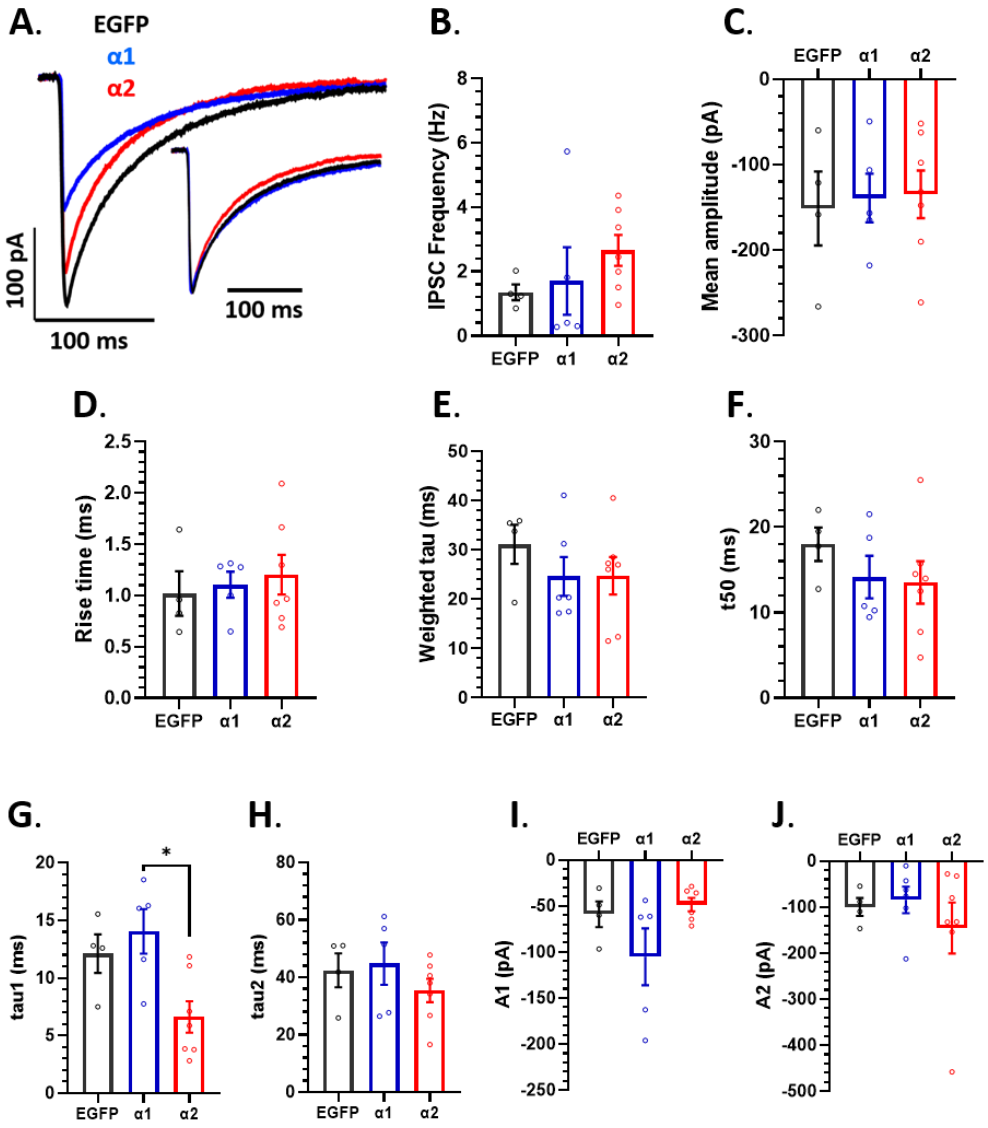

Figure 4.7 sIPSC analysis of eGFP, α1 and α2 transfected hippocampal cultured neurons. **A.** Example mean sIPSC waveforms from representative EGFP (black), $GABA_AR$ α1 (blue), and α2 (red) subunit transfected hippocampal cultured neurons. The inset trace represents peak-scaled mean sIPSC waveforms from the same cells. **B.** sIPSC frequencies of EGFP (○) (n = 4, 1.4 ± 0.2 Hz), α1 (○) (n = 5, 1.7 ± 1.04 Hz), and α2 (○) (n = 7, 2.7 ± 0.5 Hz) transfected neurons. **C**. Bar chart representing the mean ± SEM sIPSC amplitudes of EGFP (○) (n = 4, -151.3 ± 43.3 pA), α1 (○) (n = 5, -139.1 ± 28.6 pA), and α2 (○) (n = 7, -134.7 ± 27.9 pA)

transfected neurons. **D**. sIPSC rise times (10 - 90 %) of EGFP (○) (n = 4, 1.01 ± 0.2 ms), α1 (○) (n = 5, 1.1 ± 0.1 ms), and α2 (○) (n = 7, 1.2 ± 0.2 ms) transfected neurons. **E.** Bar chart representing the mean sIPSC weighted decay tau values of EGFP (○) (n = 4, 31.1 ± 3.9 ms), α1 (○) (n = 5, 24.6 ± 3.9 ms), and α2 (○) (n = 7, 24.7 ± 3.8 ms) transfected neurons. **F.** The time for sIPSCs to decay by half (t_{50}) of EGFP (○) (n = 4, 18.0 ± 1.9 ms), α1 (○) (n = 5, 14.1 ± 2.5 ms), and α2 (○) (n = 7, 13.5 ± 2.5 ms) transfected neurons. **G.** The faster decay tau from the two-exponential fit (tau1) of sIPSCs, means ± SEMs, of EGFP (○) (n = 4, 12.1 ± 1.7 ms), α1 (○) (n = 5, 14.1 ± 1.9 ms), and α2 (○) (n = 7, 6.6 ± 1.4 ms) transfected neurons. **H.** Mean ± SEM values of the slower decay tau, tau2, of EGFP (○) (n = 4, 42.5 ± 5.9 ms), α1 (○) (n = 5, 44.8 ± 7.4 ms), and α2 (○) (n = 7, 35.5 ± 4.1 ms) transfected neurons. **I.** Mean amplitudes of the fast sIPSC component (A1) of EGFP (○) (n = 4, -58.9 ± 13.9 pA), α1 (○) (n = 5, -105.1 ± 30.9 pA), and α2 (○) (n = 7, -48.4 ± 7.3 pA) transfected neurons. J. Mean amplitudes of the slow sIPSC component (A2) of EGFP (○) (n = 4, -99.7 ± 19.3 pA), α1 (○) (n = 5, -84.4 ± 28.6 pA), and α2 (○) (n = 7, -145.2 ± 55.4 pA) transfected neurons. For **B, E, I, J** – Kruskal-Wallis test with Tukey's post hoc test for multiple comparisons between all groups, P ≥ 0.05 n.s. For **C, D, F – H** – ordinary one-way ANOVA test with Tukey's post hoc test, P ≥ 0.05 n.s., ≤ 0.05 *.

Furthermore, no differences were observed between rise times (quantified as the 10-90% rise time), the weighted decay times and the time it takes for sIPSCs to decay by half, t50s, (***Figure 4.7 D, E, and F*** respectively) in eGFP, α1, and α2 transfections (P ≥ 0.05 between all groups). Further analysis into the individual components of the bi-exponential fits (tau1, tau2, A1 and A2) revealed that the faster tau, tau1, is significantly smaller in α2 (6.6 ± 1.4 ms) compared to α1 (14.1 ± 1.9 ms) transfections (P value ≤ 0.05). Since an increased number of synaptic α1/α2 PLA dots was observed in α2 transfected cultured hippocampal neurons, together with sIPSC analysis, we conclude that 'hetero-alpha' α1α2-containing $GABA_A$Rs could potentially have distinct kinetics to their 'homo-alpha' counterparts (α1α1- and α2α2-containing).

4.2.6 Exploring effect of chemical inhibitory long-term potentiation on sIPSCs in cultured hippocampal neurons

GABAergic synapses are dynamic in nature, able to undergo modulation-dependent long-term changes that regulate synaptic strength (Castillo et al., 2011; Field et al., 2021). A prominent example where $GABA_A$Rs undergo rapid synaptic clustering is during the induction of inhibitory long-term potentiation, iLTP (Marsden et al., 2007; Rajgor et al., 2020). Since chemical iLTP induction is associated with an increased

recruitment of $GABA_AR$ to synapses (Marsden et al., 2007; Petrini et al., 2014; Rajgor et al., 2018), our aim was to explore the role of 'hetero-alpha' $GABA_A$ receptors during this synaptic plasticity mechanism.

To achieve this, we first assayed a previously reported chemical iLTP protocol (Marsden et al., 2007; Petrini et al., 2014; Rajgor et al., 2018) and tested its effects on sIPSC frequency and amplitude. This protocol is based on activation of N-methyl-D-aspartate receptors (NMDARs), which induces long-term depression (LTD) at excitatory synapses and simultaneously potentiates inhibitory transmission *via* increased $GABA_AR$ surface expression (Marsden et al., 2007).

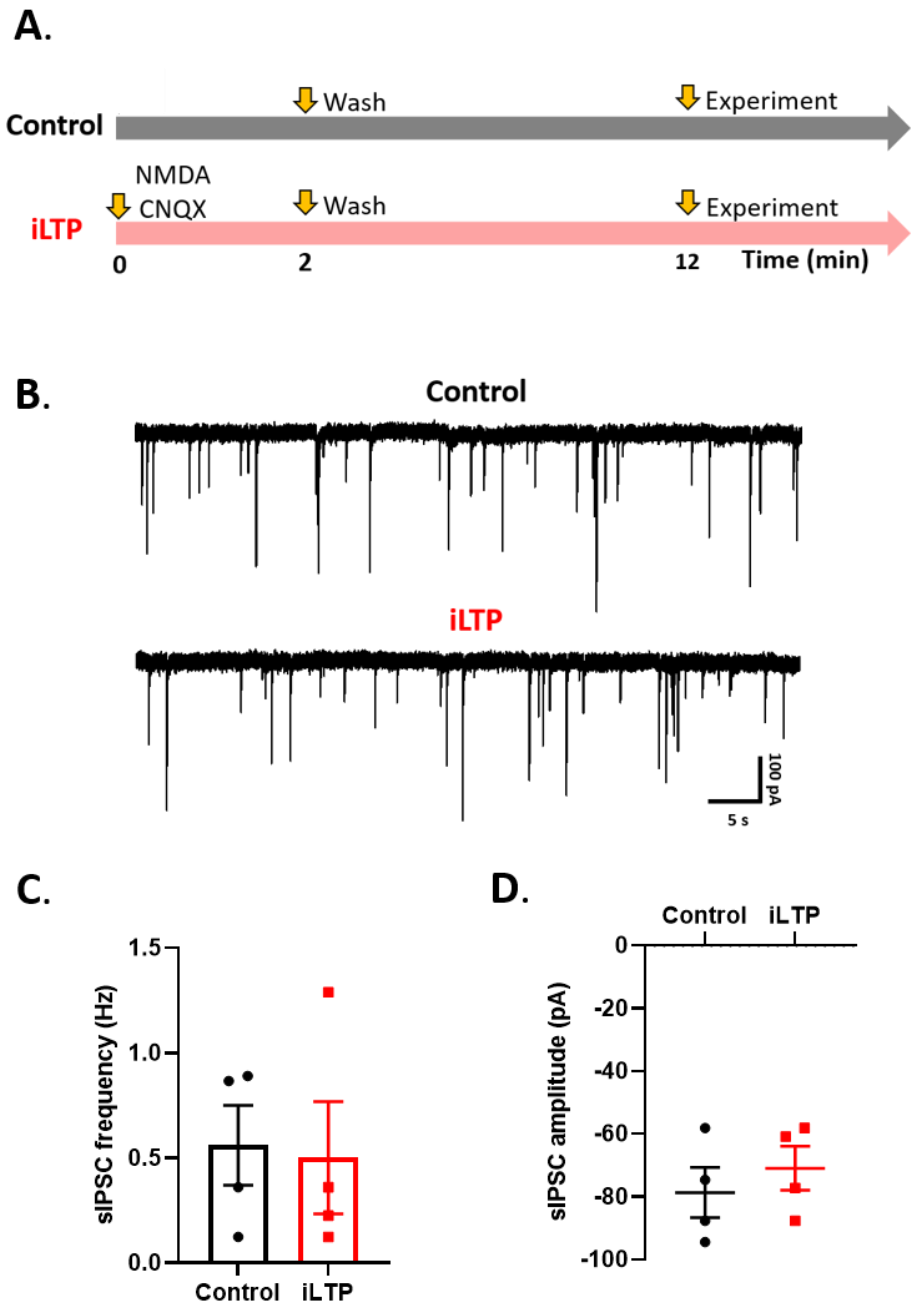

Figure 4.8 Effects on sIPSC frequency and mean amplitude of a chemical iLTP protocol. **A.** Schematic timeline of the protocol used for chemical iLTP induction in cultured hippocampal neurons with 20 µM NDMA and 10 µM CNQX. **B.** Representative example traces from whole-cell voltage-clamp recordings showing sIPSCs from control-treated (top), or iLTP induced (bottom trace) neurons. **C.** Bar chart displaying the sIPSC frequency of control treated (●) (n = 4, 0.6 ± 0.19 Hz) and iLTP treated (■) (n = 4, 0.5 ± 0.3 Hz) cultured hippocampal neurons. Unpaired t-test, P value ≥ 0.05 not significant. **D.** Scatter dot plot representing the sIPSC amplitude values for control-treated (●) (n = 4, -78.7 ± 8.0 pA) and iLTP treated (■) (n = 4, -71.0 ± 7.0 pA) neurons. Each point represents a cell. Unpaired t-test, P ≥ 0.05 not significant.

DIV11-14 cultured hippocampal neurons were treated with 20 µM NMDA and 10 µM 6-cyano-7-nitroquinoxaline-2,3-dione (CNQX), an α-amino-3-hydroxy-methyl-4-isoxazolepropionic acid receptor (AMPAR) antagonist, for two minutes to induce chemical iLTP. A control treatment was performed alongside, by treating neurons with the same volume of HEPES buffered saline, HBS (used to make up NMDA and CNQX stock solutions) (***Figure 4.8 A***). The neurons were then washed with maintenance media and left for 10 minutes prior to the start of electrophysiological recordings. No significant differences were found between sIPSC frequencies (0.6 ± 0.19 Hz and 0.5 ± 0.3 Hz) or amplitudes (-78.7 ± 8.0 pA and - 71.0 ± 7.0 pA) in iLTP induced and control treated neurons respectively. This suggests that the number of synaptic $GABA_A$Rs does not increase with the iLTP NMDA protocol.

This is surprising, since previous reports showed that the sIPSC amplitude increases post NMDA treatment and that the increase persists for up to 30 minutes (Petrini et al., 2014). Other studies demonstrated an NMDA-dependent increase in $GABA_A$R clustering at synapses as well as an increase in miniature IPSC (mIPCS) amplitude (Marsden et al., 2007; Rajgor et al., 2020). The differences between our data and previous studies could potentially be attributed to variability of cultured neurons and their age. We used DIV 11-14 cultured hippocampal neurons, whereas previous reports performed this iLTP protocol in DIV14-21 neurons (Marsden et al., 2007; Petrini et al., 2014).

4.2.7 Chemical induction of LTP increases both sIPSC amplitude and frequency

Since the chemical iLTP protocol did not appear to enhance sIPSC amplitude or frequency, we decided to explore the impact on inhibitory transmission of protocols previously found to induce excitatory LTP. One of the ways LTP is induced is *via* an overactivation of NMDA receptors leading to a rapid recruitment of AMPARs in postsynaptic membranes (Goldin et al., 2001; Liao et al., 2001; Lu et al., 2001). One of the most widely used protocols to achieve this is by enhancing activation of NMDARs through application of the NMDAR co-agonist glycine (Molnár, 2011).

Cultured hippocampal neurons were incubated with 200 µM glycine for three minutes and then left for 10 minutes prior to electrophysiological recordings. For controls, neurons were also treated with glycine but in the presence of 50 µM (2R)-amino-5-phosphonovaleric acid, APV, a competitive antagonist of NMDARs and with a five-minute pre-conditioning in APV (***Figure 4.9 A***). This protocol was previously validated in our lab (*unpublished data*), where a significant increase in frequency and amplitude of excitatory post-synaptic currents, sEPSCs, was observed, which is in agreement with previous findings (Molnár, 2011). Therefore, the effects of this glycine-induced excitatory LTP protocol on sIPSCs were studied here.

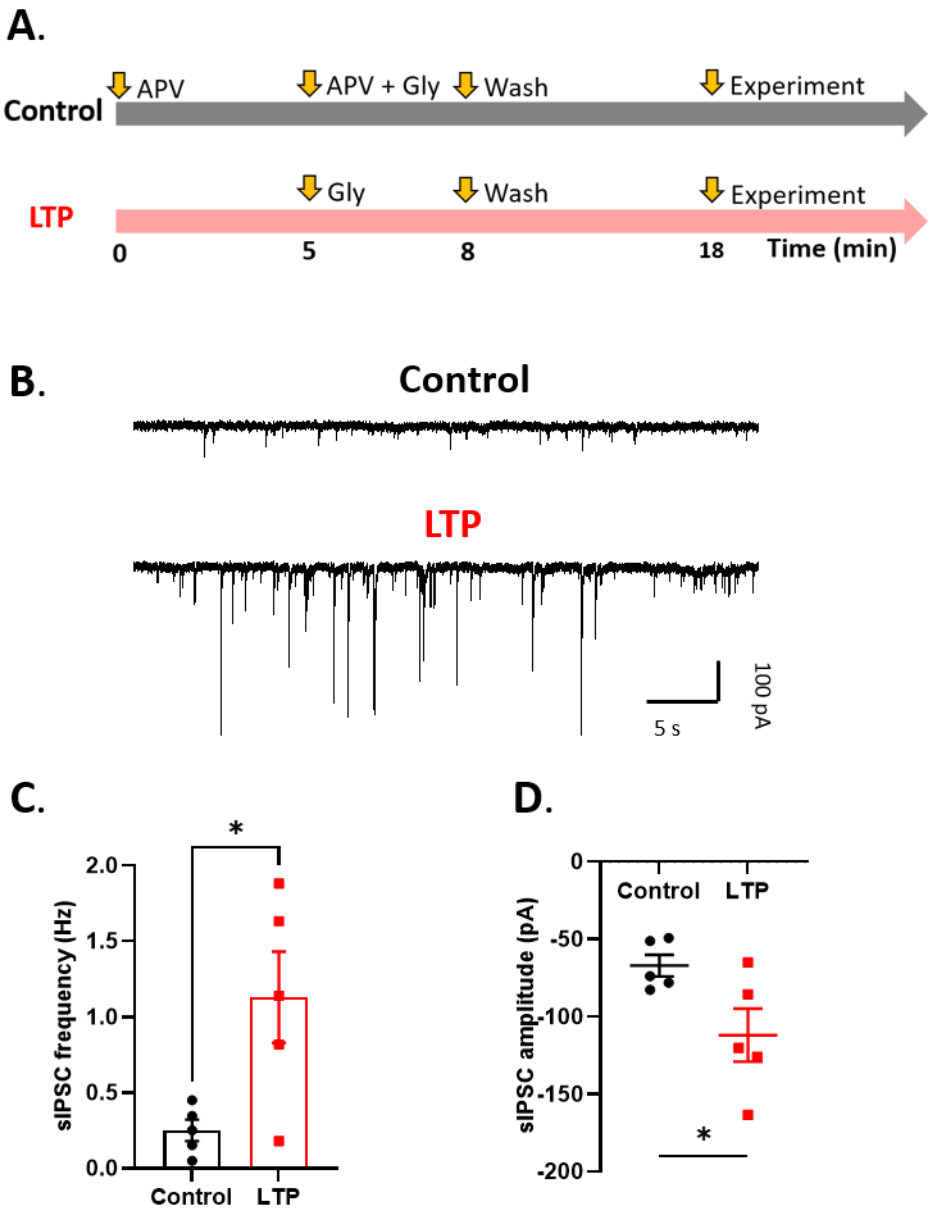

Figure 4.9 Chemical induction of excitatory LTP with glycine significantly increases both sIPSC frequency and amplitude. **A.** Schematic timeline of the protocol used for chemical LTP induction in cultured hippocampal neurons using 200 µM glycine, Gly. For control-treated neurons, an NMDA receptor antagonist, APV (50 µM) was used prior to, and during glycine application. **B.** Representative example traces from whole-cell voltage-clamp recordings showing sIPSCs from control-treated (top), or glycine LTP treated (bottom trace) neurons. **C.** Bar chart displaying the sIPSC frequency of control treated (●) (n = 5, 0.3 ± 0.07 Hz) and glycine treated (■) (n = 5, 1.1 ± 0.03 Hz) neurons. Unpaired t-test, P value: ≤ 0.05 *. **D.** Scatter dot plot representing the sIPSC amplitude values for control-treated (●) (n = 5, -67.1 ± 7.0 pA) and glycine treated (■) (n = 5, -112.0 ± 17.0 pA) neurons. Each point represents a cell. Unpaired t-test, P value: ≤ 0.05 *.

Representative traces of sIPSC recordings in control-treated (top) and glycine-treated (bottom) are shown in ***Figure 4.9 B***. Upon chemical LTP induction with glycine, sIPSC frequency increased by almost 4-fold compared to control treatment (***Figure 4.9 C***). Additionally, the mean sIPSCs amplitude exhibited a significant increase, from -67.1 ± 7.0 pA in control-treated, compared to -112.0 ± 17.0 pA in glycine-treated neurons ($P \leq 0.05$) (***Figure 4.9 D***). We therefore conclude that the glycine-induced LTP protocol increases sIPSC frequency and amplitude.

4.2.8 Investigating the effect of the glycine LTP protocol on 'hetero-alpha' $GABA_A$Rs using proximity ligation assay

The last aim of this chapter was to investigate the effects of LTP on 'hetero-alpha' $GABA_A$ receptors. Given our unexpected finding that the chemical glycine LTP protocol can also be considered an iLTP protocol (since both sIPSCs frequency and amplitude increase thereby having a postsynaptic effect in increasing the number of $GABA_A$Rs at inhibitory synapses), we assessed the presence, expression level and subcellular localisation (synaptic or extrasynaptic) of α1α2-containing $GABA_A$Rs post-LTP induction.

To achieve this goal, we subjected glycine LTP- or control -treated DIV 11-14 neurons to a PLA protocol between cell surface native α1 and α2 $GABA_A$R subunits (red). Following permeabilization, neurons were immunolabelled for MAP2 (green) and VIAAT (blue) ***(Figure 4.10 A***). The number of PLA signals in z-stack confocal images was counted and their co-localisation with VIAAT was quantified.

Interestingly, a significant increase in PLA signal was observed post glycine LTP treatment, compared to control-treated neurons ($P \leq 0.001$) (***Figure 4.10 B***). Furthermore, the co-localisation of PLA dots with VIAAT clusters significantly increased, from 26.2 ± 4.6 % in control-treated neurons, compared to 44.1 ± 5.6 % in glycine-treated LTP-induced neurons ($P \leq 0.05$) (***Figure 4.10 E***). Similarly, the percentage of PLA-positive VIAAT clusters exhibited a significant increase, by almost 50 %, from control-treated (34.6 ± 7.9 %) compared to glycine-treated (61.7 ± 8.6 %)

neurons (P ≤ 0.05) (***Figure 4.10 F***). Lastly, both the volume and mean intensity of VIAAT clusters significantly increased post LTP-induction (P ≤ 0.0001, ***Figure 4.10 G and H***).

Taken together, our data suggests that the number of 'hetero-alpha' $GABA_A$Rs increases after chemical LTP induction with glycine, and these receptors show increased expression at synapses, compared with extrasynaptic areas. Various LTP protocols induce plastic changes in inhibitory transmission, including increased postsynaptic clustering of α1, α2, and β3 $GABA_A$R subunits (Bannai et al., 2020; Battaglia et al., 2018; Petrini et al., 2014). Therefore, it is not surprising that 'hetero-alpha' α1α2-containing $GABA_A$Rs could play a role in synaptic plasticity.

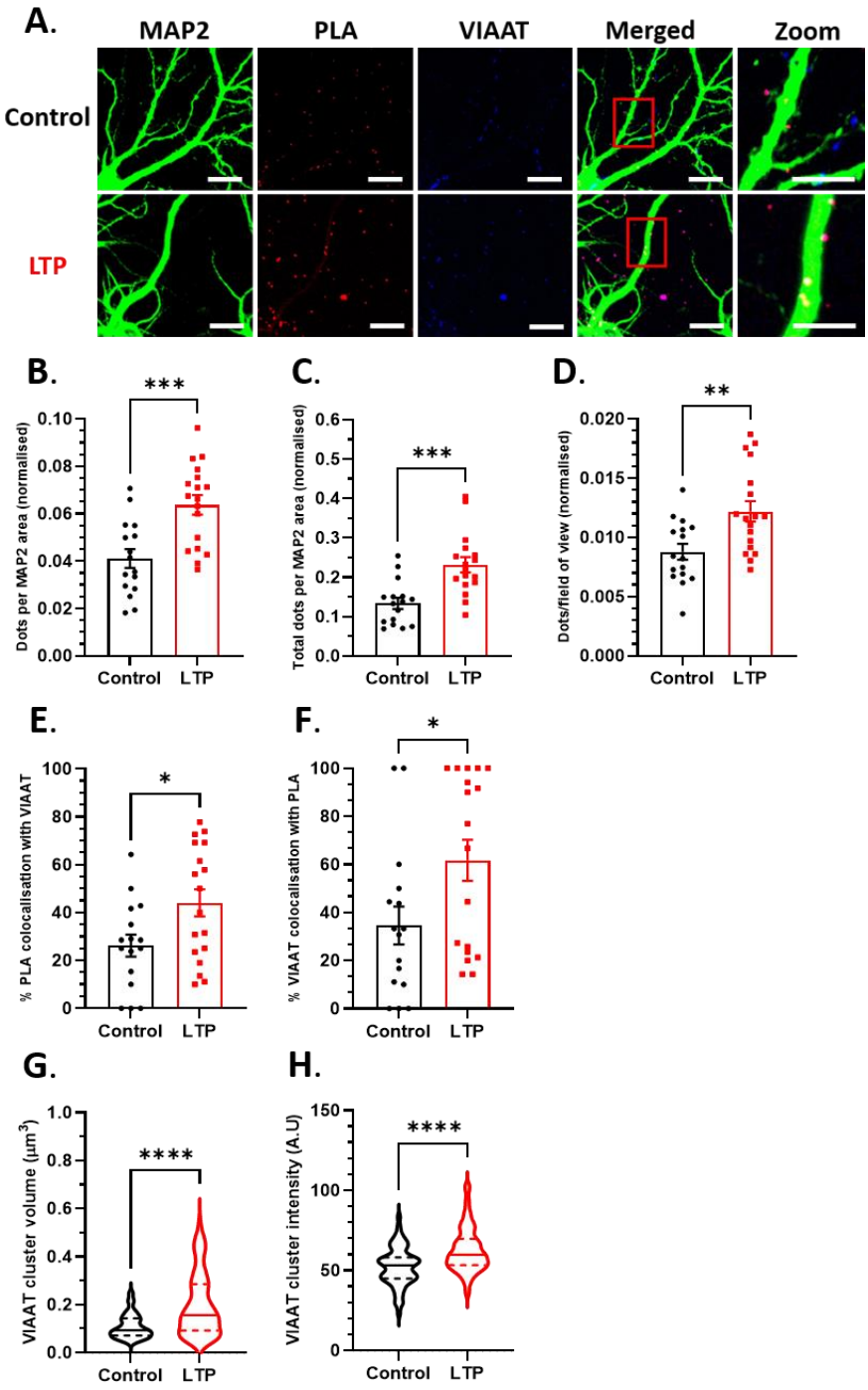

Figure 4.10 Chemical induction of LTP significantly increases GABA$_A$R α1 and α2 subunit synaptic PLA signal. **A.** Example confocal images of PLA dots (red) between GABA$_A$R α1 and α2 subunit antibodies, and intracellular MAP2 (green) and VIAAT (blue) labelling. PLA was performed prior to permeabilization of neurons. Neurons were subjected to LTP induction with glycine (bottom row), or control treatment (top row). Scale bars 15 µm (overview images) and 5 µm (zoomed inserts). **B.** Bar chart representing PLA dots within the MAP2 mask (normalised to MAP2 mask area). The mean ± SEM of PLA signals of control (●) (n = 16, 0.04 ± 0.004) and glycine (■) (n = 18, 0.06 ± 0.004) treated neurons. Unpaired t-test, P ≤ 0.001 ***. **C.** Bar chart representing the total number of PLA dots in the field of view (zoomed images; normalised to MAP2 mask area). Neurons were either control (●) (n = 16, 0.13 ± 0.014) or

glycine (■) (n = 17, 0.23 ± 0.019) treated to induce chemical LTP. Mann-Whitney test, P value: ≤ 0.001 ***. **D**. Total number of PLA dots per field of view (normalised to area). The mean ± SEM PLA signal values of control (●) (n = 16, 0.008 ± 0.0006) or glycine (■) (n = 18, 0.012 ± 0.0008) treated neurons. Unpaired t-test, P value: ≤ 0.01 **. **E.** Percentage PLA dots colocalization with VIAAT clusters for control (●) (n = 16, 26.2 ± 4.6 %) and glycine treated (■) (n = 18, 44.1 ± 5.6 %) neurons. Unpaired t-test, P value: ≤ 0.05 *. **F.** Bar chart representing percentage means ± SEMs of VIAAT clusters colocalising with PLA dots in control-treated (●) (n = 16, 34.6 ± 7.9 %) and glycine-treated (■) (n = 18, 61.7 ± 8.6 %) neurons. **G.** Violin plot displaying the median (solid line) and quartiles (dashed lines) of mean VIAAT cluster volume per cell. The mean ± SEM values in control (●) (n = 71, 0.19 ± 0.03 μm^3) or glycine (■) (n = 109, 0.24 ± 0.03 μm^3) treated neurons. Mann-Whitney test, P ≤ 0.0001 ****. **H.** Violin plot representing the mean VIAAT cluster intensity per cell. The mean ± SEM values in control (●) (n = 71, 54.7 ± 2.2 a.u.) or glycine (■) (n = 109, 62.7 ± 1.3 a.u.) treated neurons. Mann-Whitney test, P ≤ 0.0001 ****.

4.3 Discussion

In the previous chapter, it was shown that $GABA_A$ receptors can assemble as 'hetero-alpha' pentamers in HEK293 cells. The present chapter focused on investigating the existence of $GABA_A$Rs with two distinct α subunit isoforms, α1 and α2 based on imaging, as well as exploring their functional role in cultured hippocampal neurons. Previous studies identified α1α2-containing $GABA_A$Rs from brain lysates with biochemical approaches and estimated their relative abundances *via* western blotting and radioligand binding techniques (Benke et al., 2004a; del Río et al., 2001a; Duggan et al., 1991; Pöltl et al., 2003). Despite the variability in reported values, there is a consensus that more than half of α1-, α2-, and α3-containing $GABA_A$Rs are α1α1 'homo-alpha'-containing, whereas α1α2 'hetero-alpha'-containing $GABA_A$Rs comprise the minority of all α2-containing receptors (32 – 39 %) (Duggan, Pollard, and Stephenson 1991; D. Benke, Michel, and Mohler 1997; del Río et al. 2001). This is not surprising, given that α1 is the most widely expressed $GABA_A$R subunit in the brain (Hörtnagl et al., 2013; Pirker et al., 2000).

Even though biochemical techniques can be powerful, there are limitations associated with their use, as discussed in the introduction section of this chapter. Here, the aim was to study 'hetero-alpha' $GABA_A$Rs in their native state and use a method that would allow for probing and visualising individual pentameric receptors.

After careful consideration, proximity-based technique – PLA – was chosen in this study.

4.3.1 PLA is a reliable method for studying stoichiometry of $GABA_A$ receptors

As described in ***Section 4.1***, PLA is a powerful method to study proximity of two proteins by utilising epitope-selective antibodies in combination with secondary probe-coupled antibodies that upon hybridisation and amplification cycles give a fluorescent readout. Unlike, other proximity-based assays, such as Forster resonance energy transfer – FRET (Sekar and Periasamy, 2003), bioluminescent resonance energy transfer – BRET (Angers et al., 2000), and protein-fragment complementation assays – PCA (Kerppola, 2006), PLA permits identification of native protein interactions with a similar resolution (17 – 30 nm) (Gomes et al., 2016a; Söderberg et al., 2006; Weibrecht et al., 2010). To our knowledge, it has not been previously applied to study the stoichiometry of ionotropic receptors. Therefore, multiple controls were performed to validate the reliability of PLA.

Firstly, PLA between α1 and α2 $GABA_AR$ subunits was performed in HEK293 cells co-transfected with α1, α2, β2/3, and γ2 subunit cDNAs (***Figure 4.1 A***). Since we previously showed that transfection of such combinations leads to assembly and expression of 'hetero-alpha' $GABA_ARs$ (***Chapter 3***), and that the proximity of the α subunits within a receptor pentamer should be within the PLA resolution limit, we were hopeful of detecting PLA signals with confocal microscopy. Given that we were, indeed, able to detect α1/α2 PLA dots after some optimisation (adjustment of antibody dilutions and incubation times) of the protocol (Gomes et al., 2016b), PLA was perfomed in cultured hippocampal neurons (***Figure 4.1 B***), where we were able to detect a PLA-positive signal between α1 and α2 subunits.

The main potential confound of a PLA signal between two different α $GABA_AR$ subunit isoforms is its origin: the interaction could be occuring between two adjacent α1βγ and α2βγ receptors, rather than between α1 and α2 subunits present in the same pentamer. $GABA_ARs$ are known to cluster at synapses at a very high density – ~ 1250

receptors per μm^2 – (Kasugai et al., 2010; Nusser et al., 1997; Specht et al., 2013), it is therefore plausible that the PLA signal arises due to inter-receptor proximity. To address this possibility, treatment with a microtubule polymerisation inhibitor, nocodazole, was used to disperse synaptic and extrasynaptic $GABA_ARs$, as has been previously shown (Petrini et al., 2004, 2003). Our results indicate that nocodazole treatment successfully declusters α1 and α2 subunits but has no effect on the number of α1/α2 PLA dots (***Figures 4.2 - 4.4***). This weakens the idea of inter-receptor interaction detection, indicating that PLA signals are more likely to arise from subunits within the same $GABA_AR$ pentamer.

Further controls were completed, by performing PLA between γ2 and δ $GABA_AR$ subunits. With conflicting evidence of γ2 subcellular localisation (Bogdanov et al., 2006; Zoltan Nusser et al., 1998; Thomas et al., 2005), it is possible that γ and δ containing receptors can exist in the same subcellular compartment, however their presence in the same pentamer has not been shown and is considered unlikely (Olsen and Sieghart, 2009). The fact that no PLA signals were observed with γ2 and δ antibodies (***Figure 4.5***) further strengthens the reliability of the PLA technique for detecting subunits in close proximity within the same receptor pentamer, rather than in adjacent receptors.

4.3.2 Limitations of proximity ligation assay-based techniques

Even though we performed the controls described above, proximity ligation assays have other potential caveats that will be outlined in this section.

PLA relies on two epitope-specific primary antibodies, both of which must be immunoglobulin G type (IgG) (Söderberg et al., 2006). Furthermore, since we wanted to study cell surface 'hetero-alpha' $GABA_ARs$, the antibodies had to recognise the extracellular domains of receptor subunits. This vastly limits the choice of antibody combinations that could be used for PLA between $GABA_AR$ α subunits. Due to rat $GABA_AR$ α1 and α2 sequence similarities, especially at the N-terminus (UniProt: P62813 and P23576 respectively), only two epitope-specific IgG antibodies with rat

reactivity were found: rabbit anti-$GABA_AR$ α1 (Ab33299) and rabbit anti-$GABA_AR$ α2 (Synaptic Systems, 224-103). Since antibodies for PLA need to be derived from two distinct species for secondary probe specificity, the anti-$GABA_AR$ α2 antibody was conjugated to a PLUS oligonucleotide probe (***Section 2.5.3***). This way we avoided the cross-reactivity of the secondary probes. All the primary antibodies were also tested in transfected HEK293 cells for cross-reactivity, and controls omitting one of the secondary probes were performed, where no PLA signal was observed.

The requirement of dual probe recognition for the signal to occur further accounts for limitations in PLA technique. Both epitopes recognised by individual probes must be available for successful antibody binding and not be obscured by other protein-protein interactions (Koos et al., 2014). In the case with α1 and α2 $GABA_AR$ subunits, both epitopes are located at the beginning of the N-terminus (***Table 2.5***). From available cryo-electron microscopy structures of $GABA_AR$, the stretch of amino acids recognised by the antibodies is located in an α-helix, that sits on top of the NTD (Laverty et al., 2019b; Zhu et al., 2018). Furthermore, no known binding sites for ligands are located at the beginning of NTD. Therefore, it is unlikely that the epitopes are obscured, suggesting that antibodies used for PLA should be able to recognise all the target epitopes.

Another caveat of the PLA method, is its ability to estimate the number of interactions (Gomes et al., 2016b; Koos et al., 2014), i.e. number of α1α2-containing $GABA_A$ receptors. Firstly, PLA signals are very limited between target proteins that are expressed at low levels (Koos et al., 2014). Both α1 and α2 $GABA_AR$ subunits are widely expressed in the brain (Hörtnagl et al., 2013; Pirker et al., 2000). Nevertheless, it is not possible to estimate the number of receptors that contain both α1 and α2 subunit isoforms. The biochemical studies only provide an approximate proportion of these receptors, where the values are given as a proportion of a certain subunit type, rather than the total receptor pool (Benke et al., 2004a; del Río et al., 2001a; Duggan et al., 1991; Pöltl et al., 2003). Additionally, these studies mostly rely on total brain extracts, however different brain regions as well as neuronal cell types express various amounts and combinations of $GABA_AR$ subunits (Bovolin et al., 1992; Killisch et al., 1991; Pirker et al., 2000; Wisden et al., n.d.). Therefore, it is possible that, even

though both α1 and α2 subunits are widely expressed, the 'hetero-alpha' $GABA_AR$ population is minor and is assembled at low levels.

Additionally, given the packing density of $GABA_ARs$ at synapses (Kasugai et al., 2010; Nusser et al., 1997; Specht et al., 2013), it is unlikely that each PLA signal represents a single interaction between α1 and α2 subunits. From the data we obtained with co-localisation assessment between VIAAT and α1α2 PLA, each VIAAT cluster had a maximum of two PLA dots co-localising with it. This could be explained by the fact that PLA signals are clustered so closely together, that they are seen as one, rather than multiple dots. Another possible explanation for this could be that the probes from one receptor obscure the binding of the probes to the adjacent $GABA_AR$.

4.3.3 Expression of synaptic 'hetero-alpha' α1α2-containing $GABA_A$ receptors: assembly, subcellular localisation and functional signatures

Here we show that α1α2-containing $GABA_A$ receptors exist in cultured hippocampal neurons, only 20 % of which are synaptic (***Figure 4.6***). Therefore, the majority of α1α2-receptors localise extrasynaptically. Freeze-fracture replica immunolabelling showed that between 33 % to 48 % of α1 subunits and 40 % of α2 subunits localise extrasynaptically (Kasugai et al., 2010). Even though Kasugai et al., were not assessing 'hetero-alpha' $GABA_ARs$, their data correlate with our results with PLA / VIAAT co-localisation studies. As mentioned previously, at the age of the neurons used here (DIV 11-14), the colocalisation of VIAAT with $GABA_AR$ γ2 subunit is between 96.6 ± 0.8 % and 99.3 ± 0.4 %, suggesting that VIAAT is a reliable synaptic marker (Danglot et al., 2003; Sagné et al., 1997).

One of the most interesting results in this chapter, is that upon α2 subunit overexpression, the number of α1α2 PLA increases by ~ 75 %, whereas no changes are observed with α1 overexpression (***Figure 4.6***). This could imply that the α2 subunit availability is a limiting factor for 'hetero-alpha' receptor assembly or trafficking. Given that $GABA_AR$ have specific subunit 'assembly boxes' that are important for correct assembly, specifically α1 H109, that is thought to 'lock' two α

subunits initiating regulated assembly of $GABA_AR$ (Sarto-Jackson and Sieghart, 2008), it is possible that the α2 subunit plays a crucial role at dictating the assembly of 'hetero-alpha' $GABA_ARs$. To investigate this idea would involve systematically mutating amino acid residues around the H109 residue on α2 subunit and assessing their effect on 'hetero-alpha' expression.

We also found that upon overexpression of α2 subunit, PLA dots preferentially co-localise with VIAAT. More than 60 % of VIAAT clusters were PLA-positive with α2 overexpression, compared with ~ 20 % in control-transfected neurons (***Figure 4.6***). Since the overall number of α1α2-containing $GABA_ARs$ increases with α2 subunit overexpression (***Figure 4.6***), it is possible that newly assembled 'hetero-alpha' $GABA_ARs$ preferentially localise at synaptic junctions. Nevertheless, with PLA we only assessed α1α2-containing $GABA_AR$ and not α1α1- and α2α2-containing receptors, thereby we cannot speculate on the changes in expression and localisation of 'homo-alpha' receptors.

Previous electrophysiological studies using fast agonist application in transfected HEK293 cells showed that α1- and α2-containing $GABA_A$ receptors show similar activation and deactivation kinetics, with the α2 subunit-containing receptors having slightly slower overall kinetic parameters than α1-containing (Lavoie et al., 1997; McClellan and Twyman, 1999; Picton and Fisher, 2007). Nevertheless, our sIPSC analysis here revealed no significant changes in rise times and weighted decay taus between eGFP, α1 and α2 transfected neurons (***Figure 4.7***). Given that our PLA data indicates that the number of synaptic 'hetero-alpha' α1α2-containing $GABA_A$ receptors increases (***Figure 4.6***) and the faster component from a two-exponential fit to the sIPSC decay (tau1) was significantly faster in α2, compared to α1-transfected neurons, we could speculate that 'hetero-alpha' α1α2-containing $GABA_ARs$ exhibit faster desensitisation than 'homo-alpha' α2α2 $GABA_ARs$. Therefore, it could be possible that the physiological role of 'hetero-alpha' $GABA_A$ receptors could be the fine-tuning of inhibitory synaptic transmission, rather than causing macroscopic changes.

4.3.4 Effects of long-term potentiation on 'hetero-alpha' $GABA_A$ expression

Our last aim was to assess the LTP effects on the α1α2-containing $GABA_A$ receptor expression. LTP was primarily used as a physiological mechanism that regulates the number of receptors at synapses and thus could also regulate the expression of 'hetero-alpha' $GABA_A$Rs at synapses. We first used an NMDAR activation-based iLTP protocol (Marsden et al., 2007) and tried to electrophysiologically confirm iLTP induction by monitoring effects on sIPSC frequency and amplitude. Previous studies, where inhibitory postsynaptic plasticity was assessed, reported increased levels of α1, α2, and β3 $GABA_A$R subunits post iLTP induction with various protocols (Bannai et al., 2020; Battaglia et al., 2018; Petrini et al., 2014). Nevertheless, we did not see any changes in sIPSC amplitude (***Figure 4.8***), suggesting that the number of $GABA_A$R at post-synaptic membranes did not change.

There are many protocols that have been shown to induce iLTP in cultured hippocampal neurons, but most of them are based on Ca^{2+} influx upon activation of NMDAR receptors, which in turn induces translocation of Ca^{2+}/calmodulin-dependent protein kinase II – CaMKII – to inhibitory synapses, leading to an enhancement of $GABA_A$R clusters (Kittler and Moss 2003; Kittler et al. 2000; Sumi and Harada 2020; Lu et al. 2001; Molnár 2011). However, the effects of the same iLTP protocol can vary between groups, and are thought to depend on the amount and duration of Ca^{2+} influx (Castillo et al., 2011; Muir et al., 2010). This precise Ca^{2+} influx could well be the reason why we did not observe any changes upon iLTP induction to sIPSCs. Additionally, another explanation could be the difference in age of cultured hippocampal neurons as well as variability of experimental procedures.

Our data with the glycine protocol previously established as a way of evoking excitatory LTP, suggests that this paradigm is also an iLTP protocol, since both the amplitude and frequency of sIPSCs increase (***Figure 4.9***). The amplitude increase is correlated with the increased postsynaptic recruitment of $GABA_A$Rs, whereas the increase in frequency is attributed to an increase in presynaptic vesicular GABA release (Castillo et al., 2011; Gaiarsa et al., 2002). It is common that LTP protocols that induce plasticity at excitatory synapses simultaneously prompt changes at

inhibitory synapses (see Castillo at al., 2011 for review). However, the aim of this experiment was not to understand the molecular mechanisms of long-term potentiation on $GABA_AR$ clustering, but rather to use the protocol to explore the potential effects of an important physiological process on 'hetero-alpha' $GABA_AR$ expression.

Performing PLA between α1 and α2 subunit specific antibodies upon glycine LTP induction showed a ~ 50 % increase in PLA signal compared to control-treated neurons (***Figure 4.10***). Furthermore, colocalization between VIAAT and PLA dots showed a 50 – 70 % increase. Since we observed an overall increase in α1α2-containing $GABA_A$ receptors on the cell surface, this is likely to be attributed to either increased *de novo* receptor synthesis or possibly an increased membrane trafficking of the α1α2-containing receptors that are already present in secretory pathways (Arancibia-Cárcamo and Kittler, 2009). This is consistent with other iLTP protocols, where an increased $GABA_AR$ surface expression is observed (Bannai et al., 2020; Battaglia et al., 2018; Petrini et al., 2014). Upregulated $GABA_AR$ cell surface expression in turn leads to an increase of $GABA_ARs$ at synapses via increased trapping by gephyrin and other mechanisms (Petrini et al., 2014, 2004). Therefore, our data showing an increased overall α1α2 PLA overall and synaptic dot number as well as sIPSC amplitude increase, are likely to correlate with the increased postsynaptic clustering of $GABA_ARs$, as for other iLTP paradigms (Bannai et al., 2020; Battaglia et al., 2018; Petrini et al., 2014).

Nevertheless, with PLA protocol we are only able to identify interactions within the α1α2-containg receptors, and not α1α1- or α2α2-containing. Hence, we are unable to note the plasticity changes to the total α1 and α2 $GABA_AR$ receptor pool due to the limitations of the technique. In the next chapter, we will, therefore, use a method that accurately estimates the number of receptors as well as their α subunit compositions.

Taken together, another approach is needed that will directly quantify the ratio of 'hetero-alpha' to 'homo-alpha' $GABA_ARs$. As such, the next chapter will present an alternative method – spatial intensity distribution analysis, SpIDA – that can determine the quaternary structure of a single receptor *in situ*.

4.4 Conclusions

1. The proximity ligation assay is a method to study the stoichiometry of 'hetero-alpha' $GABA_A$ receptors. Nocodazole treatment successfully dispersed α1- and α2-containing $GABA_A$Rs but had no effect on the number of α1α2 PLA dots. Furthermore, analysis of PLA between γ2 and δ subunits showed no PLA signal, further validating the method.

2. 'Hetero-alpha' α1α2-$GABA_A$Rs are present in pyramidal cultured neurons, and the majority of these (~ 80 %) are localised extrasynaptically.

3. Overexpression of α2, but not the α1 subunit leads to a ~ 75 % increase in the α1α2 PLA signal. This suggests that α2 subunit synthesis is a limiting factor for α1α2-containg $GABA_A$ receptors. As such, the α2 subunit could play a key role in the assembly of 'hetero-alpha' $GABA_A$ receptors.

4. The percentage co-localisation of α1α2 PLA dots and VIAAT significantly increases upon α2 subunit overexpression, suggesting that if 'hetero-alpha' $GABA_A$R are assembled *de novo*, their preferential localisation is synaptic.

5. Glycine-induced excitatory long-term potentiation protocol has a long-lasting modulatory effect on both sIPSC frequency and amplitude, suggesting this method is also an iLTP protocol.

6. Upon glycine-LTP induction, the number of α1α2 PLA dots exhibit a ~ 50 % increase, compared to control treated neurons, suggesting increased expression of cell-surface 'hetero-alpha' $GABA_A$ receptors. Post-LTP, there is also an increase in 'hetero-alpha' $GABA_A$Rs at inhibitory synapses as indicated by an increase in the colocalisation between α1α2 PLA dots and VIAAT clusters and sIPSC amplitude.

Chapter 5: Exploring synaptic $GABA_AR$ composition changes post long-term potentiation induction

5.1 Introduction

In the previous chapter we assessed the presence and the changes occurring post-LTP induction of 'hetero-alpha' α1α2-containing $GABA_A$ receptors in cultured hippocampal neurons. The proximity ligation assay-based method (PLA) was used to achieve this aim. As mentioned previously, the PLA technique allows the fluorescent visualisation of α1 and α2 $GABA_AR$ subunits in the same receptor pentamer, only if both subunits are in close proximity of <30 nm. However due to its limitations (see ***Chapter 4 Discussion section***), it does not accurately estimate the number of α1α2-containing $GABA_ARs$. Furthermore, PLA does not provide any information about the 'homo-alpha' α1α1- or α2α2-containing $GABA_AR$ populations, i.e., their presence and numbers.

To increase the precision of our imaging techniques, we used spatial intensity distribution analysis (SpIDA) – a method that measures protein oligomerisation states (related to subunit counts) and receptor density from individual fluorescence confocal images (Barbeau et al., 2013c). This approach was previously used to study oligomerisation states of cell membrane epidermal factor receptors (EGFRs), serotonin 5-hydroxytryptamine 2C (5-HT2C), $GABA_A$ and $GABA_B$ receptors (Barbeau et al., 2013a, 2013b; Bouvier, 2001; Lorenzo et al., 2020; Sergeev et al., 2012a, 2012b; Ward et al., 2015).

5.1.1 Principle behind spatial intensity distribution analysis

SpIDA is based on fluorescence intensity histogram compilations that permit the calculation of the total number of pixels and their intensities from 12 bit images obtained through a confocal laser-scanning microscope (CLSM) equipped with an analogue photomultiplier tube (PMT) detector (Barbeau et al., 2013c, 2013b). The analysis relies on differentiating oligomerisation states of fluorescently labelled

proteins, not through direct visualisation, but through the intensity of brightness that the oligomer emits. As the fluorescent dimer emits twice as many photons as the monomer (assuming there is no quenching of the fluorophore), the quantal brightness, QB, of the former would have twice the fluorescent intensity of the latter (Godin et al., 2010, 2011).

A sample (live or fixed) is labelled with epitope-specific antibodies *via* conventional immunocytochemistry protocols (***Section 2.5.1***). The cells are then imaged with confocal microscopy at predetermined constant parameters to minimise photobleaching and optimise optical saturation (Humpolickova et al., 2009) (***Section 5.2.1***). For SpIDA analysis, pixel intensity histograms are produced for selected regions of interest (ROIs (Barbeau et al., 2013a). The analysis relies upon fitting the intensity histograms with a function derived from the expected emission intensity for a population of particles containing various numbers of fluorescent monomers, dimers and higher order oligomers. The fluorescence intensity contributed by each possible oligomeric state is weighted by their spatial probability using a Poisson distribution (Barbeau et al., 2013a; Sergeev et al., 2012a). If the quantal brightness of the monomeric fluorophore is known, then this analysis can quantify the numbers of monomers or dimers contained within the population (Barbeau et al., 2013a; Sergeev et al., 2012a).

The generalised intensity histogram for an infinite number of particles, *N*, excited inside the beam area of the laser and randomly distributed in space, assuming a Poisson (Poi) distribution, can be described by the function below:

$$H(\varepsilon, N; k) = \sum_{n} \rho^{n}(\varepsilon; k) \cdot Poi(n, N),$$

Where ε is the quantal brightness measured as arbitrary intensity units, i.u., per pixel integrated over a specified time unit; *N* – fluorescent particle density per laser beam area; ρ – probability of observing light intensity, *k*, (assuming it is proportional to the number of emitted photons). The Poisson histogram fitting, *H*, is determined from all the plausible distributions of particles (n) of fluorescence intensities in a defined volume, characterised by the point spread function (PSF) (see ***Section 5.2.1). Figure***

5.1 A schematically illustrates the principle behind the probability distribution, ρ, in the laser beam area.

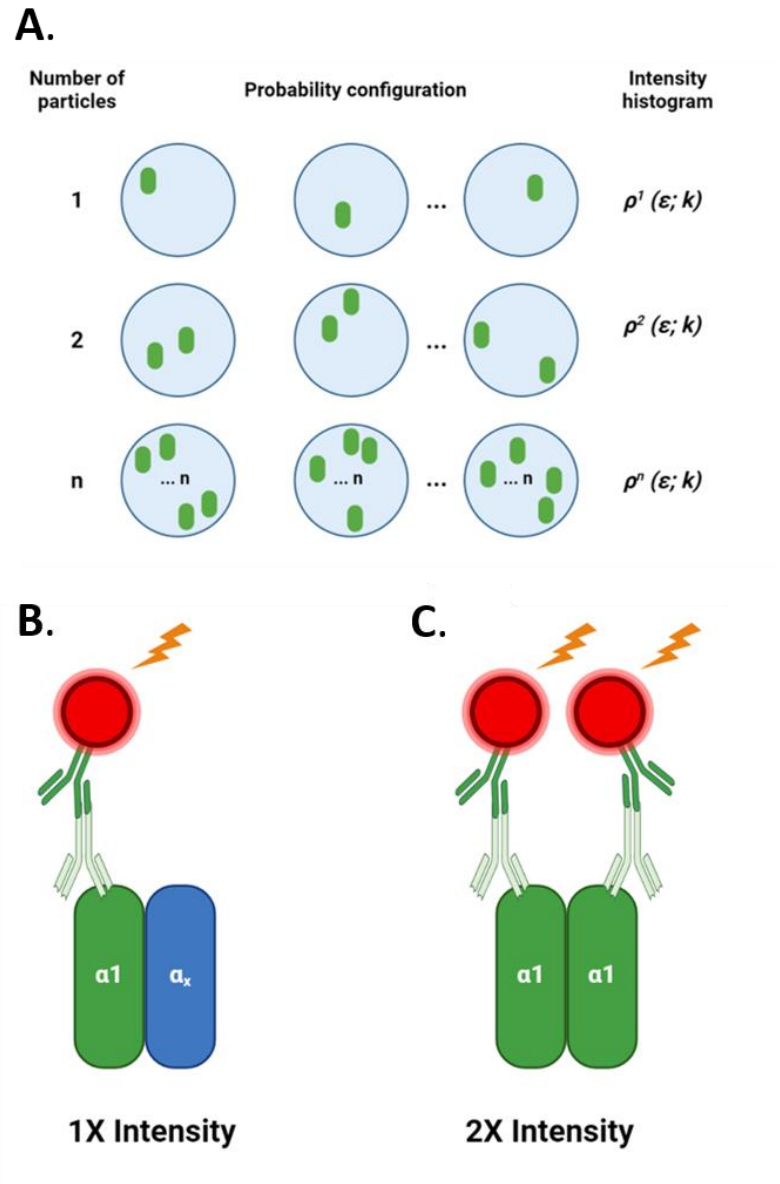

Figure 5.1 Basis of spatial intensity distribution analysis. **A.** Schematic representation showing how intensity histogram for 1, 2, … *n* number of particles (green oval) in a defined laser illumination area (light blue circle) is modelled. Each configuration shown consists of a number of particles emitting photons, to generate an intensity characterised by the quantal brightness, ε, of the monomeric fluorophore. Resulting pixel intensity histograms are associated with all possible configurations containing 1, 2, … *n* particles: ρ^n *(ε; k).* **B and C.** Cartoon representations of fluorescence intensity scenarios in $GABA_AR$s pentamers immuno-labelled for α1 subunit. The α1 monomeric forms – 'hetero-alpha' $\alpha1\alpha_x$-containing $GABA_AR$s (**B**) will emit half as many photons as the α1 dimers – 'homo-alpha' α1α1-containing $GABA_AR$s (**C**). This means that the latter (**C**) will manifest a QB twice as high as the former (**B**).

5.1.2 SpIDA as a functional tool to study the oligomerisation state of native $GABA_ARs$

The advantage of SpIDA is its ability to extrapolate data from single images taken by confocal laser-scanning microscopy, providing information on fluorescent particles in the spatial domain. As mentioned above, it is a useful tool to establish the oligomerisation state of receptor complexes (Barbeau et al., 2013a, 2013b; Bouvier, 2001; Lorenzo et al., 2020; Sergeev et al., 2012a, 2012b; Ward et al., 2015). It can, therefore, be used as a powerful method to identify the oligomerisation states of $GABA_A$ receptors in relation to the nature of their α subunits.

In order to do so, we first established the QB of a monomeric population: γ2 subunit immuno-labelling was used, as synaptic $GABA_ARs$ contain a single copy of this subunit (Farrar et al., 1999; Laverty et al., 2017; Masiulis et al., 2019a; Tretter et al., 1997). Then independent labelling of either α1 or α2 subunits was performed. From our previous results (***Chapters 3 and 4***) we have shown that $GABA_ARs$ are expressed as mixtures of α1α1-, α1α2-, and α2α2-subunit containing receptors. In this case, our predictions suggest that the Poisson distribution fitting with SpIDA for a one-population model would yield an intermediate value of QB (between ε and 2ε), compared to just ε for γ2 data fitting. This suggests that a higher order model must be used for the analysis. As such, a two-population model (monomer and dimer) was used to fit the data obtained from our images. The analysis was kindly performed by Dr. Antoine Godin from Laval university, Quebec.

Here, we estimated the density and QB of fluorescently labelled native α1 or α2 $GABA_A$ receptor subunits in cultured hippocampal neurons. The stoichiometry of a synaptic $GABA_AR$ is 2 α: 2 β: 1 γ (Farrar et al., 1999; Olsen and Sieghart, 2009; Tretter et al., 1997). Therefore, with fluorescent labelling of the α1 subunit, CSLM will only detect fluorescent particles in a pentameric receptor complex. The Poisson distribution fit with SpIDA will therefore fit two components: $GABA_ARs$ with one fluorescent protein – monomeric form of α1-containing receptors ('hetero-alpha' α1-containing receptors), and $GABA_ARs$ with two fluorescent proteins - dimeric forms of α1-containing receptors – 'homo-alpha' α1α1-containing population (***Figure 5.1 B***).

In this chapter, the aim was to identify the oligomerisation states (related to subunit counts) of native $GABA_ARs$ and establish changes in $GABA_AR$ stoichiometry upon chemical LTP induction (see ***Section 4.2.7***). We have used gephyrin staining alongside $GABA_AR$ subunit labelling as a binary mask, which allowed for synaptic receptor analysis (Lorenzo et al., 2020).

5.2 Results

5.2.1 Parameter calibration: analogue detector and point spread function (PSF) measurements

5.2.1.1 Analogue detector calibration

To reliably use SpIDA for probing the oligomerisation state of $GABA_ARs$, the acquisition parameters for CLSM must be calibrated. One of the most important factors to consider for any quantitative fluorescence-based analysis method are the sources of noise (Godin et al., 2011; Wiseman et al., 2012; Zhao et al., 2003; Zimmer, 2002). There are different types of noise associated with fluorescence-based confocal imaging: dark noise (the minimum background fluorescence when the detector is not illuminated), white noise (frequency independent continuous noise), background noise (consisting of autofluorescence of the sample and non-specific background, arising from fluorescent probes that are not bound to the epitope of interest), and detector noise (Barbeau et al., 2013a). The dark and white noise produce relatively constant signals whilst imagining, and the variance of the signal is negligible, thus they are not taken into account during the analysis. Autofluorescence and non-specific background noise can be subtracted from the analysis by performing necessary controls, such as sequentially omitting primary/secondary antibodies during immuno-labelling protocols (see ***Methods Section 2.5.1***).

The major source of noise during CLSM imaging is the noise of the detector also known as shot noise (Godin et al., 2011). This arises due to the fluctuations that originate from photon counters (that detect and record photons) and photomultiplier

tubes. The PMTs are immensely sensitive photocathode light detectors, that amplify the signal (Unruh and Gratton, 2008). This noise is inherent within the detector and follows a Gaussian distribution (Barbeau et al., 2013a). Specifically, PMTs broaden the signal due to the detector's current amplification steps (Godin et al., 2010). As SpIDA measures fluctuation fluorescence intensity of a sample to determine protein oligomerisation states from the QB values, it is essential to distinguish fluctuations that arise from the fluorescently labelled proteins from fluctuations arising from the detector (Barbeau et al., 2013c).

The variance in the signal arising from an analogue PMT detector can be measured for a given voltage value through either reflection of the laser from a mirror or a homogeneously bright fluorescent sample. Since all the samples (labelled $GABA_AR$ subunits) were excited using the 488 nm line of the Argon laser, the detector calibration was performed using this line. As described in ***Section 2.5.5,*** the analogue detector intrinsic noise was established by systematically spot scanning chroma-slides (that emit a uniform fluorescent signal) at increasing dwell times and detector gain voltages. Example images of spot scanning mode, at a detector gain of 500 V, scan speed 7, dwell time 3.84 µs/pixel, 0 % to 90% detector output, are shown ***in Figure 5.2 A***. The resulting signal variance of the 488 nm line was plotted as a function of the mean laser intensity.

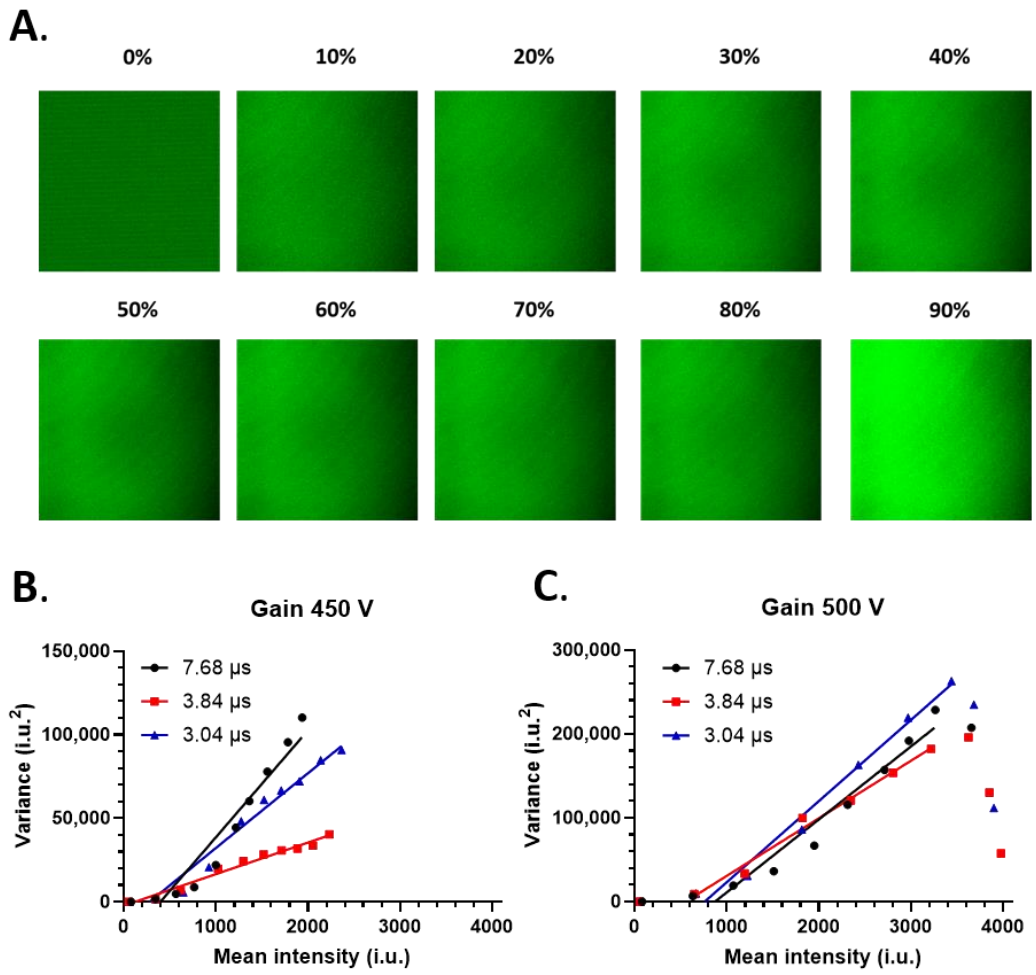

***Figure 5.2 Analogue detector calibration procedure*. A.** Example images from spot scanning mode of the Zeiss LSM510 confocal microscope using Plan-APOCHROMAT 63X/1.4NA oil DIC objective lenses. Detector gain 500 V, amplifier offset 0, scan speed 7, dwell time 3.84 µs/pixel. The values on top of the images represent the percentage detector output. Noise calibration of the PMT at detector gain 450 V (**B**) and 500 V (**C**) in the Zeiss LSM510 confocal microscope. **B.** The variances for each mean intensity signal at 450 V detector gain were collected. A linear regression was fitted to mean intensity, $\mu < 2500$ i.u., scan speed 6, dwell time 7.68 µs (●): $y_{7.68\,\mu s} = 64.01x - 25335$, $R^2 = 0.92$; scan speed 7, dwell time 3.84 µs (■): $y_{3.84\,\mu s} = 18.87x - 2227$, $R^2 = 0.98$; scan speed 8, dwell time 3.04 µs (▲): $y_{3.04\,\mu s} = 44.70x - 12420$, $R^2 = 0.97$. **C.** The variance of each mean intensity signal at 500 V detector gain were collected. A linear regression was fitted to mean intensity, $\mu < 3300$ i.u., scan speed 6, dwell time 7.68 µs (●): $y_{7.68\,\mu s} = 86.94x - 75786$, $R^2 = 0.95$; scan speed 7, dwell time 3.84 µs (■): $y_{3.84\,\mu s} = 68.59x - 37751$, $R^2 = 0.99$; scan speed 8, dwell time 3.04 µs (▲): $y_{3.04\,\mu s} = 96.69x - 73422$, $R^2 = 0.98$. The fall-off in signal variance beyond mean intensity 3300 iu was due to an increased number of saturated pixels in a scanned image, resulting in a decreased variance.

The slopes of the linear part of the curves were determined by linear regression fitting (***Figure 5.2 B***). The linear part of the curves defines the limit of the maximal intensity that can be used with SpIDA software. From our results, we concluded that the variance at 450 V detector gain was linear over the whole mean intensity range (i.u.) for all three dwell times tested (***Figure 5.2 B***). However, the recorded mean intensity for such parameters did not engage the whole theoretical range (12-bit image, the intensity range should be between 0 and 4096 i.u.). As such, we recorded the variance of the PMT at a higher detector gain – 500 V, keeping other parameters constant (tube current, amplifier gain and detector offset). Detector calibration procedure was performed for the same scan speeds (6, 7, and 8), as shown in ***Figure 5.2 C***. We concluded, that the PMT response stays linear between intensity range, $0 < \mu < 3300$ i.u. The slopes of the linear regression were extrapolated from the data ($m_{7.68\ \mu s}$ = 84.94, $m_{3.84\ \mu s}$ = 68.59, $m_{3.04\ \mu s}$ = 96.69) and used in the SpIDA software by Dr. Antoine Godin to allow the detector noise to be accounted for. The final CLSM parameters for imaging were optimised to minimise pixel saturation and fluorophore photobleaching. Thus, these parameters are set within the linear range of the detector and are outlined in ***Table 5.1***. These were kept constant throughout the course of the experimental procedure.

Table 5.1 Parameters chosen for SpIDA post detector calibration. Imaging was undertaken with the Zeiss LSM510 confocal microscope equipped with 63X/1.4NA oil DIC objective lenses. The listed parameters were selected for the 488 nm line of the Argon laser.

Parameter identity	Value
Data depth	12 bits
Data resolution	1024 x 1024 pixels
Pinhole	1.0 Airy unit
Scan speed	7
Dwell time	3.84 µs/pixel
Tube current	6.3 A
Laser intensity	10 %
Detector gain	600 V
Detector offset	0
Amplifier gain	1

5.2.1.2 Point spread function

Next, measurements of the laser beam waist area were performed. This was done through generation of the point spread function report, PSF, which allowed us to estimate the laser beam radius, and hence convert it to metric units (μm^2). ***Figure 5.3 A*** shows a diagram of the cone of illumination narrowing, with a three-dimensional laser beam waist at the focal plane. The laser beam waist radius of the 488 nm line of the multi Argon laser was estimated by z-stack imaging of 100 nm diameter fluorescent beads (***Section 2.5.6***) to quantify the beam waist *x*, *y*, and *z* values. The PSF report generated *x, y,* and *z* radii parameters of 0.179 µm, 0.135 µm, and 0.266 µm respectively. Assuming the area of the beam waist at the xy-plane is circular, the area calculation was performed with the formula:

$$A = \pi r^2,$$

Where A is the area of a circle, *r* – radius of the circle, which is the average of the *x* and *y* PSF reported values. The waist beam area was calculated to be 0.1005 μm^2. This value is in agreement with the previously reported value on the same lens (Plan-APOCHROMAT 63X/1.4NA oil DIC objective lens) with a 488 nm laser line (Ward et al., 2015), and was used to convert monomeric and dimeric α1/α2-labelled $GABA_AR$ numbers per laser beam to receptor numbers per gephyrin cluster.

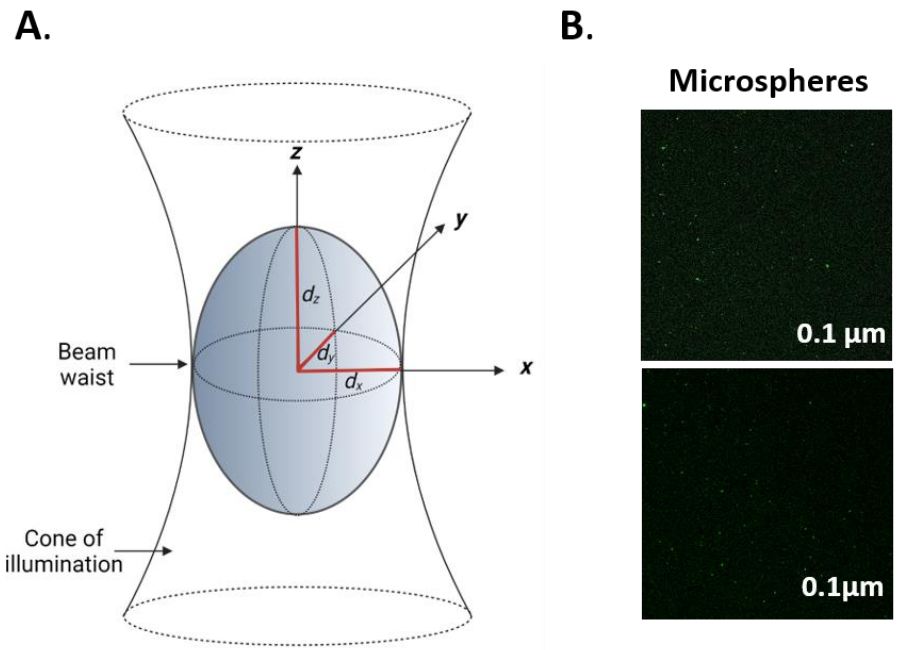

Figure 5.3 Measuring the laser beam waist area. **A.** Diagrammatic representation of the laser beam narrowing, with the beam waist located at the focal plane. PSF report generates the *x*, *y*, and *z* values, from which the beam waist area in different planes can be calculated. **B.** Example z-stack maximal projections of fluorescent microspheres used to generate the PSF report with MetroloJ plugin in Image J software.

Here, we optimised the detector PMT parameters on the 488 nm Argon laser line for SpIDA imaging and analysis. These were specifically chosen to minimise pixel saturation, fluorophore photobleaching whilst enabling the subtraction of PMT noise from the fluorescent signal. We also calculated the waist beam area that will be used to calculate the number of monomers and dimers of α1, α2 $GABA_AR$ subunits within gephyrin clusters.

5.2.2 Mean intensity of α1 and α2 $GABA_AR$ subunit labelling significantly increases post LTP induction

In the previous chapter we showed that a glycine-induced LTP protocol (Molnár, 2011) significantly increases the amplitude of sIPSCs, suggesting an increase in $GABA_AR$ numbers at synapses (***Figure 4.9***). Our results also indicate a significant increase in the proximity of α1/α2 subunit $GABA_ARs$ post glycine treatment (***Figure 4.10***), likely to be due to an upregulated expression of 'hetero-alpha' α1α2-containing receptors on postsynaptic membranes. As discussed previously, the fact that an increase in the number of α1α2 PLA spots is observed, does not necessarily mean that the proportion of 'hetero-alpha' $GABA_ARs$ changes, compared to the total receptor pool. Furthermore, the PLA method is unable to quantify the plasticity changes to 'homo-alpha' α1α1- and α2α2-receptor populations induced post LTP. Therefore, we used SpIDA methodology to accurately estimate changes in $GABA_AR$ number and oligomerisation states.

To achieve this aim, DIV11-14 cultured hippocampal neurons were control or glycine treated as previously described (see ***Section 4.2.7*** for detail). The neurons were then fixed and cell surface α1, α2, or both α1 and α2 $GABA_AR$ subunits were probed with external epitope selective antibodies (see ***Table 2.5***). Neurons were subsequently permeabilised and immunolabelled for gephyrin and MAP2. Gephyrin was used as a marker for inhibitory synapses, as it has been previously used as a binary mask in SpIDA (Lorenzo et al., 2020; Niwa et al., 2012), whereas MAP2 was used to label neuronal somas and dendrites. MAP2 labelling was also used to identify selected regions of interest (***Figure 5.4***). We used Alexa Fluor® 488 secondary antibodies to label anti-α1 and anti-α2 primary antibodies. Alexa Fluor® 555 was used as a secondary for gephyrin and Alexa Fluor® 647 for MAP2. Since we are measuring the number and oligomerisation states of $GABA_ARs$, we used the Alexa Fluor® 488 antibodies as the primary fluorescent signal since they are excited by the 488 nm-line of the multi Argon laser – the parameters of which were calibrated as described in ***Section 5.2.1***.

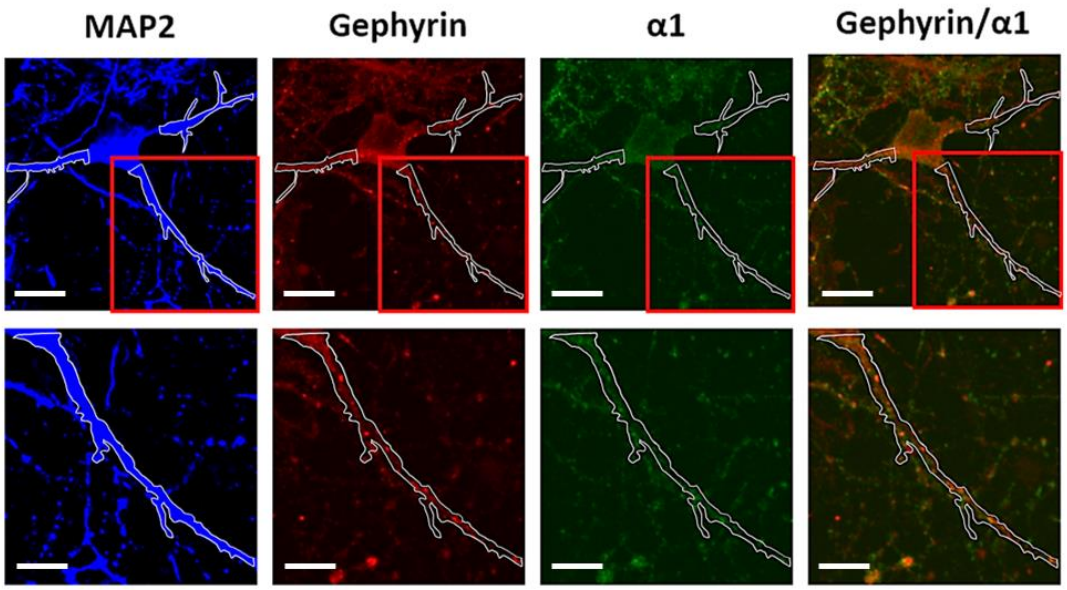

Figure 5.4 Regions of interest selected for spatial intensity distribution analysis. Example confocal image of MAP2 (blue), gephyrin (red) and $GABA_AR$ α1 subunit (green) in control treated cultured hippocampal neurons. 12-bit 1024 x 1024 px images were taken with the calibrated parameters applied to the 488 nm line of the multi Argon laser (see ***Table 5.1***). Regions of interest were selected by drawing an outline of the MAP2 staining (white outline). SpIDA of α1 subunit was performed only within the gephyrin clusters. Scale bar – bottom left corner – 30 µm (overview) and 15 µm (zoomed inserts).

It is important to note that alongside α1 or α2 subunit labelling, we used a control – labelling neuronal cell surface $GABA_ARs$ for both subunits (using the same species primary antibodies), followed by a labelling with the fluorophore-tagged secondary antibody – Alexa Fluor® 488. Theoretically, the arithmetic sum of values obtained for α1 or α2 labelling (mean intensity, receptor number and subunit number) – should equate to the value obtained for α1 + α2 labelling.

Firstly, we assessed the mean intensity of α1, α2, and α1 + α2 $GABA_AR$ subunit labelling in regions of interest selected through MAP2 staining (***Figure 5.4***). Our data indicate that α1 mean intensity increased by 22.5 % ($P \leq 0.05$) – from 37.4 ± 1.9 i.u. in control treated compared to 45.8 ± 2.5 i.u. in LTP-induced cultured hippocampal neurons (***Figure 5.5 A***). Furthermore, the mean intensity of α2 subunit immunolabelling exhibited a 35.2 % (P value ≤ 0.0001) increase post iLTP, from 85.4 ± 2.6 i.u. to 115.7 ± 4.5 i.u. (***Figure 5.5 B***). These findings suggest that the cell surface expression of α1- and α2- containing receptors increase after iLTP induction,

consistent with previous findings regarding plastic changes induced with other iLTP protocols – i.e., increased $GABA_AR$ surface expression (Bannai et al., 2020; Battaglia et al., 2018; Petrini et al., 2014).

Additionally, the arithmetic sum of α1 and α2 mean intensities was close to the mean intensity value of α1 + α2 immunolabelling in both control treated (α1 and α2 sum: 122.8 i.u compared to α1 + α2: 161.6 ± 5.0 i.u.) and LTP-induced (α1 and α2 sum: 161.5 compared to α1 + α2: 181.6 ± 7.9 i.u.) (***Figure 5.5 D and E***). This was predicted given that the secondary antibody used (goat anti-rabbit Alexa Fluor® 488) recognises both rabbit anti-α1 and rabbit anti-α2 subunit antibodies.

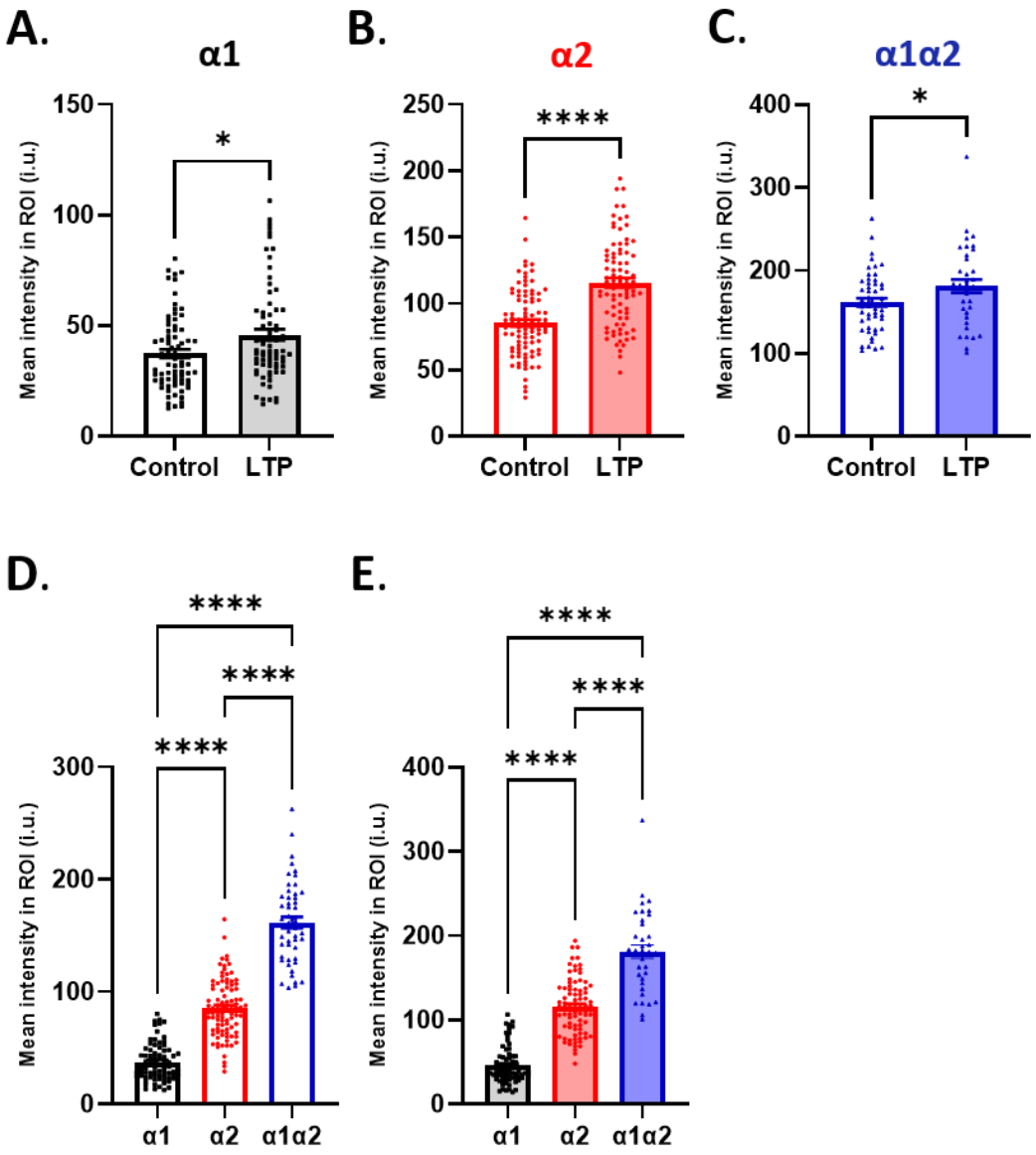

Figure 5.5 Mean intensity of GABA$_A$R labelling increases post iLTP induction in cultured hippocampal neurons. **A.** The mean intensity in regions of interest (ROIs) of cell surface α1 GABA$_A$R subunit labelling of control (n = 76, 37.4 ± 1.9 i.u.) and iLTP (n = 73, 45.8 ± 2.5 i.u.) treated cultured hippocampal neurons. Mann-Whitney test, P value ≤ 0.05 *. **B.** Bar chart representing the mean intensity in ROIs of cell surface α2 GABA$_A$R subunit labelling of control (n = 94, 85.4 ± 2.6 i.u.) and post iLTP (n = 86, 115.7 ± 4.5 i.u.) cultured hippocampal neurons. Unpaired t-test, P ≤ 0.0001 ****. **C.** The mean intensity in ROIs of cell surface α1α2 GABA$_A$R subunit labelling of control (n = 51, 161.6 ± 5.0 i.u.) and after iLTP (n = 37, 181.6 ± 7.9 i.u.) neurons. Unpaired t-test, P value ≤ 0.05 *. **D and E**. The mean intensity in ROIs of α1, α2, and α1α2 cell surface labelling in control treated (**D**) or iLTP induced (**E**) neurons. Data point are the same as in **A-C**. For both **D and E** – Kruskal-Wallis test with Tukey's post hoc test, P value ≤ 0.001 ***, ≤ 0.0001 ****. Values are for bar charts are given as mean ± SEM with single data points representing a cell in this and proceeding figures.

5.2.3 Effects of the iLTP induction on α1 $GABA_A$Rs oligomerisation states

To assess changes in $GABA_A$R stoichiometry after iLTP induction, SpIDA was applied to α1 (this section), α2 (***Section 5.2.4***), and α1 + α2 (***Section 5.2.5***) subunit staining in selected ROIs within gephyrin clusters. The SpIDA method provides information about the oligomerisation state of a single $GABA_A$R. For example, a 'homo-alpha' α1α1-containing $GABA_A$R would be registered as a dimer, whereas a 'hetero-alpha' α1-contianing receptor would be registered as a monomer. For the latter state, the identity of the second α subunit is unknown.

The analysis of the α1 staining in control-treated cultured hippocampal neurons revealed that the majority of α1-containing $GABA_A$Rs are present as monomers - 32.6 ± 3.8 which corresponds to 79.5 ± 3.2 % of the total α1-subunit receptor pool (***Figure 5.6 A and B***). Interestingly, the number of α1 subunit monomers significantly decreases post iLTP, from 32.6 ± 3.8 to 23.2 ± 2.2 ($P \leq 0.05$) in control and iLTP neurons respectively. Nevertheless, no significant differences were observed between the number of α1 dimers: 5.7 ± 1.7 in control treated and 10.2 ± 1.6 after iLTP ($P \geq 0.05$).

Furthermore, the total number of receptors (sum of α1 monomers and dimers), revealed that the number of all α1-containing receptors is 41.2 ± 3.1 per gephyrin cluster (***Figure 5.6 C***). This value is consistent with previously reported values, where the number of $GABA_A$Rs within the gephyrin cluster is estimated between tens to a few hundred (Kasugai et al., 2010; Nusser et al., 1997). The number of receptors also corresponds to whole-cell voltage-clamp sIPSC recordings of control treated neurons (-67.1 ± 7.0 pA) shown in the previous chapter (***Figure 4.9***). Given that a mean current amplitude of a single αβγ-containing $GABA_A$R was previously reported as 2.16 ± 0.29 pA, a value that would also apply to our α1-containing $GABA_A$Rs (Nusser et al., 1997). From our sIPSC data, we can estimate the number of receptors at an inhibitory synapse to be between 30 and 40 receptors, in agreement with α1-containing receptor numbers observed with SpIDA.

Surprisingly, no change was observed in the total α1-containing $GABA_A$ receptor number post iLTP induction (***Figure 5.6 C***). The total number of α1 subunits (one per

monomer and two per dimer) was calculated to be 52.9 ± 5.1 for control and 48.9 ± 2.9 for iLTP expressing neurons (***Figure 5.6 D***). Taken overall, the α1 receptor dimers form a small proportion of the total a1 population.

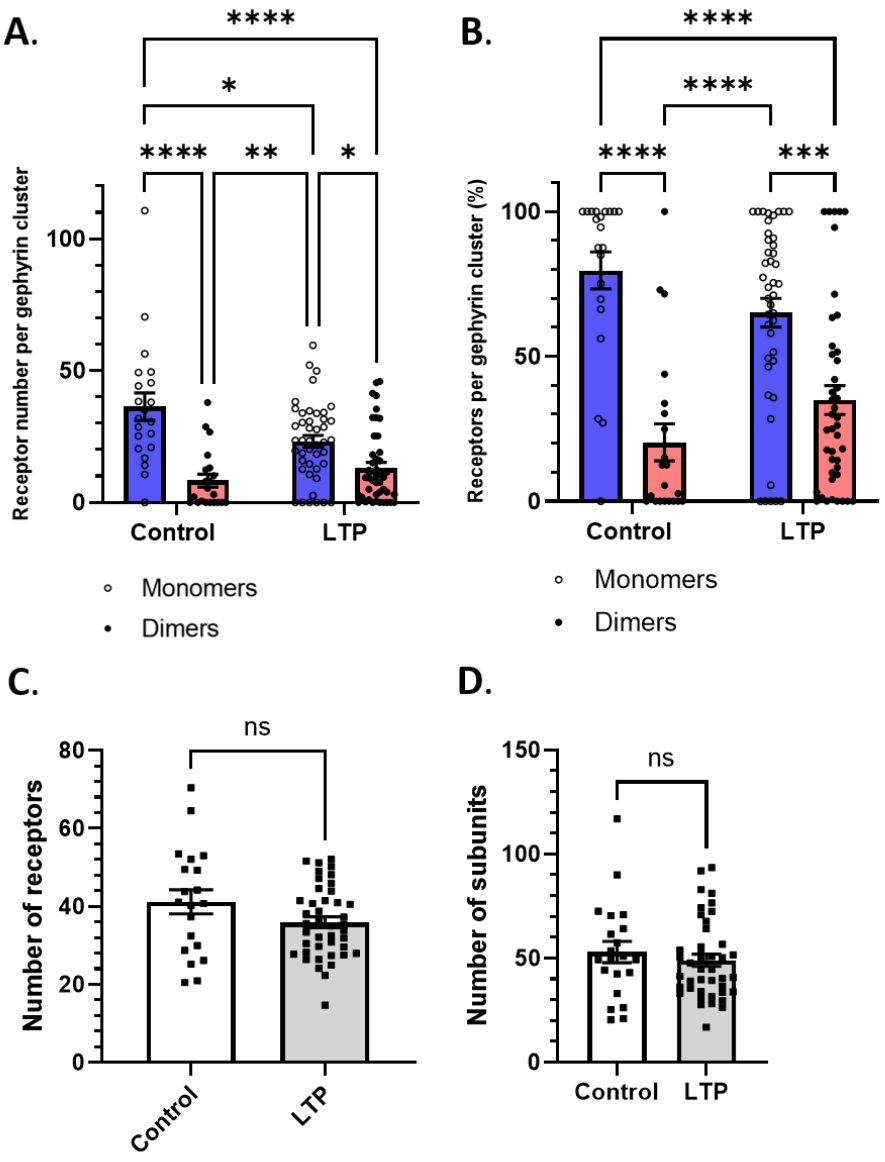

Figure 5.6 Effects of the iLTP induction on α1 GABA$_A$R oligomerisation states. **A.** Bar chart representing SpIDA of the α1 GABA$_A$R subunit monomer (○) and dimer (●) numbers within gephyrin clusters in control or iLTP expressing cultured hippocampal neurons. The mean ± SEM values are: control-treated monomers (n = 20, 32.6 ± 3.8), control-treated dimers (n = 20, 5.7 ± 1.7), iLTP-expressing monomers (n = 44, 23.2 ± 2.2), and iLTP dimers (n = 44, 10.2 ± 1.6). **B.** Monomer (○) and dimer (●) α1 GABA$_A$R percentages in sham-treated and iLTP induced neurons. The mean ± SEM values are: control-treated monomers (n = 20, 79.5 ± 3.2

%), control-treated dimers (n = 20, 20.5 ± 3.3 %), LTP-treated monomers (n = 44, 65.1 ± 4.9 %), and LTP-treated dimers (n = 44, 34.9 ± 4.9 %). For both **A and B**, two-way ANOVA with Tukey's post hoc test for multiple comparisons, P ≤ 0.05 *, ≤ 0.01 **, ≤ 0.001 ***, ≤ 0.0001 ****. **C.** Mean number of α1 subunit containing $GABA_A$ receptors per gephyrin cluster in control (n = 20, 41.2 ± 3.1) and iLTP (n = 44, 35.9 ± 1.4) neurons. Unpaired t-test, P ≥ 0.05 n.s. **D.** Total mean number of α1 subunits within the gephyrin cluster in control (n = 20, 52.9 ± 5.1) and iLTP (n = 44, 48.9 ± 2.9) neurons. Mann-Whitney test, P ≥ 0.05 n.s.

5.2.4 Effects of the glycine LTP induction on α2 $GABA_AR$ oligomerisation states

Next, we assessed the oligomerisation states of α2-containing $GABA_A$ receptors with SpIDA. Our results indicate that in control sham-treated neurons, the number of α2 monomers and α2 dimers at inhibitory synapses is similar: 30.6 ± 4.1 and 31.5 ± 2.9, with relative proportions equating to 43.8 ± 5.2 % and 57.0 ± 5.1 % (***Figure 5.7 A and B***). Interestingly, the number of α2 monomers (26.6 ± 3.5) compared to α2 dimers (41.9 ± 2.7) significantly decreases by 57.5 % (P ≤ 0.01) upon LTP induction (***Figure 5.7***). This correlates with a decreased percentage of α2 monomers 34.0 ± 3.9 % compared to α2 dimers 66.0 ± 3.9 %. This implies that there are more 'homo-alpha' α2α2-containing $GABA_A$Rs at synapses than 'hetero-alpha' α2-containing receptors after the induction of iLTP.

The total number of α2-containing receptors at synapses was estimated to be 62.1 ± 2.2 (***Figure 5.7 C***), consistent with the previously reported number of synaptic $GABA_A$Rs per gephyrin cluster (Kasugai et al., 2010). We observed a significant increase (P ≤ 0.01) post LTP in the α2-containing $GABA_A$R number. Previous studies reported an increase in postsynaptic clustered α2-containing $GABA_A$Rs post iLTP induction with various protocols (Bannai et al., 2020), which is consistent with our data. Furthermore, the total α2 subunit count significantly increases (P ≤ 0.0001) from control treated (93.6 ± 3.1) to glycine treated (115.8 ± 3.5) neurons.

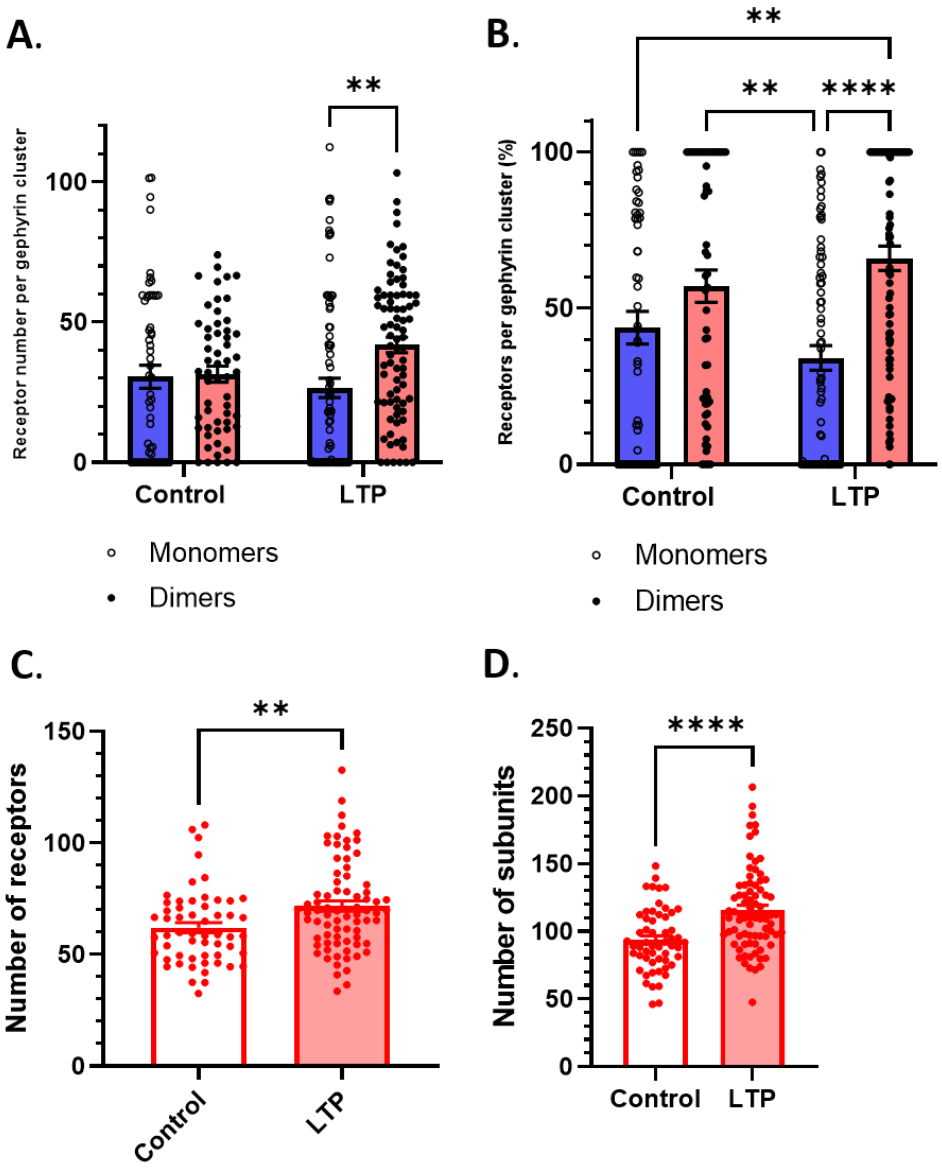

Figure 5.7 Effects of the glycine LTP induction on α2 GABA$_A$Rs oligomerisation states. **A.** SpIDA results for the α2 GABA$_A$R subunit monomer (○) and dimer (●) numbers within gephyrin clusters in control or LTP induced cultured hippocampal neurons. The mean ± SEM values are: control-treated monomers (n = 56, 30.6 ± 4.1), control-treated dimers (n = 56, 31.5 ± 2.9), LTP-treated monomers (n = 81, 26.6 ± 3.5), and LTP-treated dimers (n = 81, 41.9 ± 2.7). **B.** Monomeric (○) and dimeric (●) α2 GABA$_A$R forms percentages within gephyrin clusters in control and glycine LTP treated neurons. The mean ± SEM values are: control-treated monomers (n = 56, 43.8 ± 5.2 %), control-treated dimers (n = 56, 57.0 ± 5.1 %), LTP-treated monomers (n = 81, 34.0 ± 3.9 %), and LTP-treated dimers (n = 81, 66.0 ± 3.9 %). For both **A and B**, two-way ANOVA with Tukey's post hoc test for multiple comparisons, P ≤ 0.01 **, ≤ 0.001 ***. **C.** Mean ± SEM number of α2 subunit containing GABA$_A$ receptors per gephyrin cluster in control (n = 56, 62.1 ± 2.2) and LTP (n = 81, 71.7 ± 2.9) treated neurons. **D.** Mean ± SEM number of α2 subunits in control (n = 56, 93.6 ± 3.1) and LTP (n = 81, 115.8 ± 3.5) treated neurons. For **C and D**, Mann-Whitney test, P ≤ 0.01 **, ≤ 0.0001 ****.

5.2.5 Effects of the glycine LTP induction on α1 and α2 $GABA_AR$ oligomerisation states

Lastly, we assessed the oligomerisation states for both α subunit isoforms (α1 + α2) in a receptor pentamer, with SpIDA. Since, both primary antibodies used for immunolabelling of α1 and α2 were raised in the same species (rabbit), we could perform simultaneous labelling of both subunits with the same secondary antibody – goat anti-rabbit Alexa Fluor® 488. With such labelling, the dimeric forms would count 'homo-alpha' α1α1- and α2α2-containing receptors, as well as 'hetero-alpha' α1α2-containing $GABA_ARs$. Whereas the monomeric form would count 'hetero-alpha' α1α_x- and α2α_x-containing $GABA_ARs$, where α_x could be any other α subunit isoform, excluding α1 or α2. The limitation of such a technique is that the α1α1, α1α2, and α2α2 dimers are indistinguishable by SpiDA from each other, and the identity of the second α subunit isoform will be unknown. Nevertheless, as mentioned previously, simultaneous labelling of α1 and α2 could serve as a control in assessing receptor and subunit numbers.

Our results indicate that 77.5 ± 5.7 % of α1 and α2 subunits exist in a mixture (α1α1, α2α2, α1α2) of dimeric forms (69.6 ± 5.4 receptors per gephyrin cluster) (***Figure 5.8 A and B***). This means that approximately a quarter – 22.5 ± 5.7 % – of α1- and α2-containing receptors contain another α subunit isoform. We would expect the proportion of these receptors to be minor, given that α1 and α2 subunits are the major subunit types found at inhibitory synapses of cultured hippocampal pyramidal cells, with minor populations of α3 and α5 subunits (Fritschy et al., 1998; Fritschy and Mohler, 1995; Z Nusser et al., 1996; Palpagama et al., 2019)

Interestingly, the percentage of α1 + α2 dimers increases from 77.5 ± 5.7 % to 94.6 ± 2.7 %. This suggest that post-LTP induction, in terms of α1- and α2-containing $GABA_ARs$ at synapses, the majority are expressed as α1α1, α1α2, and α2α2 mixtures, with just 5.4 ± 2.8 % expressed as α1α_x and α2α_x mixtures.

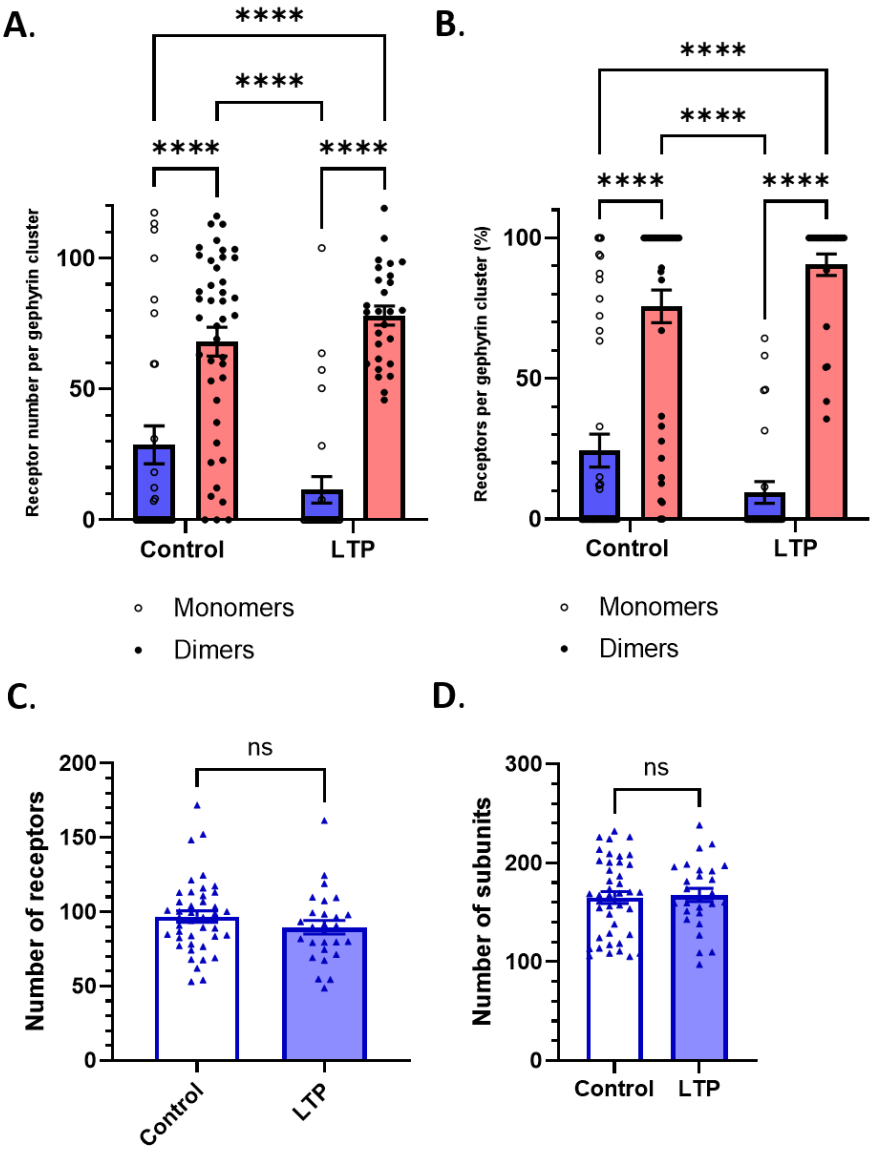

Figure 5.8 Effects of the glycine LTP induction on both α1 and α2 GABA$_A$Rs oligomerisation states. **A.** Bar chart representing SpIDA for α1 and α2 GABA$_A$R subunit monomer (○) and dimer (●) numbers within gephyrin clusters in control sham-treated or LTP treated cultured hippocampal neurons. The mean ± SEM values are: control-treated monomers (n = 41, 25.9 ± 4.1), control-treated dimers (n = 41, 69.6 ± 5.4), LTP-treated monomers (n = 25, 5.7 ± 3.1), and LTP-treated dimers (n = 25, 79.3 ± 3.5). **B.** Monomeric (○) and dimeric (●) α1 and α2 GABA$_A$R percentages within gephyrin clusters in control and glycine LTP treated neurons. The mean ± SEM values are: control-treated monomers (n = 41, 22.5 ± 5.7 %), control-treated dimers (n = 41, 77.5 ± 5.7 %), LTP-treated monomers (n = 25, 5.4 ± 2.8 %), and LTP-treated dimers (n = 25, 94.6 ± 2.7 %). For both **A and B**, two-way ANOVA with Tukey's post hoc test for multiple comparisons, P ≤ 0.0001 ****. **C.** Mean ± SEM number of both α1 and α2 subunit containing GABA$_A$ receptors per gephyrin cluster in control (n = 41, 96.8 ± 3.8) and LTP (n = 25, 89.6 ± 4.6) treated neurons. **D.** Mean ± SEM number for both α1 and α2 subunits in control (n = 41, 165.0 ± 3.1) and LTP (n = 25, 167.7 ± 6.6) treated neurons. For **C and D**, Unpaired t test, P ≥ 0.05 n.s.

5.2.6 Number of α1 and α2 subunits in α1/α2 immunolabelling is consistent with that of α1 + α2 simultaneous immunolabelling

As mentioned above, simultaneous labelling of α1 and α2 with the same secondary antibody was performed as a control for receptor and subunit counts. The arithmetic sum of individual α1 and α2 values should theoretically add up to the combined α1 + α2 values.

Firstly, we compared the number of receptors per gephyrin cluster in control treated neurons. The sum of α1 and α2 receptors (both monomers and dimers) was calculated to be ~ 104 receptors, which equated to the value obtained from α1 + α2 immunolabelling (96.9 ± 3.8) (***Figure 5.9 A***). Similarly, the sum of α1- and α2-containing receptors in LTP treated neurons (~ 107 receptors) was close to the total receptor number count in α1 + α2 immunolabelling (89.6 ± 4.6) (***Figure 5.9 C***).

Furthermore, we compared the total subunit count (one per monomer and two per dimer) in α1, α2, and α1 + α2 images. The sum of α1 and α2 $GABA_AR$ subunits (~ 147) was close to the total subunit count in α1 + α2 immunolabelling (165.0 ± 6.0) in control treated cultured hippocampal neurons (***Figure 5.9 B***). Similar internal consistency was observed in subunit counts of LTP-induced neurons.

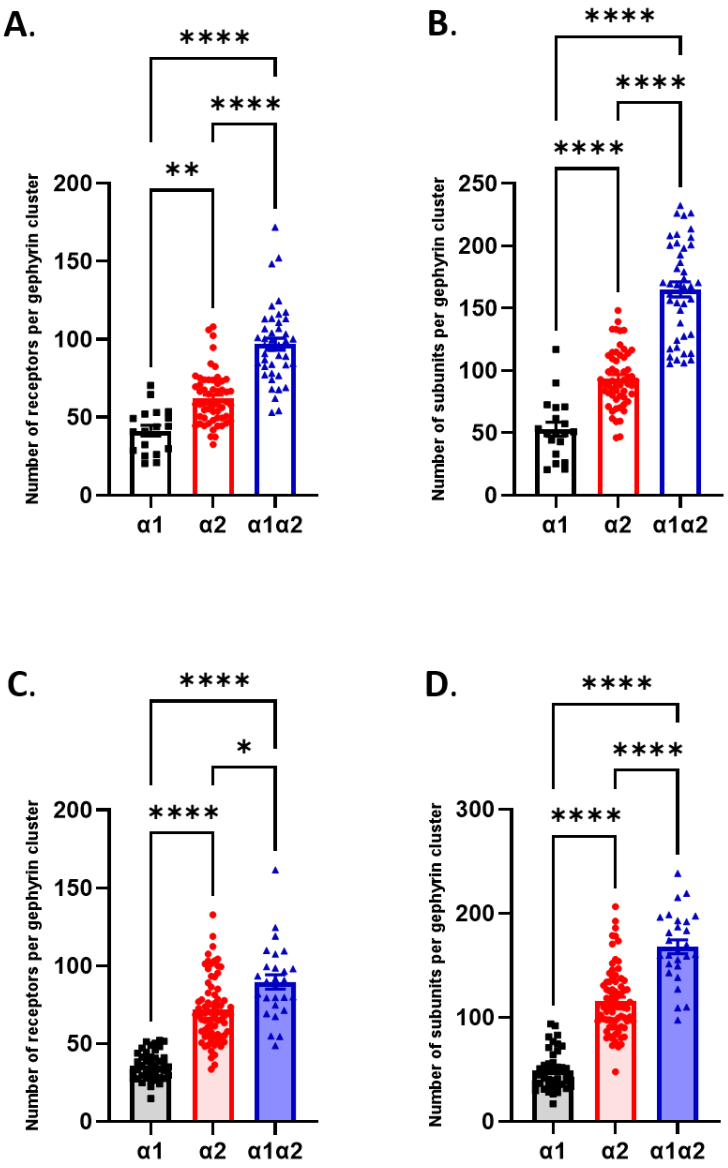

Figure 5.9 GABA$_A$R subunit and receptor number for combined α1 and α2 immuno-labelling corresponds to those obtained from α1 + α2 immuno-labelling. **A.** Bar chart representing mean ± SEM numbers of α1, α2 and α1 + α2 subunit containing GABA$_A$ receptors per gephyrin cluster in control treated cultured hippocampal neurons: α1 (■) (n = 20, 41.5 ± 3.1), α2 (●) (n = 56, 62.1 ± 2.2), and α1 + α2 (▲) (n = 41, 96.9 ± 3.8). Kruskal-Wallis test with Tukey's post hoc test, P ≤ 0.01 **, ≤ 0.0001 ****. **B.** Mean ± SEM number of α1 (■) (n = 20, 52.9 ± 5.6), α2 (●) (n = 56, 93.6 ± 3.1), and α1 + α2 (▲) (n = 41, 165.0 ± 6.0) subunits in control treated neurons. One-way ANOVA with Tukey's post hoc test for multiple comparisons, P ≤ 0.0001 ****. **C.** Mean ± SEM number of α1 (■) (n = 44, 35.9 ± 1.4), α2 (●) (n = 81, 71.7 ± 2.9), and α1 + α2 (▲) (n = 25, 89.6 ± 4.6) subunit-containing GABA$_A$Rs in LTP induced neurons. Kruskal-Wallis test with Tukey's post hoc test, P ≤ 0.05 *, ≤ 0.0001 ****. **D.** Mean ± SEM number of α1 (■) (n = 44, 48.9 ± 2.9), α2 (●) (n = 81, 115.8 ± 3.5), and α1 + α2 (▲) (n = 25, 167.7 ± 6.6) subunit counts in LTP induced neurons. Kruskal-Wallis test with Tukey's post hoc test, P ≤ 0.0001 ****.

5.3 Discussion

In this chapter, we aimed to determine the number and oligomerisation states of α1- and α2-containing $GABA_A$ receptors at inhibitory synapses by using SpIDA methodology. This technique was developed by Dr. Antoine Godin and we used his expertise to help us perform the analyses (Barbeau et al., 2013c). This type of imaging and analysis was previously used to study oligomerisation states of α2- and α3-containing $GABA_A$Rs at inhibitory synapses of the spinal dorsal horn after nerve injury (Lorenzo et al., 2020).

In ***Chapter 4*** we showed that a glycine-induced LTP protocol (Molnár, 2011) has a positive modulatory effect on the GABAergic transmission – increasing sIPSC amplitude – and hence it is also an iLTP protocol. Therefore, by chemically inducing iLTP in cultured hippocampal neurons, the changes in monomeric and dimeric α1/α2 $GABA_A$R subunit populations were assessed.

5.3.1 α1/α2-containing $GABA_A$R expression in control treated neurons

Our data indicate that ~ 80 % of the synaptic α1 $GABA_A$R receptors exist as monomers (in terms of α subunits) in cultured hippocampal neurons (***Figure 5.6***). This implies that the majority of α1-containing $GABA_A$Rs must exist as 'hetero-alpha' $GABA_A$ receptors. However, previous studies reported that 'homo-alpha' α1-containing $GABA_A$R populations are predominant, accounting for around 60 % of all α1-containing receptors (Benke et al., 2004a; Duggan et al., 1991), which is not in accord with our findings. The reason(s) for such a discrepancy can be attributed to the fact that the biochemical methods used in these former studies and the SpIDA methodology used here assess distinct $GABA_A$R pools. Immunoaffinity purification- and immunoprecipitation-based methods used to quantify the abundance of receptor mixtures rely on whole brain lysate purification – i.e. they detect 'bulk' levels of $GABA_A$Rs, intracellular, synaptic and extrasynaptic. Thus, these assess macroscopic abundance of receptor populations and do not distinguish between brain regions, cellular and subcellular subunit variation. By using SpiDA, however, we exclusively

imaged pyramidal hippocampal cultured neurons (through identification of their distinct morphology (Graves et al., 2012)) and analysed synaptic $GABA_ARs$ within gephyrin clusters – a recognised protein that plays a major role in anchoring $GABA_ARs$ at inhibitory synaptic membranes (Essrich et al., 1998; Jacob et al., 2008; Kneussel et al., 1999; Mukherjee et al., 2011). Thus, we are sampling a very discrete cellular and regional population(s) of $GABA_ARs$.

As discussed above, the limitation in the present study is that the identity of the second α subunit in the monomeric α1-receptor population cannot be resolved through SpIDA. However, we can confidently speculate, that the identity of the second α subunit in α1 receptor pool is unlikely to be α4 or α6. This is due to α6 subunit expression being almost exclusively limited to cerebellar granule cells and the cochlear nucleus (Fritschy and Mohler, 1995; Pirker et al., 2000), whilst in our experiments, cultured hippocampal neurons were used. Additionally, α4 and α6 subunits are thought to localise extrasynaptically (Brickley et al., 1996; Jechlinger et al., 1998; Nusser et al., 1998). Since we are looking specifically at $GABA_ARs$ within the gephyrin 'imaging mask' (***Figure 5.4***), it is unlikely that extrasynaptic α subunits (α4 or α6) could contribute to SpIDA monomeric α1 subunit pool mixtures. Other α subunit isoforms that can localise synaptically are: α2 (Kasugai et al., 2010; Z. Nusser et al., 1998), α3 (Maric et al., 2014; Tretter et al., 2011) and α5 (Serwanski et al., 2006). This implies, that the 'hetero-alpha' α1-containing $GABA_ARs$ could be expressed with α2, α3, or α5 subunits.

With regards to α2-subunit containing $GABA_ARs$ (***Figure 5.7***), our data indicate that the 'hetero-alpha' to 'homo-alpha' receptor ratio is distinct to that of α1-containing ratio. The ratio of monomers to dimers of α1 subunit was estimated to be 8 : 2, whereas the same ratio for α2 receptors was 1 : 1. This implies that synaptic α2-containing $GABA_ARs$ are expressed as 'homo-alpha' (~ 32 receptors) and 'hetero-alpha' (~ 31 receptors) forms at similar levels. The best comparison we can draw here, with prior studies, is with the percentages of 'homo-' and 'hetero-alpha' receptor pools established from biochemical studies. One study performed immunoprecipitation with anti-α2 $GABA_AR$ antibodies from hippocampal lysates, to pull-down α2-containing $GABA_ARs$, and subsequently probed the receptors for α1

and α5 subunits (del Río et al., 2001a). The study found that 36.6 ± 5.2 % and 20.2 ± 2.1 % are α1α2 or α2α5 receptors respectively (del Río et al., 2001a). The remaining ~ 44 % of α2-containing receptors in this study are probably α2α2 'homo-alpha' $GABA_A$Rs, given that α2α4 and α2α6 combinations are unlikely to be present (due to the reasons discussed in the paragraph above). This percentage is close to the value we have observed for 'homo-alpha' α2-receptors (~ 57 %) (***Figure 5.7***). However, it is possible that the remaining proportion of α2-containing receptors established by del Río and colleagues could contain some α2α3 $GABA_A$R, as this subunit was not probed for in the western blot analysis. Nevertheless, such receptor combination has been reported as being 'minor' (~ 2 %) in other studies (Benke et al., 2004a; Duggan et al., 1991).

From SpIDA of α1 + α2 $GABA_A$R subunits we observed that ~ 22 % were monomers, whereas the remaining ~ 78 % of receptors were expressed as dimers in control treated neurons (***Figure 5.8***). These data imply that ~ 22 % of 'hetero-alpha' $GABA_A$Rs (either α1- or α2-containing) are expressed with other subunit isoforms. These are likely to be combinations of α1α3-, α1α5-, α2α3-, and α3α5-containing $GABA_A$Rs, as these subunit mixtures were previously suggested to exist in the brain (Araujo et al., 1999, 1996; Benke et al., 2004a; del Río et al., 2001a; Duggan et al., 1991; Ju et al., 2009).

To achieve a degree of quantification, the percentage of α1α2 'hetero-alpha' $GABA_A$Rs from α1, α2 and α1 + α2 immunolabelling data was estimated. The number of synaptic α1 dimers – these could only be 'homo-alpha' α1α1-containing receptors – was estimated to be ~ 6 receptors in control treated neurons (***Figure 5.6 A***), whereas the number of α2 dimers – 'homo-alpha' α2α2-containing $GABA_A$Rs – was ~ 32 receptors (***Figure 5.7 A***). The number of dimers in α1 + α2 was measured to be ~ 70 receptors. These dimers could represent 'homo-alpha' α1α1, 'homo-alpha' α2α2, or 'hetero-alpha' α1α2 receptor populations, and are not distinguishable in SpIDA analysis as all these subunit combinations would emit a QB of 2ε. Since the labelling of these two subunits was performed with the same secondary antibody (anti-rabbit Alexa Fluor® 488) and the total number of receptors in α1 + α2 immunolabelling approximately equated to the arithmetic sum of total α1 and α2 receptors (***Figure***

5.9 A), we can subtract α1α1 and α2α2 $GABA_AR$ values (6 and 32 receptors respectively) from α1 + α2 dimeric receptor number. This means that ~ 32 $GABA_AR$ of all possible α1 + α2 dimers are 'hetero-alpha' α1α2-$GABA_AR$. As we know the total number of receptors per gephyrin cluster in α1 + α2 immunolabelling – ~ 96 receptors (monomers and dimers) (***Figure 5.8 C***), the percentage of 'hetero-alpha' α1α2 receptors equates to ~ 33 % out of all α1- and α2-containing $GABA_ARs$.

5.3.2 α1/α2-containing $GABA_AR$ expression changes following iLTP induction

Our data suggests that only the number of α2-containing $GABA_ARs$ increases significantly post glycine-based LTP induction, whereas the number of α1- and overall number of α1- + α2-containing $GABA_ARs$ does not change (***Figures 5.6 - 5.8***). However, our electrophysiology data suggests that there is an increase in postsynaptic $GABA_ARs$, due to a significant increase in sIPSC current amplitude (***Figure 4.9***), which does not reflect the results obtained here. It is worth reiterating, that SpIDA of $GABA_ARs$ is performed strictly within the gephyrin mask. One of the possible explanations for the lack of change in receptor numbers with SpiDA, is that we could also be including extrasynaptic $GABA_ARs$ in our calculations. Although we used a gephryin mask, it has been previously reported that localisation of gephyrin – synaptic or extrasynaptic – can vary hugely during development in cultured hippocampal neurons (Danglot et al., 2003). Strikingly, as much as 42 % of gephyrin was found extrasynaptically at DIV10 cultured hippocampal neurons, with the value decreasing to 10 % at DIV21 (Danglot et al., 2003). As we are using DIV11-15 cultured hippocampal neurons in these experiments, it is likely that we are also assessing some extrasynaptic $GABA_ARs$, thereby diluting the effect of iLTP on receptor numbers within gephyrin clusters. However, our data indicates that the overall mean intensity of α1, α2, and α1 + α2 immunolabelling significantly increases in our ROIs post LTP induction (ROIs selected through MAP2 labelling) (***Figure 5.5***), supporting the idea of increased receptor density. This also correlates with the changes observed with other iLTP protocols – ie, increased postsynaptic clustering of $GABA_ARs$ (Bannai et al., 2020; Battaglia et al., 2018; Petrini et al., 2014).

With regards to α1 oligomerisation state changes post LTP induction, we did not observe any significant changes in monomer/dimer ratios. Nevertheless, we observed a trend towards a decrease in α1 monomers, and an increase in α1 dimers. Furthermore, we observed that four ROIs had 100 % of dimers post LTP induction (***Figure 5.6 B***), suggesting that these α1-containing receptor pools were expressed as 'homo-alpha' α1α1-$GABA_A$Rs. Again, it is possible that the apparent lack of significant changes in oligomerisation states within the synaptic α1-receptor pool is because some receptors we are looking at are extrasynaptic.

In comparison to α1 oligomerisation, glycine LTP evoked changes in the oligomerisation states of α2-containing $GABA_A$Rs, where the proportion of α2 monomers to dimers exhibited a change from 30 : 32 receptors in control treated neurons, to 27 : 42 in LTP treated neurons (***Figure 5.7 A***). Such a change implies that post iLTP induction there are more 'homo-alpha' α2α2- than 'hetero-alpha' α2α_x-receptors expressed within gephyrin clusters. Furthermore, the overall number of α2 subunits significantly increased – a result that was previously observed with overall α2 $GABA_A$R subunit numbers being upregulated expression post-iLTP (Petrini et al., 2014). Since the overall number of α2 receptors increases post glycine treatment, we can speculate that the ratio of α2 monomers to dimers changes due to either increased *de novo* α2α2-containing receptor synthesis, or possibly an increased exocytosis of the α2α2-containing receptors that are already present in secretory pathways (Arancibia-Cárcamo and Kittler, 2009).

The data obtained for α1 + α2 immunolabelling however, suggested that there was no significant change in oligomerisation states post glycine LTP treatment. One possible explanation for this could be that in control treated neurons, the majority (~ 78 %) of α1- and α2-$GABA_A$R pool already exists as a dimer (α1α1, α1α2, or α2α2). Therefore, changes towards an increase of dimeric receptor populations could be missed. Interestingly, post LTP induction almost 95 % of α1- and α2-$GABA_A$Rs are expressed as dimers. By using immunolabelling, we can estimate the number (proportion) of 'hetero-alpha' α1α2-containing $GABA_A$Rs out of all α1 and α2 receptors, which comes to ~ 43 %, a 10 % increase compared to control treated neurons. The total number of α1 and α2 subunits does not change after glycine

treatment (***Figure 5.8 D***), but the ratios of monomers to dimers does. This may occur if the glycine LTP protocol induces reassembly of α1- and α2-containing receptors. To summarise, a schematic diagram of glycine LTP induced changes on α1, α2, and α1α2 oligomerisation states is shown in ***Figure 5.10***. Note that out of all the α1- and α2-containing 'hetero-alpha' $GABA_ARs$ some receptors could be α1α2-receptors.

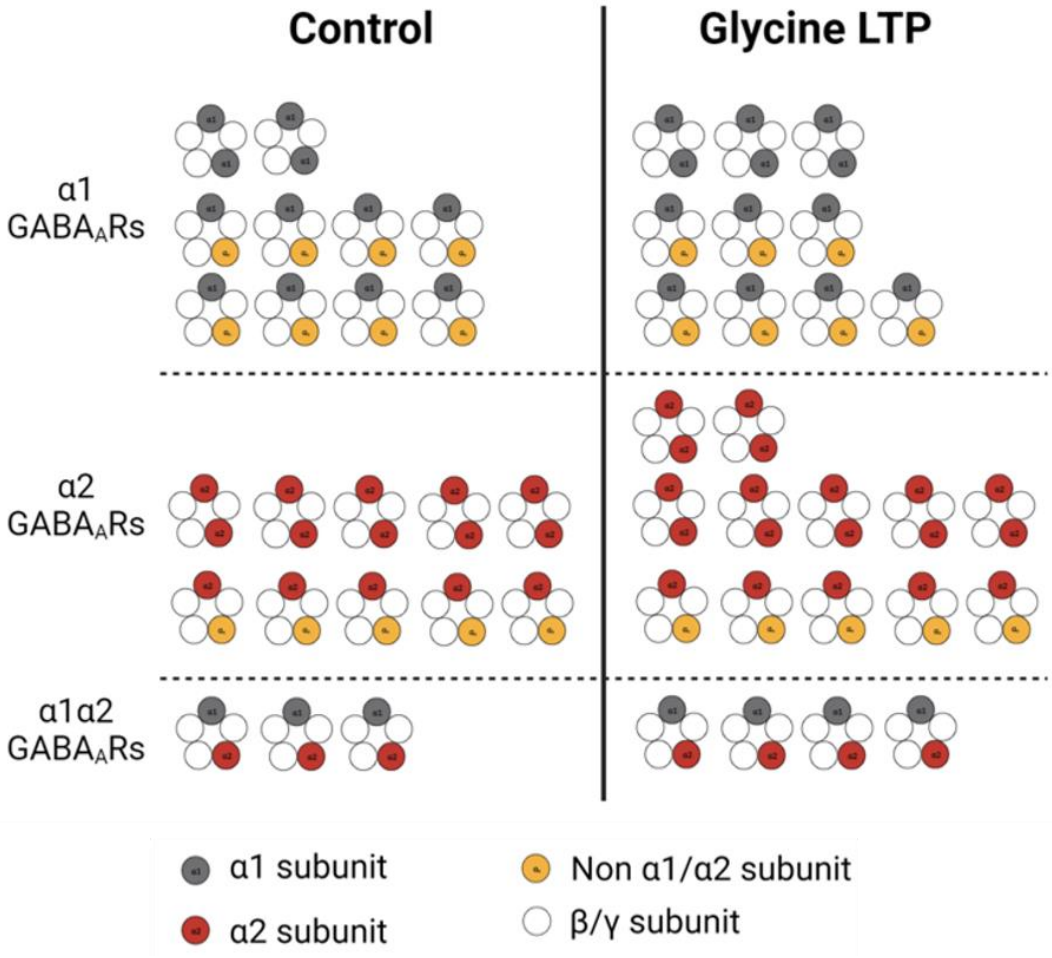

Figure 5.10 Schematic diagram of $GABA_AR$ changes induced by glycine LTP. With regards to α1 containing $GABA_ARs$ (top panel), the ratio of 'homo-alpha' to 'hetero-alpha' $GABA_ARs$ is 2 : 8 in control treated neurons. Upon glycine LTP treatment, the number of receptors does not change, however the ratio of 'homo-alpha' to 'hetero-alpha' shifts to 3 : 7. The identity of the second α subunit in 'hetero-alpha' α1-containing receptors is unknown. In terms of α2-containing $GABA_ARs$ (middle panel), the ratio of 'homo-alpha' to 'hetero-alpha' $GABA_ARs$ is 1:1 in control treated neurons. Post LTP treatment, the ratio shifts to 7 : 5, additionally with the number of α2-containing receptors increasing. The identity of the second pairing α subunit for α2 is unknown. Lastly, the percentage of α1α2 'hetero-alpha' $GABA_ARs$ (out of all α1 and α2 receptors) increases from 33 % to 43 %. Note the relative receptor number between panels is not to scale.

5.3.3 Limitations of SpIDA

One of the most obvious limitations, of such analysis is the image quality. Here, we performed a calibration of the PMT linked to our confocal microscope as discussed in ***Section 5.2.1*** to avoid pixel saturation and minimise variation in data acquisition. Furthermore, the same parameters, once set, were used across all image acquisitions to enable image comparison (see table 5.1). We also ensured that the images were taken at a consistent resolution (1024 x 1024 px). Alongside α1, α2 and α1 + α2 immunolabelling, we also used γ2 labelling as a control to allow quantification of the monomeric fluorophore brightness, given the receptor stoichiometry of 2α1:2β2/3:1γ2L.

It is important to reiterate here, that the major limitation of SpIDA is that the identity of the second α subunit in a monomeric oligomerisation state cannot be resolved since the same secondary antibody is used. We therefore estimated the percentages of α1α2-containing receptors in α1 + α2 immunolabelled images through subtraction of separately immunolabelled α1 and α2 containing receptors

Lastly, we recorded an increase in total α2-, but not α1- or α1- + α2-containing $GABA_AR$ numbers post glycine LTP induction. This is surprising, given that we observed an increase in sIPSC current amplitude with the same protocol (***Figure 4.9***). As already mentioned, the lack of a significant increase in total receptor numbers could be attributed to using gephyrin as a binary mask to look at synaptic $GABA_ARs$, whilst gephyrin is likely to also localise at extrasynaptic locations, given the age of neurons we use here (DIV11-15) (Danglot et al., 2003). Therefore, the effects of LTP induction on synaptic $GABA_ARs$ could be diluted by including part of the extrasynaptic $GABA_AR$ pool into our analysis.

5.4 Conclusions

1. Approximately 80 % of all synaptic α1-containing $GABA_ARs$ are expressed as ‘hetero-alpha’ receptors in control treated cultured hippocampal neurons, whereas

~ 50 % of all synaptic α2-containing $GABA_ARs$ are expressed as 'hetero-alpha' $GABA_ARs$.

2. Around 30 % of all synaptic α1- and α2-containing $GABA_ARs$ are expressed as α1α2-containing 'hetero-alpha' $GABA_ARs$ in control treated neurons.

3. Other combinations of 'hetero-alpha' $GABA_ARs$ (excluding α1- and α2-paired receptors) are also expressed, which are likely to be combinations of α1α3-, α1α5-, α2α3-, and α3α5-receptors.

4. Post glycine-based LTP induction, the overall mean intensity of α1, α2, and α1 + α2 immunolabelling increases, suggesting an increased overall cell surface expression of $GABA_ARs$.

5. The number of α2-containing $GABA_ARs$ within the gephyrin mask increases post LTP induction, and the number of 'homo-alpha' α2α2-$GABA_ARs$ also increases from 50 % to 66 %.

6. The number of α1α2 'hetero-alpha' $GABA_ARs$ (out of all α1- and α2-containing receptors) increases by 10 % post LTP induction. The number of other α1- and α2-containing $GABA_ARs$ decreases by 17 %.

7. iLTP is likely to induce reassembly of α1- and α2-containing receptors, by decreasing the number of α2α2 'homo-alpha' and increasing the number of α1α1 'homo-alpha' as well as α1α2 'hetero-alpha' $GABA_ARs$ within gephyrin clusters.

8. Some receptors within the gephyrin mask could be extrasynaptic, diluting the effect of glycine LTP treatment on synaptic $GABA_ARs$.

Chapter 6: General discussion

6.1 Literature overview and project aims

$GABA_A$ receptor subunit composition determines its biophysical and pharmacological properties – agonist sensitivity, kinetic profiles; subcellular localisation – synaptic or extrasynaptic, as well as pharmacological properties (Carter et al., 2010; Colquhoun, 1998; Farrant and Nusser, 2005; Sieghart, 1995; Sigel and Steinmann, 2012) In particular, the identity of the α subunit isoform present in the $GABA_AR$ pentamer determines GABA potency (Mortensen et al., 2012b) and plays a crucial role in shaping pharmacological sensitivity and the effects of the benzodiazepines (McKernan et al., 2000; Sigel and Ernst, 2018; Skolnick, 2012).

In the brain, the majority of $GABA_AR$ subtypes are expressed as pentamers containing two α, two β and one γ subunits (Laverty et al., 2019b; Olsen and Sieghart, 2009). Although only a small number of subunit combination permutations are thought to be expressed *in vivo* (McKernan and Whiting, 1996; Olsen and Sieghart, 2009) there is extensive evidence, that distinct α subunit isoforms – 'hetero-alpha' – may exist in a single receptor complex (see ***Table 1.2*** for detail). Specifically, α1 and α2 subunits – the two most widely expressed α subunit types in the brain (Pirker et al., 2000) – were reported to exist in the same $GABA_AR$ pentamer (Benke et al., 2004a; del Río et al., 2001b; Duggan et al., 1991). Existence of such receptors can vastly increase subunit permutations and hence receptor isoforms, producing $GABA_AR$ subtypes with unique GABA and allosteric modulator sensitivities.

Even though the evidence for 'hetero-alpha' $GABA_ARs$ exists, the majority of the reports used biochemical immunoaffinity purification methods to assess their presence and abundance *in vivo*. However, such methodology assesses 'bulk' receptors, and is unable to provide insight into functional and pharmacological signatures of specific receptor subtypes (see ***Section 1.4.1***). To overcome this issue, receptor concatenation has been previously used to study pharmacological fingerprints of $GABA_A$ receptors with two different isoforms of α or β subunits (see ***Section 1.4.2***). However, receptor concatenation studies are limited, as they only

assessed two subunit combinations: α1 and α6 (Minier and Sigel, 2004c; Simeone et al., 2019), and β1 and β2 (Boulineau et al., 2005). Furthermore, this is a constrained system and does not explore free subunit assembly.

Given the above, the present work primarily focused on investigating $GABA_A$Rs with two distinct α subunit isoforms: α1 and α2. We established the existence and abundance of both recombinant and native 'hetero-alpha' α1α2-containing $GABA_A$Rs. We attempted to assess functional signatures of these receptors – this aim was addressed in ***Chapters 3 and 4***. Furthermore, subcellular localisation of 'hetero-alpha' $GABA_A$Rs was also investigated (***Chapter 4***). Finally, the physiological role of these receptors post-LTP induction was assessed ***(Chapter 4 and 5***).

6.2 Major findings

6.2.1 Existence and abundance of α1α2-containing $GABA_A$Rs in vitro and in vivo

Our first aim was to establish the existence of 'hetero-alpha' α1α2-containing $GABA_A$Rs receptors in a recombinant system. Our data indicates that α1α2β3γ2L-transfected HEK293 cells have a higher GABA apparent affinity than pure α1β3γ2L- or α2β3γ2L-expressing cells, suggesting that a distinct receptor population must be present: α1α2β3γ2L (***Figure 3.3***). Furthermore, co-expression of $\alpha1^{L263S}$ and α2 subunits with β2/3 and γ2L yielded three population multi-component Hill equation fits (***Figure 3.9***), further confirming the presence of 'hetero-alpha' $GABA_A$R receptor populations. We also demonstrated that α1 and α2 subunits are in close enough proximity for PLA to produce a signal (PLA spot) in both α1α2β2γ2L- and α1α2β3γ2L-transfected HEK293 cells (***Figure 4.1***).

We demonstrate the existence of native α1α2-containing $GABA_A$Rs with PLA methodology (***Figure 4.4***). By performing nocodazole treatment to decluster $GABA_A$Rs (Petrini et al., 2004, 2003) (***Figures 4.2-4.4***) and PLA between γ2 and δ subunits (***Figure 4.5***), we established that the PLA signal is unlikely to occur between 'inter-receptor' PLA probes, thereby validating α1α2 PLA spots as indicative of 'intra-

receptor' subunit interactions. Lastly, SpIDA analysis of α1 + α2 immunolabelled cultured hippocampal neurons indicated the presence of 'hetero-alpha' $GABA_ARs$ (***Section 5.3.1***). Overall, given that we used different methods (whole-cell patch-clamp electrophysiology, PLA and SpIDA imaging based techniques), we can confidently say that 'hetero-alpha' α1α2-containing $GABA_ARs$ are expressed both *in vitro* and *in vivo*.

Our data indicates that the abundance of α1α2β2/3γ2L is between 45 % and 68 % of the total receptor pool in transfected HEK293 cells (***Figure 3.9***) and ~ 33 % at synapses in cultured hippocampal neurones (***Section 5.3.1***). These values are in agreement with previous reports, where the α1α2-containing receptor population was estimated to be between 33 % and 36 % (Benke et al., 2004a; del Río et al., 2001b; Duggan et al., 1991). Additionally, our data indicates that ~ 22 % of all α1- and α2-containing receptors at synapses are expressed as $\alpha1\alpha_x$- and $\alpha2\alpha_x$-$GABA_ARs$ (***Figure 5.8***). This suggests that the diversity of 'hetero-alpha' $GABA_ARs$ is not limited to α1α2-containing receptors - other types of 'hetero-alpha' $GABA_AR$ pentamers are likely to exist These subunit combinations are likely to be α1α3-, α1α5-, α2α3-, and α3α5-containing $GABA_ARs$, as these subunit mixtures were previously reported to exist in the brain (Araujo et al., 1999, 1996; Benke et al., 2004a; del Río et al., 2001a; Duggan et al., 1991; Ju et al., 2009). This implies that the diversity of $GABA_ARs$ expression is far greater than previously thought (Olsen and Sieghart, 2009).

6.2.2 Determinants of 'hetero-alpha' $GABA_AR$ expression and assembly

We show that only ~ 10 % of native synaptic α1-containing receptors are expressed as 'homo-alpha' $GABA_ARs$ in cultured hippocampal neurons (***Figure 5.6***). This suggests that α1-containing receptors mainly harbour other α subunit isoforms, probably predominantly the α2 subunit. Glycosylation of the α1 subunit at N110, located within the ECD of the receptor occupies a significant part of the vestibule above the channel pore (Laverty et al., 2019b) and has been proposed to play an important role in assembly of $GABA_ARs$, by blocking the formation of $GABA_AR$ pentamers with more than two α subunits (Buller et al., 1994; Chen et al., 2012b;

Phulera et al., 2018). We could speculate that N-linked glycans of the α1 subunit are structurally distinct from those on other α subunits, where the glycans association between α1 and α_x is preferential over that of α1 and α1 glycans interaction. This could potentially work like a 'lock and key', where the size and compatibility of the α subunits' N110 glycans regulate the assembly of 'hetero-alpha' $GABA_AR$s.

GABAergic transmission in frontotemporal regions of the brain and hippocampus has been reported to be altered in schizophrenia (de Jonge et al., 2017; Marques et al., 2021). Interestingly, previous reports indicate that glycosylation patterns of $GABA_AR$s, specifically α1, β1 and β2 subunits, are altered in patients with schizophrenia (Mueller et al., 2014). The glycans of the α1 subunit in the cortex taken from patients with schizophrenia were reported to have a smaller molecular mass compared to healthy patients (Mueller et al., 2014). Following our proposed 'lock and key' theory above, we could speculate, that $GABA_AR$ assembly, including 'hetero-alpha' receptors could be altered in schizophrenia.

PLA between α1 and α2 subunits indicate that overexpression of α2, but not the α1 subunit results in an increase of PLA puncta (***Figure 4.6***). This could imply that α2 subunit expression is the limiting factor in α1α2-containing $GABA_AR$ assembly. SpIDA results indicate that ~ 50 % of all α2-containing $GABA_AR$s are expressed as 'homo-alpha' α2α2-receptors (***Figure 5.7***) – a percentage that is significantly higher than 'homo-alpha' α1α1-receptor expression (~ 10 %). Taken together, we could speculate that there are rules to $GABA_AR$ subtypes assembly and expression, where assembly of α2α2-containing $GABA_AR$s is preferential over α1α2-containing $GABA_AR$s. Similarly, assembly of 'hetero-alpha' α1α2-receptors is dominant over that of 'homo-alpha' α1α1-containing $GABA_AR$s.

Our data also suggests that the identity of the β subunit regulates the abundance of 'hetero-alpha' α1α2-containing $GABA_AR$ expression in HEK293 cells (***Figure 3.9***). The β subunit identity determines $GABA_AR$ assembly and clustering (Connolly et al., 1996; Jacob et al., 2008; Nguyen and Nicoll, 2018). The evidence on β2/3-containing $GABA_A$ receptors localisation is conflicting, nevertheless there seem to be subcellular localisation differences in $GABA_AR$ expression, dependent on the identity of the β subunit (Herd et al., 2008; Kasugai et al., 2010; Thomas et al., 2005). It is therefore

possible that the β subunit identity in the pentamer regulates the abundance as well as localisation of 'hetero-alpha' $GABA_A$Rs.

6.2.3 Subcellular localisation of 'hetero-alpha' $GABA_A$Rs

The majority of native α1α2-containing $GABA_A$ receptors (~ 80 %) are located distinct from VIAAT clusters (***Figure 4.6***) in cultured hippocampal neurons. This implies that the majority of α1α2-$GABA_A$Rs must localise perisynaptically or extrasynaptically. Previous studies revealed that $GABA_A$ receptors containing the α2 subunit are localised at synaptic sites, whereas α1 -containing $GABA_A$R expression is more diffuse in cultured hippocampal neurons (Nusser et al. 1996; Nyíri, Freund, and Somogyi 2001). This difference is attributed to the differential binding affinities of α1 and α2 subunits to the major inhibitory postsynaptic scaffolding protein – gephyrin (Tretter et al., 2008). Even though gephyrin directly binds to the α1 subunit with high affinity (~ 20 μM), phosphorylation of residue T375 significantly decreases the affinity of α1 for gephyrin, and hence synaptic clustering (Mukherjee et al., 2011). Therefore, it is possible that the extrasynaptic/perisynaptic localisation of α1α2-containing $GABA_A$Rs is regulated through α1 subunit phosphorylation.

Interestingly, out of the two α subunits, α2 seems to drive the expression of 'hetero-alpha' $GABA_A$Rs, and their subsequent localisation at synapses (***Figure 4.6***). As discussed above, the availability of the α2 subunits could be a limiting factor in α1α2-receptor assembly. Since the overall number of α1α2-containing $GABA_A$Rs increases with the increased availability of α2 subunits, it is possible that *de novo* 'hetero-alpha' $GABA_A$Rs preferentially localise at synaptic junctions. Their synaptic localisation could be attributed to the basal phosphorylation of the α1 subunit at T375 (described above), resulting in an increased synaptic clustering *via* a gephyrin-dependent mechanism (Sassoè-Pognetto and Fritschy, 2000).

6.2.4 Functional role of 'hetero-alpha' $GABA_ARs$

As discussed in ***Sections 3.5.1 and 4.3.3***, 'hetero-alpha' α1α2-containing $GABA_ARs$ do not seem to hugely affect GABA apparent affinity or sIPSC kinetics compared to 'homo-alpha' counterparts (α1α1 and α2α2). One of the explanations could be that α1- and α2- 'homo-alpha' $GABA_ARs$ have similar kinetic profiles, thereby mixtures of these two subunits would potentially result in a receptor with a GABA potency and kinetic profile similar to 'homo-alpha' receptors. We show that an increased number of synaptic 'hetero-alpha' α1α2-containing receptors correlates with a faster tau1 component in the biexponential sIPSC decay (***Figure 4.7***), suggesting that these receptors could play a role in fine-tuning GABAergic transmission, rather than evoking large scale changes to IPSCs.

Since 'hetero-alpha' receptor mixtures can reside in synaptic and extrasynaptic cellular compartments (***Figure 4.6***), we could speculate that 'hetero-alpha' δ-containing α4/6α_xβ1-3δ $GABA_ARs$ may also form part of the extrasynaptic receptor population (Nusser et al. 1995; Nusser, Sieghart, and Somogyi 1998). Immunoprecipitation studies estimated α1α6βδ receptor mixtures from mice cerebellar extracts to be around 14 % of the total α1- and α6-receptor pools (Jechlinger et al., 1998; Pöltl et al., 2003). Previous studies of recombinant $GABA_AR$ mixtures estimated GABA EC_{50} values of the α1βδ and α6βδ receptors at 3.7 μM and 0.17 μM respectively (Farrant and Nusser, 2005; Mortensen et al., 2012b; Picton and Fisher, 2007). This could imply that 'hetero-alpha' α1α6βδ receptors would have an apparent affinity for GABA between the two 'pure receptor' EC_{50} values for corresponding 'homo-alpha' populations. Having a receptor population with such GABA potency could provide a dynamic regulatory mechanism for balancing responses to ambient GABA outside inhibitory synapses.

The two GABA binding sites in a $GABA_AR$ do not carry the same contribution to receptor activation, with site 2 (flanked by the α and γ subunits) carrying a three-fold higher GABA affinity than site 1 (flanked by the γ and β subunits) determined using concatamers (Baumann et al., 2003). Therefore, the relative α subunit positioning in a 'hetero-alpha' $GABA_AR$ could play an important role in receptor activation

mechanisms and pharmacology. Since the sensitivity to GABA in a $GABA_AR$ pentamer is largely determined by the α isoform present (Böhme et al., 2004), relative positioning of the α subunits in 'hetero-alpha' $GABA_ARs$ becomes important when α subunits exhibit distinct potencies towards GABA. For example, the α3-containing $GABA_AR$ apparent affinity is between 6- and 8-fold lower than that of α1-containing receptors (Ebert et al., 1994; Mortensen et al., 2012a). Thus, in the α1α3-containing $GABA_ARs$, the relative positioning of these two α subunits could dictate the GABA apparent affinity: γ2β2**α3**β2**α1** would have a lower GABA potency than γ2β2**α1**β2**α3**, since the former has an α3 subunit at GABA binding site 2. This idea has been confirmed in concatenated $GABA_AR$ studies, where the GABA apparent affinity of γ2β2**α1**β2**α6** was found to be two times lower than of γ2β2**α6**β2**α1** (94 ± 38 μM and 42 ± 14 μM respectively) (Minier and Sigel, 2004a).

Furthermore, the identity of the α subunit at the α/γ interface plays a major role in the sensitivity towards, and modulatory effects of, the benzodiazepines (Sigel and Ernst, 2018; Sigel and Lüscher, 2011). Since we discussed possible modulatory effects of BDZ on 'hetero-alpha' $GABA_ARs$ in ***Section 3.5.3***, it is important to consider the possible modulation of 'hetero-alpha' $GABA_ARs$ by endogenous benzodiazepines – endozepines. This group of molecules was hypothesised to exist endogenously in the brain after the discovery of the benzodiazepine binding site on $GABA_ARs$, and later putative endozepine candidates were identified (Costa and Guidotti, 1985; Cravatt et al., 1995; Rothstein et al., 1992). One of the most well-characterised putative endozepines is the diazepam-binding inhibitor (DBI) peptide (Farzampour et al., 2015; Guidotti et al., 1983). This is a 10 kDa protein, which has been previously shown to displace exogenous benzodiazepines from whole brain lysates, suggesting that the binding site of DBI is overlapping with the exogenous BDZ binding site (Guidotti et al., 1983).

The effects of DBI on $GABA_AR$ appear conflicting, with some studies claiming it acts as a NAM (Bormann, 1991; Costa and Guidotti, 1985), whereas others suggested it has positive modulatory effects (Christian et al., 2013). Such conflicting results could be attributed to selective modulatory effects of DBI, dependent on the identity of the α subunit isoform at the α/γ interface, as well as overall subunit composition of the

$GABA_AR$ pentamer. As such, similar to benzodiazepines, endozepines could produce multicomponent patterns of modulation, that are dependent on the subunit arrangement in 'hetero-alpha' $GABA_ARs$.

By introducing a mutation into the α subunit (H101R) to render the receptor insensitive to benzodiazepines, we also tried to determine if the α1 and α2 subunits had preferential stoichiometric locations within the hetero-alpha receptor complex. However, our data suggested that the relative proportion of receptors with α1/γ and α2/γ interfaces is apparently similar, with each interface representing approximately 50% (see ***Section 3.4***).

Lastly, we outlined the functional role of 'hetero-alpha' α1α2-containing $GABA_ARs$ during the induction of inhibitory long-term potentiation (see ***Sections 4.3.4 and 5.3.2***). To summarise, 'hetero-alpha' $GABA_AR$ expression at synapses increases post LTP induction. Our results are in agreement with previous studies, where post-synaptic clustering of $GABA_ARs$ as well as upregulated expression of the α2 subunit has been previously observed with various iLTP protocols (Bannai et al., 2020; Battaglia et al., 2018; Petrini et al., 2014). Hence, 'hetero-alpha' $GABA_ARs$ could contribute to macroscopic changes induced during LTP, alongside 'homo-alpha' $GABA_ARs$.

This work focused on establishing the existence, abundance and function of 'hetero-alpha' α1α2-containing $GABA_ARs$, however as previously mentioned, there is evidence that other α subunit combinations may exist in the brain (see ***Table 1.2***). To add to the complexity, some studies proposed the existence of 'hetero-beta' $GABA_ARs$ (Jechlinger et al., 1998; Li and De Blas, 1997) and in our study the β subunit influenced the properties of hetero-alpha receptors. This further adds to the complexity of $GABA_ARs$ expression and function. It is possible that receptors with five distinct subunits, where the identity of each subunit as well as their positioning could potentially contribute to the fine-tuning of GABAergic transmission.

6.3 Future directions

6.3.1 Concatenated receptor studies

To study the pharmacological fingerprints of $GABA_A$ receptors with two different isoforms of α or β subunits it is essential to know the predetermined positioning of subunits in a pentameric complex, as the relative positioning of subunits around the channel could influence GABA binding (Baumann et al., 2003). We studied α1α2-containing 'hetero-alpha' $GABA_AR$ in a recombinant HEK293 system, where various stoichiometric subunit combinations could potentially form: α1α1, α1α2, α2α1 and α2α2. However, to establish the GABA affinity and BDZ effects on pure 'hetero-alpha' populations, it is essential to fix the positioning of subunits. Future work would require receptor concatenation, either by using concatenated dimer/trimer mixtures or preferred concatenated pentamers (see ***Section 1.4.2***). By forcing the position of either **α1**γ2β**α2**β or **α2**γ2β**α1**β subunit combinations, we could obtain more insight into the pharmacological properties of such receptors.

6.3.2 Atomic Force and Cryo-electron Microscopy

In this work, we used two different fluorescent imaging-based method: PLA and SpIDA to study stoichiometry of native $GABA_ARs$. However, both of these techniques have limitations preventing clear conclusions on stoichiometry as discussed in ***Sections 4.3.2 and 5.3.3***. A method for direct visualisation of $GABA_ARs$, where specific α subunits could be distinguishable between one another in the same pentamer could be highly useful for future work. One of the possible ways to study receptor stoichiometry is through atomic force microscopy, AFM, previously used to establish the stoichiometry of α1β2γ2 and α4β3δ $GABA_ARs$ (Barrera et al., 2008; Neish et al., 2003). For assessment of stoichiometry by AFM, receptors are firstly purified, decorated with subunit-specific distinguishable sized-tags (eg. antibodies and Fab fragments) and subsequently imaged by a sharp oscillating tip mounted on a

cantilever beam that is scanned across the surface of the sample. Van der Waals forces between the sample and the tip cause deflections of the cantilever, which when raster scanned across the sample surface, produces a 3D topographic map (Barrera et al., 2008). By purifying $GABA_ARs$ from brain lysates and subsequently using anti-α1 antibodies together with anti-α2 Fab fragments, we can decorate native $GABA_ARs$. AFM images should allow us to distinguish between α1α1- (double antibody labelled), α1α2- (antibody and Fab fragment labelled), and α2α2-containing $GABA_ARs$ (double Fab fragment labelled) in the same sample. An alternative approach, also allowing direct visualisation of the receptor complex is to subject hetero-alpha receptors to cryo-EM (Laverty et al., 2019b), which will definitely show if there is a preferred stoichiometry for α1α2 receptors.

6.4 Concluding Remarks

Previously, the existence and functional role of 'hetero-alpha' α1α2-containing $GABA_ARs$ was relatively unexplored. In the present study, we established the expression of such receptors *in vivo* as well as estimated their relative abundance. We also demonstrate that 'hetero-alpha' $GABA_ARs$ are expressed both synaptically and extrasynaptically, and their expression is predominant over α1α1-containing receptors with implications for their activation and pharmacological properties.

Finally, from this study taking all the data into consideration, the functional role of 'hetero-alpha' $GABA_ARs$ appears to be the refinement of GABAergic transmission, rather than an induction of substantial changes. Nevertheless, hetero-alpha $GABA_A$ receptors have the potential to modify the receptor's response to drugs. Finally, we show that 'hetero-alpha' $GABA_AR$ synaptic recruitment occurs upon long-term potentiation induction, suggesting a role of these receptors in synaptic plasticity.

References

Abramian, A.M., Comenencia-Ortiz, E., Modgil, A., Vien, T.N., Nakamura, Y., Moore, Y.E., Maguire, J.L., Terunuma, M., Davies, P.A., Moss, S.J., 2014. Neurosteroids promote phosphorylation and membrane insertion of extrasynaptic $GABA_A$ receptors. PNAS 111, 7132–7137.

Abramian, A.M., Comenencia-Ortiz, E., Vithlani, M., Tretter, E.V., Sieghart, W., Davies, P.A., Moss, S.J., 2010. Protein kinase C phosphorylation regulates membrane insertion of $GABA_A$ receptor subtypes that mediate tonic inhibition. Journal of Biological Chemistry 285, 41795–41805.

Absalom, N.L., Ahring, P.K., Liao, V.W., Balle, T., Jiang, T., Anderson, L.L., Arnold, J.C., McGregor, I.S., Bowen, M.T., Chebib, M., 2019. Functional genomics of epilepsy-associated mutations in the $GABA_A$ receptor subunits reveal that one mutation impairs function and two are catastrophic. Journal of Biological Chemistry 294, 6157–6171.

Adkins, C.E., Pillai, G.V., Kerby, J., Bonnert, T.P., Haldon, C., McKernan, R.M., Gonzalez, J.E., Oades, K., Whiting, P.J., Simpson, P.B., 2001. α4β3δ $GABA_A$ receptors characterized by fluorescence resonance energy transfer-derived measurements of membrane potential. Journal of Biological Chemistry 276, 38934–38939.

Agís-Balboa, R.C., Pinna, G., Zhubi, A., Maloku, E., Veldic, M., Costa, E., Guidotti, A., 2006. Characterization of brain neurons that express enzymes mediating neurosteroid biosynthesis. PNAS 103, 14602–14607.

Ahring, P.K., Liao, V.W.Y., Balle, T., 2018. Concatenated nicotinic acetylcholine receptors: A gift or a curse? Journal of General Physiology 150, 453–473.

Akabas, M.H., Stauffer, D.A., Xu, M., Karlin, A., 1992. Acetylcholine receptor channel structure probed in cysteine-substitution mutants. Science 258, 307–310.

Akk, G., Bracamontes, J., Steinbach, J.H., 2001. Pregnenolone sulfate block of $GABA_A$ receptors: mechanism and involvement of a residue in the M2 region of the α subunit. Journal of Physiology 532, 673–684.

Angelotti, T.P., Macdonald, R.L., 1993. Assembly of $GABA_A$ receptor subunits: α1β1 and α1β1γ2S subunits produce unique ion channels with dissimilar single-channel properties. Journal of Neuroscience 13, 1429–1440.

Angers, S., Salahpour, A., Joly, E., Hilairet, S., Chelsky, D., Dennis, M., Bouvier, M., 2000. Detection of β2-adrenergic receptor dimerization in living cells using bioluminescence resonance energy transfer (BRET). PNAS 97, 3684–3689.

Arama, J., Abitbol, K., Goffin, D., Fuchs, C., Sihra, T.S., Thomson, A.M., Jovanovic, J.N., 2015. $GABA_A$ receptor activity shapes the formation of inhibitory synapses between developing medium spiny neurons. Frontiers in Cellular Neuroscience 9, 290.

Arancibia-Cárcamo, I.L., Kittler, J.T., 2009. Regulation of $GABA_A$ receptor membrane trafficking and synaptic localization. Pharmacological Therapeutics 123, 17–31.

Araujo, F., Ruano, D., Vitorica, J., 1999. Native γ-aminobutyric acid type A receptors from rat hippocampus, containing both α1 and α5 subunits, exhibit a single benzodiazepine binding site with α5 pharmacological properties. Journal of Pharmacology and Experimental Therapeutics 290, 989–997.

Araujo, F., Tan, S., Ruano, D., Schoemaker, H., Benavides, J., Vitorica, J., 1996. Molecular and pharmacological characterization of native cortical γ-aminobutyric acid A receptors containing both α1 and α3 subunits. Journal of Biological Chemistry 271, 27902–27911.

Ardito, F., Giuliani, M., Perrone, D., Troiano, G., Muzio, L.L., 2017. The crucial role of protein phosphorylation in cell signaling and its use as targeted therapy (Review). International Journal of Molecular Medicine 40, 271–280.

Baker, C., Sturt, B.L., Bamber, B.A., 2010. Multiple roles for the first transmembrane domain of $GABA_A$ receptor subunits in neurosteroid modulation and spontaneous channel activity. Neuroscience Lett 473, 242–247.

Balic, E., Rudolph, U., Fritschy, J.-M., Mohler, H., Benke, D., 2009. The α5(H105R) mutation impairs α5 selective binding properties by altered positioning of the α5 subunit in $GABA_A$ receptors containing two distinct types of α subunits. Journal of Neurochemistry 110, 244–254.

Bannai, H., Niwa, F., Sakuragi, S., Mikoshiba, K., 2020. Inhibitory synaptic transmission tuned by Ca^{2+} and glutamate through the control of $GABA_AR$ lateral diffusion dynamics. Development, Growth and Differentiation 62, 398–406.

Barbeau, A., Godin, A.G., Swift, J.L., De Koninck, Y., Wiseman, P.W., Beaulieu, J.-M., 2013a. Chapter Seven - Quantification of receptor tyrosine kinase activation and transactivation by G-protein-coupled receptors using spatial intensity distribution analysis (SpIDA). Methods in Enzymology, G Protein Coupled Receptors. Academic Press, 109–131.

Barbeau, A., Godin, A.G., Swift, J.L., De Koninck, Y., Wiseman, P.W., Beaulieu, J.-M., 2013b. Quantification of receptor tyrosine kinase activation and transactivation by G-

protein-coupled receptors using spatial intensity distribution analysis (SpIDA). Methods in Enzymology 522, 109–131.

Barbeau, A., Swift, J.L., Godin, A.G., De Koninck, Y., Wiseman, P.W., Beaulieu, J.-M., 2013c. Chapter 1 - Spatial Intensity Distribution Analysis (SpIDA): A new tool for receptor tyrosine kinase activation and transactivation quantification, in: Conn, P.M. (Ed.), Methods in Cell Biology, Receptor-Receptor Interactions. Academic Press, 1–19.

Barnard, E.A., Skolnick, P., Olsen, R.W., Mohler, H., Sieghart, W., Biggio, G., Braestrup, C., Bateson, A.N., Langer, S.Z., 1998. International Union of Pharmacology. XV. Subtypes of γ-aminobutyric acid A receptors: classification on the basis of subunit structure and receptor function. Pharmacological Review 50, 291–314.

Barrera, N.P., Betts, J., You, H., Henderson, R.M., Martin, I.L., Dunn, S.M.J., Edwardson, J.M., 2008. Atomic force microscopy reveals the stoichiometry and subunit arrangement of the α4β3δ $GABA_A$ receptor. Molecular Pharmacology. 73, 960–967.

Battaglia, S., Renner, M., Russeau, M., Côme, E., Tyagarajan, S.K., Lévi, S., 2018. Activity-dependent inhibitory synapse scaling is determined by gephyrin phosphorylation and subsequent regulation of $GABA_A$ receptor diffusion. eNeuro 5.

Baulieu, E.E., Robel, P., Schumacher, M., 2001. Neurosteroids: beginning of the story. International Review in Neurobiology 46, 1–32.

Baumann, S.W., Baur, R., Sigel, E., 2003. Individual properties of the two functional agonist sites in $GABA_A$ receptors. Journal of Neuroscience. 23, 11158–11166.

Baumann, S.W., Baur, R., Sigel, E., 2002. Forced subunit assembly in α1β2γ2 $GABA_A$ receptors. Insight into the absolute arrangement. Journal of Biological Chemistry 277, 46020–46025.

Baumann, S.W., Baur, R., Sigel, E., 2001. Subunit arrangement of γ-aminobutyric acid type A receptors. Journal of Biological Chemistry 276, 36275–36280.

Baur, R., Tan, K.R., Lüscher, B.P., Gonthier, A., Goeldner, M., Sigel, E., 2008. Covalent modification of $GABA_A$ receptor isoforms by a diazepam analogue provides evidence for a novel benzodiazepine binding site that prevents modulation by these drugs. Journal of Neurochemistry 106, 2353–2363.

Belelli, D., Casula, A., Ling, A., Lambert, J.J., 2002. The influence of subunit composition on the interaction of neurosteroids with $GABA_A$ receptors. Neuropharmacology 43, 651–661.

Belelli, D., Lambert, J.J., Peters, J.A., Wafford, K., Whiting, P.J., 1997. The interaction of the general anesthetic etomidate with the γ-aminobutyric acid type A receptor is influenced by a single amino acid. PNAS 94, 11031–11036.

Ben-Ari, Y., Gaiarsa, J.-L., Tyzio, R., Khazipov, R., 2007. GABA: a pioneer transmitter that excites immature neurons and generates primitive oscillations. Physiology Review 87, 1215–1284.

Bencsits, E., Ebert, V., Tretter, V., Sieghart, W., 1999. A significant part of native γ-aminobutyric acid A receptors containing α4 subunits do not contain γ or δ subunits. Journal of Biological Chemistry 274, 19613–19616.

Benke, D., Fakitsas, P., Roggenmoser, C., Michel, C., Rudolph, U., Mohler, H., 2004a. Analysis of the presence and abundance of $GABA_A$ receptors containing two different types of α subunits in murine brain using point-mutated α subunits. Journal of Biological Chemistry 279, 43654–43660.

Benke, D., Michel, C., Mohler, H., 1997. $GABA_A$ receptors containing the α4 subunit: prevalence, distribution, pharmacology, and subunit architecture *in situ*. Journal of Neurochemistry 69, 806–814.

Benkwitz, C., Banks, M.I., Pearce, R.A., 2004. Influence of $GABA_A$ receptor γ2 splice variants on receptor kinetics and isoflurane modulation. Anesthesiology 101, 924–936.

Benson, J.A., Löw, K., Keist, R., Mohler, H., Rudolph, U., 1998a. Pharmacology of recombinant γ-aminobutyric acid A receptors rendered diazepam-insensitive by point-mutated α-subunits. FEBS Lett 431, 400–404.

Berg, K.A., Rowan, M.P., Gupta, A., Sanchez, T.A., Silva, M., Gomes, I., McGuire, B.A., Portoghese, P.S., Hargreaves, K.M., Devi, L.A., Clarke, W.P., 2012. Allosteric interactions between δ and κ opioid receptors in peripheral sensory neurons. Molecular Pharmacology 81, 264–272.

Bergmann, R., Kongsbak, K., Sørensen, P.L., Sander, T., Balle, T., 2013. A unified model of the $GABA_A$ receptor comprising agonist and benzodiazepine binding sites. PLOS ONE 8, e52323.

Bianchi, M.T., Macdonald, R.L., 2003. Neurosteroids shift partial agonist activation of $GABA_A$ receptor channels from low- to high-efficacy gating patterns. Journal of Neuroscience 23, 10934–10943.

Blom, N., Sicheritz-Pontén, T., Gupta, R., Gammeltoft, S., Brunak, S., 2004. Prediction of post-translational glycosylation and phosphorylation of proteins from the amino acid sequence. Proteomics 4, 1633–1649.

Bogdanov, Y., Michels, G., Armstrong-Gold, C., Haydon, P.G., Lindstrom, J., Pangalos, M., Moss, S.J., 2006. Synaptic $GABA_A$ receptors are directly recruited from their extrasynaptic counterparts. EMBO J 25, 4381–4389.

Bohlhalter, S., Weinmann, O., Mohler, H., Fritschy, J.-M., 1996. Laminar compartmentalization of $GABA_A$-receptor subtypes in the spinal cord: an immunohistochemical study. The Journal of Neuroscience, 16, 283–97.

Böhme, I., Rabe, H., Lüddens, H., 2004. Four amino acids in the α subunits determine the γ-aminobutyric acid sensitivities of $GABA_A$ receptor subtypes. Journal of Biological Chemistry 279, 35193–35200.

Boileau, A.J., Pearce, R.A., Czajkowski, C., 2005. Tandem subunits effectively constrain $GABA_A$ receptor stoichiometry and recapitulate receptor kinetics but are insensitive to $GABA_A$ receptor-associated protein. Journal of Neuroscience 25, 11219–11230.

Bormann, J., 1991. Electrophysiological characterization of diazepam binding inhibitor (DBI) on $GABA_A$ receptors. Neuropharmacology, Diazepam Binding Inhibitor: A Novel Peptide with Multiple Functions 30, 1387–1389.

Boulineau, N., Baur, R., Minier, F., Sigel, E., 2005. Consequence of the presence of two different β subunit isoforms in a $GABA_A$ receptor. Journal of Neurochemistry 95, 1724–1731.

Bouvier, M., 2001. Oligomerization of G-protein-coupled transmitter receptors. Nature Reviews Neuroscience 2, 274–286.

Bovolin, P., Santi, M.R., Puia, G., Costa, E., Grayson, D., 1992. Expression patterns of γ-aminobutyric acid type A receptor subunit mRNAs in primary cultures of granule neurons and astrocytes from neonatal rat cerebella. PNAS 89, 9344–9348.

Bowery, N.G., Smart, T.G., 2006. GABA and glycine as neurotransmitters: a brief history. British Journal of Pharmacology 147, 109–119.

Brandon, N.J., Delmas, P., Hill, J., Smart, T.G., Moss, S.J., 2001. Constitutive tyrosine phosphorylation of the $GABA_A$ receptor γ2 subunit in rat brain. Neuropharmacology 41, 745–752.

Brandon, N.J., Jovanovic, J.N., Smart, T.G., Moss, S.J., 2002. Receptor for activated C kinase-1 facilitates protein kinase C-dependent phosphorylation and functional modulation of $GABA_A$ receptors with the activation of G-protein-coupled receptors. Journal of Neuroscience 22, 6353–6361.

Brickley, S.G., Cull-Candy, S.G., Farrant, M., 1996. Development of a tonic form of synaptic inhibition in rat cerebellar granule cells resulting from persistent activation of $GABA_A$ receptors. Journal of Physiology 497, 753–759.

Brickley, S.G., Mody, I., 2012. Extrasynaptic $GABA_A$ receptors: Their function in the CNS and implications for disease. Neuron 73, 23–34.

Bright, D.P., Renzi, M., Bartram, J., McGee, T.P., MacKenzie, G., Hosie, A.M., Farrant, M., Brickley, S.G., 2011. Profound desensitization by ambient GABA limits activation of δ-containing $GABA_A$ receptors during spillover. Journal of Neuroscience 31, 753–763.

Bright, D.P., Smart, T.G., 2013. Protein kinase C regulates tonic $GABA_A$ receptor-mediated inhibition in the hippocampus and thalamus. European Journal of Neuroscience 38, 3408–3423.

Brown, N., Kerby, J., Bonnert, T.P., Whiting, P.J., Wafford, K.A., 2002. Pharmacological characterization of a novel cell line expressing human α4β3δ GABAA receptors. British Journal of Pharmacology 136, 965–974.

Buller, A.L., Hastings, G.A., Kirkness, E.F., Fraser, C.M., 1994. Site-directed mutagenesis of N-linked glycosylation sites on the γ-aminobutyric acid type A receptor α1 subunit. Molecular Pharmacology 46, 858–865.

Burckhardt, C.J., Minna, J.D., Danuser, G., 2021. Co-immunoprecipitation and semi-quantitative immunoblotting for the analysis of protein-protein interactions. STAR Protocols 2, 100644.

Burgard, E.C., Tietz, E.I., Neelands, T.R., Macdonald, R.L., 1996. Properties of recombinant γ-aminobutyric acid A receptor isoforms containing the α5 subunit subtype. Molecular Pharmacology 50, 119–127.

Callén, L., Moreno, E., Barroso-Chinea, P., Moreno-Delgado, D., Cortés, A., Mallol, J., Casadó, V., Lanciego, J.L., Franco, R., Lluis, C., Canela, E.I., McCormick, P.J., 2012. Cannabinoid receptors CB1 and CB2 form functional heteromers in brain. Journal of Biological Chemistry 287, 20851–20865.

Caraiscos, V.B., Elliott, E.M., You-Ten, K.E., Cheng, V.Y., Belelli, D., Newell, J.G., Jackson, M.F., Lambert, J.J., Rosahl, T.W., Wafford, K.A., MacDonald, J.F., Orser, B.A., 2004. Tonic inhibition in mouse hippocampal CA1 pyramidal neurons is mediated by α5 subunit-containing γ-aminobutyric acid type A receptors .PNAS 101, 3662–3667.

Carter, C.R.J., Kozuska, J.L., Dunn, S.M.J., 2010. Insights into the structure and pharmacology of $GABA_A$ receptors. Future of Medical Chemistry 2, 859–875.

Carver, C.M., Chuang, S.-H., Reddy, D.S., 2016. Zinc selectively blocks neurosteroid-sensitive extrasynaptic δ $GABA_A$ receptors in the hippocampus. Journal of Neuroscience 36, 8070–8077.

Castillo, P.E., Chiu, C.Q., Carroll, R.C., 2011. Long-term plasticity at inhibitory synapses. Current Opinion in Neurobiology, Synaptic function and regulation 21, 328–338.

Chang, Y., Wang, R., Barot, S., Weiss, D.S., 1996. Stoichiometry of a recombinant $GABA_A$ receptor. Journal of Neuroscience 16, 5415–5424.

Chang, Y., Weiss, D.S., 1999. Allosteric activation mechanism of the α1β2γ2 γ-aminobutyric acid type A receptor revealed by mutation of the conserved M2 leucine. Biophysical Journal 77, 2542–2551.

Chen, L., Wang, H., Vicini, S., Olsen, R.W., 2000. The γ-aminobutyric acid type A ($GABA_A$) receptor-associated protein (GABARAP) promotes $GABA_A$ receptor clustering and modulates the channel kinetics. PNAS 97, 11557–11562.

Chen, Z.-W., Fuchs, K., Sieghart, W., Townsend, R.R., Evers, A.S., 2012a. Deep amino acid sequencing of native brain $GABA_A$ receptors using high-resolution mass spectrometry. Molecular & Cellular Proteomics 11.

Christian, C.A., Herbert, A.G., Holt, R.L., Peng, K., Sherwood, K.D., Pangratz-Fuehrer, S., Rudolph, U., Huguenard, J.R., 2013. Endogenous positive allosteric modulation of $GABA_A$ receptors by diazepam binding inhibitor. Neuron 78, 1063–1074.

Christie, S.B., de Blas, A.L., 2002. α5 subunit-containing $GABA_A$ receptors form clusters at GABAergic synapses in hippocampal cultures. Neuroreport 13, 2355–2358.

Chua, H.C., Chebib, M., 2017. Chapter One - $GABA_A$ receptors and the diversity in their structure and pharmacology, in: Geraghty, D.P., Rash, L.D. (Eds.), Advances in Pharmacology, 1–34.

Cole, R.W., Jinadasa, T., Brown, C.M., 2011. Measuring and interpreting point spread functions to determine confocal microscope resolution and ensure quality control. Nature Protocols 6, 1929–1941.

Collinson, N., Kuenzi, F.M., Jarolimek, W., Maubach, K.A., Cothliff, R., Sur, C., Smith, A., Otu, F.M., Howell, O., Atack, J.R., McKernan, R.M., Seabrook, G.R., Dawson, G.R., Whiting, P.J., Rosahl, T.W., 2002. Enhanced learning and memory and altered GABAergic synaptic transmission in mice lacking the α5 Subunit of the $GABA_A$ receptor. Journal of Neuroscience 22, 5572–5580.

Colquhoun, D., 1998. Binding, gating, affinity and efficacy: the interpretation of structure-activity relationships for agonists and of the effects of mutating receptors. British Journal of Pharmacology 125, 924–947.

Connolly, C.N., Krishek, B.J., McDonald, B.J., Smart, T.G., Moss, S.J., 1996. Assembly and cell surface expression of heteromeric and homomeric γ-aminobutyric acid type A receptors. Journal of Biological Chemistry 271, 89–96.

Connolly, C.N., Uren, J.M., Thomas, P., Gorrie, G.H., Gibson, A., Smart, T.G., Moss, S.J., 1999. Subcellular localization and endocytosis of homomeric γ2 subunit splice variants of γ-aminobutyric acid type A receptors. Molecular Cellular Neuroscience 13, 259–271.

Connolly, C.N., Wafford, K.A., 2004. The Cys-loop superfamily of ligand-gated ion channels: the impact of receptor structure on function. Biochemical Society Transactions 32, 529–534.

Costa, E., Guidotti, A., 1985. Endogenous ligands for benzodiazepine recognition sites. Biochemical Pharmacology 34, 3399–3403.

Cravatt, B.F., Prospero-Garcia, O., Siuzdak, G., Gilula, N.B., Henriksen, S.J., Boger, D.L., Lerner, R.A., 1995. Chemical characterization of a family of brain lipids that induce sleep. Science 268, 1506–1509.

Crestani, F., Keist, R., Fritschy, J.-M., Benke, D., Vogt, K., Prut, L., Blüthmann, H., Möhler, H., Rudolph, U., 2002. Trace fear conditioning involves hippocampal α5 $GABA_A$ receptors. PNAS 99, 8980–8985.

Danglot, L., Triller, A., Bessis, A., 2003. Association of gephyrin with synaptic and extrasynaptic $GABA_A$ receptors varies during development in cultured hippocampal neurons. Molecular and Cellular Neuroscience 23, 264–278.

Datta, D., Arion, D., Lewis, D.A., 2015. Developmental expression eatterns of $GABA_A$ receptor subunits in layer 3 and 5 pyramidal cells of monkey prefrontal cortex. Cerebral Cortex 25, 2295–2305.

Davenport, E.C., Szulc, B.R., Drew, J., Taylor, J., Morgan, T., Higgs, N.F., López-Doménech, G., Kittler, J.T., 2019. Autism and schizophrenia-associated CYFIP1 regulates the balance of synaptic excitation and inhibition. Cell Reports 26, 2037-2051.

Davies, M., Bateson, A.N., Dunn, S.M., 1996. Molecular biology of the $GABA_A$ receptor: functional domains implicated by mutational analysis. Frontiers in Bioscience 1, 214-233.

de Jonge, J.C., Vinkers, C.H., Hulshoff Pol, H.E., Marsman, A., 2017. GABAergic mechanisms in schizophrenia: linking postmortem and *in vivo* studies. Frontiers in Psychiatry 8, 118.

del Río, J.C., Araujo, F., Ramos, B., Ruano, D., Vitorica, J., 2001a. Prevalence between different α subunits performing the benzodiazepine binding sites in native heterologous $GABA_A$ receptors containing the α2 subunit. Journal of Neurochemistry 79, 183–191.

DeLorey, T.M., Handforth, A., Anagnostaras, S.G., Homanics, G.E., Minassian, B.A., Asatourian, A., Fanselow, M.S., Delgado-Escueta, A., Ellison, G.D., Olsen, R.W., 1998. Mice Lacking the β3 subunit of the $GABA_A$ receptor have the epilepsy phenotype and many of the behavioral characteristics of angelman syndrome. Journal of Neuroscience. 18, 8505–8514.

Dias, R., Sheppard, W.F.A., Fradley, R.L., Garrett, E.M., Stanley, J.L., Tye, S.J., Goodacre, S., Lincoln, R.J., Cook, S.M., Conley, R., Hallett, D., Humphries, A.C., Thompson, S.A., Wafford, K.A., Street, L.J., Castro, J.L., Whiting, P.J., Rosahl, T.W., Atack, J.R., McKernan, R.M., Dawson, G.R., Reynolds, D.S., 2005. Evidence for a significant role of α3-containing $GABA_A$ receptors in mediating the anxiolytic effects of benzodiazepines. Journal of Neuroscience 25, 10682–10688.

Dieck, S. tom, Kochen, L., Hanus, C., Bartnik, I., Nassim-Assir, B., Merk, K., Mosler, T., Garg, S., Bunse, S., Tirrell, D.A., Schuman, E.M., 2015. Direct visualization of identified and newly synthesized proteins in situ. Nature Methods 12, 411–414.

Ding, Y., Zheng, Y., Liu, T., Chen, T., Wang, C., Sun, Q., Hua, M., Hua, T., 2017. Changes in GABAergic markers accompany degradation of neuronal function in the primary visual cortex of senescent rats. Science Reports 7, 14897.

Draguhn, A., Verdorn, T.A., Ewert, M., Seeburg, P.H., Sakmann, B., 1990. Functional and molecular distinction between recombinant rat $GABA_A$ receptor subtypes by Zn^{2+}. Neuron 5, 781–788.

Duggan, M.J., Pollard, S., Stephenson, F.A., 1991. Immunoaffinity purification of $GABA_A$ receptor α-subunit iso-oligomers. Demonstration of receptor populations containing α1α2, α1α3, and α2α3 subunit pairs. Journal of Biological Chemistry 266, 24778–24784.

Ebert, B., Thompson, S.A., Saounatsou, K., McKernan, R., Krogsgaard-Larsen, P., Wafford, K.A., 1997. Differences in agonist/antagonist binding affinity and receptor transduction using recombinant human γ-aminobutyric acid type A receptors. Molecular Pharmacology 52, 1150–1156.

Ebert, B., Wafford, K.A., Whiting, P.J., Krogsgaard-Larsen, P., Kemp, J.A., 1994. Molecular pharmacology of γ-aminobutyric acid type A receptor agonists and partial agonists in oocytes injected with different α, β, and γ receptor subunit combinations. Molecular Pharmacology 46, 957–963.

Ehya, N., Sarto, I., Wabnegger, L., Sieghart, W., 2003. Identification of an amino acid sequence within $GABA_A$ receptor β3 subunits that is important for receptor assembly. Journal of Neurochemistry 84, 127–135.

Ericksen, S.S., Boileau, A.J., 2007. Tandem couture: Cys-loop receptor concatamer insights and caveats. Molecular Neurobiology 35, 113–127.

Ernst, M., Bruckner, S., Boresch, S., Sieghart, W., 2005. Comparative models of $GABA_A$ receptor extracellular and transmembrane domains: important insights in pharmacology and function. Molecular Pharmacology 68, 1291–1300.

Essrich, C., Lorez, M., Benson, J.A., Fritschy, J.M., Lüscher, B., 1998. Postsynaptic clustering of major $GABA_A$ receptor subtypes requires the γ2 subunit and gephyrin. Nature Neuroscience 1, 563–571.

Farrant, M., Nusser, Z., 2005. Variations on an inhibitory theme: phasic and tonic activation of $GABA_A$ receptors. Nature Reviews Neuroscience 6, 215–229.

Farrar, S.J., Whiting, P.J., Bonnert, T.P., McKernan, R.M., 1999. Stoichiometry of a ligand-gated ion channel determined by fluorescence energy transfer. Journal of Biological Chemistry 274, 10100–10104.

Farzampour, Z., Reimer, R.J., Huguenard, J., 2015. Endozepines. Advances in Pharmacology 72, 147–164.

Feng, G., Tintrup, H., Kirsch, J., Nichol, M.C., Kuhse, J., Betz, H., Sanes, J.R., 1998. Dual requirement for gephyrin in glycine receptor clustering and molybdoenzyme activity. Science 282, 1321–1324.

Field, M., Dorovykh, V., Thomas, P., Smart, T.G., 2021. Physiological role for $GABA_A$ receptor desensitization in the induction of long-term potentiation at inhibitory synapses. Nature Communications 12, 2112.

Filatov, G.N., White, M.M., 1995. The role of conserved leucines in the M2 domain of the acetylcholine receptor in channel gating. Molecular Pharmacology 48, 379–384.

Fisher, J.L., Macdonald, R.L., 1997. Single channel properties of recombinant $GABA_A$ receptors containing γ2 or δ subtypes expressed with α1 and β3 subtypes in mouse L929 cells. Journal of Physiology 505, 283–297.

Forman, S.A., Miller, K.W., 2016. Mapping general anaesthetic sites in heteromeric γ-aminobutyric acid type A receptors reveals a potential for targeting receptor subtypes. Anaesthesia and Analgesia 123, 1263–1273.

Fritschy, J.M., Benke, D., Mertens, S., Oertel, W.H., Bachi, T., Möhler, H., 1992. Five subtypes of type A γ-aminobutyric acid receptors identified in neurons by double and triple immunofluorescence staining with subunit-specific antibodies. PNAS 89, 6726–6730.

Fritschy, J.M., Mohler, H., 1995. $GABA_A$-receptor heterogeneity in the adult rat brain: differential regional and cellular distribution of seven major subunits. Journal of Computational Neurology 359, 154–194.

Fritschy, J.M., Weinmann, O., Wenzel, A., Benke, D., 1998. Synapse-specific localization of NMDA and $GABA_A$ receptor subunits revealed by antigen-retrieval immunohistochemistry. Journal of Computational Neurology 390, 194–210.

Gaiarsa, J.-L., Caillard, O., Ben-Ari, Y., 2002. Long-term plasticity at GABAergic and glycinergic synapses: mechanisms and functional significance. Trends in Neuroscience 25, 564–570.

Galarreta, M., Hestrin, S., 1997. Properties of $GABA_A$ receptors underlying inhibitory synaptic currents in neocortical pyramidal neurons. Journal of Neuroscience 17, 7220–7227.

Gallagher, M.J., Song, L., Arain, F., Macdonald, R.L., 2004. The juvenile myoclonic epilepsy $GABA_A$ receptor α1 subunit mutation A322D produces asymmetrical, subunit position-dependent reduction of heterozygous receptor currents and α1 subunit protein expression. Journal of Neuroscience 24, 5570–5578.

Gilles, J.-F., Dos Santos, M., Boudier, T., Bolte, S., Heck, N., 2017. DiAna, an ImageJ tool for object-based 3D co-localization and distance analysis. Methods 115, 55–64.

Gingrich, K.J., Roberts, W.A., Kass, R.S., 1995. Dependence of the $GABA_A$ receptor gating kinetics on the α-subunit isoform: implications for structure-function relations and synaptic transmission. Journal of Physiology 489, 529–543.

Godin, A., Swift, J., Doré, K., Sergeev, M., Freland, L., Koninck, Y., Beaulieu, J.-M., Wiseman, P., 2010. Receptor transactivation measured in live cells using spatial intensity distribution analysis (SpIDA). Biophysical Journal - BIOPHYS J 98.

Godin, A.G., Costantino, S., Lorenzo, L.-E., Swift, J.L., Sergeev, M., Ribeiro-da-Silva, A., De Koninck, Y., Wiseman, P.W., 2011. Revealing protein oligomerization and densities *in situ* using spatial intensity distribution analysis. Proceedings of the National Academy of Sciences 108, 7010–7015.

Goldin, M., Segal, M., Avignone, E., 2001. Functional plasticity triggers formation and pruning of dendritic spines in cultured hippocampal networks. Journal of Neuroscience 21, 186–193.

Gomes, I., Ayoub, M.A., Fujita, W., Jaeger, W.C., Pfleger, K.D.G., Devi, L.A., 2016a. G protein-coupled receptor heteromers. Annual Reviews of Pharmacology and Toxicology 56, 403–425.

Gomes, I., Sierra, S., Devi, L.A., 2016b. Detection of receptor heteromerization using *in situ* proximity ligation assay. Current Protocols in Pharmacology 75, 1-31.

Gorrie, G.H., Vallis, Y., Stephenson, A., Whitfield, J., Browning, B., Smart, T.G., Moss, S.J., 1997. Assembly of $GABA_A$ receptors composed of α1 and β2 subunits in both cultured neurons and fibroblasts. Journal of Neuroscience 17, 6587–6596.

Graves, A.R., Moore, S.J., Bloss, E.B., Mensh, B.D., Kath, W.L., Spruston, N., 2012. Hippocampal pyramidal neurons comprise two distinct cell types that are countermodulated by metabotropic receptors. Neuron 76, 776–789.

Guidotti, A., Forchetti, C.M., Corda, M.G., Konkel, D., Bennett, C.D., Costa, E., 1983. Isolation, characterization, and purification to homogeneity of an endogenous polypeptide with agonistic action on benzodiazepine receptors. PNAS 80, 3531–3535.

Günther, U., Benson, J., Benke, D., Fritschy, J.M., Reyes, G., Knoflach, F., Crestani, F., Aguzzi, A., Arigoni, M., Lang, Y., Bluethmann, H., Mohler, H., Lüscher, B., 1995. Benzodiazepine-insensitive mice generated by targeted disruption of the γ2 subunit gene of γ-aminobutyric acid type A receptors. PNAS 92, 7749–7753.

Haas, K.F., Macdonald, R.L., 1999. $GABA_A$ receptor subunitγ2 and δ subtypes confer unique kinetic properties on recombinant $GABA_A$ receptor currents in mouse fibroblasts. Journal of Physiology 514, 27–45.

Halff, E.F., Hannan, S., Smart, T.G., Kittler, J.T., 2020. PKA-mediated phosphorylation of Neuroligin-2 regulates its cell surface expression and synaptic stabilisation (preprint). Neuroscience.

Halliwell, R.F., Thomas, P., Patten, D., James, C.H., Martinez-Torres, A., Miledi, R., Smart, T.G., 1999. Subunit-selective modulation of $GABA_A$ receptors by the non-steroidal anti-inflammatory agent, mefenamic acid. European Journal of Neuroscience 11, 2897–2905.

Hansen, Suzanne L, Ebert, B., Fjalland, B., Kristiansen, U., 2001. Effects of $GABA_A$ receptor partial agonists in primary cultures of cerebellar granule neurons and cerebral cortical neurons reflect different receptor subunit compositions. British Journal of Pharmacology 133, 539–549.

Hansen, S. L., Ebert, B., Fjalland, B., Kristiansen, U., 2001. Effects of $GABA_A$ receptor partial agonists in primary cultures of cerebellar granule neurons and cerebral cortical

neurons reflect different receptor subunit compositions. British Journal of Pharmacology 133, 539–549.

Harney, S.C., Frenguelli, B.G., Lambert, J.J., 2003. Phosphorylation influences neurosteroid modulation of synaptic $GABA_A$ receptors in rat CA1 and dentate gyrus neurones. Neuropharmacology 45, 873–883.

Harvey, R.J., Chinchetru, M.A., Darlison, M.G., 1994. Alternative splicing of a 51-nucleotide exon that encodes a putative protein kinase C phosphorylation site generates two forms of the chicken γ-aminobutyric acid A receptor β2 subunit. Journal of Neurochemistry 62, 10–16.

Harvey, V.L., Duguid, I.C., Krasel, C., Stephens, G.J., 2006. Evidence that GABA ρ subunits contribute to functional ionotropic GABA receptors in mouse cerebellar Purkinje cells. The Journal of Physiology 577, 127–139.

Heintzmann, R., Huser, T., 2017. Super-resolution structured illumination microscopy. Chemistry Review 117, 13890–13908.

Herd, M.B., Haythornthwaite, A.R., Rosahl, T.W., Wafford, K.A., Homanics, G.E., Lambert, J.J., Belelli, D., 2008. The expression of $GABA_AR$ β subunit isoforms in synaptic and extrasynaptic receptor populations of mouse dentate gyrus granule cells. Journal of Physiology 586, 989–1004.

Hevers, W., Lüddens, H., 1998. The diversity of $GABA_A$ receptors. Pharmacological and electrophysiological properties of $GABA_A$ channel subtypes. Molecular Neurobiology 18, 35–86.

Hoestgaard-Jensen, K., O'Connor, R.M., Dalby, N.O., Simonsen, C., Finger, B.C., Golubeva, A., Hammer, H., Bergmann, M.L., Kristiansen, U., Krogsgaard-Larsen, P., Bräuner-Osborne, H., Ebert, B., Frølund, B., Cryan, J.F., Jensen, A.A., 2013. The orthosteric GABAA receptor ligand Thio-4-PIOL displays distinctly different functional properties at synaptic and extrasynaptic receptors. British Journal of Pharmacology 170, 919–932.

Hörtnagl, H., Tasan, R.O., Wieselthaler, A., Kirchmair, E., Sieghart, W., Sperk, G., 2013. Patterns of mRNA and protein expression for 12 $GABA_A$ receptor subunits in the mouse brain. Neuroscience 236, 345–372.

Hosie, A.M., Clarke, L., da Silva, H., Smart, T.G., 2009. Conserved site for neurosteroid modulation of $GABA_A$ receptors. Neuropharmacology 56, 149–154.

Hosie, A.M., Dunne, E.L., Harvey, R.J., Smart, T.G., 2003. Zinc-mediated inhibition of $GABA_A$ receptors: discrete binding sites underlie subtype specificity. Nature Neuroscience 6, 362–369.

Hosie, A.M., Wilkins, M.E., da Silva, H.M.A., Smart, T.G., 2006. Endogenous neurosteroids regulate $GABA_A$ receptors through two discrete transmembrane sites. Nature 444, 486–489.

Hosie, A.M., Wilkins, M.E., Smart, T.G., 2007. Neurosteroid binding sites on $GABA_A$ receptors. Pharmacology & Therapeutics, Neurosteroids Special Issue 116, 7–19.

Houston, C.M., He, Q., Smart, T.G., 2009. CaMKII phosphorylation of the $GABA_A$ receptor: receptor subtype- and synapse-specific modulation. Journal of Physiology 587, 2115–2125.

Houston, C.M., Lee, H.H.C., Hosie, A.M., Moss, S.J., Smart, T.G., 2007. Identification of the sites for CaMKII-dependent phosphorylation of $GABA_A$ receptors. Journal of Biological Chemistry 282, 17855–17865.

Houston, C.M., Smart, T.G., 2006. CaMKII modulation of $GABA_A$ receptors expressed in HEK293, NG108-15 and rat cerebellar granule neurons. European Journal of Neuroscience 24, 2504–2514.

Humpolickova, J., Benda, A., Enderlein, J., 2009. Optical saturation as a versatile tool to enhance resolution in confocal microscopy. Biophysical Journal 97, 2623–2629.

Hutcheon, B., Fritschy, J.M., Poulter, M.O., 2004. Organization of $GABA_A$ receptor α-subunit clustering in the developing rat neocortex and hippocampus. European Journal of Neuroscience 19, 2475–2487.

Im, W.B., Pregenzer, J.F., Binder, J.A., Dillon, G.H., Alberts, G.L., 1995. Chloride channel expression with the tandem construct of α6β2 $GABA_A$ receptor subunit requires a monomeric subunit of α6 or γ2. Journal of Biological Chemitry 270, 26063–26066.

Jacob, T.C., Moss, S.J., Jurd, R., 2008. $GABA_A$ receptor trafficking and its role in the dynamic modulation of neuronal inhibition. Nature Reviews Neuroscience 9, 331–343.

Jaeger, W., Armstrong, S., Hill, S., Pfleger, K., 2014. Biophysical detection of diversity and bias in GPCR function. Frontiers in Endocrinology 5.

Jansen, M., 2019. An in-depth structural view of a $GABA_A$ brain receptor. Nature 565, 436–438.

Jayakar, S.S., Zhou, X., Savechenkov, P.Y., Chiara, D.C., Desai, R., Bruzik, K.S., Miller, K.W., Cohen, J.B., 2015. Positive and negative allosteric modulation of an α1β3γ2 γ-

aminobutyric acid type A ($GABA_A$) receptor by binding to a site in the transmembrane domain at the γ+-β- Interface. Journal of Biological Chemistry 290, 23432–23446.

Jechlinger, M., Pelz, R., Tretter, V., Klausberger, T., Sieghart, W., 1998. Subunit composition and quantitative importance of hetero-oligomeric receptors: $GABA_A$ receptors containing α6 subunits. Journal of Neuroscience 18, 2449–2457.

Johnston, G.A.R., 2014. Muscimol as an ionotropic GABA receptor agonist. Neurochemical Reseach 39, 1942–1947.

Johnston, G.A.R., 2013. Advantages of an antagonist: bicuculline and other GABA antagonists. British Journal of Pharmacology 169, 328–336.

Johnston, G.A.R., 1996. $GABA_A$ receptor pharmacology. Pharmacology & Therapeutics 69, 173–198.

Jones, A., Korpi, E.R., McKernan, R.M., Pelz, R., Nusser, Z., Mäkelä, R., Mellor, J.R., Pollard, S., Bahn, S., Stephenson, F.A., Randall, A.D., Sieghart, W., Somogyi, P., Smith, A.J., Wisden, W., 1997. Ligand-gated ion channel subunit partnerships: $GABA_A$ receptor α6 subunit gene inactivation inhibits δ subunit expression. Journal of Neuroscience 17, 1350–1362.

Jovanovic, J.N., Thomas, P., Kittler, J.T., Smart, T.G., Moss, S.J., 2004. Brain-derived neurotrophic factor modulates fast synaptic inhibition by regulating $GABA_A$ receptor phosphorylation, activity, and cell-surface stability. Journal of Neuroscience 24, 522–530.

Ju, Y.H., Guzzo, A., Chiu, M.W., Taylor, P., Moran, M.F., Gurd, J.W., MacDonald, J.F., Orser, B.A., 2009. Distinct properties of murine α5 γ-aminobutyric acid type A receptor revealed by biochemical fractionation and mass spectroscopy. Journal of Neuroscience Research 87, 1737–1747.

Juge, N., Muroyama, A., Hiasa, M., Omote, H., Moriyama, Y., 2009. Vesicular inhibitory amino acid transporter Is a Cl^-/γ-aminobutyrate co-transporter. Journal of Biological Chemistry 284, 35073–35078.

Julenius, K., Mølgaard, A., Gupta, R., Brunak, S., 2005. Prediction, conservation analysis, and structural characterization of mammalian mucin-type O-glycosylation sites. Glycobiology 15, 153–164.

Kasugai, Y., Swinny, J.D., Roberts, J.D.B., Dalezios, Y., Fukazawa, Y., Sieghart, W., Shigemoto, R., Somogyi, P., 2010. Quantitative localisation of synaptic and extrasynaptic $GABA_A$ receptor subunits on hippocampal pyramidal cells by freeze-fracture replica immunolabelling. European Journal of Neuroscience 32, 1868–1888.

Kellenberger, S., Malherbe, P., Sigel, E., 1992. Function of the α1β2γ2S γ-aminobutyric acid type A receptor is modulated by protein kinase C *via* multiple phosphorylation sites. Journal of Biological Chemistry 267, 25660–25663.

Keramidas, A., Moorhouse, A.J., Schofield, P.R., Barry, P.H., 2004. Ligand-gated ion channels: mechanisms underlying ion selectivity. Progress Biophysics and Molecula Biology 86, 161–204.

Kerppola, T.K., 2006. Complementary methods for studies of protein interactions in living cells. Nature Methods 3, 969–971.

Khan, Z.U., Gutiérrez, A., De Blas, A.L., 1996. The α1 and α6 subunits can coexist in the same cerebellar $GABA_A$ receptor maintaining their individual benzodiazepine-binding specificities. Journal of Neurochemistry 66, 685–691.

Killisch, I., Dotti, C.G., Laurie, D.J., Lüddens, H., Seeburg, P.H., 1991. Expression patterns of $GABA_A$ receptor subtypes in developing hippocampal neurons. Neuron 7, 927–936.

Kittler, J.T., Chen, G., Honing, S., Bogdanov, Y., McAinsh, K., Arancibia-Carcamo, I.L., Jovanovic, J.N., Pangalos, M.N., Haucke, V., Yan, Z., Moss, S.J., 2005. Phospho-dependent binding of the clathrin AP2 adaptor complex to $GABA_A$ receptors regulates the efficacy of inhibitory synaptic transmission. PNAS 102, 14871–14876.

Kittler, J.T., Delmas, P., Jovanovic, J.N., Brown, D.A., Smart, T.G., Moss, S.J., 2000. Constitutive endocytosis of $GABA_A$ receptors by an association with the adaptin AP2 complex modulates inhibitory synaptic currents in hippocampal neurons. Journal of Neuroscience 20, 7972–7977.

Kittler, J.T., Moss, S.J., 2003. Modulation of $GABA_A$ receptor activity by phosphorylation and receptor trafficking: implications for the efficacy of synaptic inhibition. Current Opinion in Neurobiology 13, 341–347.

Klausberger, T., Fuchs, K., Mayer, B., Ehya, N., Sieghart, W., 2000. $GABA_A$ receptor assembly. Identification and structure of γ2 sequences forming the intersubunit contacts with α1 and β3 subunits. Journal of Biological Chemistry 275, 8921–8928.

Kleingoor, C., Wieland, H.A., Korpi, E.R., Seeburg, P.H., Kettenmann, H., 1993. Current potentiation by diazepam but not GABA sensitivity is determined by a single histidine residue. Neuroreports 4, 187–190.

Kneussel, M., Brandstätter, J.H., Laube, B., Stahl, S., Müller, U., Betz, H., 1999. Loss of postsynaptic $GABA_A$ receptor clustering in gephyrin-deficient mice. Journal of Neuroscience 19, 9289–9297.

Knoflach, F., Benke, D., Wang, Y., Scheurer, L., Lüddens, H., Hamilton, B.J., Carter, D.B., Mohler, H., Benson, J.A., 1996. Pharmacological modulation of the diazepam-insensitive recombinant γ-aminobutyric acid A receptors α4β2γ2 and α6β2γ2. Molecular Pharmacology 50, 1253–1261.

Koos, B., Andersson, L., Clausson, C.-M., Grannas, K., Klaesson, A., Cane, G., Söderberg, O., 2014. Analysis of protein interactions *in situ* by proximity ligation assays. Current Topics in Microbiology and Immunology 377, 111–126.

Korpi, E.R., Gründer, G., Lüddens, H., 2002. Drug interactions at $GABA_A$ receptors. Progress in Neurobiology 67, 113–159.

Korpi, E.R., Seeburg, P.H., 1993. Natural mutation of $GABA_A$ receptor α6 subunit alters benzodiazepine affinity but not allosteric GABA effects. European Journal of Pharmacology 247, 23–27.

Korshoej, A., Holm, M., Jensen, K., Lambert, J., 2010. Kinetic analysis of evoked IPSCs discloses mechanism of antagonism of synaptic $GABA_A$ receptors by picrotoxin. British Journal of Pharmacology 159, 636–649.

Koulen, P., Brandstätter, J.H., Enz, R., Bormann, J., Wässle, H., 1998. Synaptic clustering of $GABA_C$ receptor ρ-subunits in the rat retina. European Journal of Neuroscience 10, 115–127.

Krishek, B.J., Moss, S.J., Smart, T.G., 1996a. Homomeric β1 γ-aminobutyric acid A receptor-ion channels: evaluation of pharmacological and physiological properties. Molecular Pharmacology 49, 494–504.

Krishek, B.J., Moss, S.J., Smart, T.G., 1996b. A functional comparison of the antagonists bicuculline and picrotoxin at recombinant $GABA_A$ receptors. Neuropharmacology 35, 1289–1298.

Krishek, B.J., Xie, X., Blackstone, C., Huganir, R.L., Moss, S.J., Smart, T.G., 1994. Regulation of $GABA_A$ receptor function by protein kinase C phosphorylation. Neuron 12, 1081–1095.

Krogsgaard-Larsen, P., Frølund, B., Liljefors, T., 2002. Specific $GABA_A$ agonists and partial agonists. The Chemical Record 2, 419–430.

Labarca, C., Nowak, M.W., Zhang, H., Tang, L., Deshpande, P., Lester, H.A., 1995. Channel gating governed symmetrically by conserved leucine residues in the M2 domain of nicotinic receptors. Nature 376, 514–516.

Laurie, D.J., Seeburg, P.H., Wisden, W., 1992. The distribution of 13 $GABA_A$ receptor subunit mRNAs in the rat brain. II. Olfactory bulb and cerebellum. Journal of Neuroscience 12, 1063–1076.

Laverty, D., Desai, R., Uchański, T., Masiulis, S., Stec, W.J., Malinauskas, T., Zivanov, J., Pardon, E., Steyaert, J., Miller, K.W., Aricescu, A.R., 2019a. Cryo-EM structure of the human α1β3γ2 $GABA_A$ receptor in a lipid bilayer. Nature 565, 516–520.

Laverty, D., Thomas, P., Field, M., Andersen, O.J., Gold, M.G., Biggin, P.C., Gielen, M., Smart, T.G., 2017. Crystal structures of a $GABA_A$-receptor chimera reveal new endogenous neurosteroid-binding sites. Nature Structural and Molecular Biology 24, 977–985.

Lavoie, A.M., Tingey, J.J., Harrison, N.L., Pritchett, D.B., Twyman, R.E., 1997. Activation and deactivation rates of recombinant $GABA_A$ receptor channels are dependent on α-subunit isoform. Biophysical Journal 73, 2518–2526.

Lecat-Guillet, N., Monnier, C., Rovira, X., Kniazeff, J., Lamarque, L., Zwier, J.M., Trinquet, E., Pin, J.-P., Rondard, P., 2017. FRET-based sensors unravel activation and allosteric modulation of the $GABA_B$ receptor. Cell Chemical Biology 24, 360–370.

Lester, H.A., 1992. The permeation pathway of neurotransmitter-gated ion channels. Annual Reviews in Biophysical and Biomolecular Structure 21, 267–292.

Li, M., De Blas, A.L., 1997. Coexistence of two β subunit isoforms in the same γ-aminobutyric acid type A receptor. Journal of Biological Chemistry 272, 16564–16569.

Liao, D., Scannevin, R.H., Huganir, R., 2001. Activation of silent synapses by rapid activity-dependent synaptic recruitment of AMPA receptors. Journal of Neuroscience 21, 6008–6017.

Liao, V.W.Y., Kusay, A.S., Balle, T., Ahring, P.K., 2020. Heterologous expression of concatenated nicotinic ACh receptors: pros and cons of subunit concatenation and recommendations for construct designs. British Journal of Pharmacology 177, 4275–4295.

Lo, W., Lagrange, A.H., Hernandez, C.C., Harrison, R., Dell, A., Haslam, S.M., Sheehan, J.H., Macdonald, R.L., 2010. Glycosylation of β2 subunits regulates $GABA_A$ receptor biogenesis and channel gating. Journal of Biological Chemistry 285, 31348–31361.

Lorenzo, L.-E., Godin, A.G., Ferrini, F., Bachand, K., Plasencia-Fernandez, I., Labrecque, S., Girard, A.A., Boudreau, D., Kianicka, I., Gagnon, M., Doyon, N., Ribeiro-da-Silva, A., De Koninck, Y., 2020. Enhancing neuronal chloride extrusion rescues α2/α3 $GABA_A$-mediated analgesia in neuropathic pain. Nature Communications 11, 869.

Löw, K., Crestani, F., Keist, R., Benke, D., Brünig, I., Benson, J.A., Fritschy, J.M., Rülicke, T., Bluethmann, H., Möhler, H., Rudolph, U., 2000. Molecular and neuronal substrate for the selective attenuation of anxiety. Science 290, 131–134.

Lu, W., Man, H., Ju, W., Trimble, W.S., MacDonald, J.F., Wang, Y.T., 2001. Activation of synaptic NMDA receptors induces membrane insertion of new AMPA receptors and LTP in cultured hippocampal neurons. Neuron 29, 243–254.

Macdonald, R.L., Kang, J.-Q., Gallagher, M.J., 2010. Mutations in $GABA_A$ receptor subunits associated with genetic epilepsies. Journal of Physiology 588, 1861–1869.

Macdonald, R.L., Rogers, C.J., Twyman, R.E., 1989. Kinetic properties of the $GABA_A$ receptor main conductance state of mouse spinal cord neurones in culture. Journal of Physiology 410, 479–499.

Maric, H.M., Hausrat, T.J., Neubert, F., Dalby, N.O., Doose, S., Sauer, M., Kneussel, M., Strømgaard, K., 2017. Gephyrin-binding peptides visualize postsynaptic sites and modulate neurotransmission. Nature Chemical Biology 13, 153–160.

Maric, H.M., Kasaragod, V.B., Hausrat, T.J., Kneussel, M., Tretter, V., Strømgaard, K., Schindelin, H., 2014. Molecular basis of the alternative recruitment of $GABA_A$ versus glycine receptors through gephyrin. Nature Communications 5, 5767.

Marques, T.R., Ashok, A.H., Angelescu, I., Borgan, F., Myers, J., Lingford-Hughes, A., Nutt, D.J., Veronese, M., Turkheimer, F.E., Howes, O.D., 2021. $GABA_A$ receptor differences in schizophrenia: a positron emission tomography study using [11C]Ro154513. Molecular Psychiatry 26, 2616–2625.

Marsden, K.C., Beattie, J.B., Friedenthal, J., Carroll, R.C., 2007. NMDA receptor activation potentiates inhibitory transmission through GABA receptor-associated protein-dependent exocytosis of $GABA_A$ receptors. Journal of Neuroscience 27, 14326–14337.

Martenson, J.S., Yamasaki, T., Chaudhury, N.H., Albrecht, D., Tomita, S., 2017. Assembly rules for $GABA_A$ receptor complexes in the brain. eLife 6, e27443.

Masiulis, S., Desai, R., Uchański, T., Serna Martin, I., Laverty, D., Karia, D., Malinauskas, T., Zivanov, J., Pardon, E., Kotecha, A., Steyaert, J., Miller, K.W., Aricescu, A.R., 2019a. $GABA_A$ receptor signalling mechanisms revealed by structural pharmacology. Nature 565, 454–459.

Matthews, C., Cordelieres, F.P., 2022. MetroloJ: an ImageJ plugin to help monitor microscopes' health. 6.

McClellan, A.M., Twyman, R.E., 1999. Receptor system response kinetics reveal functional subtypes of native murine and recombinant human $GABA_A$ receptors. Journal of Physiology 515, 711–727.

McDonald, B.J., Amato, A., Connolly, C.N., Benke, D., Moss, S.J., Smart, T.G., 1998. Adjacent phosphorylation sites on $GABA_A$ receptor β subunits determine regulation by cAMP-dependent protein kinase. Nature Neuroscience 1, 23–28.

McDonald, B.J., Moss, S.J., 1997. Conserved phosphorylation of the intracellular domains of $GABA_A$ receptor β2 and β3 subunits by cAMP-dependent protein kinase, cGMP-dependent protein kinase protein kinase C and Ca^{2+}/calmodulin type II-dependent protein kinase. Neuropharmacology 36, 1377–1385.

McDonald, B.J., Moss, S.J., 1994. Differential phosphorylation of intracellular domains of γ-aminobutyric acid type A receptor subunits by calcium/calmodulin type 2-dependent protein kinase and cGMP-dependent protein kinase. Journal of Biological Chemistry 269, 18111–18117.

McKernan, R.M., Rosahl, T.W., Reynolds, D.S., Sur, C., Wafford, K.A., Atack, J.R., Farrar, S., Myers, J., Cook, G., Ferris, P., Garrett, L., Bristow, L., Marshall, G., Macaulay, A., Brown, N., Howell, O., Moore, K.W., Carling, R.W., Street, L.J., Castro, J.L., Ragan, C.I., Dawson, G.R., Whiting, P.J., 2000. Sedative but not anxiolytic properties of benzodiazepines are mediated by the $GABA_A$ receptor α1 subtype. Nature Neuroscience 3, 587–592.

McKernan, R.M., Whiting, P.J., 1996. Which $GABA_A$-receptor subtypes really occur in the brain? Trends in Neuroscience 19, 139–143.

Mertens, S., Benke, D., Mohler, H., 1993. $GABA_A$ receptor populations with novel subunit combinations and drug binding profiles identified in brain by α5- and δ-subunit-specific immunopurification. Journal of Biological Chemitry 268, 5965–5973.

Michels, G., Moss, S.J., 2007. $GABA_A$ receptors: properties and trafficking. Critical Reviews in Biochemical and Molecular Biology 42, 3–14.

Middendorp, S.J., Hurni, E., Schönberger, M., Stein, M., Pangerl, M., Trauner, D., Sigel, E., 2014. Relative positioning of classical benzodiazepines to the γ2-subunit of $GABA_A$ receptors. ACS Chemistry and Biology 9, 1846–1853.

Miller, C., 1989. Genetic manipulation of ion channels: a new approach to structure and mechanism. Neuron 2, 1195–1205.

Miller, P.S., Aricescu, A.R., 2014. Crystal structure of a human $GABA_A$ receptor. Nature 512, 270–275.

Miller, P.S., Scott, S., Masiulis, S., De Colibus, L., Pardon, E., Steyaert, J., Aricescu, A.R., 2017. Structural basis for $GABA_A$ receptor potentiation by neurosteroids. Nature Structe and Molecular Biology 24, 986–992.

Miller, P.S., Smart, T.G., 2010. Binding, activation and modulation of Cys-loop receptors. Trends in Pharmacological Science 31, 161–174.

Milligan, C., Buckley, N., Garret, M., Deuchars, J., Deuchars, S., 2004. Evidence for inhibition mediated by co-assembly of $GABA_A$ and $GABA_C$ receptor subunits in native central neurons. The Journal of neuroscience: the official journal of the Society for Neuroscience 24, 7241–50.

Minier, F., Sigel, E., 2004a. Positioning of the α-subunit isoforms confers a functional signature to γ-aminobutyric acid type A receptors. PNAS 101, 7769–7774.

Minier, F., Sigel, E., 2004b. Techniques: use of concatenated subunits for the study of ligand-gated ion channels. Trends in Pharmacological Science 25, 499–503.

Minier, F., Sigel, E., 2004c. Positioning of the α-subunit isoforms confers a functional signature to γ-aminobutyric acid type A receptors. PNAS 101, 7769–7774.

Mody, I., 2001. Distinguishing between $GABA_A$ receptors responsible for tonic and phasic conductances. Neurochemical Research 26, 907–913.

Möhler, H., 2006. $GABA_A$ receptor diversity and pharmacology. Cell Tissue Research 326, 505–516.

Mohorko, E., Glockshuber, R., Aebi, M., 2011. Oligosaccharyltransferase: the central enzyme of N-linked protein glycosylation. Journal of Inherited Metabolic Disease 34, 869–878.

Molnár, E., 2011. Long-term potentiation in cultured hippocampal neurons. Seminars in Cell and Developmental Biology 22, 506–513.

Mortensen, M., Ebert, B., Wafford, K., Smart, T.G., 2010. Distinct activities of GABA agonists at synaptic- and extrasynaptic-type $GABA_A$ receptors. Journal of Physiology 588, 1251–1268.

Mortensen, M., Frølund, B., Jørgensen, A.T., Liljefors, T., Krogsgaard-Larsen, P., Ebert, B., 2002. Activity of novel 4-PIOL analogues at human $\alpha1\beta2\gamma2S$ $GABA_A$ receptors-correlation with hydrophobicity. European Journal of Pharmacology 451, 125–132.

Mortensen, M., Patel, B., Smart, T., 2012. GABA Potency at $GABA_A$ Receptors Found in Synaptic and Extrasynaptic Zones. Frontiers in Cellular Neuroscience 6.

Mortensen, M., Smart, T.G., 2006. Extrasynaptic αβ subunit $GABA_A$ receptors on rat hippocampal pyramidal neurons. Journal of Physiology 577, 841–856.

Moss, S.J., Doherty, C.A., Huganir, R.L., 1992a. Identification of the cAMP-dependent protein kinase and protein kinase C phosphorylation sites within the major intracellular domains of the β1, γ2S, and γ2L subunits of the γ-aminobutyric acid type A receptor. Journal of Biological Chemistry 267, 14470–14476.

Moss, S.J., Gorrie, G.H., Amato, A., Smart, T.G., 1995. Modulation of $GABA_A$ receptors by tyrosine phosphorylation. Nature 377, 344–348.

Moss, S.J., Smart, T.G., 2001. Constructing inhibitory synapses. Nature Reviews Neuroscience 2, 240–250.

Moss, S.J., Smart, T.G., 1996. Modulation of amino acid-gated ion channels by protein phosphorylation. International Reviews in Neurobiology 39, 1–52.

Moss, S.J., Smart, T.G., Blackstone, C.D., Huganir, R.L., 1992b. Functional modulation of $GABA_A$ receptors by cAMP-dependent protein phosphorylation. Science 257, 661–665.

Mueller, T.M., Haroutunian, V., Meador-Woodruff, J.H., 2014. N-glycosylation of $GABA_A$ receptor subunits is altered in schizophrenia. Neuropsychopharmacology 39, 528–537.

Muir, J., Arancibia-Carcamo, I.L., MacAskill, A.F., Smith, K.R., Griffin, L.D., Kittler, J.T., 2010. NMDA receptors regulate $GABA_A$ receptor lateral mobility and clustering at inhibitory synapses through serine 327 on the γ2 subunit. PNAS 107, 16679–16684.

Mukherjee, J., Kretschmannova, K., Gouzer, G., Maric, H.-M., Ramsden, S., Tretter, V., Harvey, K., Davies, P.A., Triller, A., Schindelin, H., Moss, S.J., 2011. The residence time of $GABA_A$Rs at inhibitory synapses is determined by direct binding of the receptor α1 subunit to gephyrin. Journal of Neuroscience 31, 14677–14687.

Nagaya, N., Macdonald, R.L., 2001. Two γ2L subunit domains confer low Zn^{2+} sensitivity to ternary $GABA_A$ receptors. Journal of Physiology 532, 17–30.

Nakamura, Y., Darnieder, L.M., Deeb, T.Z., Moss, S.J., 2015. Regulation of $GABA_A$Rs by phosphorylation. Advances in Pharmacology 72, 97–146.

Nakamura, Y., Morrow, D.H., Modgil, A., Huyghe, D., Deeb, T.Z., Lumb, M.J., Davies, P.A., Moss, S.J., 2016. Proteomic characterization of inhibitory synapses using a novel pHluorin-tagged γ-aminobutyric acid receptor, type A ($GABA_AR$), α2 subunit knock-in mouse. Journal of Biological Chemistry 291, 12394–12407.

Nakamura, Y., Morrow, D.H., Nathanson, A.J., Henley, J.M., Wilkinson, K.A., Moss, S.J., 2020. Phosphorylation on Ser-359 of the α2 subunit in GABA type A receptors down-regulates their density at inhibitory synapses. Journal of Biological Chemistry 295, 12330–12342.

Neish, C.S., Martin, I.L., Davies, M., Henderson, R.M., Edwardson, J.M., 2003. Atomic force microscopy of ionotropic receptors bearing subunit-specific tags provides a method for determining receptor architecture. Nanotechnology 14, 864–872.

Newland, C.F., Cull-Candy, S.G., 1992. On the mechanism of action of picrotoxin on GABA receptor channels in dissociated sympathetic neurones of the rat. Journal of Physiology 447, 191–213.

Nguyen, Q.-A., Nicoll, R.A., 2018. The $GABA_A$ Receptor β subunitIs required for inhibitory transmission. Neuron 98, 718-725.

Niwa, F., Bannai, H., Arizono, M., Fukatsu, K., Triller, A., Mikoshiba, K., 2012. Gephyrin-independent $GABA_AR$ mobility and clustering during plasticity. PLoS One 7, e36148.

Norkett, R., Modi, S., Birsa, N., Atkin, T.A., Ivankovic, D., Pathania, M., Trossbach, S.V., Korth, C., Hirst, W.D., Kittler, J.T., 2016. DISC1-dependent regulation of mitochondrial dynamics controls the morphogenesis of complex neuronal dendrites. Journal of Biological Chemistry 291, 613–629.

Nusser, Z., Ahmad, Z., Tretter, V., Fuchs, K., Wisden, W., Sieghart, W., Somogyi, P., 1999. Alterations in the expression of $GABA_A$ receptor subunits in cerebellar granule cells after the disruption of the α6 subunit gene. European Journal of Neuroscience 11, 1685–1697.

Nusser, Z., Cull-Candy, S., Farrant, M., 1997. Differences in synaptic $GABA_A$ receptor number underlie variation in GABA mini amplitude. Neuron 19, 697–709.

Nusser, Z., Hájos, N., Somogyi, P., Mody, I., 1998. Increased number of synaptic $GABA_A$ receptors underlies potentiation at hippocampal inhibitory synapses. Nature 395, 172–177.

Nusser, Z., Roberts, J.D., Baude, A., Richards, J.G., Sieghart, W., Somogyi, P., 1995a. Immunocytochemical localization of the α1 and 2/3 subunits of the $GABA_A$ receptor in relation to specific GABAergic synapses in the dentate gyrus. European Journal of Neuroscience 7, 630–646.

Nusser, Z., Roberts, J.D., Baude, A., Richards, J.G., Somogyi, P., 1995b. Relative densities of synaptic and extrasynaptic $GABA_A$ receptors on cerebellar granule cells as determined by a quantitative immunogold method. Journal of Neuroscience 15, 2948–2960.

Nusser, Z, Sieghart, W., Benke, D., Fritschy, J.M., Somogyi, P., 1996. Differential synaptic localization of two major γ-aminobutyric acid type A receptor α subunits on hippocampal pyramidal cells. PNAS 93, 11939–11944.

Nusser, Zoltan, Sieghart, W., Somogyi, P., 1998. Segregation of different $GABA_A$ receptors to synaptic and extrasynaptic membranes of cerebellar granule cells. Journal of Neuroscience 18, 1693–1703.

Nusser, Z., Sieghart, W., Stephenson, F.A., Somogyi, P., 1996. The α6 subunit of the $GABA_A$ receptor is concentrated in both inhibitory and excitatory synapses on cerebellar granule cells. Journal of Neuroscience 16, 103–114.

Nyíri, G., Freund, T.F., Somogyi, P., 2001. Input-dependent synaptic targeting of α2 subunit-containing $GABA_A$ receptors in synapses of hippocampal pyramidal cells of the rat. European Journal of Neuroscience 13, 428–442.

Ogris, W., Lehner, R., Fuchs, K., Furtmüller, B., Höger, H., Homanics, G.E., Sieghart, W., 2006. Investigation of the abundance and subunit composition of $GABA_A$ receptor subtypes in the cerebellum of α1 subunit-deficient mice. Journal of Neurochemistry 96, 136–147.

Olsen, R.W., 2018. GABAA receptor: Positive and negative allosteric modulators. Neuropharmacology 136, 10–22.

Olsen, R.W., Lindemeyer, A.K., Wallner, M., Li, X., Huynh, K.W., Zhou, Z.H., 2019. Cryo-electron microscopy reveals informative details of $GABA_A$ receptor structural pharmacology: implications for drug discovery. Annals of Translational Medicine 7, S144.

Olsen, R.W., Sieghart, W., 2009. $GABA_A$ receptors: subtypes provide diversity of function and pharmacology. Neuropharmacology 56, 141–148.

Olsen, R.W., Sieghart, W., 2008. International Union of Pharmacology. LXX. Subtypes of γ-aminobutyric acid A receptors: classification on the basis of subunit composition, pharmacology, and function. Update. Pharmacological Reviews 60, 243–260.

Olsen, R.W., Tobin, A.J., 1990. Molecular biology of $GABA_A$ receptors. FASEB J 4, 1469–1480.

Padgett, C.L., Hanek, A.P., Lester, H.A., Dougherty, D.A., Lummis, S.C.R., 2007. Unnatural amino acid mutagenesis of the $GABA_A$ receptor binding site residues reveals a novel cation–π interaction between GABA and β2Tyr97. Journal of Neuroscience 27, 886–892.

Palpagama, T.H., Sagniez, M., Kim, S., Waldvogel, H.J., Faull, R.L., Kwakowsky, A., 2019. $GABA_A$ receptors are well preserved in the hippocampus of aged mice. eNeuro 6.

Pan, Z.H., Zhang, D., Zhang, X., Lipton, S.A., 1997. Agonist-induced closure of constitutively open γ-aminobutyric acid channels with mutated M2 domains. PNAS 94, 6490–6495.

Parodi, A.J., 2000a. Protein glycosylation and its role in protein folding. Annual Reviews in Biochemistry 69, 69–93.

Parodi, A.J., 2000b. Role of N-oligosaccharide endoplasmic reticulum processing reactions in glycoprotein folding and degradation. Biochemical Journal 348 Pt 1, 1–13.

Patel, B., Bright, D.P., Mortensen, M., Frølund, B., Smart, T.G., 2016. Context-dependent modulation of $GABA_A$R-mediated tonic currents. Journal of Neuroscience 36, 607–621.

Patel, B., Mortensen, M., Smart, T.G., 2014. Stoichiometry of δ subunit containing $GABA_A$ receptors. British Journal of Pharmacology 171, 985–994.

Petrini, E.M., Marchionni, I., Zacchi, P., Sieghart, W., Cherubini, E., 2004. Clustering of extrasynaptic $GABA_A$ receptors modulates tonic inhibition in cultured hippocampal neurons. Journal of Biological Chemistry 279, 45833–45843.

Petrini, E.M., Ravasenga, T., Hausrat, T.J., Iurilli, G., Olcese, U., Racine, V., Sibarita, J.-B., Jacob, T.C., Moss, S.J., Benfenati, F., Medini, P., Kneussel, M., Barberis, A., 2014. Synaptic recruitment of gephyrin regulates surface $GABA_A$ receptor dynamics for the expression of inhibitory LTP. Nature Communications 5, 3921.

Petrini, E.M., Zacchi, P., Barberis, A., Mozrzymas, J.W., Cherubini, E., 2003. Declusterization of $GABA_A$ receptors affects the kinetic properties of GABAergic currents in cultured hippocampal neurons. Journal of Biological Chemistry 278, 16271–16279.

Phulera, S., Zhu, H., Yu, J., Claxton, D.P., Yoder, N., Yoshioka, C., Gouaux, E., 2018. Cryo-EM structure of the benzodiazepine-sensitive α1β1γ2S tri-heteromeric $GABA_A$ receptor in complex with GABA. eLife 7, e39383.

Picton, A.J., Fisher, J.L., 2007. Effect of the α subunit subtype on the macroscopic kinetic properties of recombinant $GABA_A$ receptors. Brain Research 1165, 40–49.

Pirker, S., Schwarzer, C., Wieselthaler, A., Sieghart, W., Sperk, G., 2000. $GABA_A$ receptors: immunocytochemical distribution of 13 subunits in the adult rat brain. Neuroscience 101, 815–850.

Pollard, S., Duggan, M.J., Stephenson, F.A., 1993. Further evidence for the existence of α subunit heterogeneity within discrete γ-aminobutyric acid A receptor subpopulations. Journal of Biological Chemistry 268, 3753–3757.

Pollard, S., Thompson, C.L., Stephenson, F.A., 1995. Quantitative characterization of α6 and α1α6 subunit-containing native γ-aminobutyric acid A receptors of adult rat cerebellum demonstrates two α subunits per receptor oligomer. Journal of Biological Chemistry 270, 21285–21290.

Pöltl, A., Hauer, B., Fuchs, K., Tretter, V., Sieghart, W., 2003. Subunit composition and quantitative importance of $GABA_A$ receptor subtypes in the cerebellum of mouse and rat. Journal of Neurochemistry 87, 1444–1455.

Rajgor, D., Purkey, A.M., Sanderson, J.L., Welle, T.M., Garcia, J.D., Dell'Acqua, M.L., Smith, K.R., 2020. Local miRNA-dependent translational control of $GABA_AR$ synthesis during inhibitory long-term potentiation. Cell Reports 31, 107785.

Rajgor, D., Sanderson, T.M., Amici, M., Collingridge, G.L., Hanley, J.G., 2018. NMDAR-dependent Argonaute 2 phosphorylation regulates miRNA activity and dendritic spine plasticity. EMBO J 37, e97943.

Ramerstorfer, J., Furtmüller, R., Sarto-Jackson, I., Varagic, Z., Sieghart, W., Ernst, M., 2011. The $GABA_A$ receptor α+/β− interface: a novel target for subtype selective drugs. Journal of Neuroscience 31, 870–877.

Reddy, D.S., 2010. Neurosteroids: endogenous role in the human brian and therapeutic potentials. Progress in Brain Research 186, 113–137.

Reynolds, J.N., Maitra, R., 1996. Propofol and flurazepam act synergistically to potentiate $GABA_A$ receptor activation in human recombinant receptors. European Journal of Pharmacology 314, 151–156.

Rogers, C.J., Twyman, R.E., Macdonald, R.L., 1994. Benzodiazepine and β-carboline regulation of single $GABA_A$ receptor channels of mouse spinal neurones in culture. Journal of Physiology 475, 69–82.

Rothstein, J.D., Garland, W., Puia, G., Guidotti, A., Weber, R.J., Costa, E., 1992. Purification and characterization of naturally occurring benzodiazepine receptor ligands in rat and human brain. Journal of Neurochemistry 58, 2102–2115.

Rudolph, U., Crestani, F., Benke, D., Brünig, I., Benson, J.A., Fritschy, J.M., Martin, J.R., Bluethmann, H., Möhler, H., 1999. Benzodiazepine actions mediated by specific γ-aminobutyric acid A receptor subtypes. Nature 401, 796–800.

Rudolph, U., Möhler, H., 2004. Analysis of $GABA_A$ receptor function and dissection of the pharmacology of benzodiazepines and general anaesthetics through mouse genetics. Annual Reviews in Pharmacology and Toxicology 44, 475–498.

Sagné, C., El Mestikawy, S., Isambert, M.-F., Hamon, M., Henry, J.-P., Giros, B., Gasnier, B., 1997. Cloning of a functional vesicular GABA and glycine transporter by screening of genome databases 1. The mouse VIAAT cDNA sequence has been submitted to the EMBL Data Bank under the accession number AJ001598.1. FEBS Letters 417, 177–183.

Sarto, I., Wabnegger, L., Dögl, E., Sieghart, W., 2002. Homologous sites of $GABA_A$ receptor α1, β3 and γ2 subunits are important for assembly. Neuropharmacology 43, 482–91.

Sarto-Jackson, I., Sieghart, W., 2008. Assembly of $GABA_A$ receptors (Review). Molecular Membrane Biology 25, 302–310.

Sassoè-Pognetto, M., Fritschy, J.M., 2000. Mini-review: gephyrin, a major postsynaptic protein of GABAergic synapses. European Journal of Neuroscience 12, 2205–2210.

Scholze, P., Pökl, M., Längle, S., Steudle, F., Fabjan, J., Ernst, M., 2020. Two distinct populations of α1α6-containing $GABA_A$ receptors in rat cerebellum. Frontiers in Synaptic Neuroscience 12, 591129.

Schumacher, M., Robel, P., Baulieu, E.E., 1996. Development and regeneration of the nervous system: a role for neurosteroids. Developmental Neuroscience 18, 6–21.

Sekar, R.B., Periasamy, A., 2003. Fluorescence resonance energy transfer (FRET) microscopy imaging of live cell protein localizations. Journal of Cell Biology 160, 629–633.

Semyanov, A., Walker, M.C., Kullmann, D.M., Silver, R.A., 2004. Tonically active $GABA_A$ receptors: modulating gain and maintaining the tone. Trends in Neuroscience 27, 262–269.

Sergeev, M., Godin, A.G., Kao, L., Abuladze, N., Wiseman, P.W., Kurtz, I., 2012a. Determination of membrane protein transporter oligomerization in native tissue using spatial fluorescence intensity fluctuation analysis. PLOS ONE 7, e36215.

Sergeev, M., Swift, J.L., Godin, A.G., Wiseman, P.W., 2012b. Ligand-induced clustering of EGF receptors: a quantitative study by fluorescence image moment analysis. Biophysical Chemistry 161, 50–53.

Serwanski, D.R., Miralles, C.P., Christie, S.B., Mehta, A.K., Li, X., De Blas, A.L., 2006. Synaptic and non-synaptic localization of $GABA_A$ receptors containing the α5 subunit in the rat brain. Journal of Computational Neurology 499, 458–470.

Sexton, C.A., Penzinger, R., Mortensen, M., Bright, D.P., Smart, T.G., 2021. Structural determinants and regulation of spontaneous activity in $GABA_A$ receptors. Nature Communications 12, 5457.

Sieghart, W., 1995. Structure and pharmacology of γ-aminobutyric acid A receptor subtypes. Pharmacological Reviews 47, 181–234.

Sieghart, W., Item, C., Buchstaller, A., Fuchs, K., Höger, H., Adamiker, D., 1993. Evidence for the existence of differential O-glycosylated α5 subunits of the γ-aminobutyric acid A receptor in the rat brain. Journal of Neurochemistry 60, 93–98.

Sieghart, W., Sperk, G., 2002. Subunit composition, distribution and function of $GABA_A$ receptor subtypes. Current Topics in Medical Chemistry 2, 795–816.

Sierra, S., Luquin, N., Rico, A.J., Gómez-Bautista, V., Roda, E., Dopeso-Reyes, I.G., Vázquez, A., Martínez-Pinilla, E., Labandeira-García, J.L., Franco, R., Lanciego, J.L., 2015. Detection of cannabinoid receptors CB1 and CB2 within basal ganglia output neurons in macaques: changes following experimental parkinsonism. Brain Structure and Function 220, 2721–2738.

Sigel, E., 2002. Mapping of the benzodiazepine recognition site on $GABA_A$ receptors. Current Topics in Medical Chemistry 2, 833–839.

Sigel, E., Baur, R., Boulineau, N., Minier, F., 2006. Impact of subunit positioning on $GABA_A$ receptor function. Biochemical Society Transactions 34, 868–871.

Sigel, E., Baur, R., Kellenberger, S., Malherbe, P., 1992. Point mutations affecting antagonist affinity and agonist dependent gating of $GABA_A$ receptor channels. EMBO J 11, 2017–2023.

Sigel, E., Baur, R., Malherbe, P., Möhler, H., 1989. The rat β1 subunit of the $GABA_A$ receptor forms a picrotoxin-sensitive anion channel open in the absence of GABA. FEBS Letters 257, 377–379.

Sigel, E., Baur, R., Trube, G., Möhler, H., Malherbe, P., 1990. The effect of subunit composition of rat brain $GABA_A$ receptors on channel function. Neuron 5, 703–711.

Sigel, E., Ernst, M., 2018. The Benzodiazepine Binding Sites of $GABA_A$ Receptors. Trends in Pharmacological Science 39, 659–671.

Sigel, E., Kaur, K.H., Lüscher, B.P., Baur, R., 2009. Use of concatamers to study $GABA_A$ receptor architecture and function: application to δ subunit-containing receptors and possible pitfalls. Biochemical Society Transactions 37, 1338–1342.

Sigel, E., Lüscher, B.P., 2011. A closer look at the high affinity benzodiazepine binding site on $GABA_A$ receptors. Current Topics in Medical Chemistry 11, 241–246.

Sigel, E., Steinmann, M.E., 2012. Structure, function, and modulation of $GABA_A$ receptors. Journal of Biological Chemistry 287, 40224–40231.

Simeone, X., Iorio, M.T., Siebert, D.C.B., Rehman, S., Schnürch, M., Mihovilovic, M.D., Ernst, M., 2019. Defined concatenated α6α1β3γ2 GABAA receptor constructs reveal dual action of pyrazoloquinolinone allosteric modulators. Bioorganic and Medical Chemistry 27, 3167–

Simon, J., Wakimoto, H., Fujita, N., Lalande, M., Barnard, E.A., 2004. Analysis of the set of GABAA receptor genes in the human genome. Journal of Biological Chemistry 279, 41422–41435.

Skolnick, P., 2012. Anxioselective anxiolytics: on a quest for the Holy Grail. Trends in Pharmacology Sci 33, 611–620.

Smart, T.G., Constanti, A., 1986. Studies on the mechanism of action of picrotoxinin and other convulsants at the crustacean muscle GABA receptor. Proceedings of the Royal Society of London B: Biological Science 227, 191–216.

Smart, T.G., Moss, S.J., Xie, X., Huganir, R.L., 1991. $GABA_A$ receptors are differentially sensitive to zinc: dependence on subunit composition. British Journal of Pharmacology 103, 1837–1839.

Smart, T.G., Stephenson, F.A., 2019. A half century of γ-aminobutyric acid. Brain and Neuroscience Advances 3, 239-249.

Söderberg, O., Gullberg, M., Jarvius, M., Ridderstråle, K., Leuchowius, K.-J., Jarvius, J., Wester, K., Hydbring, P., Bahram, F., Larsson, L.-G., Landegren, U., 2006. Direct observation of individual endogenous protein complexes i*n situ* by proximity ligation. Nature Methods 3, 995–1000.

Somogyi, P., Fritschy, J.M., Benke, D., Roberts, J.D., Sieghart, W., 1996. The γ 2 subunit of the $GABA_A$ receptor is concentrated in synaptic junctions containing the alpha 1 and β2/3 subunits in hippocampus, cerebellum and globus pallidus. Neuropharmacology 35, 1425–1444.

Song, I., Savtchenko, L., Semyanov, A., 2011. Tonic excitation or inhibition is set by $GABA_A$ conductance in hippocampal interneurons. Nature Communications 2, 376.

Specht, C.G., Izeddin, I., Rodriguez, P.C., El Beheiry, M., Rostaing, P., Darzacq, X., Dahan, M., Triller, A., 2013. Quantitative nanoscopy of inhibitory synapses: counting gephyrin molecules and receptor binding sites. Neuron 79, 308–321.

Srinivasan, S., Nichols, C.J., Lawless, G.M., Olsen, R.W., Tobin, A.J., 1999. Two invariant tryptophans on the α1 subunit define domains necessary for $GABA_A$ receptor assembly. Journal of Biological Chemistry 274, 26633–26638.

Stell, B.M., Brickley, S.G., Tang, C.Y., Farrant, M., Mody, I., 2003. Neuroactive steroids reduce neuronal excitability by selectively enhancing tonic inhibition mediated by δ subunit-containing $GABA_A$ receptors. PNAS 100, 14439–14444.

Stell, B.M., Mody, I., 2002. Receptors with different affinities mediate phasic and tonic $GABA_A$ conductances in hippocampal neurons. Journal of Neuroscience 22, RC223.

Stórustovu, S.I., Ebert, B., 2006. Pharmacological characterization of agonists at δ-containing $GABA_A$ receptors: functional selectivity for extrasynaptic receptors is dependent on the absence of γ2. Journal of Pharmacology and Experimental Therapeutics 316, 1351–1359.

Sumi, T., Harada, K., 2020. Mechanism underlying hippocampal long-term potentiation and depression based on competition between endocytosis and exocytosis of AMPA receptors. Science Reports 10, 14711.

Sumikawa, K., Parker, I., Miledi, R., 1988. Effect of tunicamycin on the expression of functional brain neurotransmitter receptors and voltage-operated channels in *Xenopus* oocytes. Brain Research 464, 191–199.

Sun, M.-Y., Shu, H.-J., Benz, A., Bracamontes, J., Akk, G., Zorumski, C.F., Steinbach, J.H., Mennerick, S.J., 2018. Chemogenetic isolation reveals synaptic contribution of δ $GABA_A$ receptors in mouse dentate granule neurons. Journal of Neuroscience. 38, 8128–8145.

Sur, C., Wafford, K.A., Reynolds, D.S., Hadingham, K.L., Bromidge, F., Macaulay, A., Collinson, N., O'Meara, G., Howell, O., Newman, R., Myers, J., Atack, J.R., Dawson, G.R., McKernan, R.M., Whiting, P.J., Rosahl, T.W., 2001. Loss of the major $GABA_A$ receptor subtype in the brain is not lethal in mice. Journal of Neuroscience 21, 3409–3418.

Tan, K.R., Baur, R., Charon, S., Goeldner, M., Sigel, E., 2009. Relative positioning of diazepam in the benzodiazepine-binding-pocket of GABA receptors. Journal of Neurochemistry 111, 1264–1273.

Tan, Y.H., Liu, M., Nolting, B., Go, J.G., Gervay-Hague, J., Liu, G., 2008. A nanoengineering approach for investigation and regulation of protein immobilization. ACS Nano 2, 2374–2384.

Tanaka, M., Olsen, R.W., Medina, M.T., Schwartz, E., Alonso, M.E., Duron, R.M., Castro-Ortega, R., Martinez-Juarez, I.E., Pascual-Castroviejo, I., Machado-Salas, J., Silva, R., Bailey, J.N., Bai, D., Ochoa, A., Jara-Prado, A., Pineda, G., Macdonald, R.L., Delgado-Escueta, A.V., 2008. Hyperglycosylation and reduced GABA currents of mutated GABRB3 polypeptide in remitting childhood absence epilepsy. American Journal of Human Genetics 82, 1249–1261.

Taylor, P.M., Thomas, P., Gorrie, G.H., Connolly, C.N., Smart, T.G., Moss, S.J., 1999. Identification of amino acid residues within $GABA_A$ receptor β subunits that mediate both homomeric and heteromeric receptor expression. Journal of Neuroscience 19, 6360–6371.

Thomas, P., Mortensen, M., Hosie, A.M., Smart, T.G., 2005. Dynamic mobility of functional $GABA_A$ receptors at inhibitory synapses. Nature Neuroscience 8, 889–897.

Thompson, C.L., Bodewitz, G., Stephenson, F.A., Turner, J.D., 1992. Mapping of $GABA_A$ receptor α5 and α6 subunit-like immunoreactivity in rat brain. Neuroscience Letters 144, 53–56.

Thompson, S.A., Arden, S.A., Marshall, G., Wingrove, P.B., Whiting, P.J., Wafford, K.A., 1999. Residues in transmembrane domains I and II determine γ-aminobutyric acid type A. A Rrceptor subtype-selective antagonism by furosemide. Molecular Pharmacology 55, 993–999.

Tia, S., Kotchabhakdi, N., Wang, J.F., Vicini, S., 1996. Distinct deactivation and desensitization kinetics of recombinant $GABA_A$ receptors. Neuropharmacology 35, 1375–1382.

Tretter, V., Ehya, N., Fuchs, K., Sieghart, W., 1997. Stoichiometry and assembly of a recombinant $GABA_A$ receptor subtype. Journal of Neuroscience 17, 2728–2737.

Tretter, V., Jacob, T.C., Mukherjee, J., Fritschy, J.-M., Pangalos, M.N., Moss, S.J., 2008. The clustering of $GABA_A$ receptor subtypes at inhibitory synapses is facilitated *via* the direct binding of receptor α2 subunits to gephyrin. Journal of Neuroscience 28, 1356–1365.

Tretter, V., Kerschner, B., Milenkovic, I., Ramsden, S.L., Ramerstorfer, J., Saiepour, L., Maric, H.-M., Moss, S.J., Schindelin, H., Harvey, R.J., Sieghart, W., Harvey, K., 2011. Molecular basis of the γ-aminobutyric acid A receptor α3 subunit interaction with the clustering protein gephyrin. Journal of Biological Chemistry 286, 37702–37711.

Tretter, V., Revilla-Sanchez, R., Houston, C., Terunuma, M., Havekes, R., Florian, C., Jurd, R., Vithlani, M., Michels, G., Couve, A., Sieghart, W., Brandon, N., Abel, T., Smart, T.G., Moss, S.J., 2009. Deficits in spatial memory correlate with modified γ-aminobutyric acid type A receptor tyrosine phosphorylation in the hippocampus. PNAS 106, 20039–20044.

Twyman, R.E., Macdonald, R.L., 1992. Neurosteroid regulation of $GABA_A$ receptor single-channel kinetic properties of mouse spinal cord neurons in culture. Journal of Physiology 456, 215–245.

Tyagarajan, S.K., Fritschy, J.-M., 2014. Gephyrin: a master regulator of neuronal function? Nature Reviews Neuroscience 15, 141–156.

Ueno, S., Bracamontes, J., Zorumski, C., Weiss, D.S., Steinbach, J.H., 1997. Bicuculline and gabazine are allosteric inhibitors of channel opening of the $GABA_A$ receptor. Journal of Neuroscience 17, 625–634.

Unruh, J.R., Gratton, E., 2008. Analysis of molecular concentration and brightness from fluorescence fluctuation data with an electron multiplied CCD camera. Biophysical Journal 95, 5385–5398.

Unwin, N., 2005. Refined structure of the nicotinic acetylcholine receptor at 4A resolution. Journal of Molecular Biology 346, 967–989.

Verdoorn, T.A., 1994. Formation of heteromeric γ-aminobutyric acid type A receptors containing two different α subunits. Molecular Pharmacology 45, 475–480.

Verdoorn, T.A., Draguhn, A., Ymer, S., Seeburg, P.H., Sakmann, B., 1990. Functional properties of recombinant rat $GABA_A$ receptors depend upon subunit composition. Neuron 4, 919–928.

Vetiska, S.M., Ahmadian, G., Ju, W., Liu, L., Wymann, M.P., Wang, Y.T., 2007. $GABA_A$ receptor-associated phosphoinositide 3-kinase is required for insulin-induced recruitment of postsynaptic $GABA_A$ receptors. Neuropharmacology 52, 146–155.

Vithlani, M., Moss, S.J., 2009. The role of $GABA_AR$ phosphorylation in the construction of inhibitory synapses and the efficacy of neuronal inhibition. Biochemical Society Transactions 37, 1355–1358.

Wafford, K.A., Bain, C.J., Quirk, K., McKernan, R.M., Wingrove, P.B., Whiting, P.J., Kemp, J.A., 1994. A novel allosteric modulatory site on the $GABA_A$ receptor β subunit. Neuron 12, 775–782.

Walters, R. J., Hadley, S.H., Morris, K.D., Amin, J., 2000. Benzodiazepines act on $GABA_A$ receptors *via* two distinct and separable mechanisms. Nature Neuroscience 3, 1274–1281.

Wang, M., 2011. Neurosteroids and $GABA_A$ Receptor Function. Frontiers in Endocrinology 2, 44.

Ward, R.J., Pediani, J.D., Godin, A.G., Milligan, G., 2015. Regulation of oligomeric organization of the serotonin 5-hydroxytryptamine 2C (5-HT2C) receptor observed by spatial intensity distribution analysis. Journal of Biological Chemistry 290, 12844–12857.

Wei, W., Zhang, N., Peng, Z., Houser, C.R., Mody, I., 2003. Perisynaptic localization of δ subunit-containing $GABA_A$ receptors and their activation by GABA spillover in the mouse dentate gyrus. Journal of Neuroscience 23, 10650–10661.

Weibrecht, I., Leuchowius, K.-J., Clausson, C.-M., Conze, T., Jarvius, M., Howell, W.M., Kamali-Moghaddam, M., Söderberg, O., 2010. Proximity ligation assays: a recent addition to the proteomics toolbox. Expert Reviews in Proteomics 7, 401–409.

Whiting, P., McKernan, R.M., Iversen, L.L., 1990. Another mechanism for creating diversity in γ-aminobutyrate type A receptors: RNA splicing directs expression of two forms of γ2 phosphorylation site. PNAS 87, 9966–9970.

Whittemore, E.R., Yang, W., Drewe, J.A., Woodward, R.M., 1996. Pharmacology of the human γ-aminobutyric acid A receptor α4 subunit expressed in *Xenopus laevis* oocytes. Molecular Pharmacology 50, 1364–1375.

Wieland, H.A., Lüddens, H., Seeburg, P.H., 1992a. A single histidine in $GABA_A$ receptors is essential for benzodiazepine agonist binding. Journal of Biological Chemistry 267, 1426–1429.

Wisden, W., Laurie, D.J., Monyer, H., Seeburg, P.H., n.d. The Distribution of 13 GABA, Receptor Subunit mRNAs in the Rat Brain. I. Telencephalon, Diencephalon, Mesencephalon 23.

Wiseman, P.W., Godin, A.G., Swift, J.L., Costantino, S., Ribeiro-da-Silva, A., Koninck, Y.D., Beaulieu, J., 2012. Spatial intensity distribution analysis (SpIDA): a fluorescence microscopy-based method to measure receptor oligomerization in cells. Microscopy and Microanalysis 18, 128–129.

Wongsamitkul, N., Maldifassi, M., Simeone, X., Baur, R., Ernst, M., Sigel, E., 2017. α subunits in $GABA_A$ receptors are dispensable for GABA and diazepam action. Scientific Reports 7.

Wooltorton, J.R., Moss, S.J., Smart, T.G., 1997. Pharmacological and physiological characterization of murine homomeric β3 $GABA_A$ receptors. European Journal of Neuroscience 9, 2225–2235.

Xu, M., Akabas, M.H., 1996. Identification of channel-lining residues in the M2 membrane-spanning segment of the $GABA_A$ receptor α1 subunit. Journal of General Physiology 107, 195–205.

Yakel, J.L., Lagrutta, A., Adelman, J.P., North, R.A., 1993. Single amino acid substitution affects desensitization of the 5-hydroxytryptamine type 3 receptor expressed in *Xenopus* oocytes. PNAS 90, 5030–5033.

Zezula, J., Sieghart, W., 1991. Isolation of type I and type II $GABA_A$-benzodiazepine receptors by immunoaffinity chromatography. FEBS Letters 284, 15–18.

Zhao, M., Jin, L., Chen, B., Ding, Y., Ma, H., Chen, D., 2003. After-pulsing and its correction in fluorescence correlation spectroscopy experiments. Applied Optics 42, 4031–4036.

Zhu, S., Noviello, C.M., Teng, J., Walsh, R.M., Kim, J.J., Hibbs, R.E., 2018. Structure of a human synaptic $GABA_A$ receptor. Nature 559, 67–72.

Zimmer, M., 2002. Green fluorescent protein (GFP): applications, structure, and related photophysical behaviour. Chemical Reviews 102, 759–781.